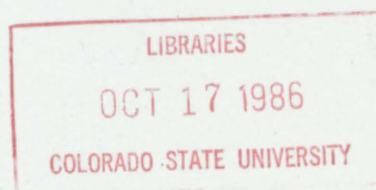NSF/NOAA ATM-8419116

An Observational Study of Tropical Cloud Cluster Evolution and Cyclogenesis In the Western North Pacific

by Cheng-Shang Lee

P.I. William M. Gray

Atmospheric Science

PAPER NO.

403

DEPARTMENT OF ATMOSPHERIC SCIENCE

COLORADO STATE UNIVERSITY

FORT COLLINS, COLORADO

AN OBSERVATIONAL STUDY OF TROPICAL CLOUD CLUSTER EVOLUTION AND

CYCLOGENESIS IN THE WESTERN NORTH PACIFIC

By

Cheng Shang Lee

Department of Atmospheric Science

Colorado State University

Fort Collins, Colorado 80523

September, 1986

ABSTRACT

     A combination of rawinsonde composite and individual case analyses
using FGGE III-b data has been used to study the evolution of pre-
cyclone tropical cloud clusters and those prominent cloud clusters which
do not develop into tropical cyclones in the western North Pacific.
These two types of cloud clusters are defined as genesis and non-genesis
cases. Results show that the non-genesis cloud clusters have about the
same magnitude of maximum mean upward vertical motion and the same
amount of cumulus activities as those of the genesis cloud clusters.
The convection associated with the non-genesis cloud clusters does not
necessarily alter the temperature, pressure or the vorticity fields, but
does transport moisture from the lower troposphere to the middle
troposphere. These cloud clusters generally form due to a large-scale
low-level forced convergence and dissipate due to a strong middle- to
upper-level shearing effect.

     Genesis cloud clusters are found to have a much stronger middle- to
low-level cyclonic circulation over $2-8^\circ$ radius than the non-genesis
cloud clusters. The buildup of this strong cyclonic circulation before
cyclogenesis is primarily due to strong large-scale surge-type forcing
processes which produce large inward eddy vorticity fluxes. These
surge-type eddy fluxes are estimated as a residual of the tropospheric
tangential momentum budget balance. The mean transverse circulation
transports are generally not efficient enough to produce the necessary
momentum buildup at the early formation stages. The eddy fluxes allow
for a cyclonic circulation buildup without increasing the transverse
circulation.

     The individual case FGGE analyses indicate three possible large-
scale surges: the cross-equatorial surges, trade wind surges, or summer
monsoon surges within the North Indian Ocean. A convection burst and a
low-level vorticity buildup are generally found to be associated with
these surges. Tropical cyclone formation generally occurs when these
surges reach the inner region of the pre-cyclone cloud cluster. The
results also indicate large variations between different individual
formation cases. In the upper level, the circulation pattern can act to
help or hinder the formation process. A weak divergent flow generally
is satisfactory for formation to occur.

TABLE OF CONTENTS

Page

LIST OF SYMBOLS AND ACRONYMS

Symbols

[ ]	Bracket denotes grid box average
–	Overbar denotes azimuthal mean
$\wedge$	Over-hat denotes an area average
B	Bowen Ratio S_{sfc} / L E_{sfc}
C	Condensation
C_D	Drag coefficient
C_p	Specific heat of dry air at constant pressure
C_r	Radial component of cyclone movement
D	Divergence
E	Evaporation
E_{sfc}	Surface evaporation
F	Vertical eddy moist static energy flux
f	Coriolis parameter
F_θ	Subgrid scale effect (tangential component)
F_{sfc}	Surface friction
g	Gravity
h	Moist static energy
L	Latent heat
M	Mean circulation flux
P	1. Precipitation 2. Pressure, vertical axis
P_{sfc}	Surface precipitation
Q_R	Radiational heating rate
q	Mixing ratio

Q_1	Apparent heat source
Q_2	Apparent moisture sink
qF	or $(-\nabla \cdot LqV)$ – horizontal latent energy (Lq) convergence
r	Radius, radial axis
SE	Standing eddy flux
S_{sfc}	Surface sensible energy flux
s	Dry static energy
sF	Horizontal dry static energy (s) convergence
sfc	Denote surface
T	Temperature
TE	Transient eddy flux
V	Total wind
V_r	Radial component of momentum, radial wind
V_t	Tangential component of momentum, tangential wind
V^2	Total wind speed square
V_{10}	Total wind speed at 10 meters height
Z	Height
θ	1. azimuth, measured counterclockwise from the north 2. as a subscript denotes tangential component
θ_e	Equivalent potential temperature
ρ	Density
τ_o	Surface stress
ω	Vertical p velocity or vertical mass flux (mb/d)
ζ_a	Absolute vorticity
ζ_r	Relative vorticity

ATR   Annual Typhoon Report

BK   Background composite - this composite contains the positions at dates and times that are the same as those of the genesis composites but at one year before and one year after. It is considered to represent the average condition where cyclones may form.

ECMWF   European Center for Medium-range Weather Forecasts

FG   Fast Genesis Composite - (estimated) intensity at Stage 1 ($5\sim10$ m s^{-1}), Stage 2 ($10\sim15$ m s^{-1}), Stage 3 (19 m s^{-1}), and Stage 4 (31 m s^{-1})

FGGE   First GARP Global Experiment

GN   Genesis Composite - (estimated) intensity at Stage 1 ($5\sim10$ m s^{-1}), Stage 2 (~10 m s^{-1}), Stage 3 (15 m s^{-1}), and Stage 4 (22 m s^{-1})

IR   (Satellite) Infrared Image

JTWC   Joint Typhoon Warning Center, Guam

NCAR   National Center for Atmospheric Research, Boulder, CO

NG   Non-Genesis Composite (average of NN and PN)

NN   Non-Persistent, Non-genesis Composite - estimated intensity at Stage 2 ($\sim5\sim10$ m s^{-1})

NOAA   National Oceanic and Atmospheric Administration

PN   Persistent, Non-genesis - estimated intensity at Stage 2 ($\sim5\sim10$ m s^{-1})

SG   Slow Genesis Composite - (estimated) intensity at Stage 1 ($5\sim10$ m s^{-1}), State 2 (10 m s^{-1}), Stage 3 (14 m s^{-1}), and Stage 4 (17 m s^{-1})

STY   Supertyphoon

TS   Tropical Storm

TUTT   Tropical Upper Tropospheric Trough

TY   Typhoon

VIS   (Satellite) Visible Image

1. INTRODUCTION

There are approximately 80 tropical cyclones with maximum sustained surface winds of 20 m s^{-1} over the globe per year (Gray, 1981). The average annual variation from this number is only about 8%. The western North Pacific is the most active region, with an annual average of about 26 tropical cyclones (or about 33% of the total number). About half to two thirds of these cyclones reach hurricane or typhoon intensity (maximum sustained surface winds > 33 m s^{-1}). However, only a very small percentage of tropical cloud clusters develop into tropical cyclones.

The physical processes that lead to the formation of a tropical cyclone from a tropical cloud cluster or disturbance are still not well understood. Complications arise because there are many different formation cases occurring under different large-scale circulation patterns and in different ocean basins. The processes that dictate the later stage of cyclone development might also vary from those that dictate the early formation stage. Moreover, no one can really answer the question of why a cloud cluster can develop into a tropical cyclone (termed genesis cloud cluster) unless he also answers the question of why many prominent cloud clusters do not form tropical cyclones (termed non-genesis cloud cluster).

The research presented here attempts to study the evolution of both genesis and non-genesis cloud clusters in the western North Pacific by using a combination of the rawinsonde composite and the individual case

analysis techniques. (Other major ocean basins – e.g., North Atlantic and eastern North Pacific – are not studied because of the lack of observations as adequate as those in the western North Pacific.) It is expected that through careful mass, energy, moisture, and angular momentum budgets analyses, most of the important physical processes influencing tropical cyclone formation and non-formation can be ascertained.

There have been a number of earlier observational studies on tropical cyclone formation at Colorado State University: (Gray, 1968; Zehr, 1976; Erickson, 1977; McBride, 1979, 1981a,b; McBride and Zehr, 1981; and Love, 1982, 1985a,b). Their results have indicated that the tropical cyclone formation event is mainly influenced by favorable surrounding larger-scale circulations. This research closely follows these previous studies, but is more detailed and has several advantages over the previous studies. The first advantage is that the current study uses 21 years (1957-1977) of rawinsonde data vs. the previous 10 years (1961-1970) of data used by some composite studies (Zehr, 1976; McBride, 1979, 1981a,b; and McBride and Zehr, 1981). The larger data set allows the possibility of added stratification of cyclone behavior. Better comparisons can then be made. The most significant improvement, however, is that by using stricter classification criteria during the various time stages of evolution, the characteristics of the cloud cluster's inner region structure can be better identified. More accurate and detailed budget analyses can also be obtained. In addition, the composite programs and procedures have been completely revised to rectify some small problems in the original version and to give better composite representations.

The second advantage of this newer study is that there are more reliable satellite data available for the current study than for the previous studies (Zehr, 1976; Erickson, 1977; McBride, 1979, 1981a, 1981b; and McBride and Zehr, 1981). This means that more, better-defined, non-genesis cloud clusters can be selected and that the centers of these cloud clusters can be better positioned. As will be shown later, some significant differences between the previous and the current non-genesis cloud cluster analyses are found. The results for the current analysis are more consistent and realistic.

The last advantage is that the FGGE III-b data set has become available at the National Center for Atmospheric Research (NCAR) in the last few years. This data set has been worked with and has been found suitable for studying the large-scale circulation influences on individual tropical cyclone formation (Lee and Gray, 1984). Although the FGGE III-b data set has some drawbacks for a very detailed study in individual cases, it offers the advantage of many cases for study and a consistent objective analysis in all cases.

The research philosophy followed is that if the results show consistencies and systematic variations among different tropical cyclones in different ocean basins, these results can then be considered very reliable. The success of the studies by Lee and Gray (1984) and Lee, et al. (1986) - regarding the large-scale circulation influence on the development of individual North Indian Ocean tropical cyclones using FGGE data - is very encouraging. The present study goes further, however, by focusing attention on all 24 tropical cyclones that formed in the western North Pacific (where raw rawinsonde observations are spread more uniformly) during the 1979 FGGE year. It is to be noted

that the FGGE III-b data were analyzed at the European Center for Medium-Range Weather Forecasts (ECMWF) and no subjective modification has been made to these data by the author.

It is well-known that both rawinsonde composites and individual case analysis have their specific advantages and drawbacks. The rawinsonde composite can give good quantitative information on the average three-dimensional structure and circulation patterns. A detailed budget analysis also can be made provided that careful composite classification criteria are imposed during case selection. The greatest drawback of this technique is that individual case characteristics are lost in the composite. Including the individual case FGGE analysis in this study is designed specifically to overcome this averaging problem.

Although the combination of the rawinsonde composite technique and individual case analysis using FGGE III-b data is very satisfactory in quantitatively studying the large-scale circulation influences on tropical cyclone formation, the detailed inner core structure and the internal dynamics associated with the meso-scale convective system can not be adequately identified. Nevertheless, if the large-scale environmental forcing is the primary dictating mechanism for tropical cyclone formation, the internal dynamics of the cloud cluster likely are not a crucial factor and can be understood much more easily afterward. Even if it should be shown later that the internal dynamics of the cloud cluster are the major factor in determining the processes responsible for cyclogenesis, understanding the large-scale circulation patterns would likely also be fundamental to a complete understanding of the cyclogenesis process.

A tropical cyclone can be classified into different stages throughout its life cycle; namely, tropical disturbance (pre-cyclone stage), tropical depression, tropical storm and typhoon or hurricane. These classifications are rather arbitrary and the evolution of a system from one stage to another stage is a continuous process rather than an abrupt discontinuous change. Ooyama (1982) has suggested that "it is far more natural to assume that genesis is a series of events, arising by chance from quantitative fluctuations of the normal disturbances, with the probability of further evolution gradually increasing as it proceeds.'' This study thus will focus on the evolution of both the structure of the meso-scale cloud cluster and its environmental circulation patterns during the formation of the tropical cyclone.

1.1 Previous Studies on Tropical Cyclone Formation

There have been many studies – including numerical model simulations, theoretical studies and observational analyses – attempting to help understand the formation and developing processes of tropical cyclones. Due to the fact that the required energy source in a tropical cyclone comes from latent heat released in convective clouds, many researchers have incorporated the cumulus convective processes (or cumulus parameterization) into their numerical models hoping to simulate the cyclone formation and developing processes through the forcing of cumulus heating (Kuo, 1965; Yamasaki, 1968; Ooyama, 1969; Rosenthal, 1970; etc.). An important concept behind some of these early studies is the so-called CISK (Conditional Instability of the Second Kind) theory (Charney and Eliassen, 1964; Ooyama, 1969) in which the cyclone and cumulus-scale motions are regarded as cooperating rather than as competing.

Fingerhut (1980) however, pointed out that ''... the CISK theory gives an early cyclone growth rate which is roughly one order of magnitude less than what is observed. Furthermore, the CISK theory gives identical growth rates for observed composite clusters which grow and which do not grow.'' Ooyama (1982) restated that the original linear CISK (which many early model simulations adopted in spirit) was not intended to explain tropical cyclogenesis but rather intensification. The closure assumption of the balanced model - the motion is in a quasi-balanced state or in gradient wind balance - is invalid in the early formation stage.

Gray (1979) and Fingerhut (1980) also have pointed out that most of the early-year numerical model simulations considered initial vortices that are roughly 10 times as intense as a typical tropical cloud cluster. Table 1 lists the intensity of initial disturbances used in several numerical experiments as summarized by Fingerhut (1980). The data used in some recent numerical model simulations are also included. It appears that those early-year numerical models (earlier than 1980) simulated cyclone intensification, not genesis. In recent years, numerical model simulations have been more carefully designed to start from weak vortices which are more similar to the observed pre-cyclone cloud clusters or easterly wave disturbances (see Fingerhut, 1980; Kurihara and Tuleya, 1981; Tuleya and Kurihara, 1981; Kurihara and Kawase, 1985; Tuleya, 1986). The studies by Challa and Pfeffer (1980, 1984) were aimed more at the hurricane development. Much stronger initial vortices were used in those model simulations.

The studies by Kurihara and Tuleya (1981) and Tuleya and Kurihara (1981) utilized a 3-dimensional model which integrated from an initial

TABLE 1

Intensity of initial disturbances utilized in several numerical experiments.

Model	V_{max} (m s^{-1})	Radius of V_{max} (km)	Mean Relative Vorticity, 2 V_{max}/r (10^{-6}s^{-1})
Kuo (1965)	10	141	142
Yamasaki (1968)	4.7	100	94
Ooyama (1969)	10 5	50 25,50,75,100	400 400,200,133,100
Miller (1969)	10	200	100
Rosenthal (1970)	7	250	56
Sundquist (1970)	15	200	150
Carrier (1971)	21	50	840
Anthes et al. (1971a,b) Anthes (1972, 1977)	18	240	150
Mathur (1972)	15	200	150
Harrison (1973)	10	120	170
Kurihara and Tuleya (1974)	12	200	120
Ceselski (1974)	17	100–150	~200
Kurihara (1975)	12	200	120
Rosenthal (1978)	7.2	220	65
Challa and Pfeffer (1980)	15	200	150
Kurihara and Tuleya (1981)	8	3-D	43 (max.)
Tuleya and Kurihara (1981)	–	3-D	18-43 (max.)
Challa and Pfeffer (1984)	14	200	140
Kurihara and Kawase (1985)	–	–	12.5 (max.)
Typical pre-genesis cloud cluster Fingerhut (1980)	3.6	550	13
Planetary vorticity at 15° at 20°			~37 ~50

condition comparable to that of an observed easterly wave disturbance originating from Africa. This model was designed to study the sensitivity of the cyclone formation and development to different environmental flow fields. Some interesting results were obtained from these model simulations. Neither of these studies, however, included in their model simulations the cumulus momentum rearrangement which acts to reduce the vertical tangential wind shears and thus slows down the cyclone development process (Lee, 1984; Challa and Pfeffer, 1984). They also did not well address the problem of why most easterly wave cloud clusters do not develop into tropical cyclones.

The numerical model simulation by Kurihara and Kawase (1985), on the other hand, used a simplified 2-D model on a zonal-vertical plane to study the sensitivity of easterly wave development from non-linear vorticity advection (Shapiro, 1977) and a CISK-type heating function. However, the vertical distribution of cumulus heating used in their simulation was arbitrarily determined. The level of maximum heating was placed at 600 mb, which is too low. McBride (1979) showed that the maximum mean vertical motion for the precyclone easterly wave cloud cluster is at about 300 mb, where the maximum cumulus heating (Q_1) should occur. Hack and Schubert (1986) found that model vortex evolution was very sensitive to the vertical heating profile. Placing the maximum heating at 600 mb (which is too low) gives a much stronger cyclone development rate as compared to the results with maximum heating placed at a more realistic level of 300 to 350 mb. The model simulations by Kurihara and Kawase (1985) thus are considered to have important physical deficiencies, especially since retarding cumulus friction effect was not included.

Schubert, et al. (1980) and Hack and Schubert (1986) have shown
that geostrophic adjustment works in a way such that the heating
efficiency is very low at the early cyclogenesis stage when the vortex
is weak. This is the major reason why many previous studies could not
properly simulate tropical cyclone formation from a weak initial vortex
in a reasonable time period when using a realistic magnitude of mean
vertical motion. As has been discussed by Fingerhut (1980) most
previous numerical model simulations (e.g. Sundquist, 1970; Anthes et
al., 1971a; Madala, 1975; Rosenthal, 1978) overestimated the 0-3° mean
vertical motion by a factor of 2 to 3. This was required in order to
spin up the model cyclone.

At the early cyclone formation stage the efficiency of a system's
momentum forcing (in comparison with its thermal forcing) is very high.
Based on the same concept, a few earlier studies (Alaka, 1962 and
Shapiro, 1977) have been directed toward finding a dynamic instability
criteria for cyclogenesis. Shapiro (1977) noted that the basic dynamics
of a weak quasi-steady pre-genesis disturbance is essentially linear.
It is suggested that if some non-linear process, which can be due to
changes in the surrounding flow, can become sufficiently large, then the
disturbance can not remain in a quasi-steady state and must grow. This
type of instability hypothesis appears to be qualitatively supported by
some of our project's previous observations and the current study. This
will be extensively discussed in Chapter 10.

Some studies have emphasized the importance of inward angular
momentum transports to account for the observed angular momentum spin-up
during the cyclone developing process and the need to balance the
surface frictional dissipation (Pfeffer, 1958; Riehl, 1961; Anthes,

1970; Kurihara, 1975; Challa and Pfeffer, 1980; Holland, 1983). Among these, the studies by Anthes (1970) and Challa and Pfeffer (1980) were specifically aimed at assessing the importance of the eddy angular momentum transports. (Note that most of the earlier-year numerical models are only in two dimensions.) They found that including an eddy angular momentum transport (or source) in the upper level helps the development of the model hurricane. Challa and Pfeffer (1984) further included the cumulus momentum mixing in their model simulation and found that the cumulus momentum mixing is primarily a retarding mechanism to tropical cyclone development.

The numerical model simulation study by Fingerhut (1980) is the first one to include in the model all physical processes, e.g., cumulus heating and momentum mixing, radial eddy momentum flux and the radiative heating (which is missing in most of the numerical simulations), and to initialize from a very weak vortex that is similar to the pre-cyclone vortex observed by McBride (1979, 1981a). As mentioned above, almost none of the numerical model simulations handle the evolution of the non-genesis cloud cluster. In other words, a numerical model simulation should be able to integrate from an initial vortex which resembles the observed non-genesis cloud cluster and yield no significant development of the vortex. Fingerhut (1980) indeed did successfully simulate the evolution of a non-genesis case. Unfortunately, an important ingredient behind the success of his simulations was the assumption of a positive cumulus friction through a rather deep layer, which later has been shown to be unrealistic by the author (Lee, 1984). In contrast, cumulus friction is primarily negative in the middle levels. The results of this study, however, indicate that Fingerhut might be right to include a

deep cyclonic spin up in his model simulations, although such a spin up

does not result from cumulus momentum transports but probably from an

environmental surge-type forcing on the poleward and/or equatorward side

of the cluster. This subject is discussed in more detail in Chapter 10.

In contrast to the numerical model simulations or theoretical

studies, observational studies have been looking for direct evidence of

the favorable large-scale or mesoscale conditions necessary for cyclone

formation and development. Gray (1968) discussed the important roles

that strong low-level relative vorticity and small vertical shear of

horizontal wind play in determining regions of high tropical cyclone

genesis frequency. Gray (1979) further demonstrated that six primary

seasonal climatological parameters appeared to explain the long-term

geographical differences in seasonal cyclone genesis frequency. These

include both dynamical and thermodynamical parameters, namely, the ocean

thermal energy to 60 m, the 500-700 mb RH, the vertical gradient of θ_e

between surface and 500 mb, the 950 mb relative vorticity, the inverse

of the 950 mb to 200 mb vertical wind shear and the Coriolis parameter.

McBride and Zehr (1981) found that the most distinctive difference

between genesis and non-genesis cloud clusters is the environmental

vorticity differences between 900 and 200 mb. The genesis cloud

clusters have much greater 900 and 200 mb vorticity difference at 6°

radius. A zero vertical wind shear line is generally found across the

center of the pre-cyclone cloud clusters but not the non-genesis cloud

clusters.

Ooyama (1982) commented that ''no doubt there exist large-scale

influences on the genesis process. However, what McBride and Zehr

(1981) found in the pre-cyclone cloud cluster composites do not

necessarily reveal causal effect of large-scale conditions, but merely confirm that the genesis process is already on its way.'' The author, though agreeing with the comment that genesis may be already on its way under this condition, does not agree with Ooyama's comment regarding the degree of the importance of the large-scale influence. This confusion arose primarily because McBride and Zehr (1981) failed to properly explain how the stronger low-level vorticity field with the genesis cases was brought about in the first place. The present study and some other studies (Love, 1982, 1985b; Lee and Gray, 1984; Lee, et al. 1986) all indicate that there are generally low-level large-scale wind surges which cause the vorticity buildup around the vicinity of the pre-cyclone disturbance prior to when the incipient tropical cyclones were first observed. Molinari and Skubis (1985), in their surface wind analysis, also found a low-level large-scale surge prior to the intensification of Hurricane Agnes in 1972. Tollerud and Esbensen (1985), in their composite analysis of the tropical cloud clusters in the North Atlantic, found a stronger low-level convergence during the cloud cluster growing stage as well. These large-scale low-level surges will be discussed extensively in later chapters.

In summary, none of the previous studies have properly addressed the physical processes responsible for tropical cyclone formation vs. non-formation. While the author's current research does not study every aspect of tropical cyclogenesis, it does provide more direct evidence on the influence of the large-scale circulation on tropical cyclogenesis. It is expected that results from this study will advance our knowledge toward fully understanding the tropical cyclone formation processes.

2. RAWINSONDE COMPOSITE

Tropical cyclones spend most of their lifetime over tropical oceans where conventional observations are limited. With the sparse rawinsonde network in the western North Pacific (shown in Fig. 1), it is impossible to obtain reliable quantitative or even qualitative analyses of meso-scale and/or synoptic-scale meteorological data associated with a tropical cyclone or cloud cluster at a given time period. However, if many similar systems at numerous time periods are composited together, observations can be located with respect to the individual system center. This results in a network of very dense data, which when averaged according to an appropriate grid system, allows quantitative analysis of mean fields of meteorological parameters associated with such types of systems.

These composite procedures undoubtedly have a significant smoothing effect. The variability among individual systems and uncertainty in determining the wind center of each system further add a scatter to this technique. Nevertheless, if the basic characteristics of those composited individual cases are basically similar, as is here assumed, then the relevant physical processes should be elucidated. The success of previous tropical cyclone rawinsonde composite studies (e.g. Izawa, 1964; Williams and Gray, 1973; Ruprecht and Gray, 1976; Frank, 1976; Zehr; 1976; etc.) lends much credibility to this research methodology. A similar composite technique has also been used to study tropical easterly waves (e.g. Reed and Recker, 1971; Reed et al., 1977; Thompson, et al., 1979) and squall lines (Gamache and House, 1982).
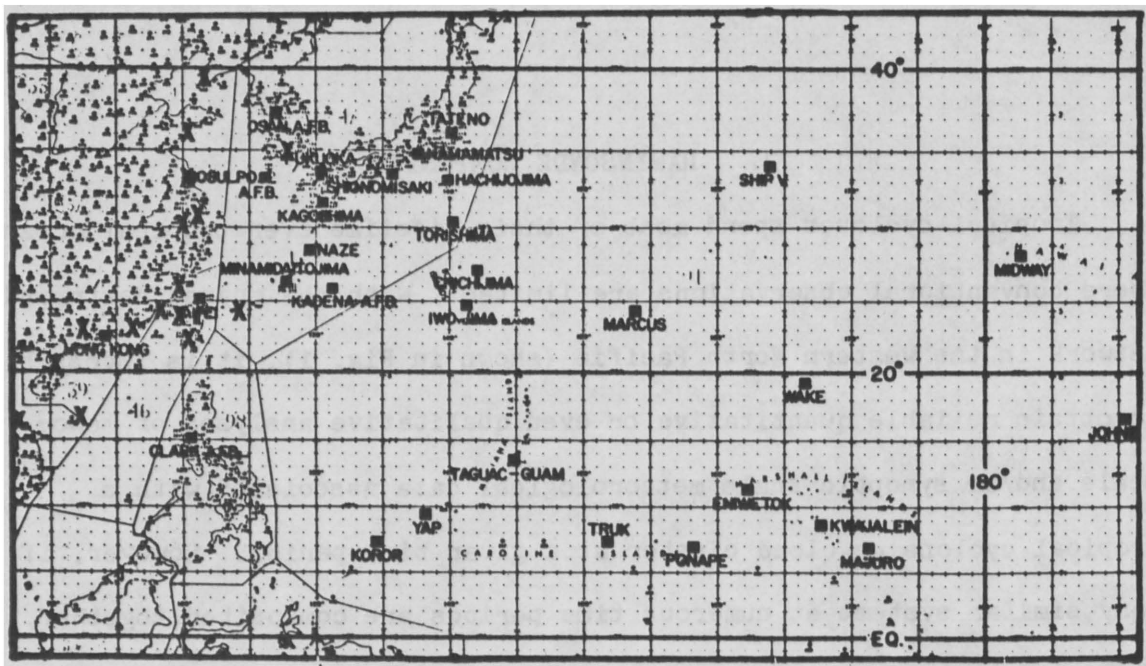
Fig. 1. Map showing the locations of the rawinsonde stations contained in the western North Pacific data set for the period 1957-1977. The X's show the new Asian coastal stations which have been incorporated into the data base in the last few years.

To obtain a realistic composite, it is necessary to have a large sample of rawinsonde data evenly distributed over the region, as well as a set of very strict classification criteria. However, there is always a trade-off between the two for a given data sample within specific time periods. A set of more strict criteria generally gives less individual cases to be included in the composite and, hence, less rawinsonde data. This is why so much time in the past few years has been spent on expanding the western North Pacific rawinsonde data set from the former total of ten years (1961-1970) to the current 21 years (1957-1977) of data. In addition, many Taiwan data and Mainland China coastal data have been included in the new data set (see Fig. 1). This increase in total rawinsonde data allows a more strict composite criteria and better results. Earlier studies - e.g., Frank, 1976; Zehr, 1976; McBride, 1979 - used only 10 years of data.

2.1 Rawinsonde Composite Technique

The rawinsonde compositing is performed on a 15° latitude radius cylindrical grid extending from the surface to 50 mb, a total of 23 vertical levels. The grid is positioned with the weather system center at the grid center. The grid spacing is 2^O latitude in radius and 45° in azimuth, as shown in Fig. 2. All observations that fall into a specific grid box (an example is shown as the shaded area in Fig. 2) are averaged together to give a mean value at that grid point (shown as dot in Fig. 2). Therefore, a parameter value described as being at 6° radius is actually the composite average of all soundings falling between 5° latitude and 7° latitude radius. Inside 7° radius, the composite results are available at 1^O radial spacing, i.e., all data are averaged between $0-1^O$, $1-2^O$, $2-3^O$, etc. However, the results at this

Vertical Levels

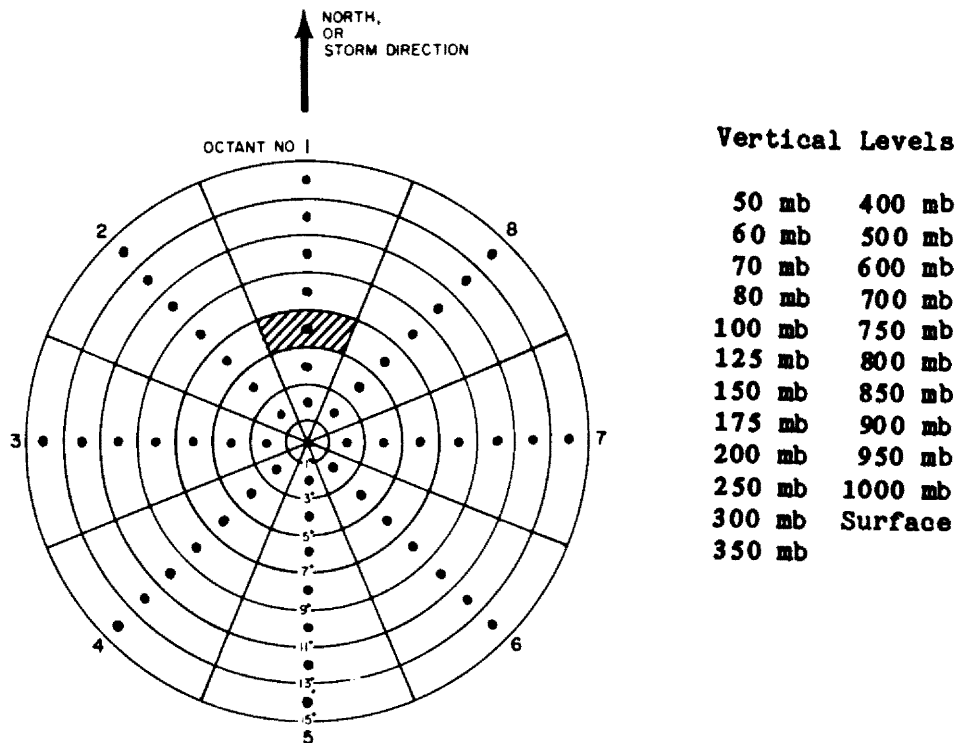|	
50 mb	400 mb
60 mb	500 mb
70 mb	600 mb
80 mb	700 mb
100 mb	750 mb
125 mb	800 mb
150 mb	850 mb
175 mb	900 mb
200 mb	950 mb
250 mb	1000 mb
300 mb	Surface
350 mb	

Fig. 2. Cylindrical grid and vertical levels for rawinsonde composites. Arrow points toward north. The radial grid spacing is 2° latitude. Each grid point value represents the average of all soundings in the grid box. A grid box is shown as the shaded area.

finer resolution tend to be noiser and generally are not used unless the data sample is very large and the results are smooth.

The meteorological parameters being composited together include dynamical and thermodynamical parameters. These are wind components, height (or surface pressure), temperature, mixing ratio and other parameters derived from these basic parameters (e.g., total wind speed, potential temperature, etc.). For the wind components, two coordinates are used during compositing: the natural or fixed coordinate (NAT) and the motion or Lagrangian coordinate (MOT). (Note that all thermodynamic parameters are in the NAT coordinate.) In the MOT system, the system motion is subtracted from all wind vectors before compositing; in other words, the wind vector in the MOT coordinate is with respect to the moving system center; or

$$\vec{V}_{MOT} = \vec{V}_{NAT} - \vec{C};$$

where ($\vec{C}$) is the system motion vector. (This notation is used throughout this paper.)

To assure the conservation of mass, the radial wind is artificially balanced from the surface to 100 mb (assumed tropopause) at any radius. The vertical mass- (or pressure) weighted average of the unbalanced radial wind is used as the correction factor. The vertical motion is calculated from the balanced radial wind to assure zero vertical motion at the surface and 100 mb. (Note that the observed tropopause is generally around 110–120 mb in the tropical atmosphere). The mass balance is a very important correction to make, especially in the budget analysis. For a budget analysis, many radial flux terms, e.g., $V_r V_t$, $V_r f$, $V_r S$, and $V_r q$, etc., are calculated from each individual sounding

before compositing, and the radial wind component has been mass-balanced during the calculation.

2.2 Background Composite

In order to understand the general circulation patterns and atmospheric conditions in the region where tropical cyclones may form, a "background" composite is made. A set of selected positions, at dates and times similar to those of the tropical cyclone, appears suitable for making this background composite run. To simplify this selection process, all tropical cyclone positions used in the genesis composites are taken for one year before and one year after the original year. This forms the position set of the background composite. The date, time and the cyclone motion remain the same. This background composite thus contains the positions (which may be clear, cloudy or within a tropical cyclone) that follow the seasonal and geographic distribution patterns of tropical cyclones. These composite results will be referred to as "background" or "mean tropical atmosphere."

Figure 3 shows that the average position of the background composite (shown as the star) is very close to the center of the other composite positions. Because of the way the background composite is chosen, the seasonal and spatial distributions are nearly identical to the other genesis composites. (Appendix A contains a detailed list of the average characteristics for all rawinsonde composites.)

To obtain a mean tropical atmospheric sounding, all soundings that fall inside 5° radius in the background composite are averaged. The values of height, temperature, and mixing ratio (and relative humidity) are tabulated in Table 2. It can be easily shown that this mean
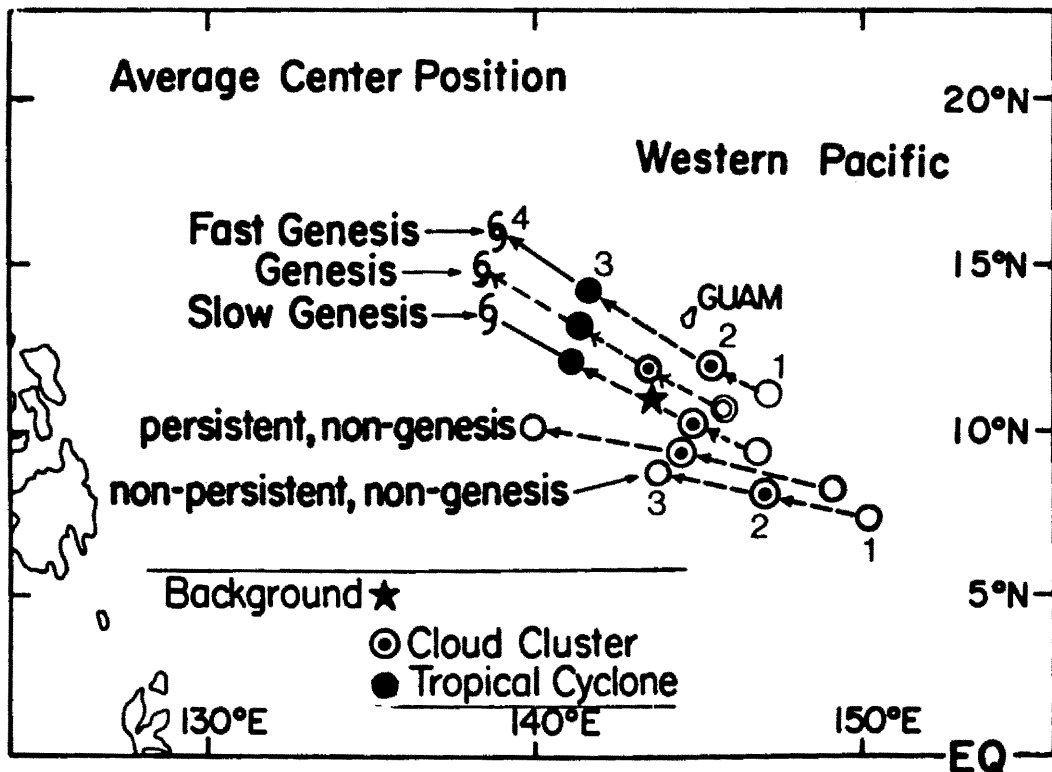
Fig. 3. The average positions of the rawinsonde composite data sets.
Five different categories and the background composite are all
shown.

tropical atmosphere is statically stable but convectively or

conditionally unstable.

Figure 4 shows the 850 mb and 200 mb circulation pattern in NAT and

MOT coordinates for the background composite. In the NAT coordinate

(left panel), flow is mostly easterly at 850 mb (or trade wind). A

subtropical high is located to the north-northeastern section, while a

convergent zone is located to the south-southeast. At 200 mb, a

subtropical ridge lies across the whole domain to the north. In the MOT

coordinate, the pattern has changed substantially, especially in the

lower levels where wind speed is weaker (about the same magnitude as the

cyclone moving speed). A trough now lies across the whole domain at 850

mb. At 200 mb, the ridge is weaker compared to that of the NAT

TABLE 2

Height, temperature, and mixing ratio (relative humidity) for the mean tropical atmosphere.

(Average of All Soundings Inside 5° of Background Composite)

|	Height (m)	Temperature (°C)	Mixing Ratio (g kg^{-1}) and Relative humidity (%)
50 mb	20680	-62.7	0
60 mb	19566	-66.7	0
70 mb	18643	-70.9	0
80 mb	17861	-75.3	0
100 mb	16583	-79.2	0
125 mb	15307	-75.2	0
150 mb	14230	-67.9	0
175 mb	13287	-60.5	0
200 mb	12441	-53.4	0
250 mb	10964	-41.0	0.1(32)
300 mb	9696	-30.7	0.3(33)
350 mb	9585	-22.4	0.7(36)
400 mb	7587	-15.7	1.1(40)
500 mb	5869	-5.4	2.5(49)
600 mb	4414	2.8	4.2(55)
700 mb	3148	9.9	6.3(58)
750 mb	2570	12.9	7.8(63)
800 mb	2025	15.5	9.6(69)
850 mb	1507	18.0	11.5(74)
900 mb	1014	20.7	13.6(78)
950 mb	540	23.6	16.1(82)
1000 mb	88	26.7	18.3(80)
Surface	1004.1 (mb)	27.1	19.0(83)
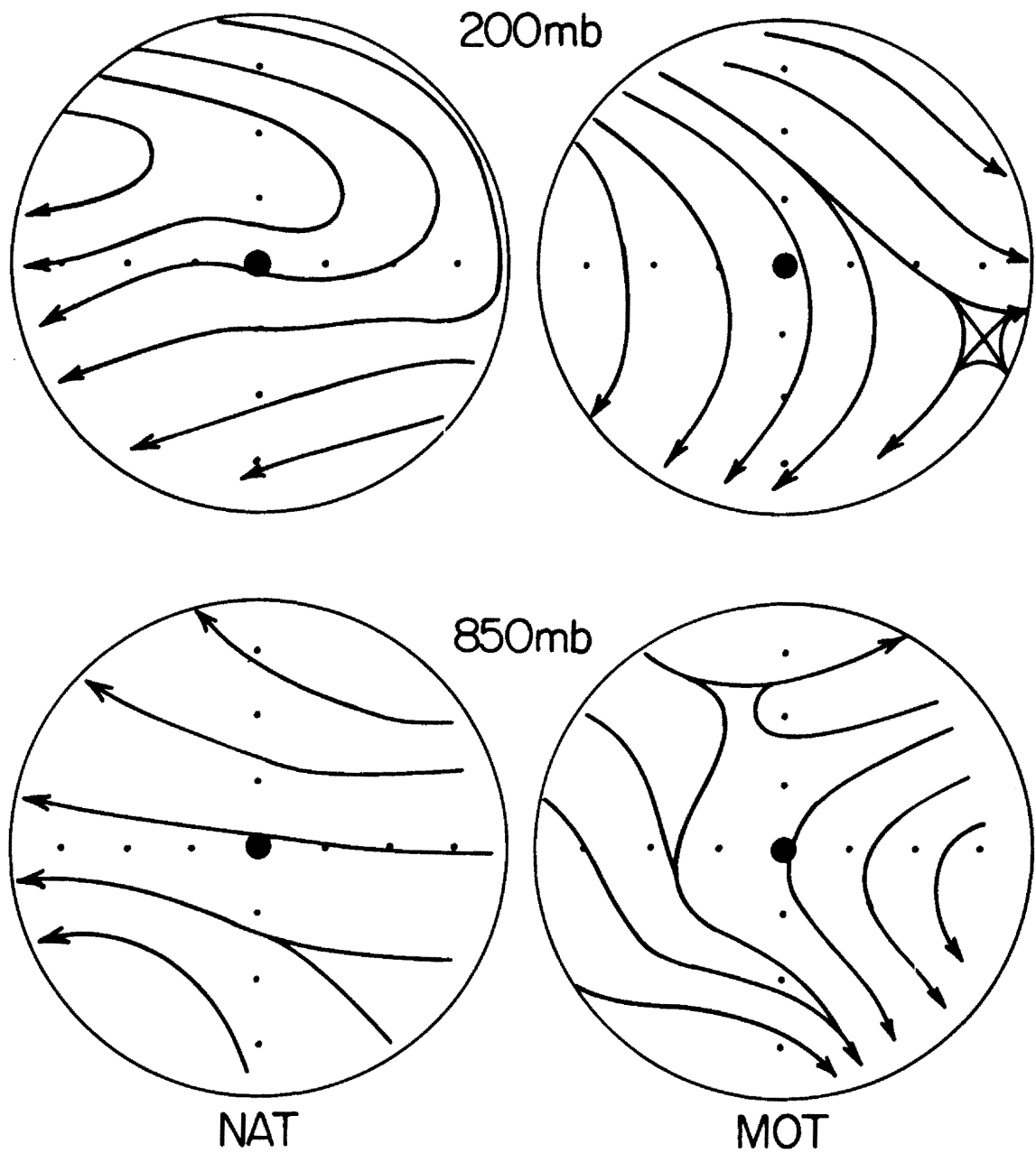
Fig. 4. Streamline patterns of the background composite at 200 mb (top)
and 850 mb (bottom) in the natural (NAT, left) and motion (MOT,
right) coordinates over 15° radial domain. The radial grid
spacing shown is 4° latitude.

coordinate. These apparent circulation pattern differences between NAT and MOT coordinates have to be kept in mind when examining the circulation pattern in MOT coordinates. Throughout the rest of this paper, all circulation patterns presented are in the MOT coordinate – which is a more appropriate coordinate choice because the systems are moving at different speeds and directions and these motion effects should be subtracted out from each system.

The mean radial wind and tangential wind at 6° radius (or mean divergence (D) and vorticity (ζ_r) inside 6° radius) and the $0-6^{\circ}$ mean vertical motion are shown in Fig. 5. Weak convergence is observed from the surface up to 500 mb, but the divergence concentrates at levels between 100 to 300 mb. A weak upward motion, maximum of 26 mb d^{-1} at 300 mb, is present throughout the whole troposphere. Since the tropical atmosphere is very stable, this weak mean upward motion must be the net result of cumulus convection occurring over a smaller space scale. The mean tangential wind profile shows cyclonic circulation at lower levels where convergence is present and anticyclonic circulation at upper levels where divergence is present. The relative vorticity is about an order of magnitude smaller than the earth vorticity. The magnitude of the divergence is about 40-50% of that of the relative vorticity. Note that $f = 29 \times 10^{-6}$ s^{-1} at 11.5°N (average latitude of the background composite center), $\zeta_r \sim 4 \times 10^{-6}$ s^{-1} and $D \sim 2 \times 10^{-6}$ s^{-1}.

The background composite results presented above form a basis for comparison purposes. It has to be noted that these circulation patterns and profiles do not represent exactly the day-to-day real atmosphere, but rather the average conditions over the same periods of time and

geographical locations as the pre-cyclone cloud clusters which will be
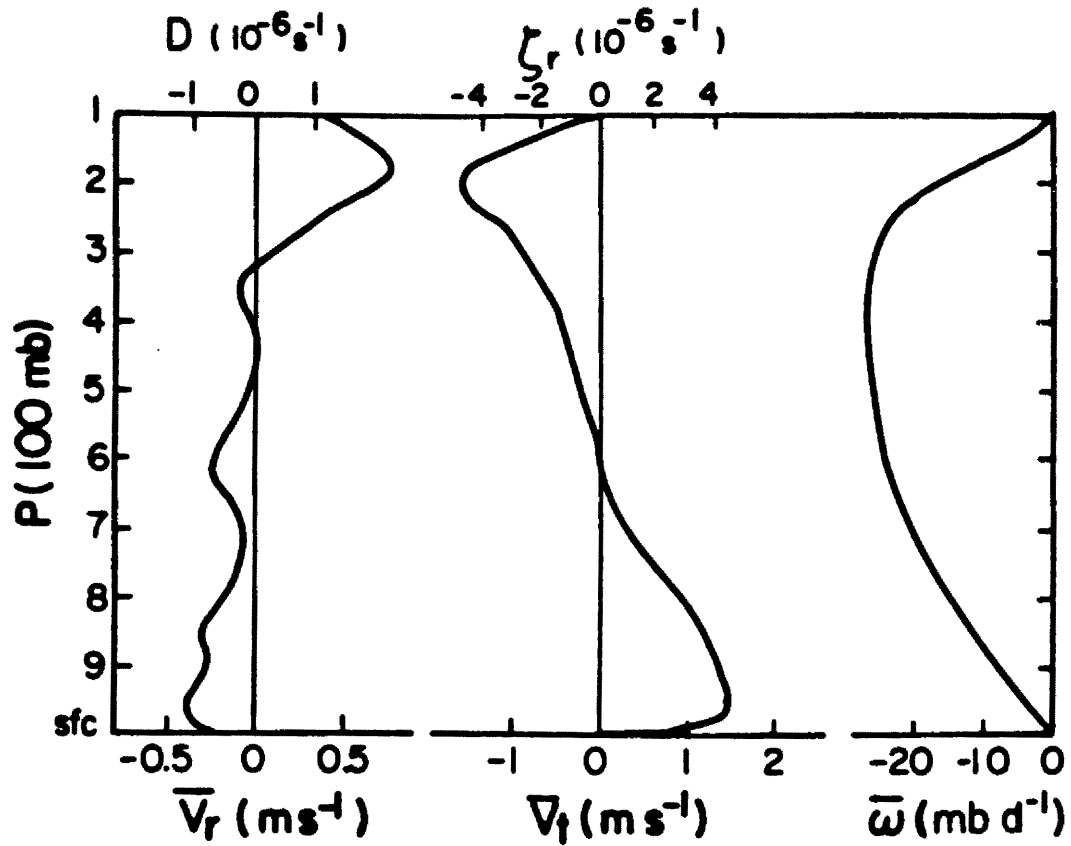discussed.

Fig. 5. Mean radial wind and tangential wind profiles at 6° radius (or
0-6° mean divergence and vorticity) and 0-6° mean vertical
motion for the background composite.

3. EVOLUTION OF NON-GENESIS CLOUD CLUSTERS

There have been only a few rawinsonde composite studies (Zehr,
1976; Erickson, 1977; McBride, 1979) of those tropical cloud clusters
which do not develop into tropical cyclones (non-genesis cloud
clusters). While these studies indicated the structural differences
between non-genesis and genesis cloud clusters they contained no
significant discussion about how those differences can come about. To
understand how these differences can occur, it is necessary to study the
evolution of both types of cloud clusters. This chapter will discuss
the non-genesis cloud cluster composites and the environmental
circulation pattern changes as cloud clusters form and dissipate. The
evolution of the genesis cloud cluster will be studied in the next
chapter and compared to the non-genesis cases.

3.1 Selection of the Non-genesis Cloud Clusters

The NOAA sun-synchronous near-polar orbiting satellite mosaics
(1967-1977) were used to select the positions of the non-genesis cloud
clusters. These satellite mosaics are available once a day for visible
images and twice a day for IR. The visible images are available at 09LT
(local-time daylight) and IR at 09LT and 21LT. These are about the 00Z
and 12Z in the western North Pacific region. The selection procedure
used only the visible data except for some cases when IR could be used
to help determine the continuity of the system. These satellite
pictures are published by NOAA in book form. The quality of these
pictures are generally good and suitable for the current purpose.

Unfortunately, the earlier years (1967-1972) have quite a few missing pictures and some pictures are of poor quality. (A few months of data were not available at the time of selection, but this does not affect the overall purpose of this research.)

There are some important criteria used in selecting the non-genesis cloud clusters. To be selected, these cloud clusters have to be:

a. Located far enough from an existing tropical cyclone and be easily separated from the cloud pattern associated with the cyclone;

b. Not mixed with those cloud clusters which later develop into tropical cyclones;

c. Large enough in size (comparable to pre-cyclone cloud clusters). Some might be smaller (still at least 3-4° in diameter) but with very good convection;

d. Not elongated in shape;

f. Located between 5-17.5°N and 120-165°E (some might move into or outside the domain at early or later time periods and still be selected). These criteria are used to make sure that only well-defined, prominent non-genesis cloud clusters are selected.

The greatest difficulty in selection was that the continuity of some cloud clusters was very hard to determine. For instance, in the situation where one cloud cluster was observed at a certain position on the first day and one cloud cluster was observed at a position a few degrees west of this position on the second day, it was possible that the cloud cluster either moved westward a few degrees longitude in 24 hours or that the original cloud cluster dissipated and a new one formed to its west in 24 hours. Since there was only one VIS image every day (the IR image sometimes is helpful in this matter), the decision

sometimes might be quite subjective — such as the case from 7 to 14 June 1976, shown as the white circles in Fig. 6. However, all possible information was used to differentiate these two situations. Factors taken into consideration were: how far apart were the two cloud clusters; how similar were their sizes and shapes and was there any indication that a cloud cluster was forming (some small cumulus) or dissipating (cirrus remainder, etc.)?

Another difficulty was determining the center of the cloud clusters. This was easily overcome by the following two procedures:

1. If a circulation center can be determined from the satellite cloud pattern, this center is used as the cloud cluster center;

2. If no circulation center can be determined, the center of the convection is used. This is similar to the procedure used by Arnold, 1977. For the monsoon surge-type cloud cluster, the surface center is generally located at the northern edge of the cloud. Figure 6 shows some examples of the selected non-genesis cloud clusters. The centers of the cloud clusters are shown as open circles or stars for persistent and non-persistent cases, respectively (see page 29 for definition).

Eleven years (1967-1977) of NOAA satellite images, June-November, have been looked at to select the non-genesis cloud clusters. A great deal of time was spent in choosing cases, and some years of data were looked over twice in order to reduce any possible inaccuracy. December through May were not considered because they had only a few tropical cyclones (only 15% occurred during these 6 months). In this 11-year period, 660 non-developing cloud clusters were selected. Among them, 332 cases could be located at only one 24-hour time period, 328 cases could be located at two time periods or more. Table 3 lists the number
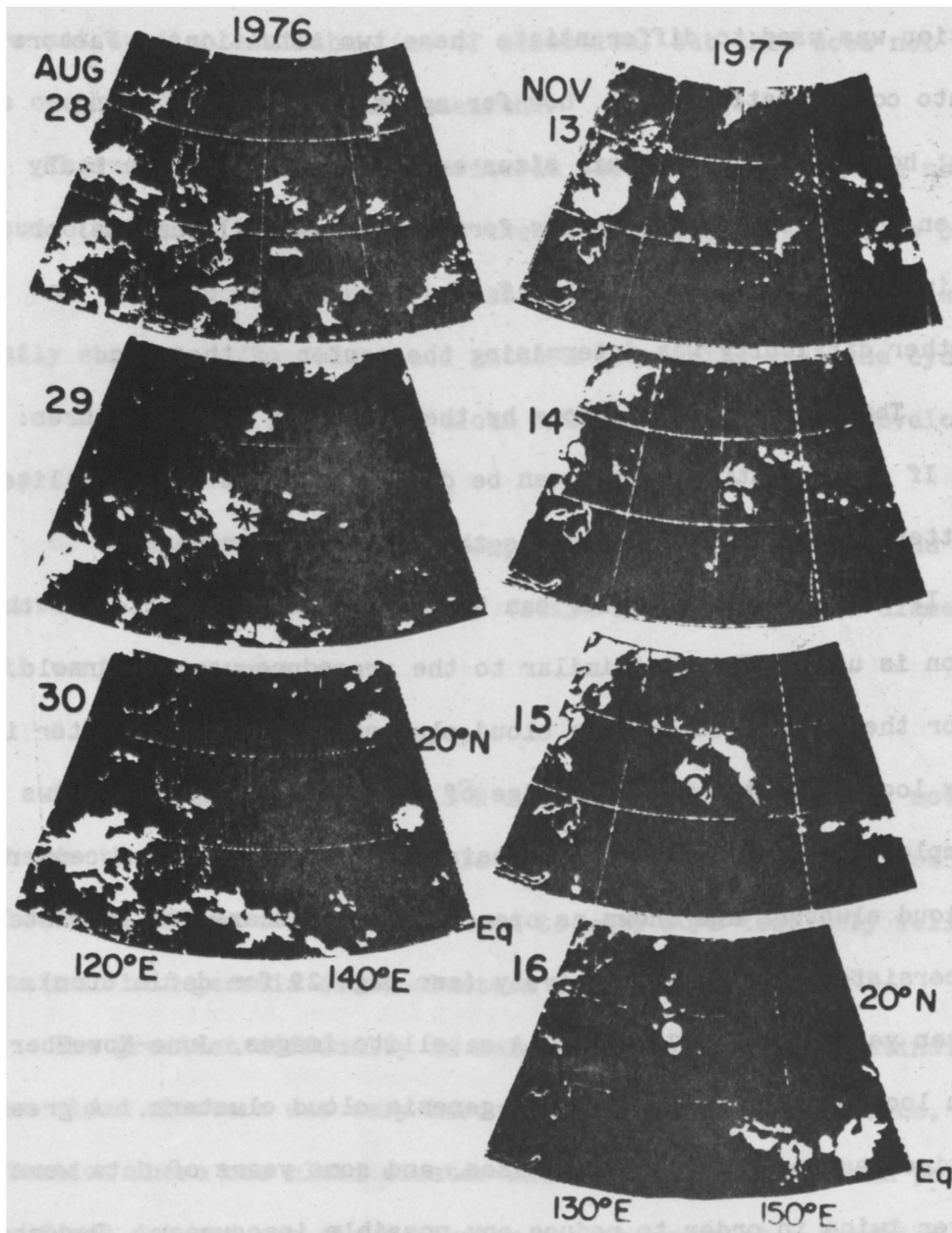
Fig. 6.   Examples of the non-genesis cloud clusters used in the
          composite. Centers of the system are shown by the circles
          (persistent) and stars (non-persistent).
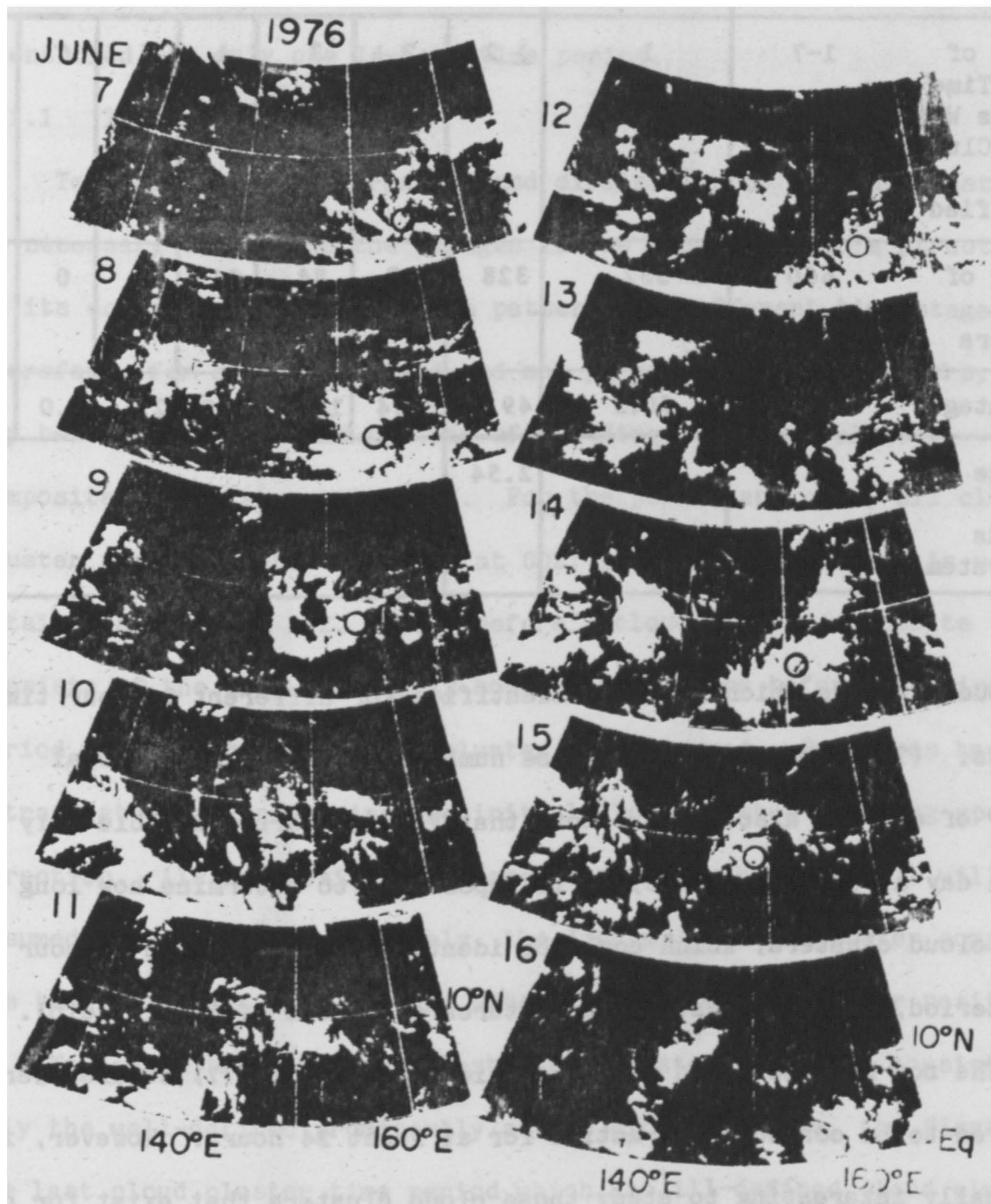
Fig. 6. Continued.

TABLE 3

Statistics of the Non-Genesis Cloud Clusters

	Total	Non Persistent	Persistent						
			≥ 2	2	3	4	5	6	7
Number of 24-hr Time Periods Where Cloud Clusters Can Be Identified	1-7	1							
Number of Cloud Clusters	660	332	328	207	84	21	14	0	2
Percentage	100	50.3	49.7	31.4	12.7	3.2	2.1	0.0	0.3
Average Time Periods Per System	1.77	1.0	2.54						

of cloud clusters which could be identified for different 24-hour time periods. (The percentages for these numbers relative to the total number of 660 are also shown.) Note that VIS data are available only once a day at 00Z, therefore, it is impossible to determine how long these cloud clusters, which could be identified for only one 24-hour time period, actually lasted (IR pictures are often of little help).

The non-genesis cloud clusters which Erickson (1977) studied were required to be convectively active for at least 24 hours. However, it is equally interesting to study those cloud clusters that exist for only a short time period. This study, therefore, classifies all the non-genesis cloud clusters into two groups:

1. Persistent non-genesis cloud cluster (PN) - these can be identified for at least two 24-hour time periods (similar to Erickson's non-genesis composite); and

2. Non-persistent, non-genesis cloud clusters (NN)- these can be identified for only one 24-hour time period.

3.1.1   Time Stages

To understand the formation and dissipation of a cloud cluster, it is necessary to examine the changes in the cloud cluster's structure and in its environmental circulation patterns at different time stages. Therefore, for both persistent and non-persistent cloud clusters, one day before (Stage 1) and one day after (Stage 3) cloud cluster composites are also constructed. For the persistent case, all cloud cluster positions are available at 00Z; linear interpolation is used to obtain positions at 12Z. The ''before'' cloud cluster composite consists of the time periods 12 hours and 24 hours before the first time period when a prominent cloud cluster was observed. Positions are extrapolated backward using the initial cloud cluster's moving speed and direction. (If the position extrapolated is south of $4^\circ N$, it will be assumed to be at $4^\circ N$.) Similarly, the ''after'' cloud cluster composites are taken 12 hours and 24 hours after the last cloud cluster position.

To assure that the persistent cloud cluster composite consists of only the well-defined prominently active cloud clusters, the first or the last cloud cluster time period which has ill-defined cloud clusters were included in the before (Stage 1) or the after (Stage 3) cloud cluster composite rather than in the cloud cluster composite (Stage 2). Under this condition, the before or the after cloud cluster composite includes three 12-hour time periods. On the other hand, the before and

the after cloud cluster composites are mostly cloud free but are in their formation or dissipation tendency. Note that due to the time resolution, cloud clusters might still exist at the 12Z time (which is included in the before or the after cloud cluster composite) previous to or following the cloud cluster composite.

It is more difficult to determine the before and the after position of the non-persistent cloud cluster because cloud clusters were observed at only one 24-hour time period. However, persistence is generally a good approximation in a tropical region. The mean motion of the persistent cloud cluster (4.0 m s^{-1} toward 283° direction) was applied to the non-persistent cloud clusters to determine the positions at other time periods. In some cases it was more appropriate to assume no motion for those cloud clusters where the original cloud cluster dissipated and a new one formed to its west. To eliminate the possible bias between 00Z and 12Z data, non-persistent cloud clusters consist of the observed 00Z time period and the time period 12 hours before. The before and the after cloud cluster stages are taken in a way similar to that of the persistent case. The average positions for these composites have been shown in Fig. 3 and the average characteristics are summarized in Appendix A. Two of the persistent cloud clusters merged into mid-latitude frontal systems; therefore, no after stage is considered for these two cases.

3.2 Evolution of Thermodynamic Fields

The height, temperature and moisture fields generally have large variations in latitude. Therefore, they are often shown as deviations from east-west 9-15° averages in order to eliminate latitudinal dependence. Values at 0-2° radius are used to represent the inner-core

structure of the system.

3.2.1   Height Field

Table 4 shows height field deviations at 950 mb instead of at the surface pressure which often encounters a degree of noise due to the sea-level pressure corrections of higher elevations of some stations. The results indicate a weak mean height gradient with a value of about 10 meters or 1 mb per 10° latitude radius. This pressure gradient is primarily due to the higher height value at the north-northeast quadrant where the subtropical high is located (as shown in Fig. 7 for both cases at Stage 2). Figure 7 also indicates the lower height field for the persistent cloud cluster (at Stage 2) is spread over a much broader region than for the non-persistent case. No apparent change is found for the overall pattern (as shown in Fig. 7) at the three time stages except for the non-persistent case at Stage 3. At that time, the lower height field near the center, which was present at the two previous stages, has disappeared (figure not shown).

As discussed before, prominent cloud clusters existed only at Stage 2; Stage 1 consisted of cloud free or cloud formation time periods for each individual cloud cluster case. The presence of a weak inward pressure gradient at Stage 1 (shown in Table 4) for both cases indicates that the cloud clusters generally form in an environment with a lower pressure field. As will be shown later, there is a large-scale low-level convergence associated with this inward pressure gradient at Stage 1 which might be an important feature in the cloud cluster's formation.

TABLE 4

Mean 950 mb height deviations (m) from 9-15°, east-west average at different radial belts for non-genesis cloud cluster composites and the background.

Radial Belt (lat.)	0-1	1-3	3-5	5-7	7-9	9-11	11-13	13-15
Background (BK)	8.3	1.6	1.9	2.8	1.0	2.4	5.1	7.6

Non-persistent, non-genesis cloud cluster (NN)

Before (Stage 1)	-2.5	-3.1	-0.8	0.8	2.4	4.1	9.5	9.0
During (Stage 2)	-5.9	-2.4	-0.3	1.9	2.2	5.9	6.1	9.4
After (Stage 3)	-0.9	0.2	0.1	3.2	2.6	5.6	6.8	-0.1

Persistent, non-genesis cloud cluster (PN)

Before (Stage 1)	-7.4	-2.8	-0.5	1.2	1.9	7.1	10.6	12.3
During (Stage 2)	-5.9	-1.3	-1.6	1.3	1.2	3.0	7.2	6.0
After (Stage 3)	-5.5	-0.7	0.8	1.3	2.3	4.7	2.3	2.9

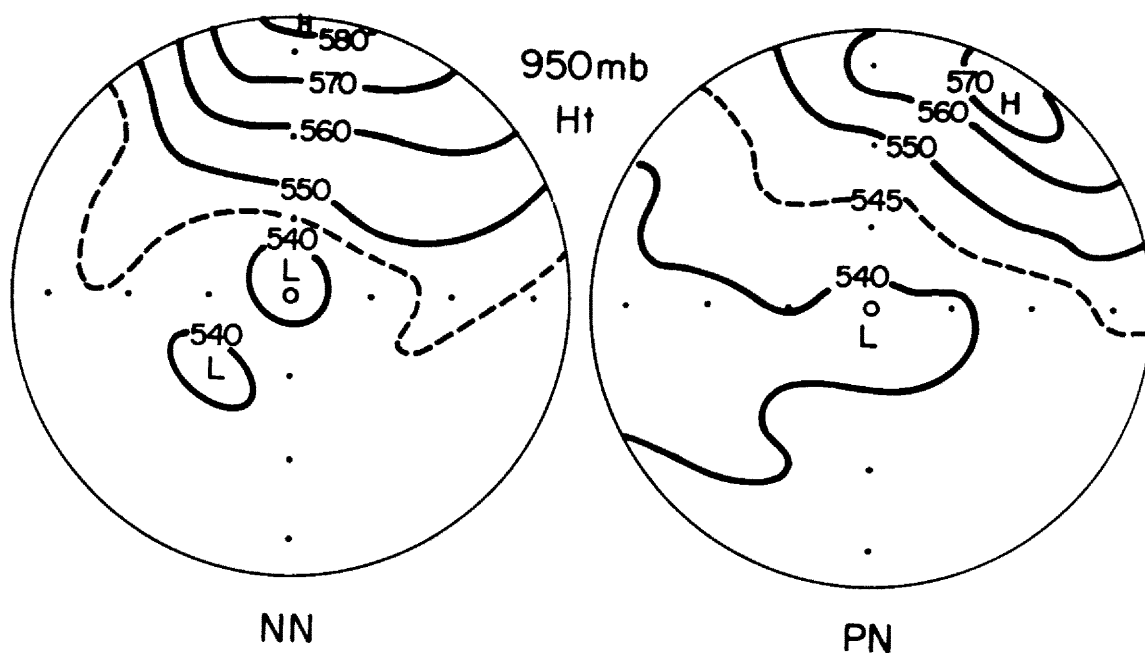NN   PN

Fig. 7. The 950 mb height field (m) for both persistent (right) and non-persistent (left) cloud clusters at Stage 2. The radial distance between dots is 4° latitude.

3.2.2 Temperature Field

The vertical profiles of the $0-2^\circ$ temperature deviation from the east and west $9-15^\circ$ average for both persistent (PN) and non-persistent (NN) cases at Stages 1, 2 and 3 are shown in Fig. 8. The background profile (BK) is also shown. Remarkable similarities exist between the two cases except above 100–150 mb. Before the formation of cloud clusters, the temperature deviation is generally small in both cases. Their vertical profiles are similar to the background profile except in the upper troposphere where a slight warming occurs.

At the prominent cloud cluster stage (Stage 2), the upper tropospheric warming increases but its magnitude is still small or about
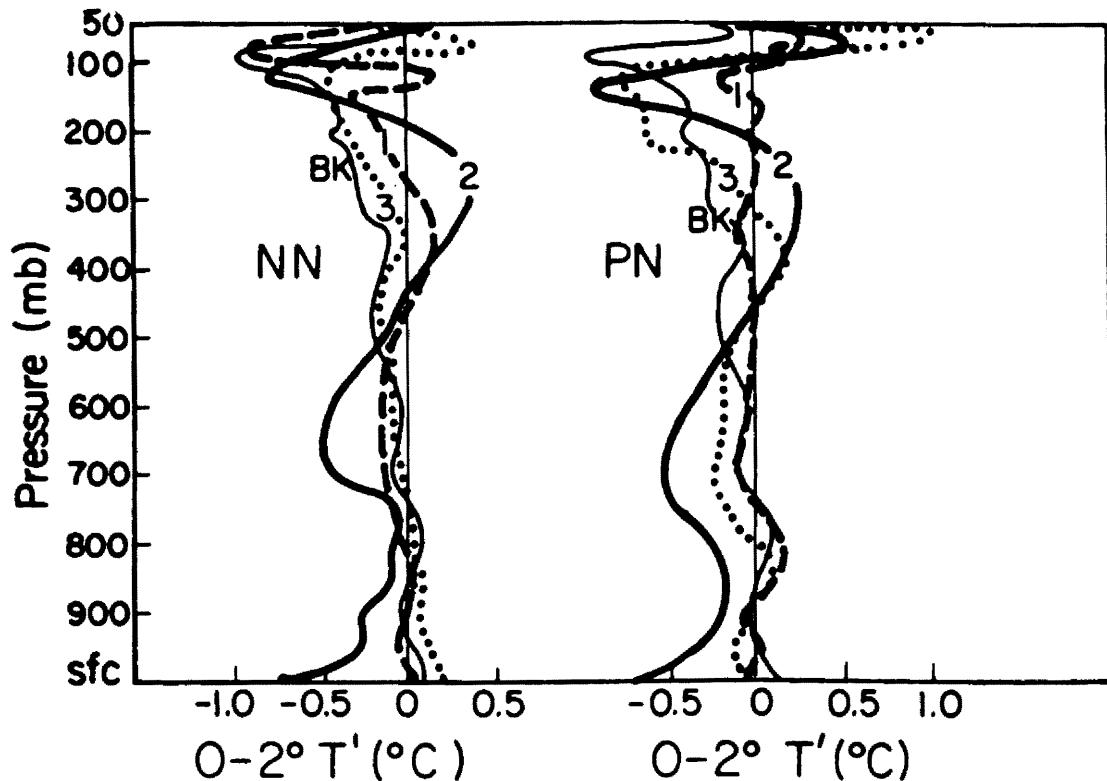
Fig. 8. The $0-2^\circ$ temperature deviation from the east-west $9-15^\circ$ average for both persistent (right) and non-persistent (left) nongenesis cloud clusters at Stage 1 (before), Stage 2 (during) and Stage 3 (after). The background profile (BK) is also shown.

0.3-0.4^{O}C. A cooling effect is found below 500 mb with maximum cooling (-0.5^{O}C) at 600-750 mb and near the surface. Entrainment and re-evaporation cooling are likely the cause of this low-level cooling. The cold core at 125 mb (near tropopause) may be due to the cumulus cloud overshooting cooling. The persistent and non-persistent cloud clusters have similar temperature deviation profiles which suggest that the duration of a cloud cluster does not necessarily greatly modulate its structure. Surprisingly, the profile of the after non-persistent cloud cluster (Stage 3 of NN) is almost the same as that of the background. The after persistent cloud cluster profile (Stage 3 of PN) is also very similar to the background profile except that a slight residual warming and cooling exist at 300-500 mb and 500-800 mb, respectively. Such remarkable consistencies found in the temperature field for the two independently selected non-genesis cases adds credibility to the composite technique and these data sets.

3.2.3   Moisture Field

Figure 9 shows the precipitable water (PPW) at 0-2^O, 0-4°, and 4-7° for both non-genesis cases. The areas 0-4° and 4-7° at the Stage 2 cloud cluster stage are considered to be the convective region and the environment, respectively. The values at these three regions are also shown for the background composite. These results indicate that tropical cloud clusters form in a environment with a higher moisture content compared to the background. The precipitable water at 0-4° and 0-2^O increases from Stage 1 to Stage 2 and decreases at Stage 3. The precipitable water at Stage 3 is generally higher than that at Stage 1 inside 4° radius; in other words, cumulus convection tends to increase the moisture content of an air column. (Note that the precipitable
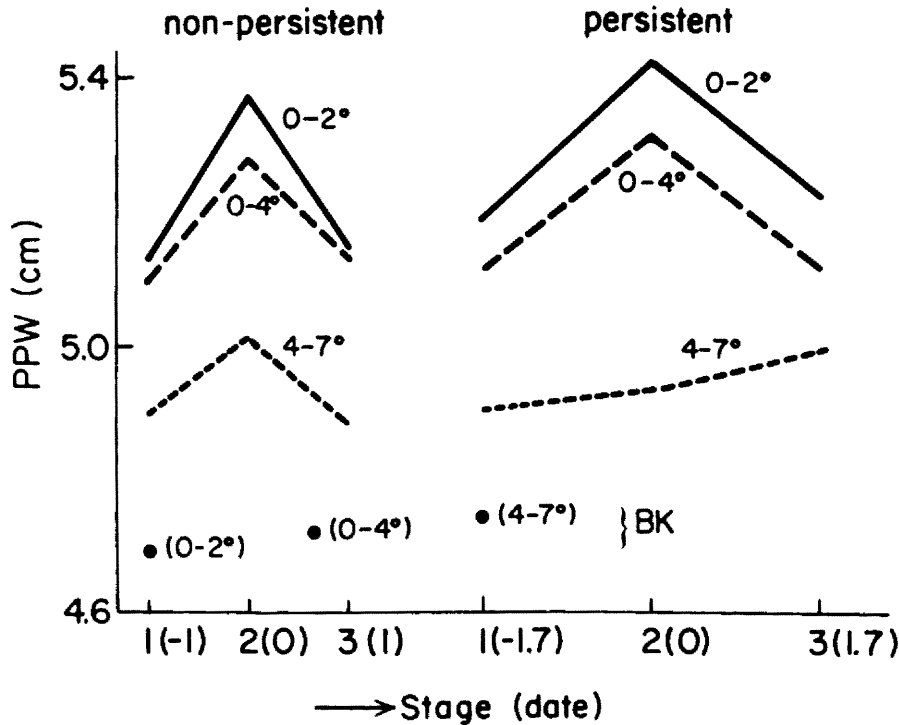
Fig. 9. The precipitable water (PPW) for both persistent (right) and non-persistent (left) cloud cluster composites at 0-2°, 0-4°, and 4-7° regions. Background (BK) values are also shown by the large dots.

water generally decreases with latitude as the cloud cluster moves poleward.) At the environmental region (4-7°), a slight drying is seen for the non-persistent case due to the strong subsidence at this stage (will be shown later), but a substantial moistening is evident for the persistent case after convection (Stage 3 minus Stage 1).

Although cumulus convection generally moistens the air column, the moistening occurs primarily above 700 mb, as shown in Fig. 10 (mixing ratio deviation from 9-15°, east-west average or q' at 0-2°). A strong similarity also exists between these two non-genesis cases. Below 700 mb a strong drying is observed after convection (Stage 3 minus Stage 1). A slight drying is also observed below 900 mb (boundary layer)
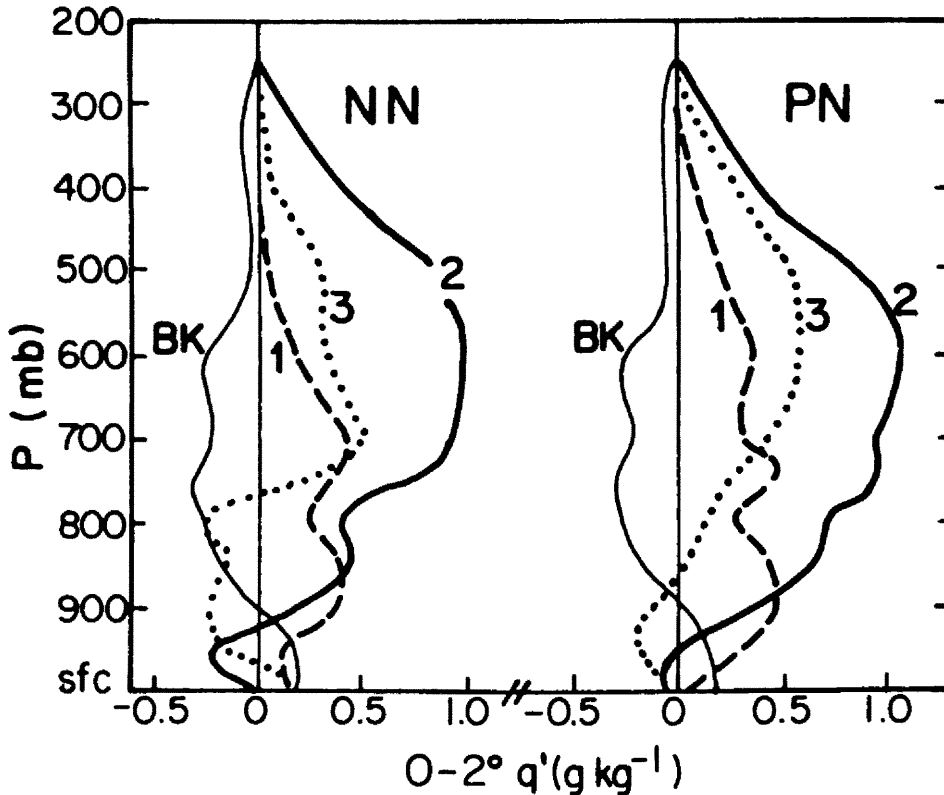
Fig. 10. The 0-2° mixing ratio deviation from the east-west 9-15° average for both persistent (right) and non-persistent (left) cloud clusters at three stages. The background (BK) profile is also shown. Shaded values show increase of moisture from Stage 1 to Stage 3.

during convection (or at Stage 2, the cloud cluster stage). This drying process is likely due to the convective downdrafts which are dry and cool when they reach the boundary layer. (Also refer to Fig. 8 for the cooling near the boundary layer.) In other words, the downdraft process brings middle-level low θ_e air and transports it into the boundary layer.

Figure 10 also indicates that cloud clusters form in a region with a higher moisture content compared to its surrounding environment. The q' profiles at Stage 1 for both cases show that the moist air (positive q') extends up to 400-500 mb. This higher moisture content is probably

the result of the horizontal convergence. As will be shown later in Fig. 14, a large-scale weak convergence exists at Stage 1 and extends as high as 400-500 mb at this stage. The moistening process due to previous cumulus convections also might have helped. The horizontal advection of moist air into this region is conducive to producing a higher moisture content, as well.

To illustrate the possible horizontal moisture advection processes, the relative humidity (RH) at 500 mb, 700 mb and 850 mb for both cases at these three stages are shown in Figs. 11 (non-persistent) and 12 (persistent). Also shown in the far left panel in Fig. 11 is the background composite. (A mid-value contour is shown by the heavy curve and moist regions are shaded.) As expected, the background composites have lower RH to the north-northeast quadrant where the subtropical high is located, and high RH to the south at all levels. At 850 mb, however, the RH variations are quite small. The RH field is even more uniform at 950 mb for all composites (figure not shown). Such uniform RH fields at 950 mb indicate a well mixed tropical boundary layer which does not significantly change with time.

At 500 mb, a slightly higher RH area is observed near the center region for both cases at Stage 1 (before cloud cluster stage). This high RH area expands and increases its magnitude at Stage 2 (formation of cloud cluster) and maintains its value at Stage 3 (dissipation of cloud cluster). At 700 mb, there is not much difference between Stage 1 and Stage 3 (before and after cloud cluster). A large area of high RH at Stage 2 correspondes to the activity of cumulus convection. These results indicate that the increase of the moisture content at these levels is mostly due to the cumulus activity.

Fig. 11. The relative humidity (RH) for the background (BK) and the non-persistent non-genesis composite at Stage 1 (before), Stage 2 (during) and Stage 3 (after) at 500 mb (top), 700 mb (middle) and 850 mb (bottom). The heavy curves are 50% (500 mb), 60% (700 mb) and 75% (850 mb) lines. Shaded areas are the moist regions. The dot shows the center of the system.
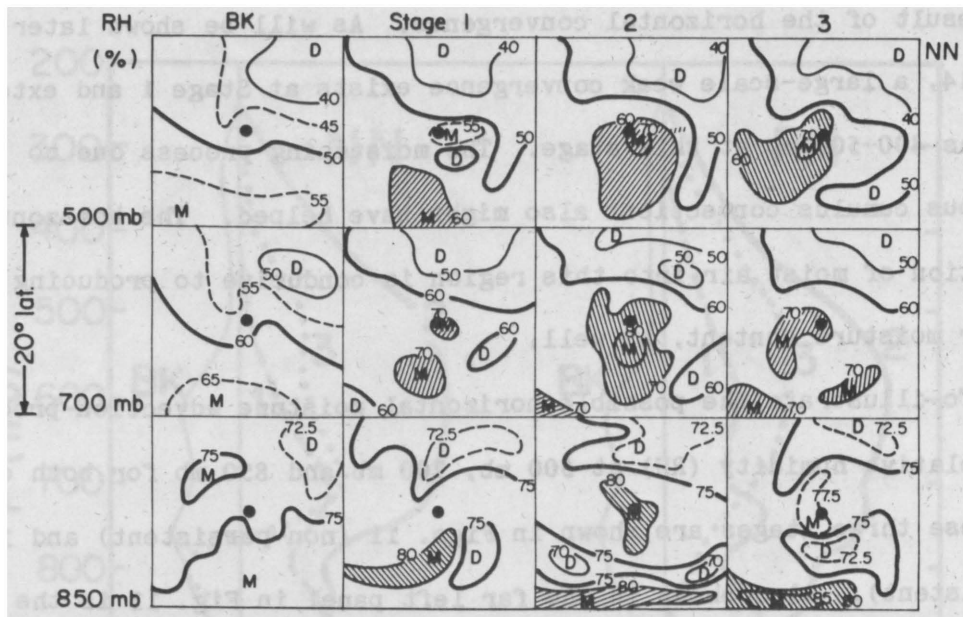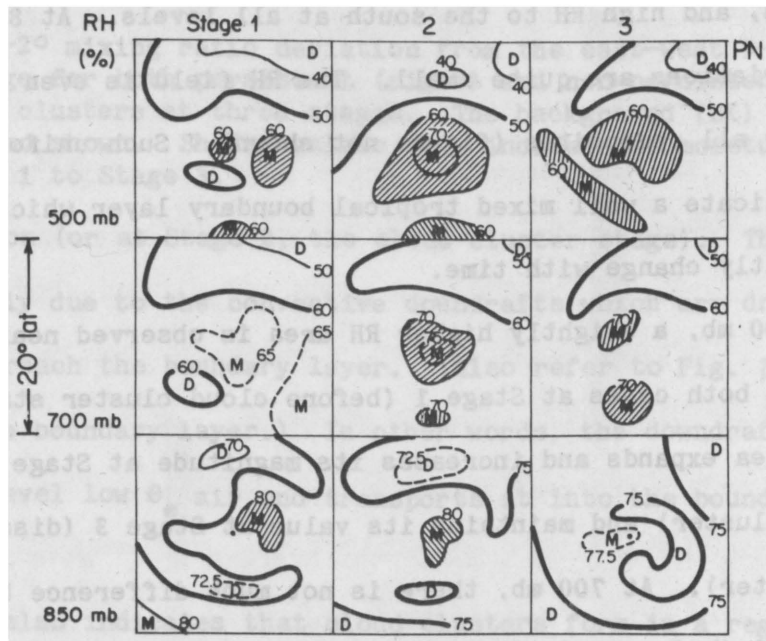

Fig. 12. The relative humidity (RH) for the background (BK) and the persistent non-genesis composite at Stage 1 (before), Stage 2 (during) and Stage 3 (after) at 500 mb (top), 700 mb (middle) and 850 mb (bottom). The heavy curves are 50% (500 mb), 60% (700 mb) and 75% (850 mb) lines. Shaded areas are the moist regions. The dot shows the center of the system.

At 850 mb, the horizontal moisture advection seems to play an observable role. As shown in the bottom panels of Figs. 11 and 12, moist air parcels were advected from the south (NN) and east (PN) to the west of the center from Stage 1 to Stage 3. However, the horizontal moisture convergence is still considered as the primary factor in giving the high moisture content at this level.

3.3 Evolution of Dynamic Fields

3.3.1 Tangential Wind and Vorticity

The mean tangential wind fields for both cases at 3 stages are shown in Fig. 13. The background field is also shown at the bottom left of the figure. For both cases throughout their three stages, a weak cyclonic circulation extends from the surface to 400-500 mb inside $8-10^{\circ}$ radius and there is an anticyclonic flow aloft. The magnitude of the maximum low-level cyclonic flow increases slightly and moves closer to the center from Stage 1 to Stage 2 and weakens quickly at Stage 3. The changes in the upper-level anticyclonic circulation are somewhat erratic. The strong upper anticyclonic circulation at Stage 3 is due to the strong mid-latitude westerlies. Compared to the background, both cloud clusters (at Stage 2) have deeper and stronger low-level cyclonic circulation but weaker upper-level anticyclonic circulation.

The vorticity fields for both cases at all three stages are very weak. Even at the cloud cluster stage (Stage 2), the maximum value of the mean relative vorticity inside 4° radius (at 850-900 mb) is very weak and on the order of 1.0×10^{-5} s^{-1}. The earth vorticity (f) however is 2.5×10^{-5} s^{-1} or 2.5 times as much as cloud cluster mean relative vorticity over $0-4^{\circ}$ radius.
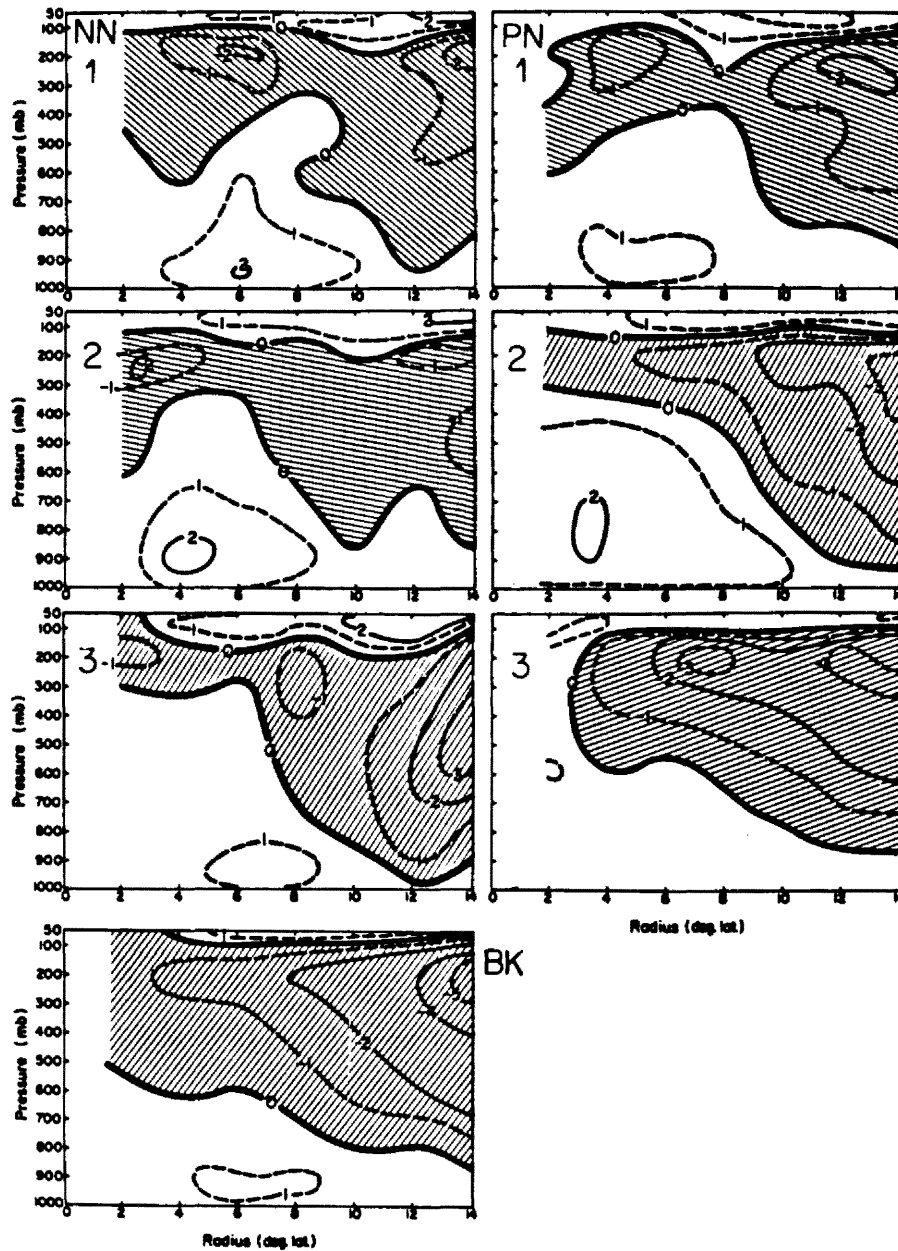
Fig. 13. The mean tangential wind ($\overline{V}_t$) for both persistent (right) and non-persistent (left) non-genesis cases at Stage 1 (before), Stage 2 (during) and Stage 3 (after). Background is shown at the bottom left.

3.3.2   Radial Wind, Divergence, and Vertical Motion

The mean radial wind profiles at 4° and 6° radii (or mean divergence at the 0-4° and 0-6° regions) for both cases are shown in Fig. 14 (in which profiles for Stages 1, 2, and 3 are labeled accordingly). The background profiles (labeled as BK) are shown as thinner curves. The mean vertical motion, derived from the kinematic method by assuming zero vertical motion at 100 mb and the surface, is shown in Fig. 15. Over 0-4° or 0-6° radius, in both the persistent and non-persistent cases, a large divergence exists at upper tropospheric levels (100-300 mb) at Stage 1, with maximum divergence located at about 175 mb. The low-level convergence extends from the surface to 500-400 mb, but strong convergence is concentrated below 800 mb. Note that these divergence/convergence fields are much stronger than those of the background composites. The upper level divergence and the middle-level convergence between 350 mb and 800 mb increase from Stage 1 to Stage 2. However, the low-level convergence near the surface decreases. The derived vertical motion profiles indicate an increase in upward motion at the middle-upper troposphere but a slight decrease at the layer below (also found by Tollerud and Esbensen, 1985).

At Stage 3 for the non-persistent case, the upward vertical motion at 0-4° radius decreases greatly to a magnitude similar to that of the background composite. Over the 0-6° radius, however, weak mean subsidence is present; in other words, there is strong subsidence at 4-6°. (A drying effect is associated with this subsidence as shown in Fig. 9.) This indicates that the non-persistent cloud cluster generally moves to the vicinity of a strong subsidence region, then dissipates quickly. For the persistent case at Stage 3, the vertical motion
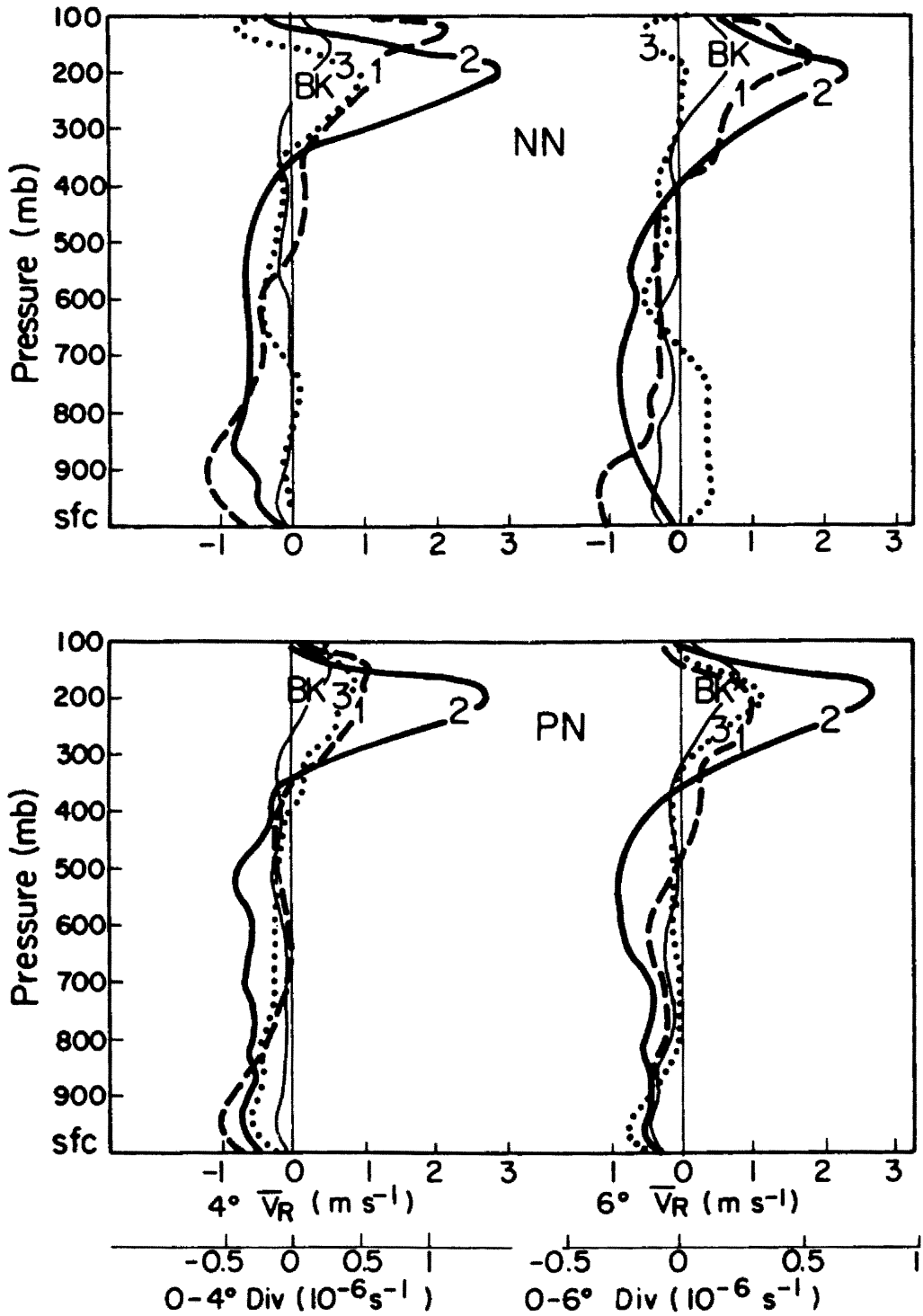
Fig. 14. The mean radial wind profiles for both persistent (bottom) and
non-persistent (top) non-genesis cloud clusters at 4° (left)
and 6° (right) radius (or 0-4° and 0-6° mean divergence) at
Stage 1 (before), Stage 2 (during) and Stage 3 (after). The
background profiles (BK) are shown in thinner curves.

Fig. 15. The 0-4° (left) and 0-6° (right) mean vertical motion ($\overline{\omega}$) for both persistent (bottom) and non-persistent (top) non-genesis cloud clusters at Stage 1 (before), Stage 2 (during) and Stage 3 (after). Background profiles (BK) are shown in thinner curves. The curve labeled 1.5 is for the composite between Stage 1 and Stage 2.
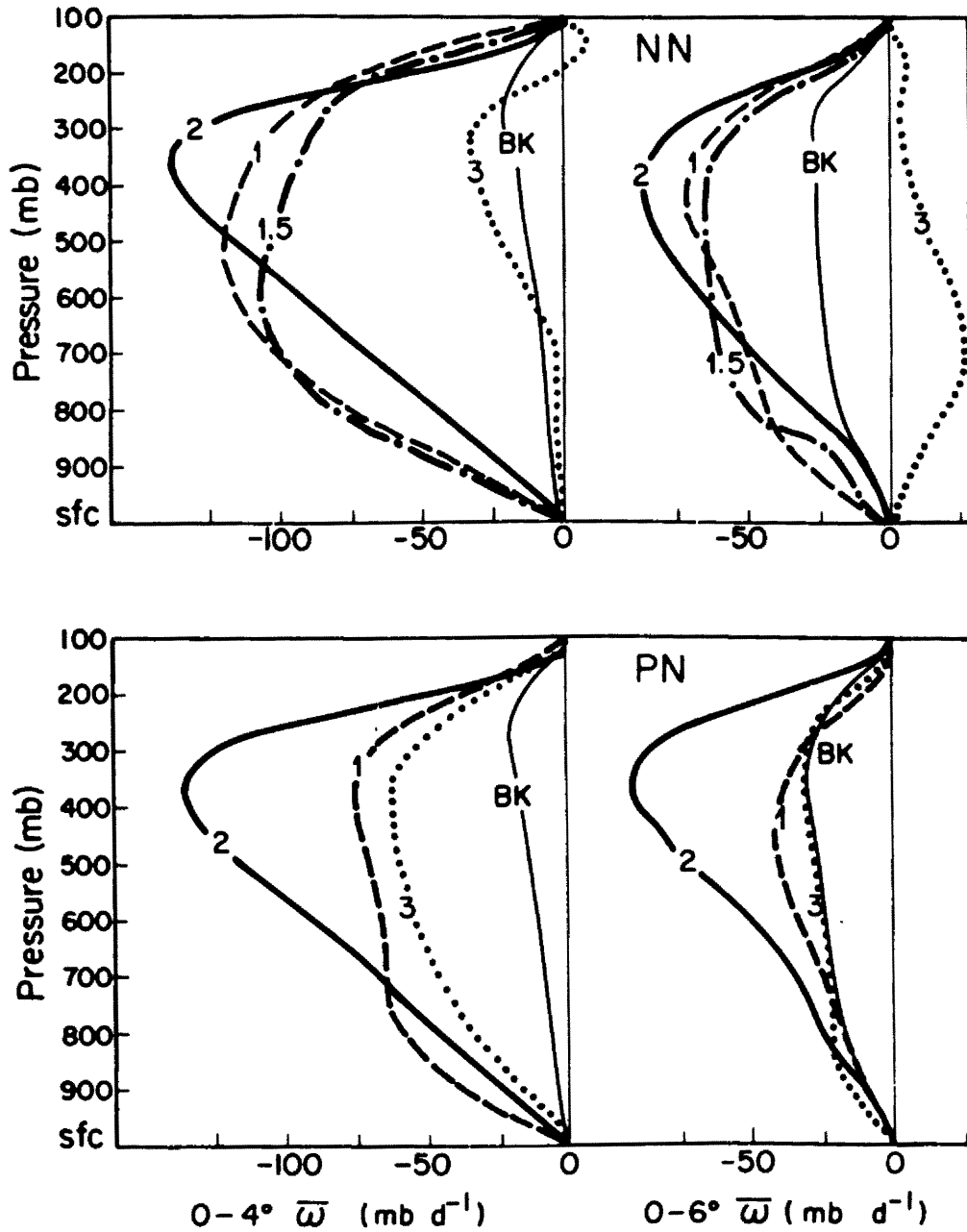
decreases to magnitudes slightly less than those of Stage 1, but still remains larger than those of the background.

The most remarkable feature in these vertical motion profiles is the much stronger than background upward motion at Stage 1 (or before the prominent cloud clusters were observed) due to the strong low-level convergence. The profiles at Stage 1 are also flatter than those at Stage 2, indicating that their convection is shallower at Stage 1 and deeper at Stage 2 (or cloud cluster stage). However, some deep convection already exists at Stage 1 because the mean upward motion extends up to the upper troposphere. In fact, both Stages 1 and 3 (especially for the persistent cases) also include a number of cases with active convection (at the 12Z time period right before and after Stage 2). This can explain why the upward motion at Stages 1 and 3 is much stronger than the background, especially at $0-4^{o}$. Despite this, there is still more upward vertical motion at Stage 1 than at Stage 3 – especially for the non-persistent case.

For the non-persistent case, the upward motion at Stage 1 is exceptionally strong, which leads the author to suspect that when extrapolated backward 24 hours and 36 hours (during the time stage classification), the positions of some pre-non-persistent cases might be within the convection region of other systems. Therefore, a supplementary composite was made. It contains two time periods 12 hours and 24 hours before when the non-persistent cloud clusters were observed (at 00Z). This composite falls exactly between Stage 1 and 2 and is labeled as Stage 1.5 in Fig. 15. The two time periods contained in this composite are similar to those in the Stage 1 composite of the persistent case, and the convection might still be present at the 12Z

time period for some cases. Results show a reduction (compared to Stage 1) in the upward vertical motion at middle levels and a slight increase at low levels. These results reinforce the concept that there is more low-level convergence and more shallow convection before the prominent cloud clusters form. This fits the previously discussed changes in the moisture profiles.

During the convection stage, the vertical motion profiles become very steep from the surface to 350 mb where the maximum vertical motion is located. Middle-level convergence increases significantly at this stage (Fig. 14). This middle-level mean convergence indicates a large amount of middle-level lower θ_e air is being entrained into the convective system. This likely helps create the meso-scale and/or convective scale downdrafts through re-evaporation cooling. This middle level convergence might also be a result of the freezing and ice-phase sublimation processes which provide extra buoyancy to the upward air parcel. The observed temperature and mixing ratio profiles (Figs. 8 and 10) supports this argument.

3.3.3 Vertical Wind Shear

As has been discussed by Gray (1968, 1975) and Zehr (1976), a strong vertical wind shear - or so-called blow-through ventilation - is unfavorable for tropical cyclone formation. These authors indicate that a strong vertical wind shear will prevent progressive accumulation of warm air in a deep vertical column, which is necessary to lower the surface pressure. (By the same argument, the strong vertical wind shear is not favorable for cloud cluster evolution either.) However, their studies did not look at progressive changes in vertical wind shear.

Thus, a more detailed discussion regarding the vertical wind shear evolution is presented here.

The vertical profiles of zonal and meridional winds (u and v) averaged over a 0-3° radius area in moving or MOT coordinates are shown in Fig. 16. Since system moving speed has been subtracted out, an easterly wind (negative u) thus means that environmental flow is blowing through the system from the east. Results show that before formation of the cloud cluster, the wind profiles are very similar for persistent and non-persistent cases. They are also similar to those of the background composite except below 800 mb. In the meridional direction, relative flow is mainly from the north with a larger magnitude in the upper troposphere. The meridional vertical wind shear is generally very weak except above 300 mb. The zonal wind profiles, on the other hand, show strong relative flow from the east in the middle troposphere and weaker relative flow from the west in the upper and lower troposphere. A strong easterly wind shear (east wind increases with height) is present below 500-600 mb and there is a westerly wind shear aloft.

The zonal and the vertical meridional wind shears do not show any significant change from Stage 1 to Stage 2. However, from Stage 2 to Stage 3 or during the dissipation of the cloud cluster the northerly shear (north wind increases with height) between 500 mb and 150 mb increases, especially for the persistent case, indicating a stronger shearing effect. The zonal vertical wind shear between 500 and 150 mb shows little change during this time period for the non-persistent case, but decreases greatly for the persistent case. In summary, the non-genesis cloud clusters occur under an environment with strong vertical
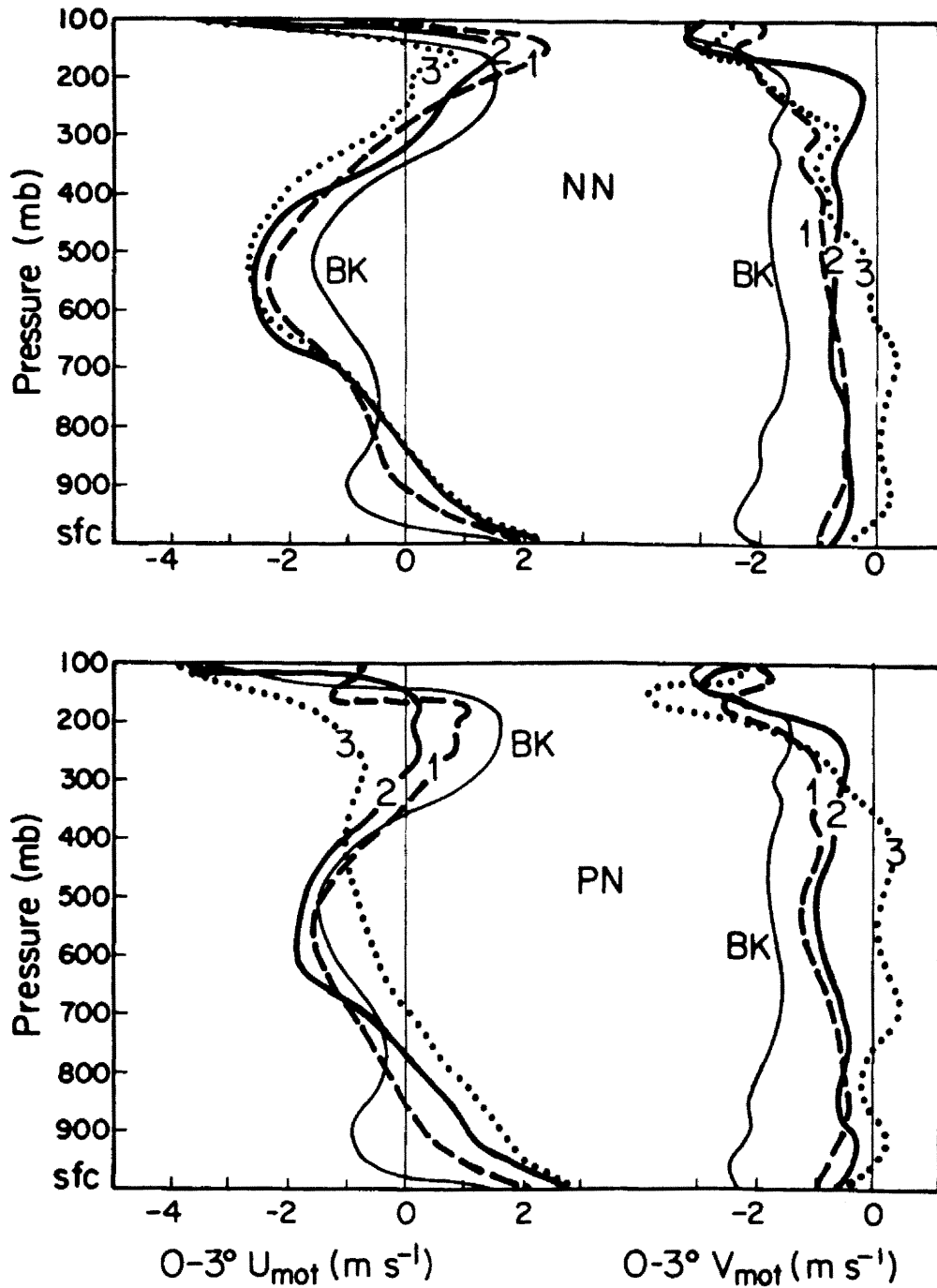
Fig. 16. The vertical profiles of the zonal (left) and meridional (right) winds at 0-3° radial area in moving or MOT coordinates for both persistent (bottom) and non-persistent (top) cases in a moving coordinate at Stage 1 (before), Stage 2 (during) and Stage 3 (after).

zonal wind shear and weak meridional vertical wind shear. The upper

level northerly relative flow generally increases during the cloud

cluster dissipation stage. These vertical wind profiles will be

compared with those of the genesis cloud cluster later.

3.3.4   Upper- and Lower-level Circulation Patterns

The 200 mb (upper troposphere) and 850 mb (lower troposphere)

streamline patterns are shown in Figs. 17 and 18. The isotachs are also

shown, as are shaded areas indicating the regions with stronger wind

speed ($\geq 6 \text{ m s}^{-1}$). The overall wind vectors are quite noisy at 200 mb

of Stages 1 and 3 and at 850 mb of Stage 3, indicating large variations

among individual cases. Some smoothing has been used in order to obtain

these streamlines. Nevertheless, the persistent and non-persistent

cases are very similar.

In the upper level, the prevailing flow for every case is mostly

from the north-northwest, with a weak ridge across the whole domain. An

anticyclonic circulation is present at Stage 2 or cloud cluster stage.

The ridge at Stage 3 appears to be stronger than that at Stage 1. The

persistent case shows an increase of the north-northwesterlies in the

region to the north and to the south of the center from Stage 2 to Stage

3. This is in agreement with the observed increasing northerly relative

flow from Stage 2 to Stage 3 as indicated in Fig. 16.

At 850 mb for the persistent case, a very good convergence or

confluence is observed around the center region at Stage 1 or before the

prominent cloud clusters were observed. An anticyclonic circulation

(subtropical high) is located in the north-northeast quadrant. The wind

speed is generally weak except on the south side where the system motion
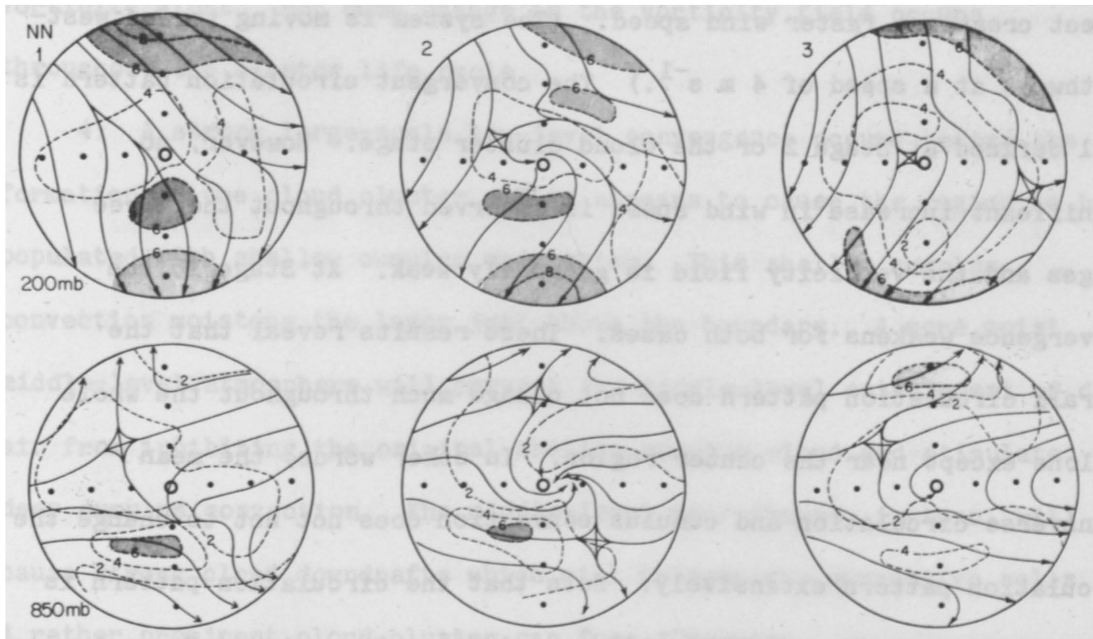
Fig. 17. The 200 mb (top) and 850 mb (bottom) streamlines in a moving
         or MOT coordinate for the non-persistent case at Stage 1
         (before), Stage 2 (during) and Stage 3 (after). The isotaches
         are shown in dashed curves. The shaded areas are regions with
         wind speed stronger than 6 m s^{-1}.
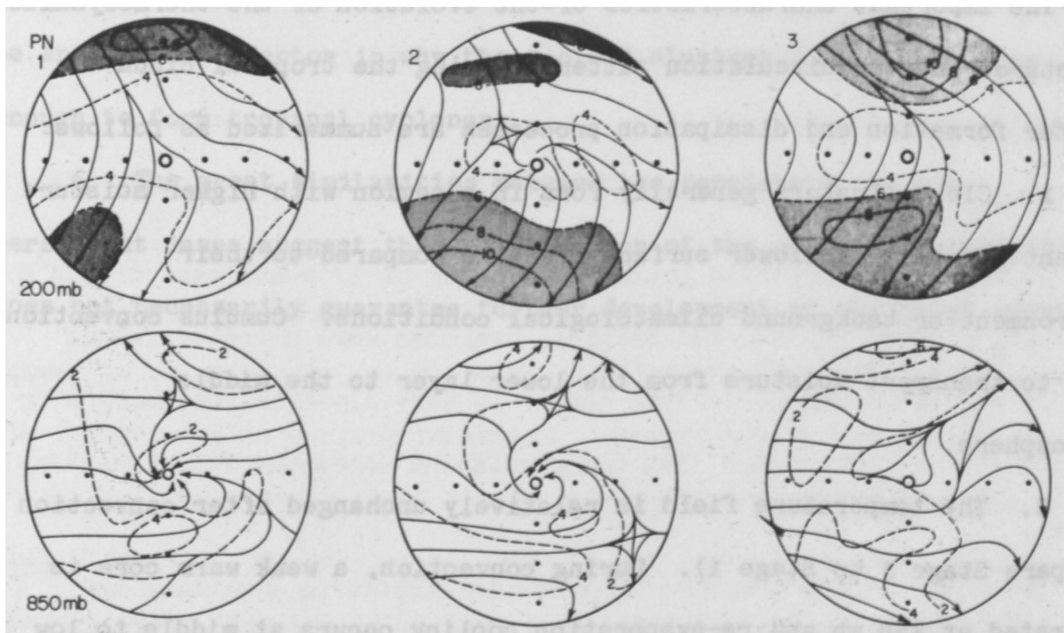
Fig. 18. The 200 mb (top) and 850 mb (bottom) streamlines in moving or
         MOT coordinate for the persistent case at Stage 1 (before),
         Stage 2 (during) and Stage 3 (after). The isotaches are shown
         in dashed curves. The shaded areas are regions with wind
         speed stronger than 6 m s^{-1}.

effect creates a faster wind speed. (The system is moving toward west-northwest at a speed of 4 m s^{-1}.) The convergent circulation pattern is well defined at Stage 2 or the cloud cluster stage. However, no significant increase in wind speed is observed throughout the three stages and the vorticity field is generally weak. At Stage 3, the convergence weakens for both cases. These results reveal that the overall circulation pattern does not change much throughout the whole cyclone except near the center region. In other words, the mean transverse circulation and cumulus convection does not act to change the circulation pattern extensively. Note that the circulation pattern is very similar (except near the center region) at Stage 1 and Stage 3, especially at the upper levels.

3.4   Summary

The important characteristics of the evolution of the thermodynamic structures and the circulation patterns during the tropical cloud cluster formation and dissipation processes are summarized as follows:

1.   Cloud clusters generally form in a region with higher moisture content and slightly lower surface pressure compared to their environment or background climatological conditions. Cumulus convection acts to transport moisture from the lower layer to the middle troposphere.

2.   The temperature field is relatively unchanged after convection (compare Stage 3 to Stage 1). During convection, a weak warm core is generated at 350 mb and re-evaporation cooling occurs at middle to low levels. Strong downdrafts cause a cool and dry boundary layer.

3.   The vorticity field is very weak (a magnitude of 0.4 f) with cyclonic vorticity at middle-lower levels and anticyclonic

vorticity aloft. Not much change in the vorticity field occurs throughout the cluster life cycle.

4. A strong large-scale low-level convergence occurs before the formation of the cloud cluster. This appears to cause the region to be populated with shallow cumulus convection. This shallow cumulus convection moistens the layer just above the boundary. A more moist middle-level atmosphere will prevent the middle-level entrainment of dry air from inhibiting the original shallow cumulus cloud and stimulate deep cumulus convection. The middle-level entrainment, in turn, will cause strong cloud downdrafts which will trigger new convective cells. A rather prominent cloud cluster can form afterward.

5. Cloud clusters form under an environment with moderately strong middle- to upper-level wind shears. A stronger shearing effect was also observed during the dissipation stage of the cloud clusters. This may be an important factor in why these cloud clusters do not last long enough to form tropical cyclones.

6. The great similarities between the persistent and non-persistent cases suggest that the duration of the cumulus convection does not necessarily guarantee further development of the cloud cluster.

4. EVOLUTION OF PRE-CYCLONE CLOUD CLUSTERS AND COMPARISONS TO THE NON-GENESIS CASES

Cloud clusters that later develop into tropical cyclones (''genesis cloud clusters'') have also been composited and studied by the author. A discussion of the structural changes during genesis cloud cluster development and a comparison of genesis and non-genesis cases are presented below. The energy, moisture and the tangential (angular) momentum budgets will be discussed in the next two chapters.

4.1 Classification Criteria and Average Characteristics of Composites

The genesis composite consists of those tropical cyclones which occurred during 1957 to 1977 - as documented in the Joint Typhoon Warning Center (JTWC) Annual Typhoon Report (ATR) - and meet the following criteria:

a) the first reported maximum intensity is equal to or less than 35 knots; and

b) the first reported position is south of 25°N and east of 120°E.

From this 21-year period, 341 tropical cyclones were selected (about half of the total number). This number is very close to the numbers in the non-genesis composites (332 non-persistent cases and 328 persistent cases).

To have better representations of the structural evolution and better budget analyses, four consecutive developing stages were taken. The incipient tropical cyclone composite (Stage 3) includes only the first two 12-hour time periods according to the best track of ATR. (Note that the best track of any tropical cyclone generally starts from the

time period when the system was upgraded to a tropical depression or a tropical cyclone.) Stage 4 consists of the two time periods immediately following the Stage 3 composite. Stage 2 includes two 12-hour time periods 12 hours and 24 hours before Stage 3; and Stage 1, 12 hours and 24 hours before Stage 2. For each stage, there are two time periods, one 00Z and one 12Z, therefore the possible diurnal bias has been minimized. The average time difference between any two consecutive stages is exactly 24 hours. It is very reasonable to assume that for every individual case the cloud cluster should have formed by Stage 2. In addition, for some cases, cumulus convection might have already organized into a prominent cloud cluster at Stage 1. The average intensity or maximum sustained surface wind velocity at Stages 1, 2, 3 and 4 is (or estimated to be) ≤ 10 m s^{-1}, 10 m s^{-1}, 15 m s^{-1} and 22 m s^{-1}, respectively.

When comparing genesis and non-genesis composites, it is only meaningful to compare them at the stages when they are of approximately similar intensity, or namely of cloud cluster stage. This is Stage 2 of non-genesis cases and Stage 2, and possibly Stage 1, of the genesis case. Noticeable changes between Stage 1 and 2 for the genesis case appear to be extremely important because they might be the indicators for later tropical cyclone formation. Because non-persistent and persistent non-genesis cloud clusters have fairly similar structures, only Stage 2 of the persistent case, or the average of these two non-genesis cases (denoted as NG), will be shown in most of the comparisons.

Since satellite images are only available after 1967, it is not feasible to use satellite images to determine the center positions at Stages 1 and 2. Instead, persistence is used in the way it was used for

the non-genesis cloud clusters. To obtain new positions at corresponding time periods, the system's position and motion at the first time period for each case is used to extrapolate backward 12 hours, 24 hours, etc. If the new position is south of 4°N, it is assumed to be at 4°N. The average characteristics for each composite are shown in Appendix A. The averaged positions have been shown in Fig. 3 (page 18). The average position for genesis cloud clusters is about $2-3^\circ$ north of those for non-genesis cloud clusters. The genesis cloud clusters have a larger northward moving component, but the westward moving speed is about the same.

4.2   Thermodynamic Structure Evolution

4.2.1   Height Field

The mean height field deviations from the $9-15^\circ$ east-west average are shown at three levels in Fig. 19. The background (BK) and the non-genesis (NG) are also shown (thinner curves). The height fields at 200 mb are generally noiser than those at 500 mb and 950 mb. The overall height field patterns for the four stages of the genesis case at 950 mb and 500 mb are fairly similar. A drop in the 950 mb height occurs over about a 6° radius domain at Stages 1 and 2, but is concentrated mainly inside $3-4^\circ$ radius at Stages 3 and 4. Although the height field drop occurs over quite a large area during Stage 1, the magnitude is only 10 m or 1 mb – which is not much larger than that of the non-genesis cases. The important feature, however, is that this height field drop creates a strong pressure gradient at $4-8^\circ$ radius, where stronger winds are also observed. At Stage 2, the strong pressure gradient moves closer in (to $2-6^\circ$ radius), and still further inward at Stages 3 and 4. These results suggest that tropical cyclone formation may be associated with those
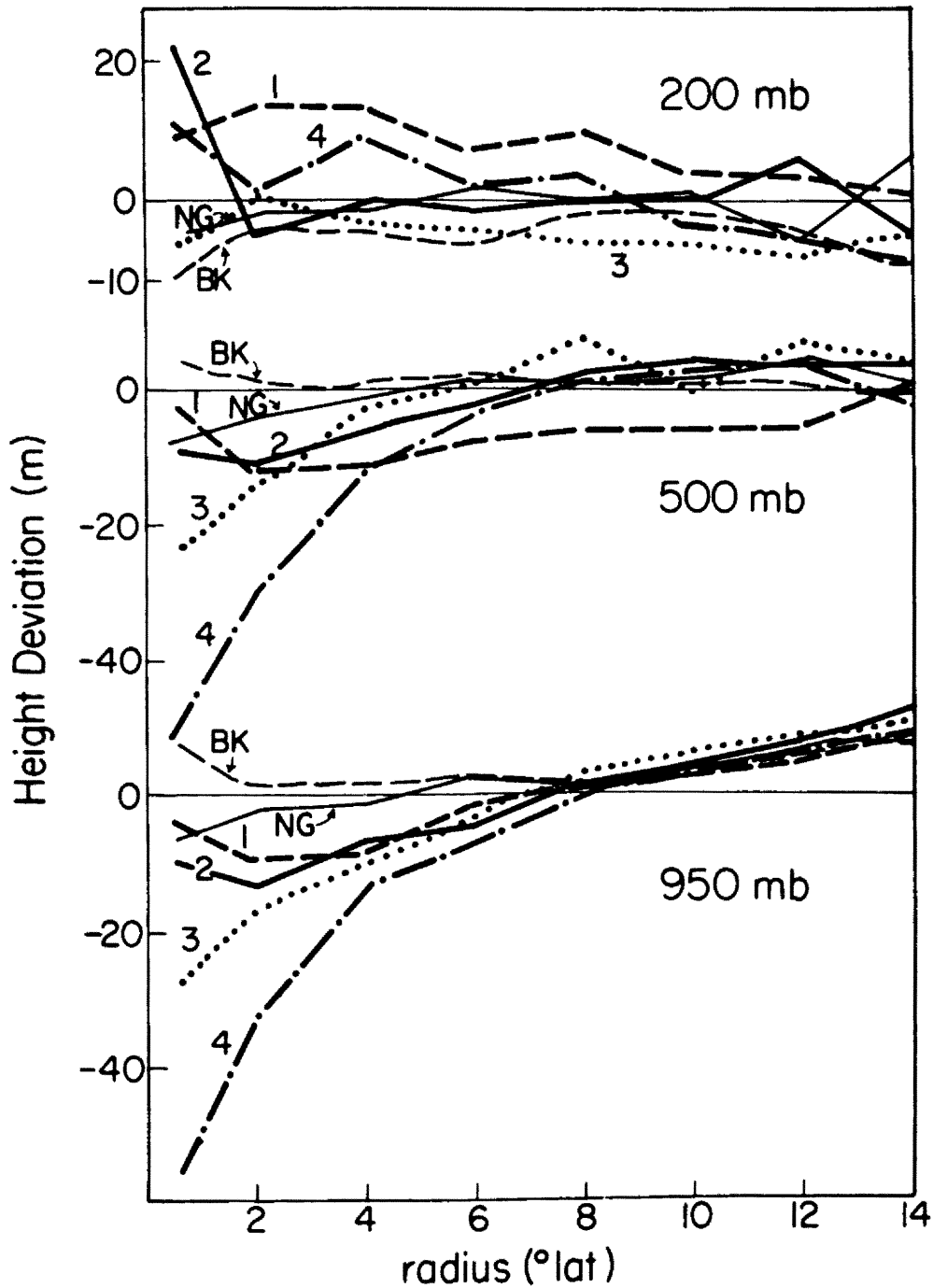
Fig. 19. The height deviation from the east-west 9-15° average at 200 mb, 500 mb, and 950 mb for the genesis case at Stage 1 (2 days before, $\leq$ 10 m s^{-1}), Stage 2 (1 day before, ~ 10 m s^{-1}), Stage 3 (incipient tropical cyclone, ~ 15 m s^{-1}) and Stage 4 (1 day after, ~ 22 m s^{-1}). The background (BK) and non-genesis (NG) composites are also shown.

larger-scale processes that cause this inward-developing surface
pressure drop evolution.

To further investigate this surface pressure evolution, Fig. 20
shows the north-south and east-west cross sections of the 950 mb height
field. Note that these are the actual height values, not deviations.
The background height field shows fairly weak north-south and east-west
pressure gradients. In the north-south direction, the pressure (height)
decreases uniformly from north to south until $8-10^{\circ}$ south of the
composite center. Since the composite center is at $11.5^{\circ}N$, this
pressure trough can be considered as the equatorial trough. This
background composite height field gives a fairly reasonable
representation of the large-scale height field in the western North
Pacific. The curves for the non-genesis cloud cluster composites are
very close to the background curves and also have fairly weak pressure
gradients. Almost no change is observed throughout the life cycle of
the non-genesis cloud cluster. (The curves at different stages are so
close to each other that they are not shown in Fig. 20.) Also see Table
4 on page 32. Note that there is a pressure drop near the center, but
the magnitude is very small.

Figure 20 (upper pannel) indicates that in the north-south
direction the lowest pressure is located away from the composite center
for the genesis case at Stages 1 and 2. This might be due to the
positioning procedure and the data resolution problem, but it could be
realistic, thus indicating that circulation centers tend to form more on
the north side of the cloud cluster. The pressure drop (compared to the
background) occurs from 8° north of the center to 6° south of the center
or over a 14° domain at Stage 1. The pressure drop from Stage 1 to
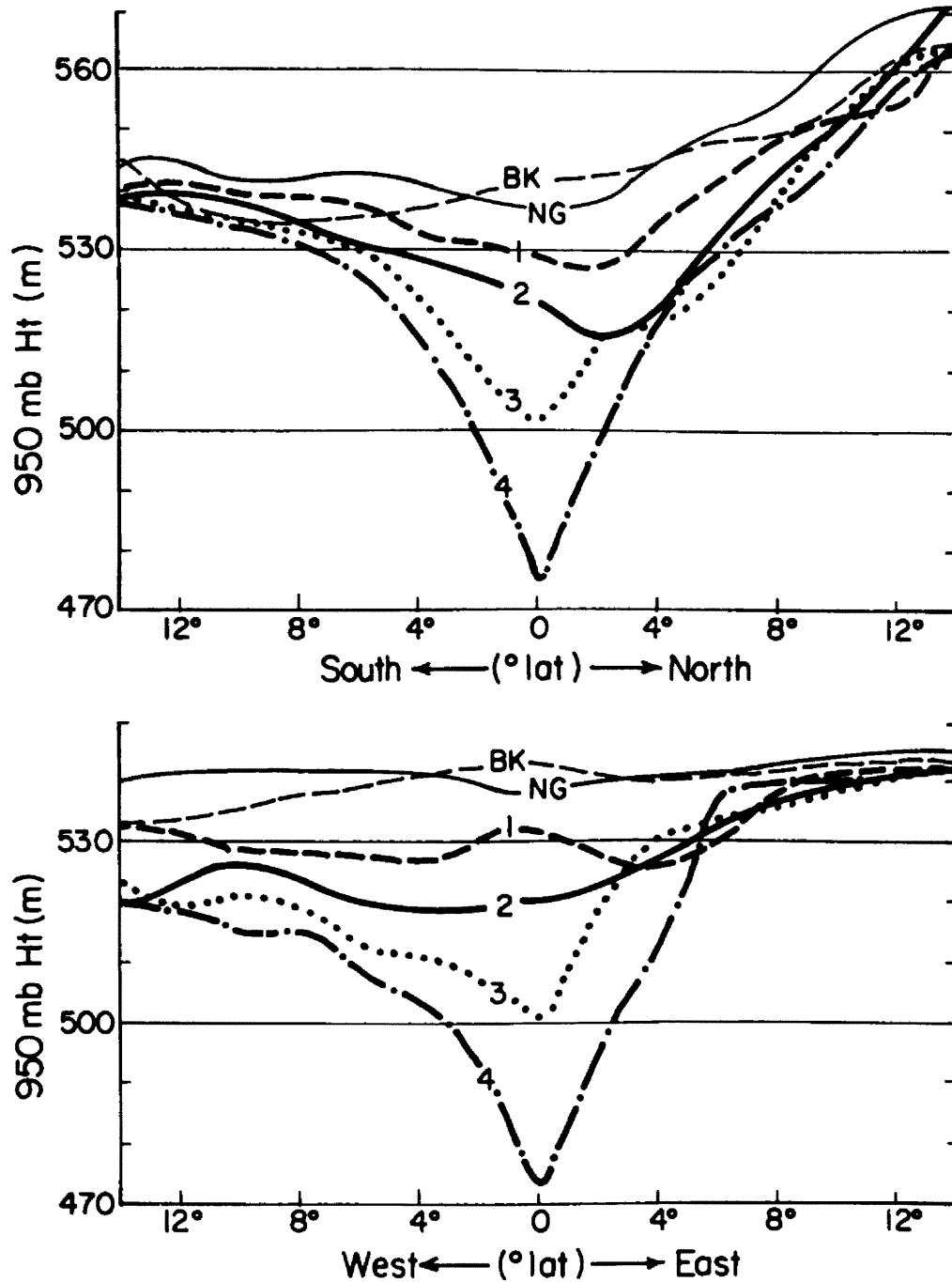
Fig. 20. The 950 mb height field along north-south (upper) and east-
west (bottom) directions for the genesis composites at Stage 1
(2 days before, $\leq$ 10 m s^{-1}), Stage 2 (1 day before, ~ 10 m s^{-}
^{1}), Stage 3 (incipient tropical cyclone, ~ 15 m s^{-1}) and Stage
4 (1 day after, ~ 22 m s^{-1}). The background (BK) and the
non-genesis (NG) cloud cluster composite.

Stage 2 also occurs over a very large area. However, from Stages 2 to 3 and from 3 to 4, the pressure drop concentrates near the center and more on the south side. In the east-west direction, the curves for the genesis composites show quite a significant pressure drop across most of the domain except outward of 6° radius east of the composite center at Stage 1. From Stage 1 to Stage 4, this already lower pressure field further falls, with the maximum drop occurring near the center.

4.2.2 Temperature Field

As in the non-genesis cases, the genesis cloud clusters possess a warm core in the middle to upper troposphere and a cold core at lower levels and near the tropopause (as shown in Fig. 21). The magnitude of the middle to upper tropospheric warm core is much stronger for the genesis case than for the non-genesis cases. It increases only slightly from Stage 1 to Stage 3, but increases significantly from Stage 3 to Stage 4. The low-level cold core shows an erratic evolution pattern and the changes are relatively small. Above 100 mb, the genesis case changes from a warm core system at Stages 1 and 2 to a cold core system at Stages 3 and 4.

The radial profiles of temperature deviations from the 9-15° east-west average at 300 mb, where the largest warm core occurs, are shown in Fig. 22. The non-genesis and background profiles are also shown. The pattern and its evolution is similar to that of the 950 mb height field. The warming occurs over a very large area at Stage 1 of the genesis case, but is concentrated near the center at later stages. The non-genesis cases have a weaker warming which occurs over a smaller region. These results are in good agreement with the observed 500 mb and 950 mb height fields. Note that although the warming at the inner region

Fig. 21. The 0-2° radius vertical profiles of the temperature
deviations from the east-west 9-15° average for the genesis
case at Stage 1 (2 days before, ≤ 10 m s⁻¹), Stage 2 (1 day
before, ~ 10 m s⁻¹), Stage 3 (incipient tropical cyclone, ~ 15
m s⁻¹) and Stage 4 (1 day after, ~ 22 m s⁻¹) and the non-
genesis cloud cluster (NG).

occurs over a deep layer, the warming at the higher levels of 200-400 mb

is more efficient (and of greater magnitude) for producing a lower

surface pressure hydrostatically.

Although Fig. 21 shows the results only at 0-2° radius, the

profiles for the region 0-5° radius show a similar pattern (figure not

shown). This latter region is the cloudiest, and the observed upper-

level warming can be explained by the cumulus convective heating (in the

form of subsidence warming) and by the environmental vertical wind

shear. However, the pressure drop shown in Figs. 19-20 occurs over an

area larger than can be explained by cumulus convection and its
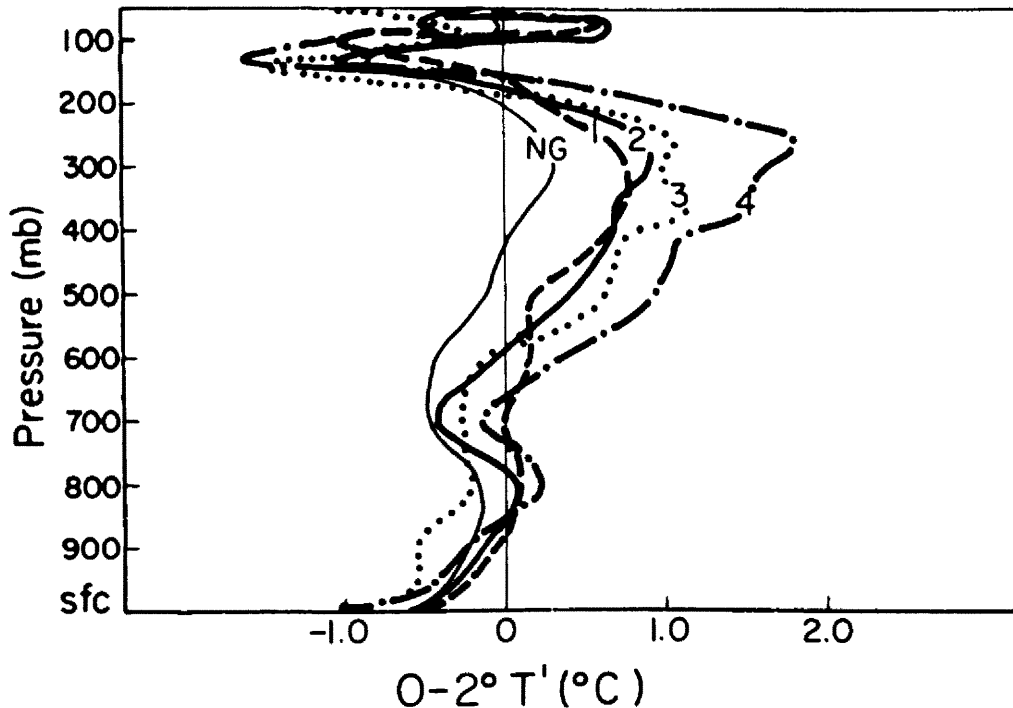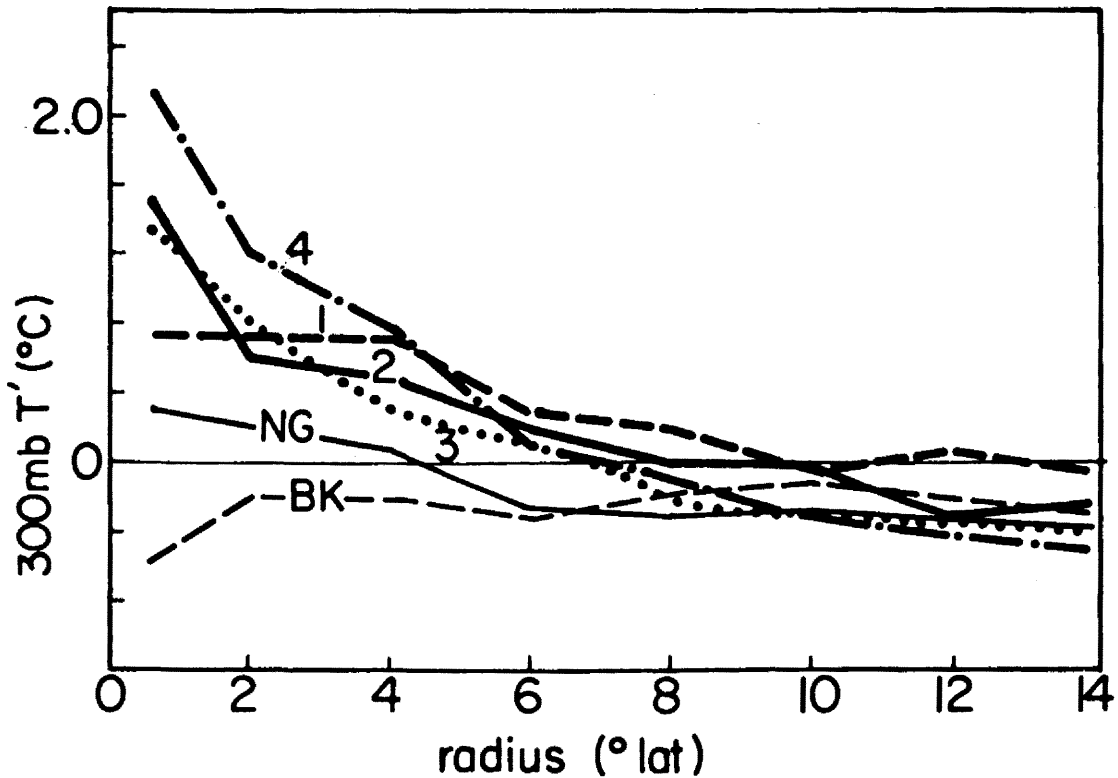
Fig. 22. The 300 mb radial profiles of the temperature deviations from the east-west 9-15° average for the genesis case at Stage 1 (2 days before, $\leq$ 10 m s^{-1}), Stage 2 (1 day before, ~ 10 m s^{-1}), Stage 3 (incipient tropical cyclone, ~ 15 m s^{-1}) and Stage 4 (1 day after, ~ 22 m s^{-1}) and the non-genesis cloud cluster (NG).

immediate environment. Therefore, the 300 mb temperature fields for the first 3 stages of the genesis case are shown in Fig. 23 (right panel) to indicate the large-scale warm and cold pools. The background and the non-genesis cloud clusters are also shown (left panel of Fig. 23). In these figures, the shaded area indicates the warm pools with temperatures higher than -30°C and the heavy curves are -30.5°C isotherms.

The background composite shows a warm region to the northwest and cold regions to the northeast and the south. The non-genesis cases

Fig. 23.   The 300 mb temperature field for the genesis case (GN) at
           Stages 1, 2, and 3 (right) and for the non-genesis and
           background composites (left).   The shaded areas are the warmer
           regions with temperatures higher than -30°C and the heavy
           curves are -30.5° isotherms.   The distance between dots is 4°.

possess a similar pattern except that the temperature is slightly higher near the center associated with the cumulus convection. The cold pool to the northeast i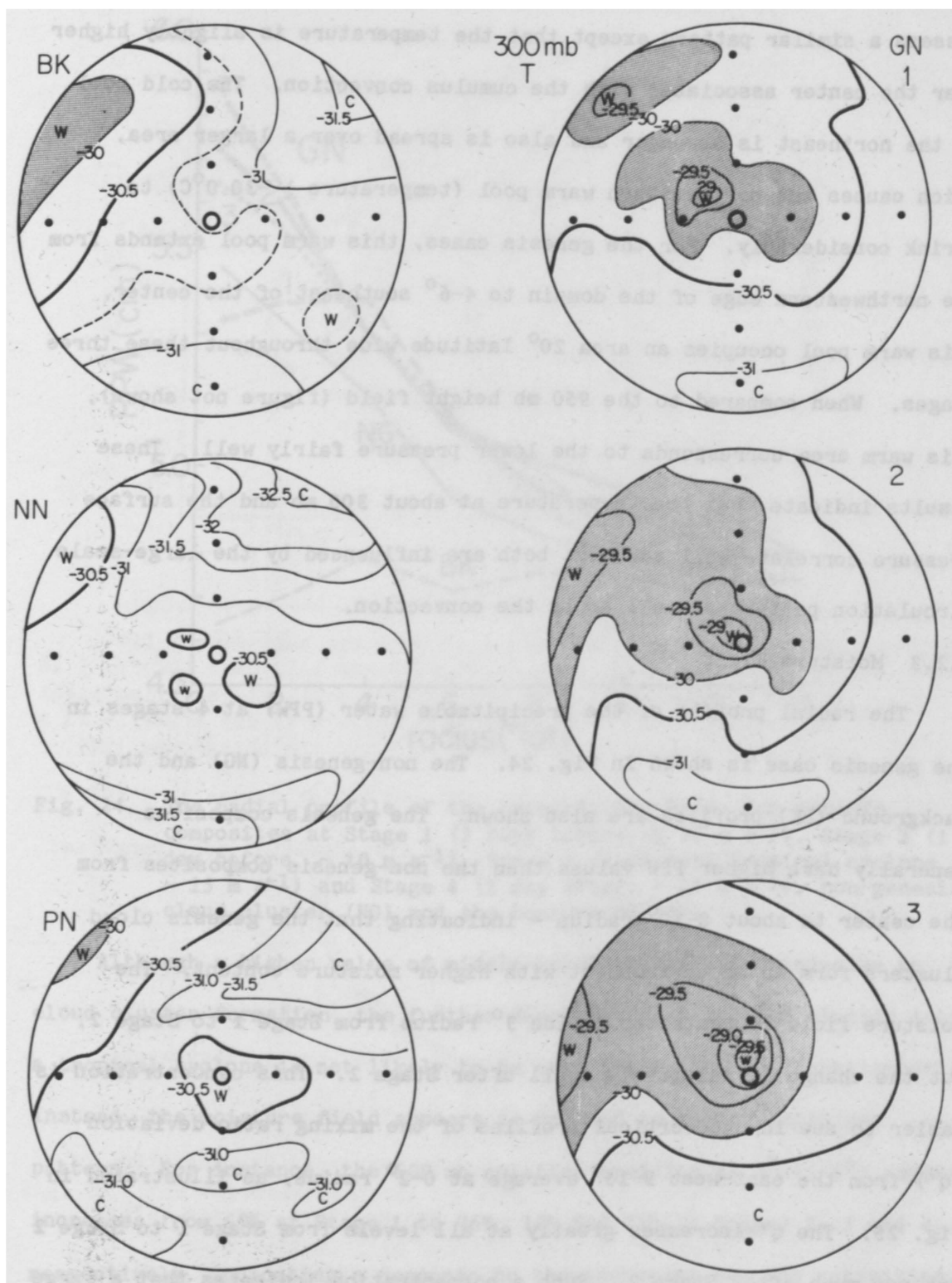s stronger and also is spread over a larger area, which causes the northwestern warm pool (temperature $\geq$ -30.0°C) to shrink considerably. For the genesis cases, this warm pool extends from the northwestern edge of the domain to 4-6° southeast of the center. This warm pool occupies an area 20° latitude wide throughout these three stages. When compared to the 950 mb height field (figure not shown), this warm area corresponds to the lower pressure fairly well. These results indicate that the temperature at about 300 mb and the surface pressure correlate well and that both are influenced by the large-scale circulation pattern as well as by the convection.

4.2.3 Moisture Field

The radial profile of the precipitable water (PPW) at 4 stages in the genesis case is shown in Fig. 24. The non-genesis (NG) and the background (BK) profiles are also shown. The genesis composites generally have higher PPW values than the non-genesis composites from the center to about 8-10° radius – indicating that the genesis cloud clusters form in an environment with higher moisture content. The moisture field concentrates inside 3° radius from Stage 1 to Stage 2, but the change is relatively small after Stage 2. This concentration is easier to see in the vertical profiles of the mixing ratio deviation (q') from the east-west 9-15° average at 0-2° radius, as illustrated in Fig. 25. The q' increases greatly at all levels from Stage 1 to Stage 2 but not much after Stage 2. Such a concentration indicates that a large moistening occurs in association with the concentration of the horizontal convergence (which will be shown later).
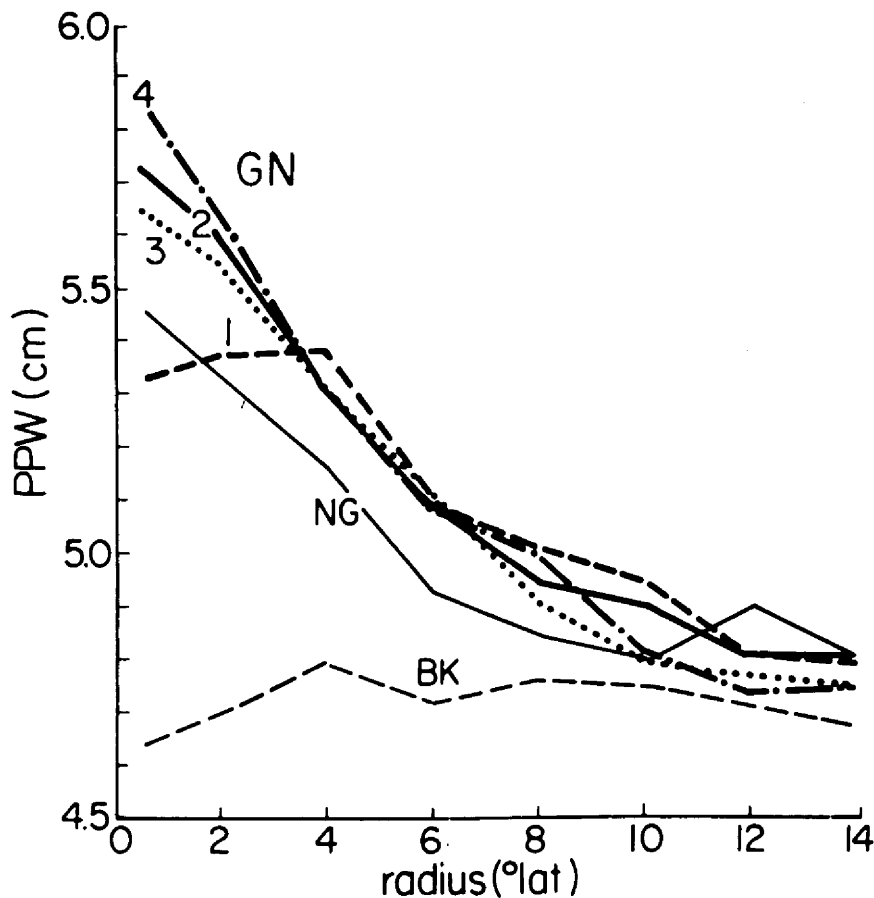
Fig. 24. The radial profile of the precipitable water for genesis composites at Stage 1 (2 days before, $\leq$ 10 m s^{-1}), Stage 2 (1 day before, ~ 10 m s^{-1}), Stage 3 (incipient tropical cyclone, ~ 15 m s^{-1}) and Stage 4 (1 day after, ~ 22 m s^{-1}), non-genesis cloud cluster (NG) and the background (BK).

Although a higher value of middle-level moisture is conducive to cloud cluster formation, the further development of a cloud cluster into a tropical cyclone is not likely to be affected by the moisture content. Instead, the moisture field appears to respond to the circulation pattern. For instance, the 600 mb relative humidity at 2° (1-3°) radius increases from 69% at Stage 1 to 76%, 78% and 78% at Stages 2, 3 and 4, respectively, indicating a response to the increased cumulus activities. The value at 6° (5-7° radial belt or the environment), however,
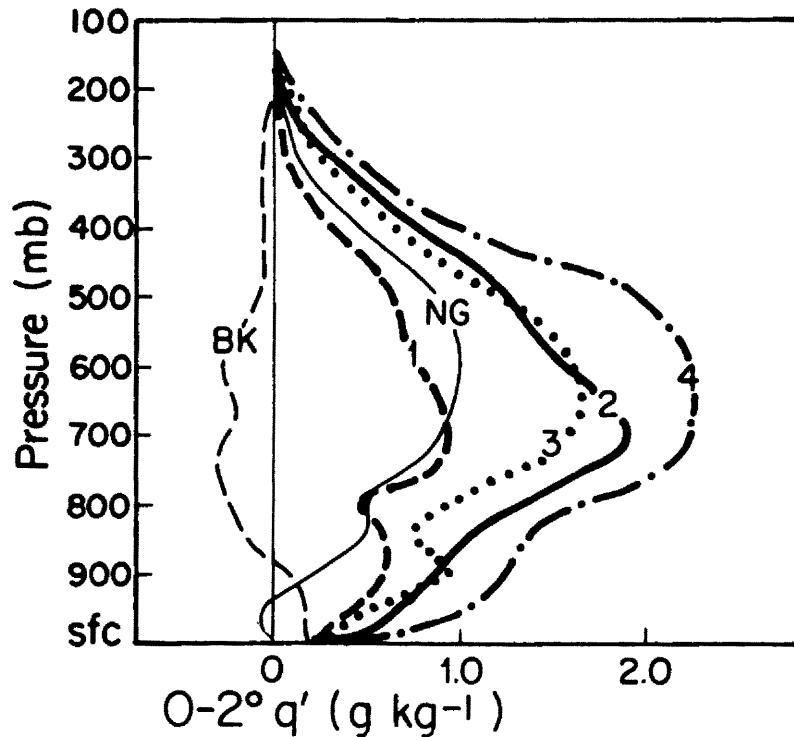
Fig. 25. The 0-2° mixing ratio deviation from the east-west 9-15°
average for genesis composites at Stage 1 (2 days before, $\leq$ 10
m s⁻¹), Stage 2 (1 day before, ~ 10 m s⁻¹), Stage 3 (incipient
tropical cyclone, ~ 15 m s⁻¹) and Stage 4 (1 day after, ~ 22 m
s⁻¹) non-genesis cloud cluster (NG) and the background (BK).

decreases from 65% at Stage 1 to 63%, 62% and 60% at Stages 2, 3 and 4,

respectively. This is due to the stronger environmental subsidence as

the system develops.

4.2.4 Equivalent Potential Temperature

The equivalent potential temperature (θ_e) is a measure of the

combination of the temperature and mixing ratio, or, approximately

equivalent to the moist static energy. The value of θ_e thus should

increase as the cloud cluster develops and increases the magnitude of

its middle to upper-level warm core and its moisture content. The

increase of θ_e, however, occurs only in the inner region or inside 3°,

as shown in Fig. 26 by the θ_e profiles at 2° (1-3°) and 4° (3-5°).

These profiles show a common θ_e pattern with lowest θ_e value at about
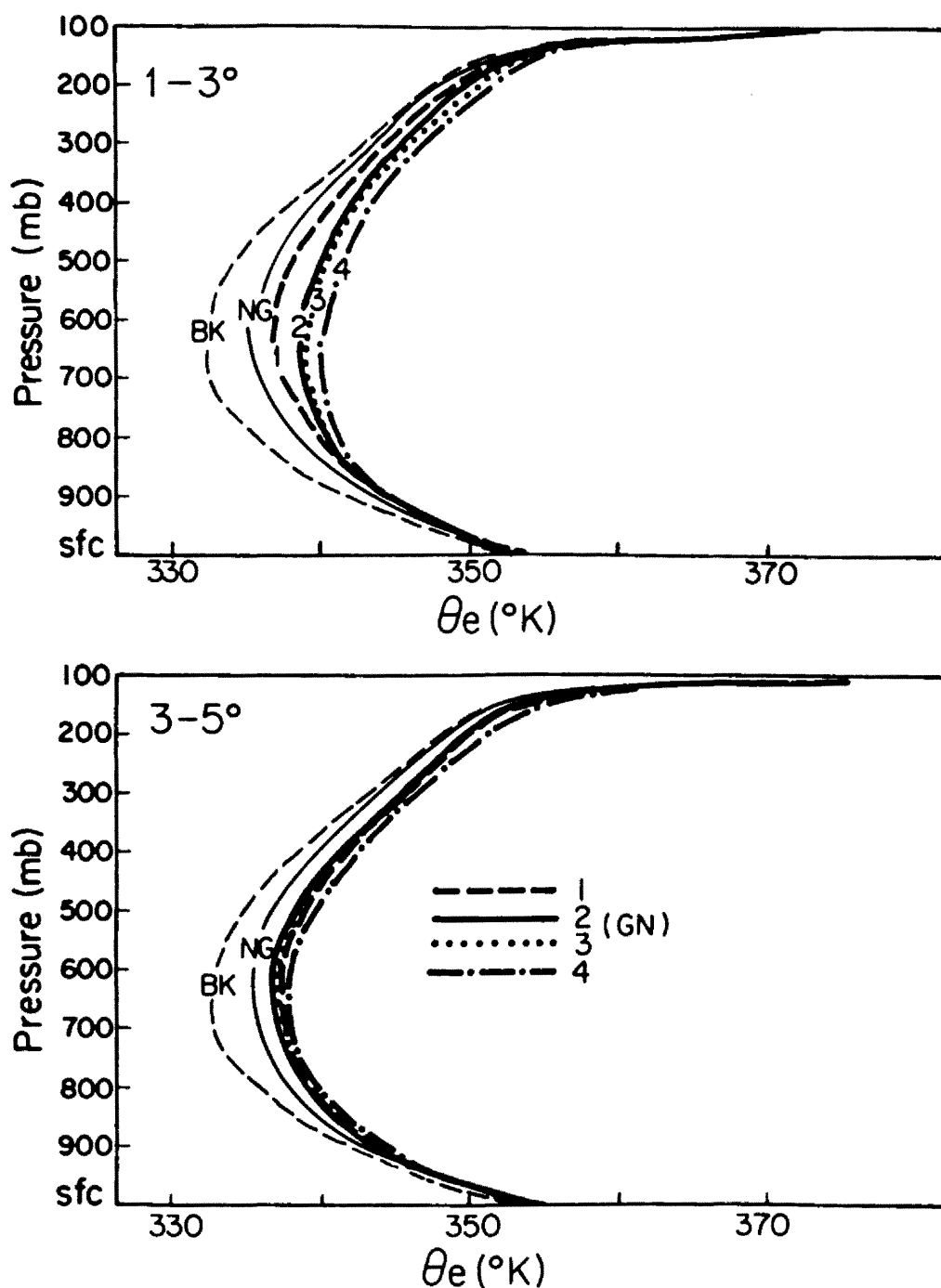
Fig. 26. The vertical profiles of equivalent potential temperature at
2° (1-3°) and 4° (3-5°) radii for the genesis case at Stage 1
(2 days before, $\leq$ 10 m s^{-1}), Stage 2 (1 day before, ~ 10 m s^{-1}), Stage 3 (incipient tropical cyclone, ~ 15 m s^{-1}) and Stage
4 (1 day after, ~ 22 m s^{-1}) stages), non-genesis cloud cluster
(NG) and the background (BK).

600 mb and higher θ_e values above and below that level. At both radii the non-genesis composite has higher θ_e values than the background, and the genesis composites have higher θ_e values than the non-genesis composite. The θ_e profile for the genesis case shows a steadily increasing trend from Stage 1 to Stage 4 at 2° radius. However, almost no change is observed at 4° and 6° radius (figure not shown). These results indicate that the outer region conditional instability is relatively unmodified during the formation of a tropical cyclone.

4.3 Dynamic Structure Evolutions

4.3.1 Radial Wind and Vertical Motion

The radius-pressure cross sections of the mean radial wind at 4 stages of the genesis composite are shown in Fig. 27. The two non-genesis cases are also shown. For all composites, the inflow extends from the surface up to 350-400 mb at most radii, while the outflow concentrates at a much shallower layer between 100-300 mb. At Stage 1 of the genesis composite, the radial wind inside $2-3^o$ radius is smaller than in the other composites. The low-level strong inflow ($V_r \leq -1$ m s^{-1}) penetrates inward from outside 14° radius to about 3.5^o radius at Stage 1 and extends to inside 1° radius at Stage 2. Similar patterns also occur for the upper-level outflow. The low-level inflow and upper-level outflow inside 6° radius reach maximum values at Stage 3 and decrease slightly at Stage 4.

When compared to the genesis cases at Stage 2, the non-genesis cloud clusters (at their Stage 2) have a much smaller inflow at the boundary layer. The upper-level outflow is also slightly smaller, but the middle-level inflow is slightly larger inside 6° radius. The weaker low-level inflow for the non-genesis cloud clusters agrees well
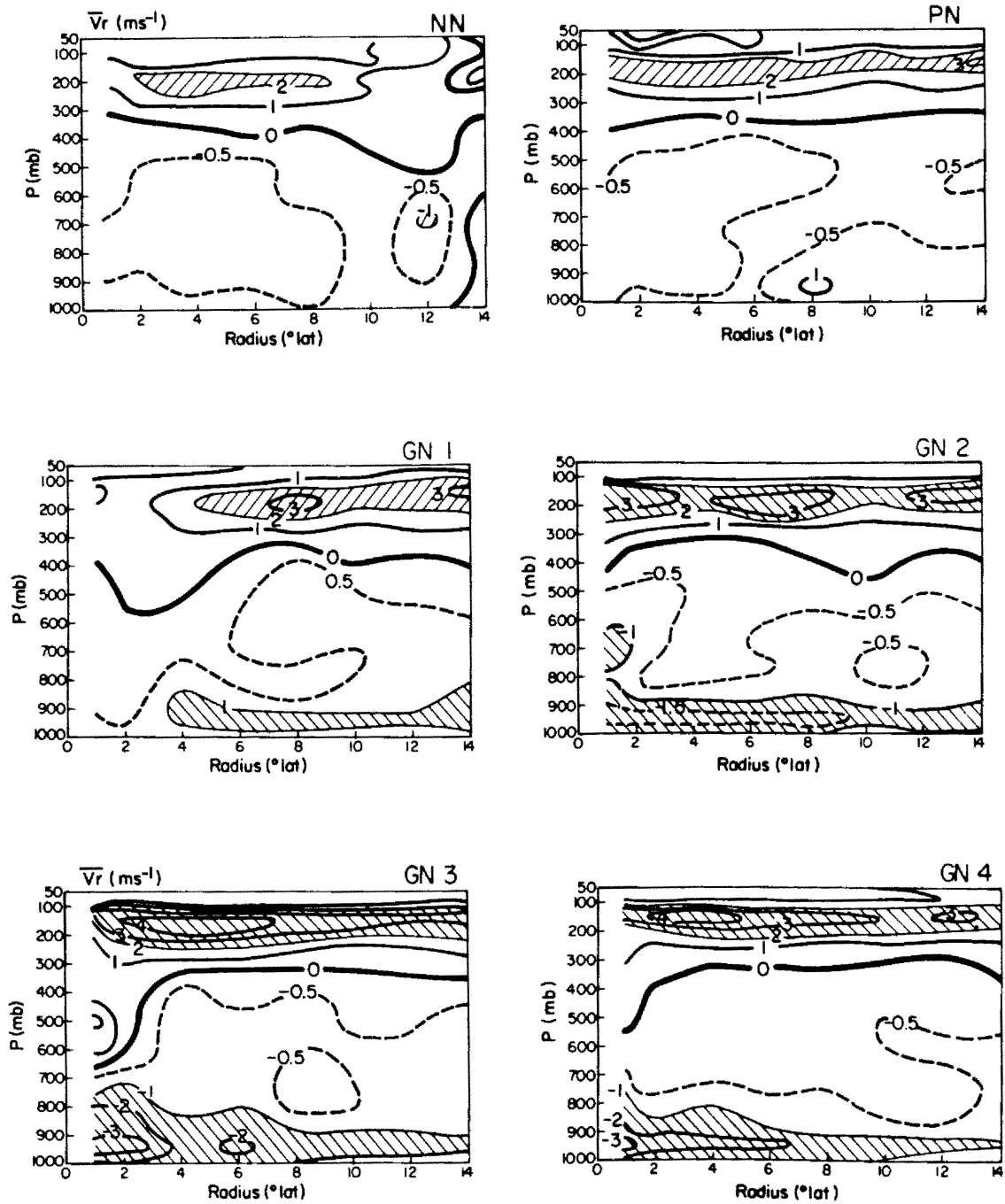
Fig. 27. The cross section of the radial wind for the genesis case at Stage 1 (2 days before, $\leq$ 10 m s^{-1}), Stage 2 (1 day before, ~ 10 m s^{-1}), Stage 3 (incipient tropical cyclone, ~ 15 m s^{-1}) and Stage 4 (1 day after, ~ 22 m s^{-1}) and the non-genesis cloud clusters (NG) at Stage 2. The heavy curves are the zero lines and the shaded regions show strong inflow ($\leq$ -1 m s^{-1}) and outflow ($\geq$ 2 m s^{-1}).

with the weaker surface pressure gradient associated with these composites. The strong upper-level outflow ($V_r \geq 2$ m s^{-1}) for the non-persistent cloud cluster extends from the inner region outward only to 8-10° radius, while it extends all the way to 14° radius for all other composites (even for the background composite, figure not shown). These results indicate that the non-persistent, non-genesis cloud clusters generally exist in an environment quite different from that of the other cases.

Although, the radial inflow shows quite different vertical distributions for the genesis and the non-genesis composites, the vertical mass-weighted integrations of the inflow are very similar. The genesis and non-genesis cloud clusters thus have about the same magnitudes of the maximum mean vertical motion ($\bar{\omega}$), as shown in Fig. 28 for the 0-4° and 0-6° regions. The genesis cloud cluster at Stage 2 has stronger vertical motion below 600 mb (due to the stronger boundary inflow) as compared to the non-genesis cloud cluster, but the maximum vertical motion at 300-350 mb is about the same for both. The evolution of the $\bar{\omega}$ profile from Stage 1 to Stage 2 of the genesis case is very similar to that of the non-genesis case. The $\bar{\omega}$ profile is flatter at the middle levels at Stage 1 and steeper at Stage 2; in other words, strong low-level large-scale convergence at Stage 1 causes more shallow convection to form at Stage 1 and more deep convection to develop at Stage 2.

A large increase in mean vertical motion occurs from Stage 2 to 3, indicating a possible convection burst during the formation of tropical cyclones. Note that the 0-4° radius upward vertical motion increases only slightly from Stage 1 to Stage 2, but its pattern changes
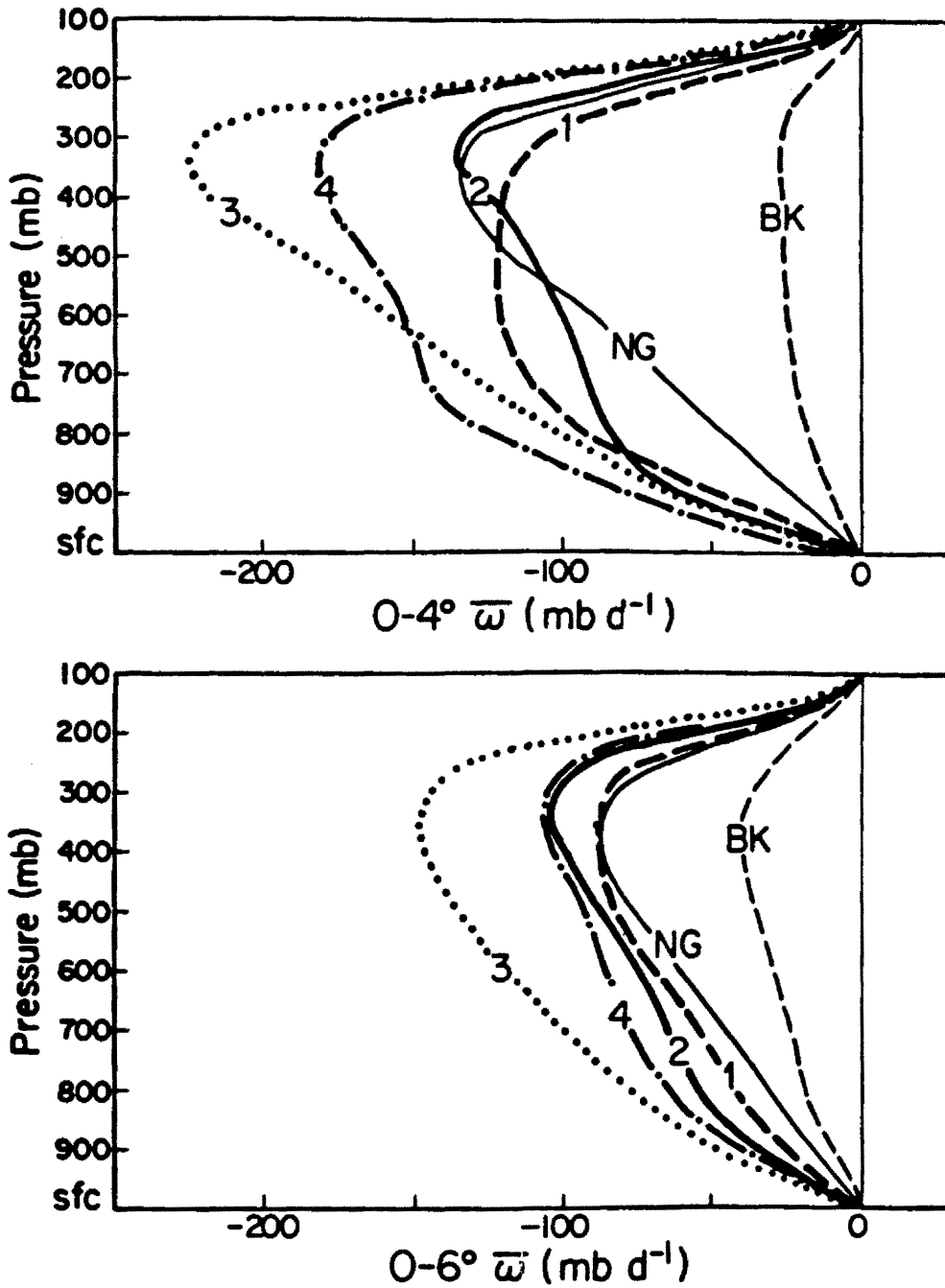
Fig. 28. The 0–4° and 0–6° mean vertical motion profiles for the
genesis case at Stage 1 (2 days before, $\leq$ 10 m s^{-1}), Stage 2
(1 day before, ~ 10 m s^{-1}), Stage 3 (incipient tropical
cyclone, ~ 15 m s^{-1}) and Stage 4 (1 day after, ~ 22 m s^{-1}) and
for the non-genesis cloud cluster (NG). The background
profile (BK) is also shown.

significantly. From Stage 2 to Stage 3, the magnitude at the middle layer increases greatly, but the pattern change is relatively small. The upward vertical motion at both regions decreases from Stage 3 to Stage 4. This convection burst at Stage 3 appears to be important to the formation of the tropical cyclone, as will be discussed in the individual case analyses.

Figure 28 gives only the mean vertical motion from the center to 4° and 6° radius. It doesn't show the radial distribution. The vertical-radial cross sections of mean vertical motion for both genesis and non-genesis composites are thus shown in Fig. 29. The mean vertical motions at $0-2^\circ$ radius are taken to represent values at 1° radius. These figures reveal a common pattern for tropical convective systems indicating that upward vertical motion generally extends from the center to about $7-8^\circ$ radius. Beyond 10° radius there is a weak upward motion with a magnitude comparable to that of the background upward motion (maximum magnitude about 40 mb/d at 300-500 mb). A weak subsidence is generally found between these two regions.

At Stage 1, maximum vertical motion is located at $2-3^\circ$ radius and a secondary maximum at 7° radius. The center region shows relatively weak vertical motion. It is possible that this weak vertical motion might be partly due to the inaccuracy in locating the system's center positions, but the author tends to view this as a real feature - but one that is magnified by the coarse data resolution. Arnold (1977) has also observed that the tropical cyclone circulation centers generally form in the clear regions outside or along the periphery of the cloud cluster.

The maximum vertical motion strengthens and moves inward to within 1° radius from Stage 1 to Stage 2. The second maximum center also moves
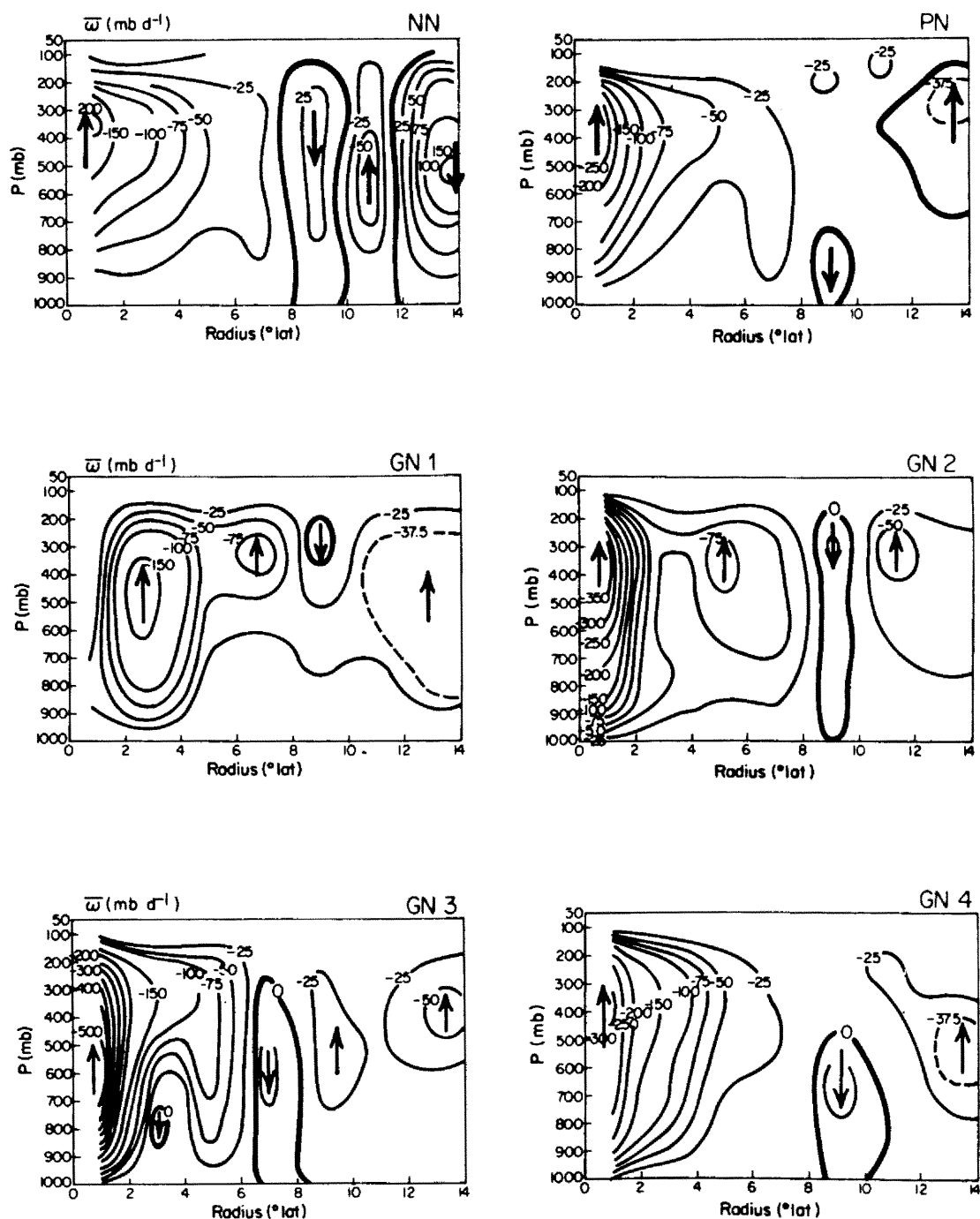
Fig. 29. The cross section of the mean vertical motion for the genesis
case at Stage 1 (2 days before, $\leq$ 10 m s^{-1}), Stage 2 (1 day
before, ~ 10 m s^{-1}), Stage 3 (incipient tropical cyclone, ~ 15
m s^{-1}) and Stage 4 (1 day after, ~ 22 m s^{-1}) and the non-
genesis cloud cluster composites (Stage 2 of NN and PN). The
heavy curves are the zero lines.

from 7° to 5° radius and strengthens slightly. The subsidence between $8-10^o$ radius becomes stronger and extends from the upper level down to the surface, indicating a better separation between cyclone convection and its environmental or weak mean ascent.

The inner region mean vertical motion reaches a maximum intensity at Stage 3. The surrounding cyclone subsidence strengthens and moves further inward to $6-8^o$ radius in response to the overall increased cyclone convection. The concentration of convection near the cyclone center also gives a weak subsidence at 700-850 mb between 2° and 4° radius. As the system develops further, the inner strong convection expands outward, pushing the environmental subsidence back to $8-10^o$ radius. Arnold (1977) also showed that the radial extent of cloudiness decreased from cloud cluster stage (Stage 2) to depression stage (Stage 3) and increased again at tropical storm stage (Stage 4), which is in good agreement with the current results.

For the non-genesis cloud clusters, the magnitude of the upward motion decreases uniformly with radius. A similar central concentration does not occur. (Note that for the genesis case, the Stage 2 or cloud cluster stage shows most of the convection concentrated at a radius inside 2° and leaving relatively weak vertical motion at $3-5^o$ radius). As discussed previously, the non-persistent cloud cluster occurs in an environment different from that in the other composites. The $8-14^o$ radius area-weighted average of $\bar{\omega}$ shows a mean subsidence over this region with a maximum magnitude of 38 mb/d at 500 mb (figure not shown). Other composites, however, have weak mean upward motion over this radial domain. These results suggest that the non-genesis cloud cluster occurs over a limited region within a generally unfavorable environment. This

might be one of the reasons why these cloud clusters last for only a very short time period. (Note that strong subsidence occurs at $4-6^o$ radius for the non-persistent case at Stage 3, the cloud cluster dissipation stage which has been indicated by Fig. 14 - page 42).

4.3.2 Tangential Wind and Vorticity

The radial-pressure cross sections of mean tangential wind at 4 stages of the genesis case are shown in Fig. 30. (The non-genesis cases are also shown). At Stage 1, the maximum cyclonic circulation is located at 900 mb between $5-6^o$ radius. The cyclonic circulation extends up to 300 mb within $6-8^o$ radius. The anticyclonic circulation exists only at 100-300 mb inside 6° radius and extends downward to below 500 mb beyond 10° radius. The maximum anticyclonic circulation is located at 200 mb. The maximum center at $12-14^o$ radius is possibly due to the strong mid-latitude westerlies which generally has no direct influence on cloud cluster development at this early stage.

As the cloud cluster develops to a tropical cyclone, the cyclonic circulation becomes stronger and extends to higher levels, with the maximum cyclonic circulation located near the system center. The outer maximum anticyclonic circulation strengthens and extends gradually inward, possibly because systems that move toward the northwest direction pick up more mid-latitude westerly influences.

When comparing the genesis (Stages 1 and 2) and non-genesis (both) cases, the most striking feature is that the genesis cases have much stronger low-level cyclonic circulation which increases with time. Although the genesis cases show a stronger upper-level anticyclonic circulation than the non-genesis cases, the difference is not as dramatic as it is for the middle to low-level cyclonic circulation. The
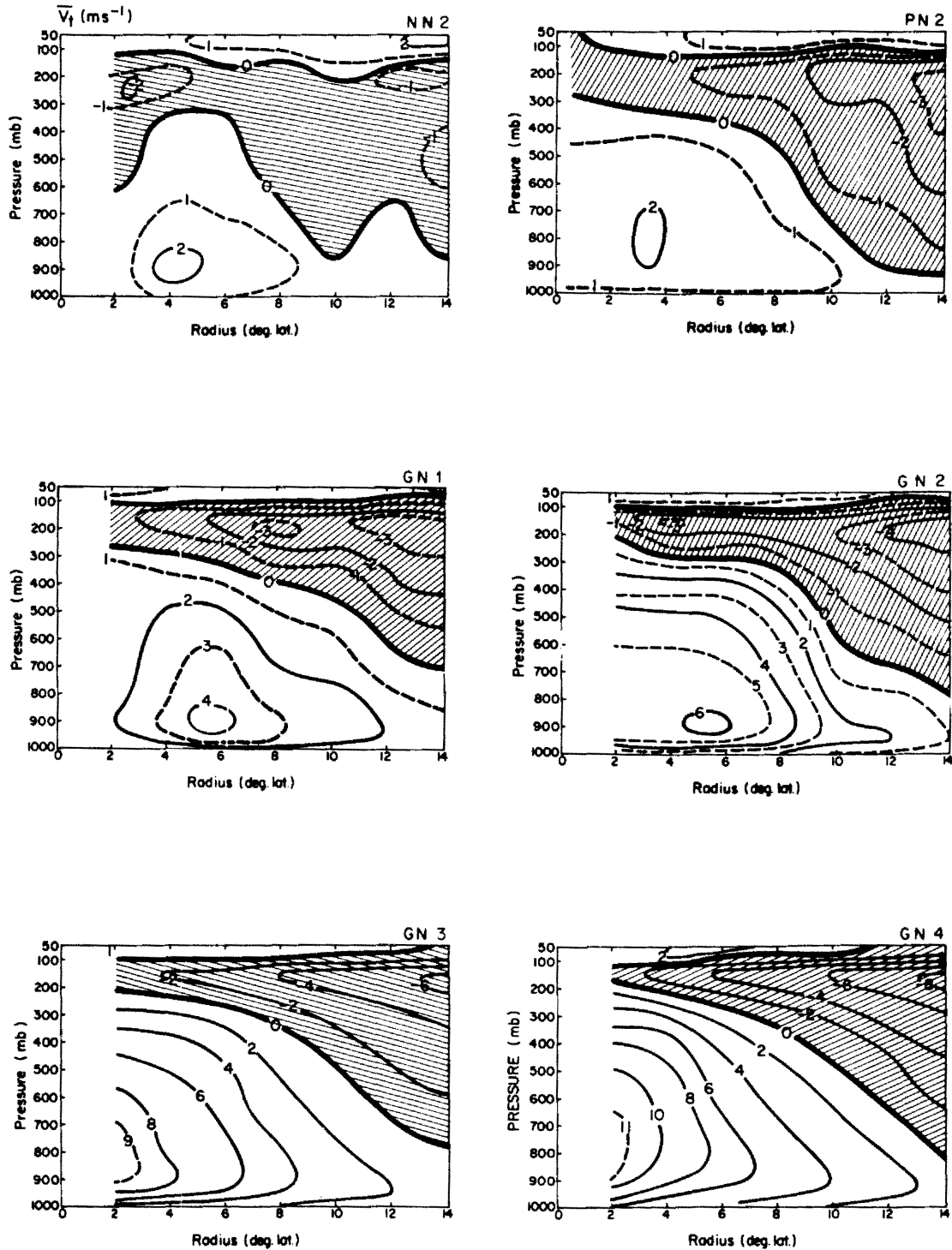
Fig. 30. The cross section of the mean tangential wind for the non-
genesis cloud clusters at Stage 2 (NN and PN) and for the
genesis case at Stage 1 (2 days before, $\leq$ 10 m s^{-1}), Stage 2
(1 day before, ~ 10 m s^{-1}), Stage 3 (incipient tropical
cyclone, ~ 15 m s^{-1}) and Stage 4 (1 day after, ~ 22 m s^{-1}).
The shaded regions indicate the anticyclonic circulation.

non-genesis pattern variations are more erratic. For example, the non-persistent non-genesis cases (NN) have a maximum upper-level anticyclonic circulation at 2-4° radius with a magnitude quite comparable to that of the genesis cases at the corresponding radius. The non-persistent cases do not have a strong anticyclone beyond 10° radius, while the genesis cases do. This is partly due to the averaged position of the non-persistent composites being at a lower latitude than that of the genesis composites. The persistent non-genesis cases (PN), on the other hand, have an anticyclonic circulation that is similar to the genesis cases at larger radii but not at smaller radii (inside 6-8° radius).

To give a better representation of tangential wind evolution, tangential wind profiles at 2^O, 4°, 6°, and 8° radius are shown in Fig. 31. At 2^O and 4° radius (or inner region), the middle to low-level tangential wind increases dramatically and steadily from Stage 1 to Stage 4. The upper-level anticyclonic circulation increases from Stage 1 to Stage 2, but decreases slightly thereafter. At 6° and 8° radius (or outer region), the middle to low-level cyclonic circulation increases significantly from Stage 1 to Stage 2, but the changes are small thereafter. In the upper level, the anticyclonic circulation generally increases from Stage 1 to Stage 4. These results indicate that the vertical anticyclonic wind shear (anticyclonic circulation increase or cyclonic circulation decrease with height) generally increases throughout the whole formation cycle at all radii. This creates a required stronger warm core at the upper troposphere and hydrostatically a lower surface pressure (through thermal wind balance) during tropical cyclone development.
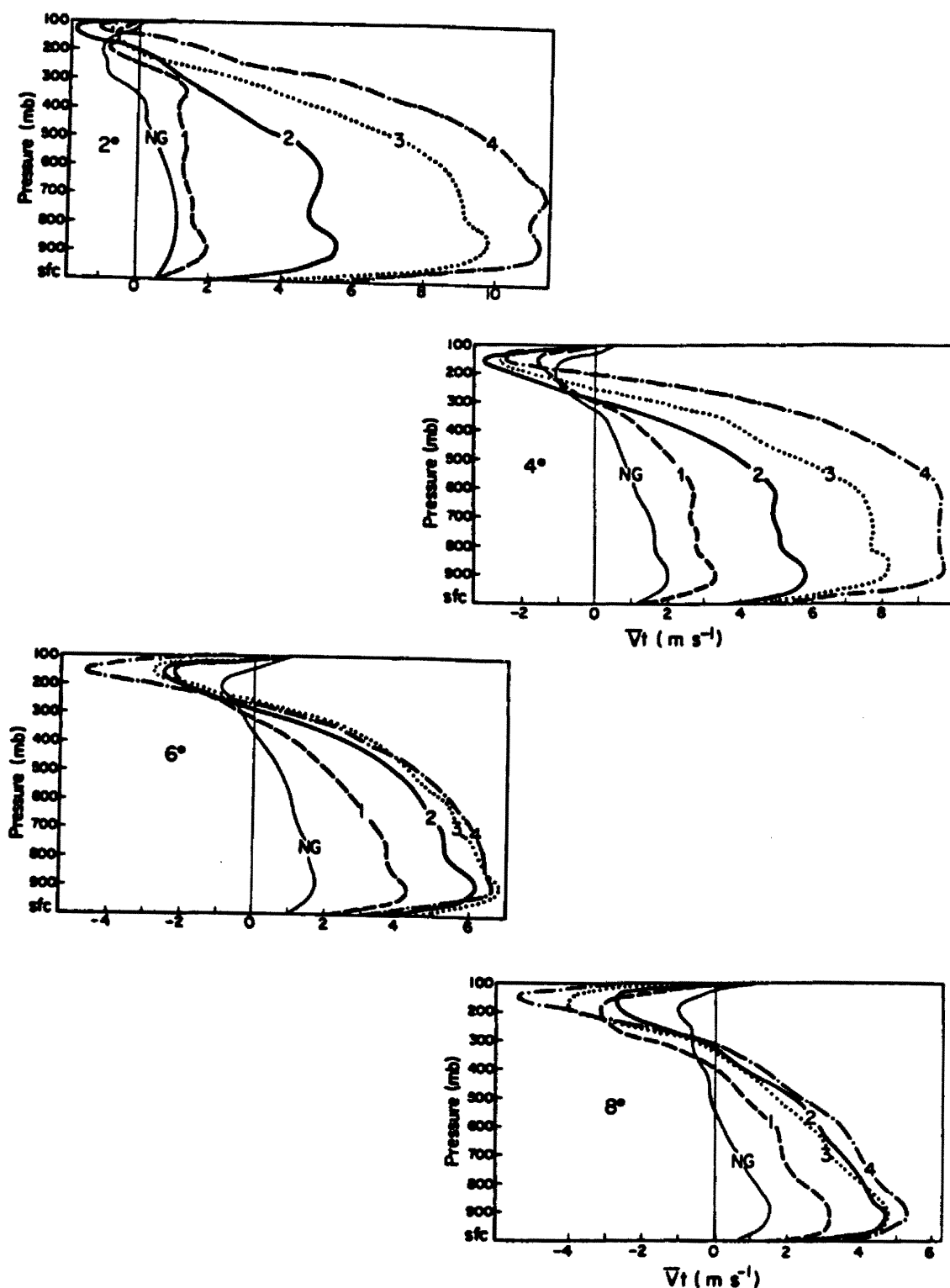
Fig. 31. The vertical profiles of the mean tangential wind at 2^O, 4°,
6°, and 8° radius for the genesis case at Stage 1 (2 days
before, $\leq$ 10 m s^{-1}), Stage 2 (1 day before, $\sim$ 10 m s^{-1}), Stage
3 (incipient tropical cyclone, $\sim$ 15 m s^{-1}) and Stage 4 (1 day
after, $\sim$ 22 m s^{-1}). The non-genesis profile (NG) is shown in
thinner curve.

Compared to the genesis cloud clusters, the non-genesis cloud clusters (NG in Fig. 31) generally have less vertical anticyclonic wind shear. McBride and Zehr (1981) found similar differences between genesis and non-genesis cloud clusters and hypothesized a genesis potential as 0-6° mean vorticity (or $2\overline{V}_t/r$ at 6° radius) difference between 900 mb and 200 mb. They used the 6° radius because that is where the vertical anticyclonic wind shear difference is the largest. The current results also show the largest difference at 6° radius. However, of more significance is that the middle to low-level cyclonic circulation (or mean positive vorticity) at 6-8° radius increases prior to the formation of the tropical cyclone but then shows no further increase thereafter. The upper-level anticyclonic circulation, on the other hand, experiences only a small increase both before and during the formation of the tropical cyclone. Therefore, the buildup of the middle to lower-level cyclonic circulation at 5-9° radius may be more crucial to tropical cyclone formation than the strengthening of the upper-level anticyclonic circulation. In other words, it is necessary to accumulate enough vorticity at the vicinity of a cloud cluster before it can develop into a tropical cyclone.

Since the vorticity at any radius takes into account the radial shear of tangential wind or

$$\overline{\zeta}_r = \frac{\partial r\overline{V}_\theta}{r\partial r} = \frac{\overline{V}_\theta}{r} + \frac{\partial \overline{V}_\theta}{\partial r} ,$$

it can look quite different from the tangential wind field (see Fig. 32). Note that the values of the vorticity are given as a factor of f, or the earth vorticity, which increases from Stage 1 to Stage 4 because
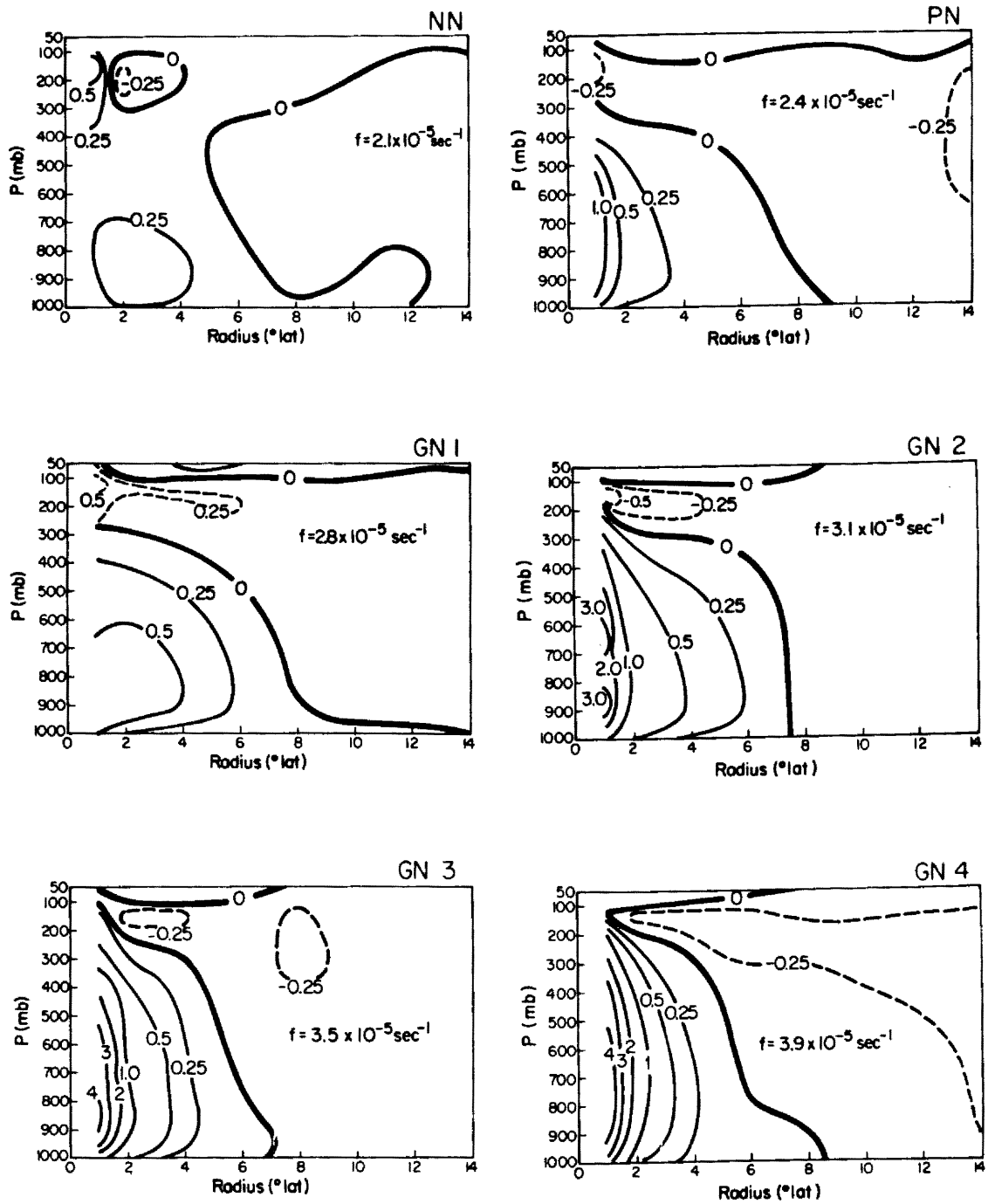
Fig. 32. The cross section of the relative vorticity in terms of the earth vorticity (f) for the genesis case at Stage 1 (2 days before, $\leq$ 10 m s^{-1}), Stage 2 (1 day before, ~ 10 m s^{-1}), Stage 3 (incipient tropical cyclone, ~ 15 m s^{-1}) and Stage 4 (1 day after, ~ 22 m s^{-1}) and the non-genesis cloud clusters (Stage 2 of NN and PN). The heavy curves show the zero lines. The value of f (calculated from the mean latitude) is also shown for each composite.

the system moves poleward. Results indicate that the cyclonic (positive) vorticity generally decreases with height and radius. The positive vorticity does not extend outward very far because the shear term changes sign (becomes negative) beyond the radius where the maximum cyclonic wind is present and cancels out much of the curvature term. The vorticity is generally small beyond this radius.

The vorticity is relatively uniform inside 6° radius at Stage 1 of the genesis case. From Stage 1 to Stage 4 the cyclonic vorticity inside $2-3^{\circ}$ radius increases and extends to higher levels. However, the change is small in the upper levels or beyond $3-4^{\circ}$ radius. The increase of the cyclonic vorticity inside 2° radius from Stage 2 to Stage 3 (during cyclone formation) or from Stage 3 to Stage 4 (after formation) is not as dramatic as that from Stage 1 to Stage 2 (before formation). In other words, a very abrupt pattern change in the vorticity field occurs one day before the formation of the tropical cyclone, but the changes are relatively small during and after the formation. This may indicate that some sudden onset conditions occur.

The non-persistent non-genesis cloud cluster (NN) has a much weaker vorticity field as compared to the other composites. The persistent non-genesis cloud cluster (PN) has a larger vorticity ($\sim$ f) at 1° radius. However, the magnitude is still much smaller than that for the genesis cloud cluster at Stage 2 and the radial extent of the 0.5f vorticity contour is also smaller in the persistent case. In the upper level, the persistent, non-genesis case does not have as strong anticyclonic (negative) vorticity as that for the genesis case.

These results indicate that the concentration of the vorticity and the vertical motion at the inner region of a tropical cloud cluster

(Stage 2) - as shown in Figs. 29 and 32 - is very crucial to tropical cyclone formation. In other words, strong cumulus heating over an area with strong vorticity is very efficient for spinning up the vortex (refer to Hack and Schubert, 1986). Therefore, the processes which can lead to a large increase in the vorticity associated with a tropical cloud cluster are conducive to tropical cyclone formation. It has to be noted, however, that cumulus convection and its associated mean transverse circulation is generally not efficient enough to cause a strong vorticity increase over a large domain at these early stages. (The non-genesis cloud clusters have about the same magnitude of mean vertical motion as the genesis cases, but do not develop to tropical cyclones.) Other processes besides the mean vertical motion or the mean transverse circulation processes must act to bring about the early stage observed vorticity increase.

4.3.3 Vertical Wind Shears

As discussed previously, the non-genesis cloud clusters occur in an environment with a strong zonal and/or meridional vertical wind shear between 500 and 200 mb, which is unfavorable for cloud cluster development. The genesis cloud clusters, however, have less zonal and meridional wind shear between 200 mb and 500 mb. Figure 33 shows $0-3^{\circ}$ averaged zonal and meridional wind profiles - in a motion coordinate - for the first 3 stages of the genesis case and for the non-genesis cloud cluster.

For the genesis cases, the zonal wind profile shows a similar pattern at all 3 stages, with a weak easterly wind shear from the surface to 500 mb and almost no wind shear at 500-200 mb where the maximum warming occurs (Fig. 22). In the meridional direction, the wind
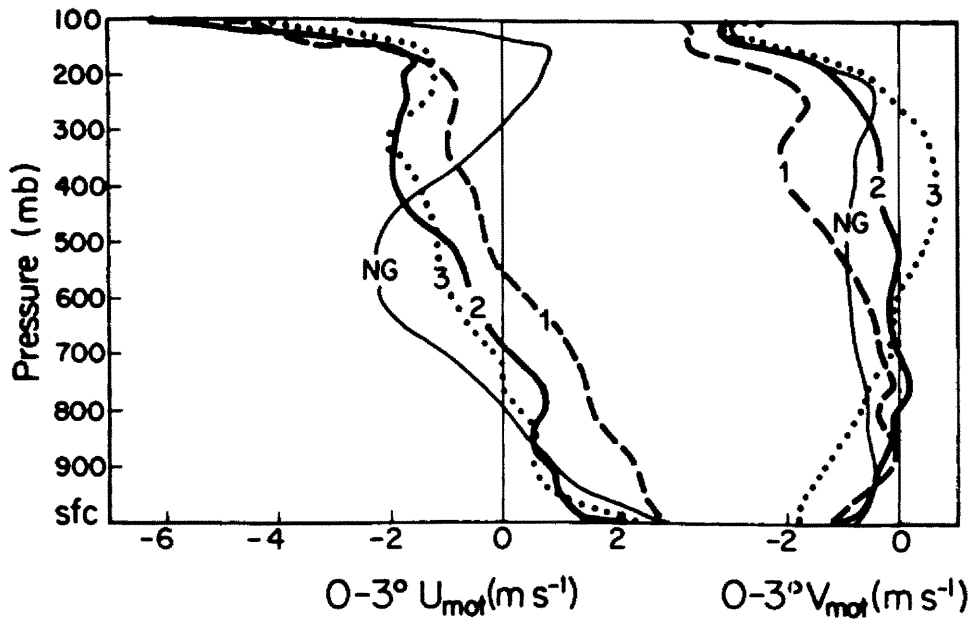
Fig. 33. The 0-3° zonal (left) and meridional (right) wind profiles for the genesis cases at the first 3 stages and for the non-genesis cloud cluster (NG) in the motion or MOT coordinate.

shear between 200 mb and 500 mb is also generally weak. Below 300 mb, it changes from a weak northerly shear at Stage 1 to a weak southerly shear at Stage 3. Note that the average moving direction is toward the northwest, which coincides with the observed easterly and southerly vertical wind shears. In contrast, between 200 and 500 mb the non-genesis cloud clusters have a strong westerly wind shear, opposite to the direction of the cloud cluster movement. This was also observed in the early composite measurements of Williams and Gray (1973). A northerly shear above 300 mb is observed for all composites. In their model simulation, Tuleya and Kurihara (1981) also found that easterly wind shear is preferred for tropical storm formation. It is thus concluded (with some speculation) that a vertical wind shear in the direction opposite to the cloud cluster motion is unfavorable for cloud cluster development.

Gray (1968) has shown that a weak vertical wind shear is required

for enthalpy and for moisture to accumulate in a vertical column, thus creating a favorable environment for tropical cyclone development. He also analyzed the plan views of the zonal wind shear for the pre-cyclone disturbance and found zero shear line in the zonal direction across the system center and strong easterly and westerly wind shears on the equatorward and poleward sides, respectively. McBride (1979) and McBride and Zehr (1981) further compared the 200 to 900 mb wind shear between the genesis and non-genesis cloud clusters and found the genesis cloud clusters to be similar to those described by Gray (1968). McBride and Zehr's results also indicated that the non-genesis cloud clusters had a different vertical wind shear pattern which showed a stronger vertical wind shear between 200 mb and 900 mb at the cloud cluster's inner region. No such zero vertical wind shear line was found for the non-genesis cloud clusters.

The current results generally agree with both Gray's and McBride's results regarding the zonal vertical wind shear for the genesis cases. Figure 34 shows plan views of the zonal and meridional vertical wind shears between 200 mb and 850 mb for the genesis case at Stages 1 and 2, the non-genesis cloud clusters (Stage 2) and the background. The 200 mb to 900 mb wind shears for the non-genesis cloud cluster composite in the western North Pacific by McBride (1979) and McBride and Zehr (1981), also known as the WPN1 data set, is shown as well (N1). Note that these plan views are in a natural coordinate (NAT).

The background composite shows that the zonal vertical wind shear changes from easterly to westerly shear from south to north with a zero line across 2° south of the center. Both non-genesis cases show similar patterns except that the zero line is now right across the system
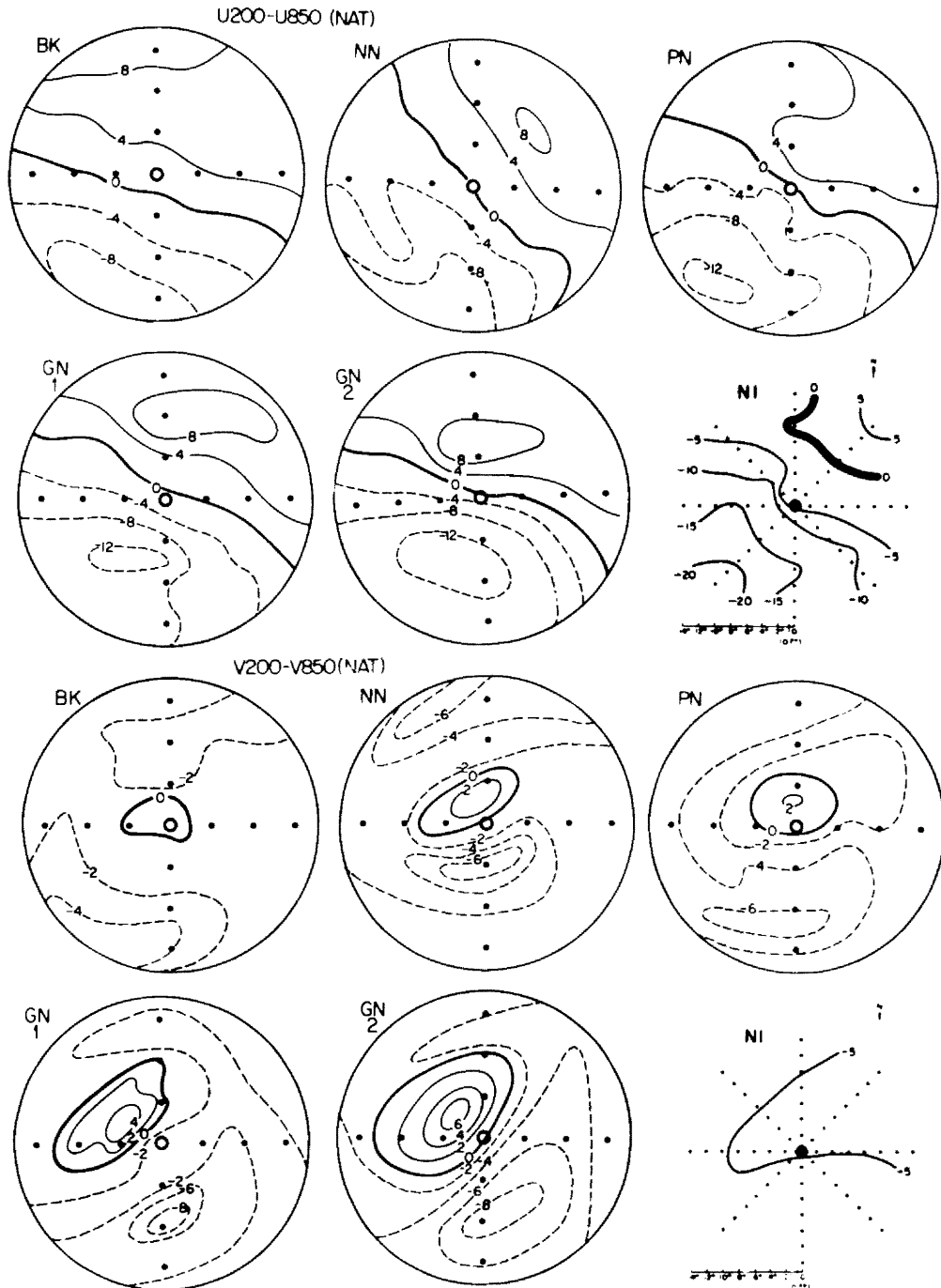
Fig. 34. The 200 mb minus 850 mb zonal and meridional vertical wind
shears in the NAT coordinate for the background composite
(BK), the non-genesis cloud clusters (NN and PN) and the first
2 stages of the genesis composites (GN1 and 2). Heavy curves
are the zero shear lines and dashed curves are the negative
shear lines. The radial grid spacing is 4° latitude.
McBride's (1979) non-genesis composite (N1) is also shown.

center. The genesis case also shows a similar pattern, but the strong shears on both sides have larger magnitudes and move in closer to the center at Stage 2.

In the meridional direction, the northerly shear is present over almost all of the domain for most of the composites. A weak southerly shear is located around the center region for the background composite. For the non-genesis cloud cluster composites, this southerly shear region expands toward the northwest direction and a stronger northerly shear is located to the south-southeast direction. The genesis composites show a similar vertical wind shear pattern except that the southerly shear in the northwest quadrant is stronger and over a larger region. The shear is generally weaker at the center region.

The shear patterns for both the persistent and non-persistent cloud clusters are very similar to each other, and they are also similar to those for the genesis composites. However, the results for the non-genesis cloud cluster by McBride (1979) and McBride and Zehr (1981) are different from the current results. McBride and Zehr's non-developing clusters did not generally have a zero shear with changing sign over the center, as the present results do. Since a much larger data set and better satellite images are used in the current study, the current results should be considered more reliable.

These results suggest that it is more realistic to view the vertical wind shear as a general hindering rather than a conducive parameter as far as early stage cyclone genesis is concerned. This is not to say that vertical wind shear is not a positive factor for later stage intensification, however. A strong upper-level shearing effect certainly will prevent the convection from getting organized; a weak

vertical wind shear near the center is just what is expected for a cloud cluster. However, it is the middle to upper tropospheric vertical wind shear that can seriously hinder the development of a tropical cloud cluster. The plan views of the zonal vertical wind shear between 200 and 500 mb do show a stronger shear around the center region for the non-genesis cloud clusters. An example is given in Fig. 35 which illustrates the 200 mb minus 500 mb zonal wind shear patterns for the persistent cloud cluster (PN) and the genesis case at Stage 2 (GN2).

4.3.4   Upper- and Lower-level Circulation Patterns

The 850 mb and 200 mb streamlines in the motion (or MOT) coordinate system at 4 stages in the genesis case are shown in Fig. 36. At 850 mb, the isotachs are also shown, as are the areas (shaded) with a wind speed greater than 6 m s^{-1}. At 200 mb, isotachs are not shown but the wind
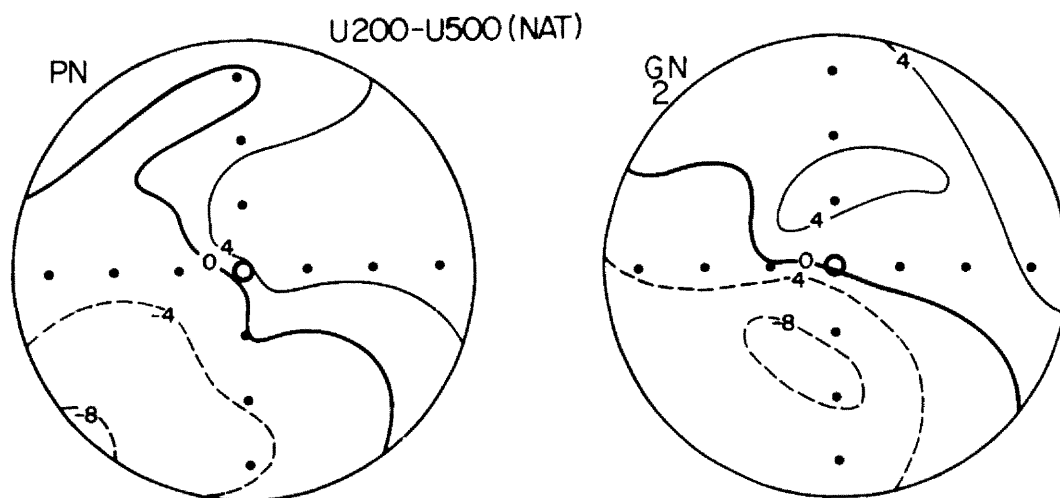
Fig. 35.   The 200 mb minus 500 mb zonal wind shear in the NAT coordinate for the persistent non-genesis cloud clusters (left) and the genesis cloud cluster at Stage 2 (right). Heavy curves are zero lines and negative shear lines are dashed.
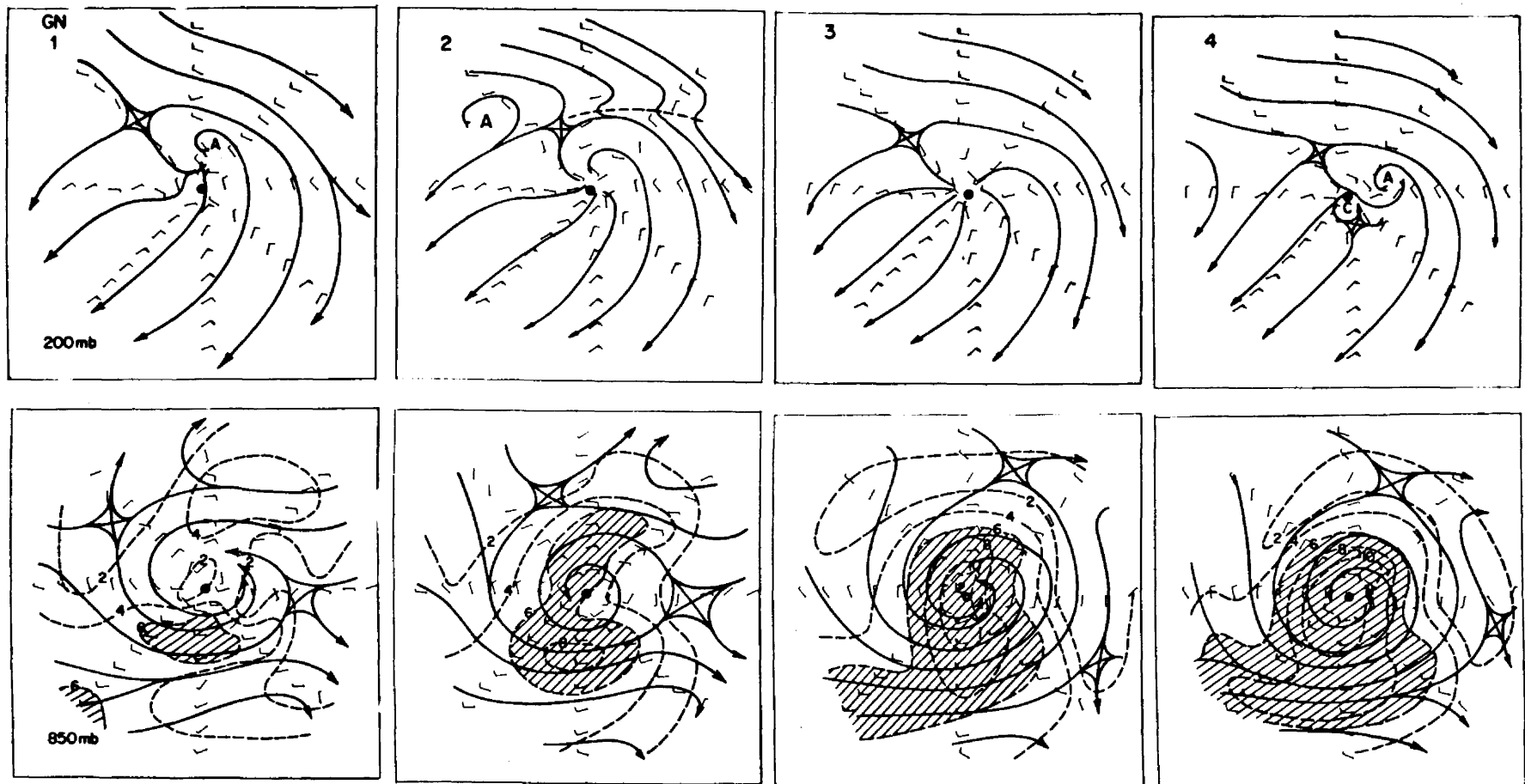
Fig. 36. The 200 mb and 850 mb streamlines in the motion (or MOT) coordinate for the genesis cases at Stage 1 (2 days before, ≤ 10 m s^{-1}), Stage 2 (1 day before, ~ 10 m s^{-1}), Stage 3 (incipient tropical cyclone, ~ 15 m s^{-1}) and Stage 4 (1 day after, ~ 22 m s^{-1}). The isotaches at 850 mb are also shown. The shaded regions are areas with a wind speed ≥ 6 m s^{-1}. The radial grid spacing is 2° latitude.

bars have been plotted. The resulting wind vectors at all levels are fairly smooth.

At 850 mb the cyclonic circulation is elongated in the east-west direction with stronger winds located on the south and north sides at Stage 1. Note that the trade wind on the north side is actually stronger because the system is moving toward the west-northwest direction. The circulation becomes more and more circular as the cloud cluster develops into a tropical cyclone. The isotach patterns also become more symmetric at later stages, although the wind speeds on the east and west sides are still weaker.

There are two important characteristics that need to be emphasized:

1) the strong wind regions are spreading from the environment inward to the center region during the cyclone formation process (Stage 1 to Stage 3). This is in good agreement with the observed surface pressure field evolution.

2) The environmental advection process may play an important role in producing the strong wind in the vicinity of the cyclone center.

The 850 mb circulation at Stage 1 shows a strong trade wind being advected toward the northwest side of the cluster system and a southwest monsoon being advected from the southwest direction toward the south-southeast side of the system. Note that the wind vectors on the southwest quadrant are from the southwest in the natural coordinate. In the western North Pacific, a trade wind to the north of the system is a prevailing feature; therefore, the southwest monsoon influence from the southwest direction appears to be very important to the cyclone formation. This subject will be discussed in more detail in Chapters 7

and 9.

At 200 mb, the circulation pattern has an anticyclonic center located above the system center and is relatively unchanged throughout the 4 stages. At Stage 4, the strong cumulus convection produces a forced cyclonic outflow at the center and pushes the anticyclone center toward the northeast direction. A trough is analyzed to be located at the north-northeast direction at Stage 2 but not at Stage 1 or Stage 3. Although this trough pattern shows up as relatively discontinuous in time, it is suspected that, to make this upper trough appear in the composite, there should be many individual cases located under an environment with an upper trough (such as a tropical upper tropospheric trough (TUTT)) in their vicinity. The tropical cyclone formation cases with this specific upper trough feature also will be discussed in Chapters 7 and 9.

At the upper troposphere the circulation pattern generally shows a big anticyclonic ridge around most of the domain; however, the flow at 100 mb is relatively undisturbed. Figure 37 shows the streamlines and wind vectors at 100 mb for the genesis case at Stages 2 and 4. The prevailing flow is basically from the northeast direction with an anticyclone located off the domain to the northwest direction. These results indicate that the flow above the tropopause (about 110-120 mb) does not have a direct influence on cyclogenesis, nor does the cyclone's associated convection substantially alter the flow pattern above the tropopause – at least at the formation stages.

When comparing the circulation patterns between the genesis (Stages 1 and 2) and the non-genesis cloud clusters (Figs. 17 and 18), the largest differences are found at the low level (850 mb). At 200 mb, the
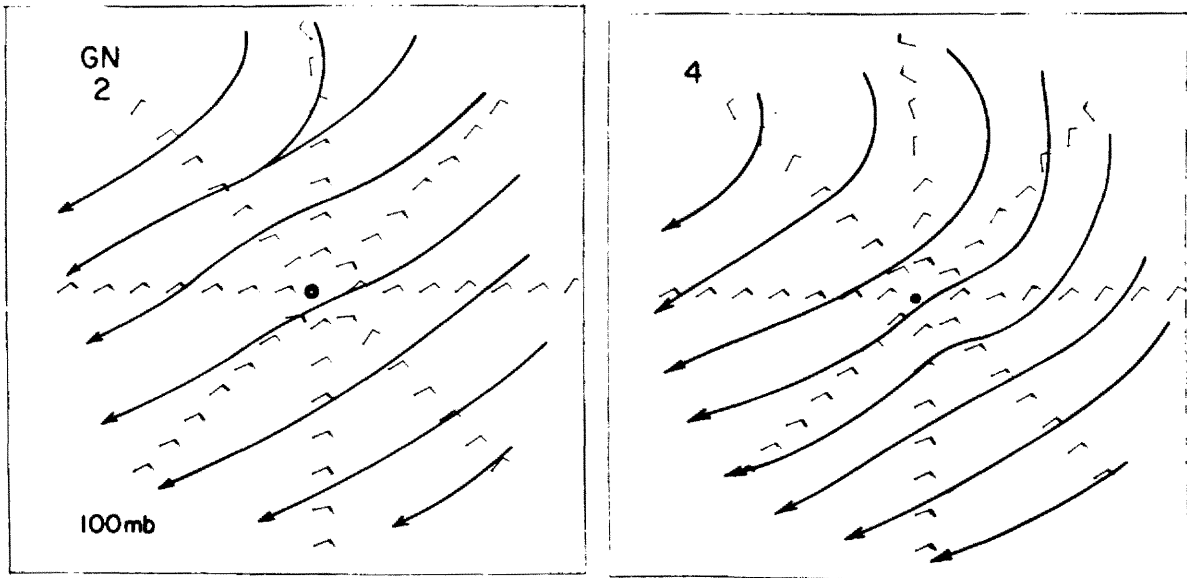
Fig. 37. The 100 mb streamlines for the genesis case at Stages 2 and 4. The radial grid spacing is 2° latitude.

overall circulation patterns for the genesis and non-genesis cloud clusters are very similar except that the anticyclonic center is stronger for the genesis case and the wind vectors for the non-genesis cases are slightly noiser. At 850 mb, the non-genesis cases have a reasonably good convergent field; however, the cyclonic vorticity is much weaker when compared to the genesis case. The genesis case also shows a concentration of the cyclonic circulation near the center before cyclogenesis, while non-genesis cases do not.

4.4 Summary

The important characteristics of the tropical cyclone formation processes and the important differences between the genesis and non-genesis cloud clusters are summarized as follows:

1) The pre-cyclone cloud clusters are generally located in a large-scale environment which gives a weak pressure fall (within a magnitude of 0.5 to 1 mb) over a very large domain. This pressure drop creates a strong pressure gradient at larger radii with respect to the

cluster center. As the cloud cluster develops into a tropical cyclone, the pressure drop is concentrated at the inner radii. The temperature field and vertical tangential wind shear evolutions correspond to the surface pressure field very well. The non-genesis cases show a weaker pressure gradient, with the pressure drop occurring over a much smaller area and being smaller in magnitude.

2) The genesis composites - especially in the inner region show a higher moisture content and higher θ_e values compared to the non-genesis composites. This is due to the concentrated cumulus activities in the genesis case. The environmental θ_e values for the genesis case show little change throughout the 4 formation stages. In short, the moisture field or θ_e values do not show a direct link to cyclogenesis, although a moistening process at the middle levels is important to the formation of the cloud cluster.

3) The genesis (Stages 1 and 2) and non-genesis cloud clusters generally have about the same amount of maximum mean vertical motion over the $0-4^o$ or $0-6^o$ region. The genesis case, however, shows an environmentally forced low-level convergence that reaches the inner region at Stage 2, and a convection burst is observed at Stage 3 (during the formation of tropical cyclone).

4) In contrast to the non-genesis cases, the genesis cloud cluster has a stronger middle to low-level cyclonic vorticity which spreads over a larger area. A beginning concentration of this vorticity is observed at Stage 2 or before the formation of the tropical cyclone. It is associated with the environmentally forced low-level convergence which reached the inner region at this time. A convection burst associated

with cyclone formation is observed within 24 hours after this time period.

5) A strong large-scale trade wind surge or a strong southwest monsoon surge might be the catalyst for the increase and the concentration of the vorticity near the vicinity of the pre-cyclone cloud cluster.

6) Based on the results presented above, it is hypothesized that cyclone formation processes are mainly dictated by the system's surrounding large-scale circulation patterns which initially causes a large buildup of the low-level cyclonic vorticity near the vicinity of the pre-cyclone cloud cluster. The cyclone's internal dynamics start to play an important role only after the cyclonic vorticity increases by a sizable amount (Stages 2-3) and the cloud cluster gets itself better organized.

5. ENERGY AND MOISTURE BUDGETS

Yanai, Esbensen and Chu (1973) defined the apparent heat source (Q_1) and the apparent moisture sink (Q_2) as:

$$Q_1 = \frac{\partial \hat{s}}{\partial t} + \widehat{\nabla \cdot s V} + \frac{\partial \widehat{\omega s}}{\partial p} = \hat{Q}_R + \widehat{L(C-E)} - \frac{\partial}{\partial p}\widehat{s'\omega'} \tag{1}$$

$$Q_2 = -L(\frac{\partial \hat{q}}{\partial t} + \widehat{\nabla \cdot q V} + \frac{\partial \widehat{q\omega}}{\partial p} = \widehat{L(C-E)} + L\frac{\partial}{\partial p}\widehat{q'\omega'} , \tag{2}$$

where s is the dry static energy, or $s = C_p T + gZ$, Q_R the radiational heating rate, C the condensation rate, E the evaporation rate and L the latent heat. The overhat ($\wedge$) represents the horizontal area average and the prime (') the deviation from the horizontal average. The terms $\widehat{s'\omega'}$, $\widehat{q'\omega'}$ are mainly due to the cumulus convective transports.

From Eqs. 1 and 2, we obtain:

$$Q_1 - Q_2 - Q_R = -\frac{\partial}{\partial p}\widehat{(s'+Lq')\omega'} = -\frac{\partial}{\partial p}\widehat{h'\omega'} , \tag{3}$$

where h is the moist static energy or $h = C_p T + gZ + Lq$. The $-\widehat{h'\omega'}$ is a measure of the vertical eddy transport of total energy (kinetic energy can be neglected) and can be used to measure the cumulus convection. Assuming no vertical motion across 100 mb, Eq. 3 can be integrated vertically to yield:

$$F_{p1} = -\frac{1}{g}\widehat{(h'\omega')}_{p1} = -\frac{1}{g}\int_{100}^{p1} (Q_1-Q_2-Q_R)dp, \tag{4}$$

where F_{p1} is the vertical eddy transport of total energy at any pressure level p1. Since Q_1 and Q_2 can be calculated from composite data and Q_R can be estimated, F_{p1} thus can be obtained.

Integrating Eq. 1 and Eq. 2 vertically from 100 mb down to the surface yields, after some rearrangements,

$$\frac{1}{g} \int_{100}^{sfc} (Q_1 - Q_R) dp = LP_{sfc} + S_{sfc} , \text{ and} \qquad (5)$$

$$\frac{1}{g} \int_{100}^{sfc} (Q_2) dp = L(P_{sfc} - E_{sfc}) , \qquad (6)$$

where P_{sfc} is the precipitation, and S_{sfc} and E_{sfc} the surface sensible heat flux and the surface evaporation, respectively. To estimate the precipitation, surface sensible and latent energy flux (or evaporation), a Bowen ratio has to be assumed. The Bowen ratio is defined as the ratio of surface sensible energy flux to latent energy flux, or $B = S_{sfc}/LE_{sfc}$. Integrating Eq. 3 from 100 mb to the surface or combining Eq. 5 and Eq. 6 gives:

$$F_{sfc} = \frac{1}{g} \int_{100mb}^{sfc} (Q_1 - Q_2 - Q_R) dp = S_{sfc} + LE_{sfc} \qquad (7)$$

where F_{sfc} is the total surface energy flux, which includes both the sensible and the latent energy fluxes.

Yanai et al. (1973) and many other researchers (e.g. Johnson, 1976, 1980) have developed complicated diagnostic models to estimate cloud ensemble properties, such as the exchanges of mass, heat, moisture and liquid water between the cloud ensemble and its environment, and the vertical cloud mass flux. The focus of this study, however, is placed on the large-scale horizontal energy and moisture transports, the total vertical energy flux by cumulus convection, the surface energy flux and the precipitation. A Bowen ratio of 0.1 is used. Yanai et al. computed the time averaged Bowen ratio to be 0.076, and other estimates

all are around this number. Since the surface sensible heat flux is generally much smaller than the surface latent energy flux, the surface evaporation estimated from Eq. 7 by assuming B = 0.1 is quite reliable. The estimated precipitation, from Eq. 6, should also be quite reliable.

5.1 Calculation of Q_1, Q_2 and Q_R

In a moving coordinate, the wind vector in the above equations should be taken as a motion wind vector, that is, with system (coordinate) moving speed being subtracted out. Since the composite technique uses a cylindrical coordinate, the horizontal convergence term takes the form,

$$\widehat{\nabla \cdot A \mathbf{W}} = \frac{\overline{\partial r V_r A}}{r \partial r},$$ (8)

where A is S, q or h; V_r the radial wind; and the overbar (–) the azimuthal average at any radius. Integrating Eq. 8 from r_1 to r_2 and around the azimuth, then dividing by the area $\pi(r_2^2 - r_1^2)$ gives

$$\widehat{\nabla \cdot A \mathbf{V}}_{r_1 - r_2} = \frac{2[\overline{(rV_r A)}_2 - \overline{(rV_r A)}_1]}{(r_2^2 - r_1^2)}$$ (9)

If $r_1 = 0$, Eq. 9 becomes:

$$(\widehat{\nabla \cdot A \mathbf{W}})_{0-r_2} = \frac{2\overline{v_r A}}{r_2}$$ (10)

where r_2 can be any radius.

The term $\overline{rV_r A}$ in Eq. 9 represents the azimuthal average of total flux $rV_r A$. In the current coordinate system there are only eight azimuthal grids, which is not an adequate number to represent the horizontal fluxes when there are lots of transient features (like squall lines) moving in a radial direction. Also, the time resolution of the

current composites is not adequate to represent the time transient features. An attempt is thus made to calculate the quantity $r \times V_r \times A$ for each individual sounding and then take the average with respect to each grid box (2° radius by 45° azimuth, as shown in Fig. 2). The grid values of rV_rA around the azimuth are then averaged to represent the average total flux, or $\overline{rV_rA}$. Unfortunately, the values of s in the upper levels are very large due to the large height values there. A slight noise in the upper-level height field can cause a severe problem in this type of estimation.

To illustrate this problem, we decompose the total flux (TF) into the mean flux (M), the standing eddy flux (SE) and the transient eddy flux (TE) or

$$TF = M + SE + TE ,$$

where $TF = \overline{rV_rA}$ and ($r \ V_r \ A$) is estimted from each individual sounding. The mean flux (M), the standing eddy flux (SE) and the transient eddy flux (TE) are defined as:

$$M = \bar{r} \ \overline{V_r} \ \bar{A},$$

$$SE = \overline{[r] \ [V_r] \ [A]} - \bar{r} \ \overline{V_r} \ \bar{A}, \text{ and}$$

$$TE = \overline{rV_rA} - SE - M = \overline{rV_rA} - \overline{[r] \ [V_r] \ [A]}$$

where bracket ([ ]) is the grid box average or the grid point value. The tropospheric mass-weighted averages of these components of moist static energy (h) flux for the first 3 stages of the genesis cases are shown in Table 5.

The mean radial h flux (M) is very realistic (generally exporting h) throughout these stages at all radii. The radial h flux by the standing eddy (SE) is also realistic (generally importing h), but is of

TABLE 5

Tropospheric mass-weighted average of mean (M), standing eddy (SE) and transient eddy (TE) fluxes of moist static energy $(rV_r h)$ for genesis case at Stages 1, 2 and 3. (Unit in degree latitude $\bar{x}$ $(m\ s^{-1})$ x (kilo Joule/KG)).

Radius	2^O	4°	6°	8°	10°	12°	14°
Stage 1							
Mean	-0.7	5.6	14.0	29.9	30.9	49.7	64.9
SE	-0.7	-0.4	-1.2	-2.0	-4.0	-3.4	-20.8
M+SE	-1.4	5.2	12.8	27.9	26.9	46.3	44.1
TE	-24.6	-82.8	-109.8	-52.8	-68.4	-0.4	46.7
TOTAL	-26.0	-77.6	-97.0	-24.9	-41.5	45.9	90.8
Stage 2							
Mean	5.3	6.8	16.2	28.8	27.8	49.1	70.6
SE	-0.2	-1.1	-1.2	-4.3	-7.0	-11.8	-17.8
M+SE	5.1	5.7	15.0	24.5	20.8	37.3	52.8
TE	42.6	-49.2	28.5	-5.3	73.9	70.6	16.1
TOTAL	47.7	-43.5	43.5	19.2	94.7	107.9	68.9
Stage 3							
Mean	6.1	15.6	24.6	29.2	41.7	50.2	76.5
SE	0.4	-0.8	-2.5	-6.5	-10.9	-12.7	-11.4
M+SE	6.5	14.8	22.1	22.7	30.8	37.5	65.1
TE	-10.8	-39.3	25.1	-33.0	25.4	65.7	53.5
TOTAL	-4.3	-24.5	47.2	-10.3	56.2	103.2	118.6

much smaller magnitude. (The standing eddy is a measure of the asymmetry and is estimated only by the 8 octants in the current system.) The calculated transient eddy flux (as a residual), however, exhibits very large variations along the radius. The magnitude of TE, unfortunately, is generally large and dominant. For example, at Stage 2 the TE term changes from +42.6 at 2^O to -49.2 at 4° and to +28.5 at 6° radius, while the mean term changes from 5.3 to 6.8 and to 16.2. The changes in the TE term from Stage 1 to Stage 3 are also erratic. Since

the total term is dominated by the TE term, any noise in the TE term will affect the total term greatly. When the total h fluxes were used in the energy budget analysis, the results were noisy and unrealistic. Therefore, it is not feasible to use the total term in the current budget studies. Only the mean and the SE term are used in the Q_1 and Q_2 calculations, and realistic results are obtained -- as will be seen later. Yanai et al. (1973) did not include transient eddies in their calculations either (only 5 stations were used).

It is possible to use this total term in the composite study if the climatological and latitudinal bias of height and temperature can be taken out and a massive data sample is used. However, the author doubts that this would significantly improve on the current results which use only the mean and standing eddy fluxes.

The total s flux is about as noisy as the total h flux, but the latent heat flux is reasonably realistic. (The mean term dominates for the latent heat flux.) Apparently, it is possible to use the total term in evaluating Q_2; however, only the mean and the standing eddy terms are used in evaluating Q_2 as well as Q_1.

The $\frac{\partial s}{\partial t}$ and $\frac{\partial q}{\partial t}$ terms for both of the non-genesis cases are taken to be zero, that is, the cloud clusters are assumed to be in a steady state. This assumption is generally good for the persistent cloud clusters because they were at their prominent cloud cluster stage when they were composited. It might not be so realistic for the non-persistent cloud cluster because of its short duration. In other words, the time resolution of the composite is not capable of resolving the non-persistent cluster's rapid changes over time. For the genesis case, the time period between any two consecutive time periods is exactly one

day. For example, Stage 1 will develop into Stage 2 in one day and the difference between Stage 2 and Stage 1, dividing by 1 day, is considered the local change rate $\partial/\partial t$ at Stage 1. Because these genesis composites are carefully made to study the time evolution, the evaluation of the local change term is very good.

The values of Q_1 and Q_2 at any radial belt, e.g. $0-2^\circ$, $2-4^\circ$, ..., etc., can be calculated simply by using Eqs. 1 and 2 (the flux form). Unfortunately, the horizontal and vertical flux convergent terms are generally very large and of opposite sign, and Q_1 and Q_2 are the residuals of these two large terms (the local changing rate is generally small). The values of Q_1 and Q_2 at any radius therefore also are computed using the advection forms of Eqs. 1 and 2; or

$$Q_1 = \frac{\overline{\partial s}}{\partial t} + \overline{V_r \ (\partial s/\partial r)} + \overline{\omega} \ (\partial \overline{s}/\partial p), \text{ and} \tag{11}$$

$$Q_2 = -L(\frac{\overline{\partial q}}{\partial t} + \overline{V_r \ (\partial q/\partial r)} + \overline{\omega} \ \frac{\partial \overline{q}}{\partial p}). \tag{12}$$

In Eqs. 11 and 12 the values of the horizontal advection term are generally small and the vertical advection term dominates. Since the variations of $\partial s/\partial p$ and $\partial q/\partial p$ between different composites are relatively small, the calculated Q_1 and Q_2 patterns are thus largely determined by the mean vertical motion pattern.

Results indicate that the calculated Q_1 and Q_2 values using the advection form agree very well with those using the flux form (but at different radial regions). An example of the radial-pressure cross section of the calculated Q_1 and Q_2 using the flux form at 1°, 3° ...(in representing $0-2^\circ$, $2-4^\circ$... radial belts) and advection form at 2°, 4°, ...etc. is shown in Fig. 38 for Stage 2 of the genesis case. The

patterns of Q_1 and Q_2 are fairly similar to that of the mean vertical motion (Fig. 29). The Q_2 generally has a maximum value at a lower level than Q_1 because the moisture (q) decreases greatly with height. The Q_1 and Q_2 for the genesis case at Stage 4 are not calculated because no later stage can be used to estimate the local change rate.

In the following energy and moisture budget analyses, two regions, $0-4^O$ and $4-8^O$, are extensively studied. The $0-4^O$ region covers most of the cumulus activities associated with a tropical cloud cluster or tropical cyclone. The study by Arnold (1977) indicates that the radial extent of the total cyclone-associated cloudiness of the western North Pacific systems is about $4-5^O$ radius at the early stages. The $0-4^O$ radius area is also comparable to the pentagon used by Yanai et al. (1973). The $4-8^O$ region represents the environment surrounding a tropical cloud cluster or tropical cyclone and is assumed to be mostly clear or partly cloudy. The calculated Q_1 and Q_2 profiles for these two regions depends primarily on the quality of the data (especially for the radial wind) at 4° and 8° radius where data are most reliable.

The radiational profiles Q_R for the clear and dense cirrus overcast regions used by Frank (1977b) are used in this study (figure not shown). The Q_R profile for a region can be obtained by averaging the cloudy and clear profiles according to the percentage of cirrus cloud coverage over that region. The percentages of the area covered by convective and cirrus clouds at different square regions (Arnold, 1977) are used to represent the values at radii corresponding to these regions. (An
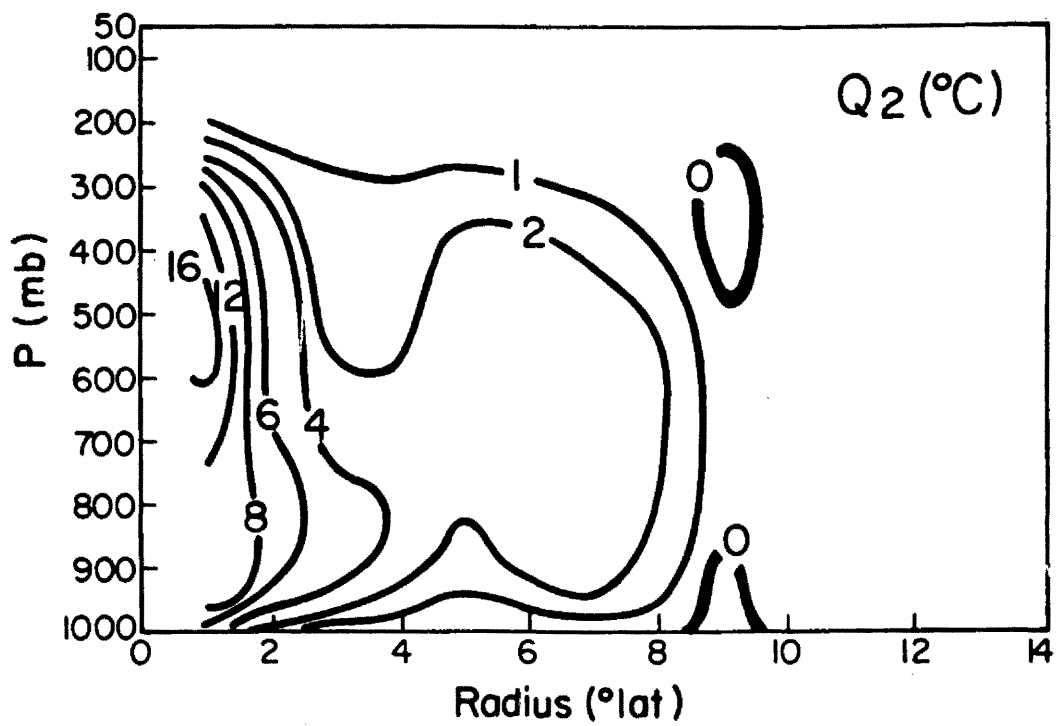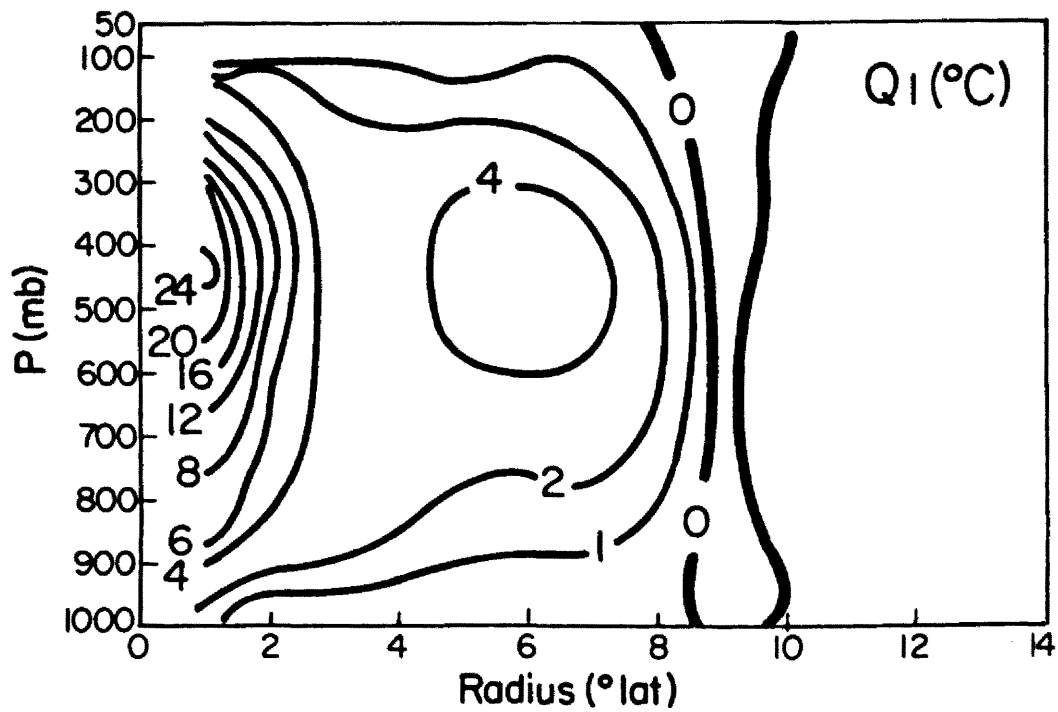
Fig. 38. The cross section of Q_1 (top) and Q_2 (bottom) in °C d^{-1} for Stage 2 of the genesis case.

averaged radius is estimated for each square region.) The cloudiness

values of the $0-4^{\circ}$ and $4-8^{\circ}$ radial belts used for each composite can

thus be estimated. The results indicate that the cloudiness variations

from cloud cluster stage to tropical storm stage are relatively small

compared to the radial variations.

5.2 Moisture and Energy Budgets of the Background Composite

Since the purpose of the background composite is to give the

average conditions for the western North Pacific where cyclones might

form, it is quite beneficial to have the average Q_1 and Q_2 profiles and

to estimate the average surface energy flux and precipitation over this

region. It is somewhat surprising to find that the surface energy flux

is very stable for the different regions of the background composite.

Values are 150, 161, 155, 148, 159 and 148 watt m^{-2} for the regions of

$0-4^{\circ}$, $4-8^{\circ}$, $0-6^{\circ}$, $6-10^{\circ}$, $0-8^{\circ}$ and $8-12^{\circ}$ radius, respectively. Because

there are still small differences between the different regions, a

linear average of the $0-4^{\circ}$, $0-6^{\circ}$ and $0-8^{\circ}$ regions is taken to represent

the average background Q_1 and Q_2 profiles. (Note that the data at 4°,

6°, and 8° are extremely good.) The results are shown in Fig. 39, in

which the Q_R profile is obtained by assuming 15% cloudiness. The

maximum Q_1 value is located at a higher level than the maximum Q_2 value.

These patterns are very similar to those of Yanai et al. (1973) – and

our project's many other similar calculations – but the magnitudes are

smaller.

The energy and moisture budgets are obtained by integrating these

Q_1, Q_2 and Q_R profiles from 100 mb (assumed tropopause) to the surface

and by assuming a Bowen ratio of 0.1. Results are portrayed in the

different units of watt m^{-2}, cm d^{-1}, and $^{\circ}C$ d^{-1} in Table 6. The

conversion between these units is also given. To keep a consistent

unit, the standard M.K.S. system (or watt m^{-2}) will be used in the

illustrations unless otherwise indicated. For individuals more used to

other units, simple approximations can be used:

300 watt $m^{-2} \sim 1$ cm d^{-1} precipitation or evaporation ,and

100 watt $m^{-2} \sim 1^{\circ}C$ d^{-1} warming of the troposphere (900 mb

depth atmosphere).
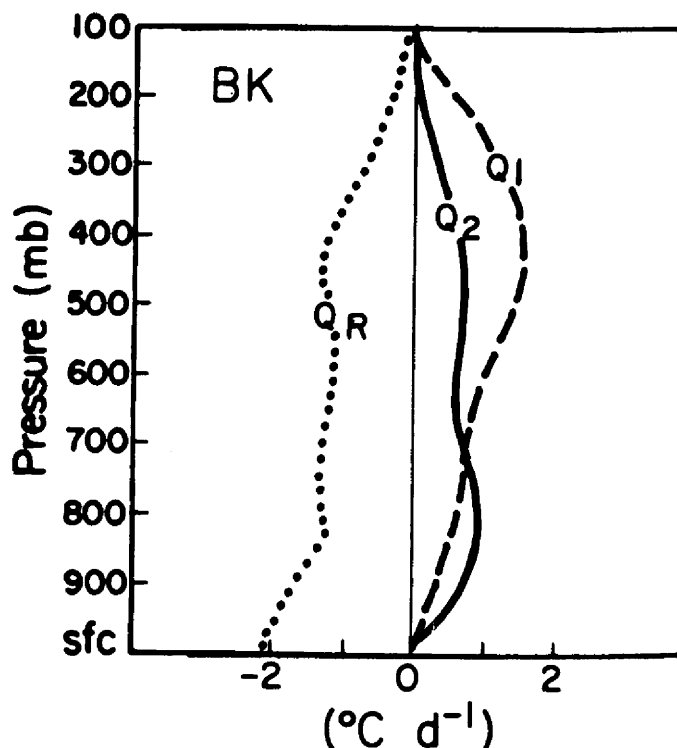
Fig. 39. The vertical profiles of Q_1 and Q_2 for the background (BK)
composite. Averages of the 0-4°, 0-6°, and 0-8° regions are
taken to give these profiles.

A schematic illustration of the energy and moisture budget for the

background composite (BK) is shown in Fig. 40. This diagram shows some

interesting results: 1) about 70% of the precipitation comes from

local evaporation and 30% from horizontal moisture convergence; 2) about

TABLE 6

Energy (h) and moisture (q) budgets for the background composite. Results are given in different units. Conversion between units is also shown.

Unit:	Watt m^{-2}	$cm\ d^{-1}$	$^{o}C\ d^{-1}$*
Horizontal h flux convergence	-34	-0.12	-0.33
Radiational heating (Q_R)	-119	0.41	-1.15
Surface energy flux (Evap + S_{sfc})	153	0.53	1.48
Horizontal q flux convergence	54	0.19	0.62
Surface precipitation	192	0.66	1.84
Surface Evaporation	138	0.47	1.32

$1\ cm\ d^{-1}$ (precipitation) = 290 watt m^{-2} = 2.78 $^{o}C\ d^{-1}$
$1\ ^{o}C\ d^{-1}$ (warming of troposphere) = 104 watt m^{-2} = 214 cal $cm^{-2}\ d^{-1}$
1 watt m^{-2} = 2.06 cal $cm^{-2}\ d^{-1}$

*Note: The troposphere is considered to be between the surface and 100 mb (or about 900 mb thick).

80% of the surface energy flux goes to balance the radiational loss; and 3) the tropical western North Pacific is primarily exporting energy, at a magnitude about 20% of its total surface energy flux or about 34 watt m^{-2}. Although these results were just as expected, it is important to show them quantitatively so that the budgets of the cloud clusters can be compared against them.

5.3 Moisture and Energy Budgets of Non-genesis Cloud Clusters

The Q_1 and Q_2 profiles for both non-persistent (NN) and persistent
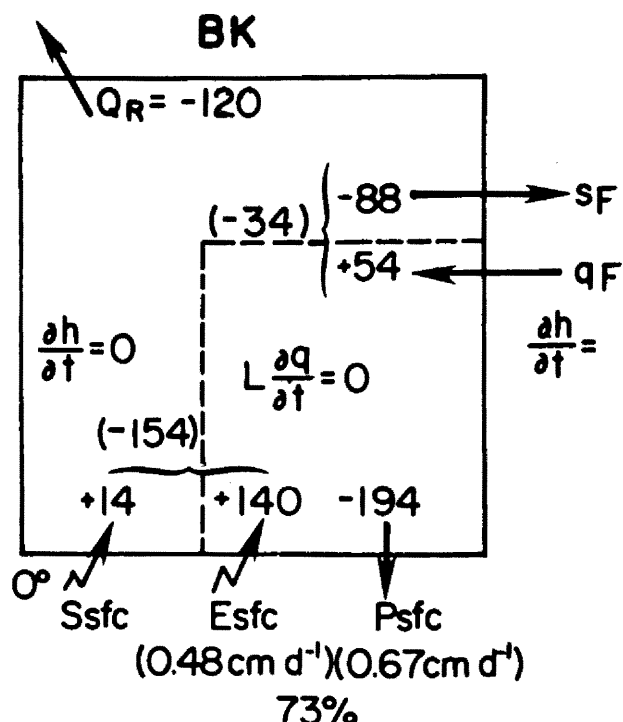
Fig. 40. Schematic diagram showing the different energy and moisture budget terms for the background composite. Units are watt m^{-2} (or cm d^{-1} where so noted). The arrows within the dashed box (at the bottom, right corner) show terms for the moisture budget. Dry static energy and latent energy flux convergence are represented by sF and qF, respectively. The percentage of the total precipitation that comes from the local evaporation is shown also.

(PN) non-genesis cloud clusters at the $0-4°$ and $4-8°$ regions are shown in Fig. 41. The profiles for these two composites are almost identical in the $0-4°$ radius region. The Q_1 profile is fairly similar to that shown in Yanai et al. (1973) except the maximum magnitude for the current profile is slightly larger. Note that the area used in Yanai et al. is about $6°$ latitude by $10°$ longitude, or about the same area as the $0-4°$ radial region used here. The Q_2 profile shows a maximum at 450-500 mb and a secondary maximum at 800-850 mb. The Q_2 profile of Yanai et al. (1973) however, shows the maximum value at 800 mb and a secondary maximum at 500 mb.
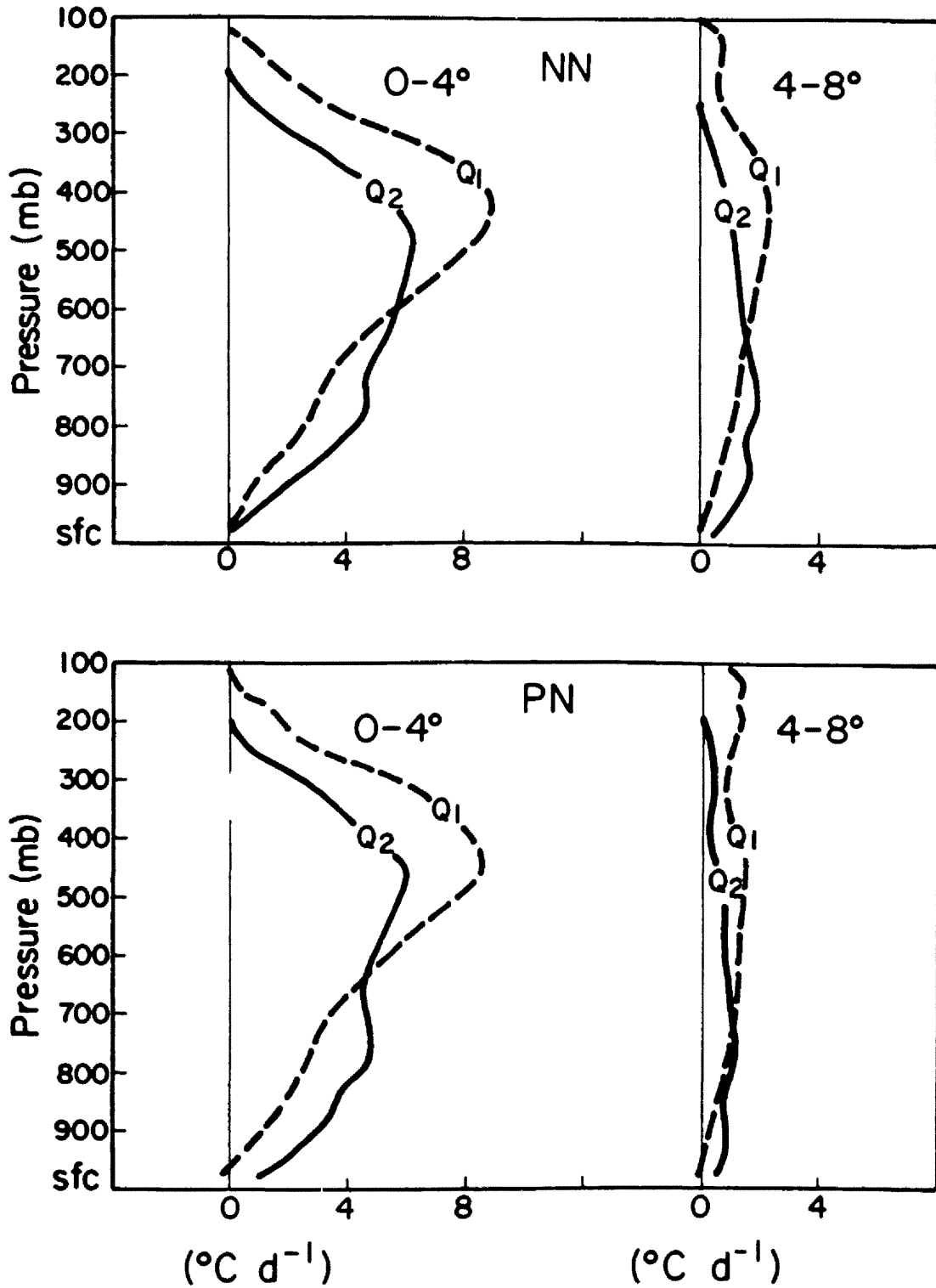
Fig. 41. The Q_1 and Q_2 profiles for the persistent (bottom) and non-persistent (top) cloud clusters at 0-4° and 4-8° regions.

The Q_1 and Q_2 profiles in the 4-8° region have much smaller magnitudes and are similar to the background profiles. The data appear to be noiser at the upper level as some data on the poleward side pick up the westerly influence. Nevertheless, these Q_1 and Q_2 profiles are very realistic and the moisture and energy budgets made from them should be quite reliable. The cloud coverage at 0-4° and 4-8° is assumed to be 60% and 23%, respectively, based on the data adopted from Arnold (1977). Note that taking an area average of 0-4° and 4-8° is likely to reduce the possible error in the radial distribution of the cloud coverage.

The moisture and energy budgets for both of the non-genesis cloud clusters in the 0-4° and 4-8° regions are depicted in Fig. 42. The terms involving the horizontal fluxes (sF and qF) are essentially the horizontal flux convergences. The results indicate that the energy and moisture budgets for both cases (NN and PN) -- including the precipitation, the surface evaporation and the sensible energy flux -- are very similar. The non-persistent cloud cluster has a slightly larger surface energy flux at the 0-4° radius. Such remarkable consistencies in the moisture and energy budgets, as well as in other parameters (e.g., vertical motion), give added credibility to these data sets.

The results depicted in Fig. 42 show some important characteristics of conservative (non-intensifying) cloud clusters in the western North Pacific:

(1) Cloud clusters rain about 1.7 cm per day over an area of 8° diameter domain, while their environment (4-8°) rains about 0.8 cm per day (very close to the background value of about 0.7 cm d^{-1}).
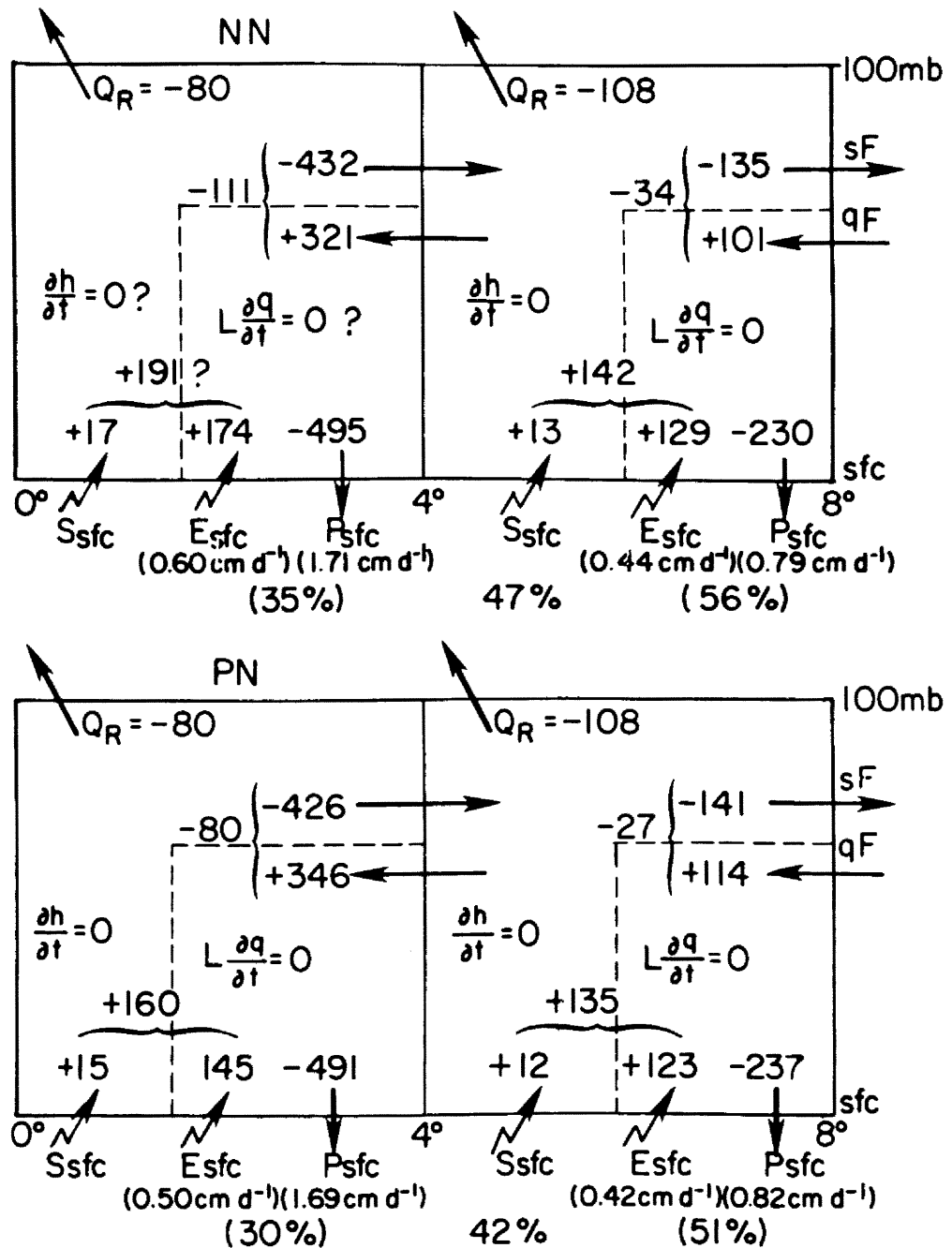
Fig. 42. Schematic diagram showing the energy and moisture budgets for both persistent and non-persistent cloud clusters at the 0-4° and 4-8° regions. Unit is watt m⁻² (or cm d⁻¹ where so noted). The arrows within the dashed box (at the bottom, right corner) show terms for the moisture budget. The horizontal dry static energy and latent energy flux convergence are represented by sF and qF, respectively. The percentages of the total precipitation which comes from the local evaporation are shown for the 0-4°, 0-8°, and 4-8° regions.

(2) The surface evaporation is relatively invariant across the
whole region. The amount is about 0.4-0.5 cm per day (about
the same as the background value) and the cluster regions
have slightly larger values.

(3) Only about 30% of precipitation within the cloud cluster region
($0-4^o$) comes from local evaporation. The local evaporation
at the $0-8^o$ radius region still accounts for less than 50%
of the local precipitation. The horizontal moisture flux
makes up more than half of the local precipitation amount.
These results are quite different from those of the background.

(4) The cloud clusters export a large amount of dry static energy.
About three-quarters of this loss is compensated for by the
latent energy import.

(5) About half of the total surface energy flux goes to compensate
for the radial export energy loss associated with the transverse
circulation. The other half goes to balance the radiational
loss.

Although these results show remarkable consistency between the two
non-genesis cases and, at $4-8^o$, are also similar to those of the
background composite, a few uncertainties still need to be noted. The
first is that the horizontal fluxes by the transient eddies are
neglected. These fluxes are likely not negligible when an active
transient banding feature is present. Fortunately, this does not seem
to affect the current energy and moisture budget analyses. The other
uncertainties are the determination of the local change rate, the Bowen
ratio and the radiational cooling. However, these errors are likely
minimal, except for the local change rate for the non-persistent, non-

genesis cloud cluster which is only observed at one time period (00Z). Assuming a zero local change rate certainly is not appropriate for these short-lived cloud clusters. This problem will be discussed later.

5.4 Moisture and Energy Budgets of the Genesis Case

The Q_1 and Q_2 profiles at the $0-4^O$ and $4-8^O$ regions for the first three stages of the genesis cases are shown in Fig. 43. At the $0-4^O$ region, the Q_1 profile remains relatively unchanged from Stage 1 to Stage 2, but increases greatly from Stage 2 to Stage 3. At the $4-8^O$ region the Q_1 profile increases slightly from Stage 1 to Stage 2 but decreases greatly from Stage 2 to Stage 3. The changes of the Q_1 profile from Stage 1 to Stage 3 correspond mainly to the changes in the mean vertical motion profile. The concentration of the cumulus heating from Stage 2 to Stage 3, however, might have a great impact on the further development of a tropical cyclone. The maximum Q_2 over the $0-4^O$ radius is located at 800-900 mb at Stages 1 and 2, but is raised to 450 mb at Stage 3. From Stage 2 to Stage 3 there is an overall increase of Q_2 at $0-4^O$ and a decrease at $4-8^O$ radius.

The moisture and energy budgets at $0-4^O$ and $4-8^O$ are depicted in Fig. 44. The cloud coverage is estimated as 60% and 23% at $0-4^O$ and $4-8^O$ radius, respectively, for all stages (the same as those for the non-genesis cloud clusters at Stage 2). The results indicate that the changes of the moisture and energy budgets for these two regions before the cyclone formation (or from Stage 1 to Stage 2) is relatively small. The differences in different budget terms between the genesis and non-genesis cloud clusters are not large either. The genesis cloud cluster experiences a large change in the moisture and energy budget terms
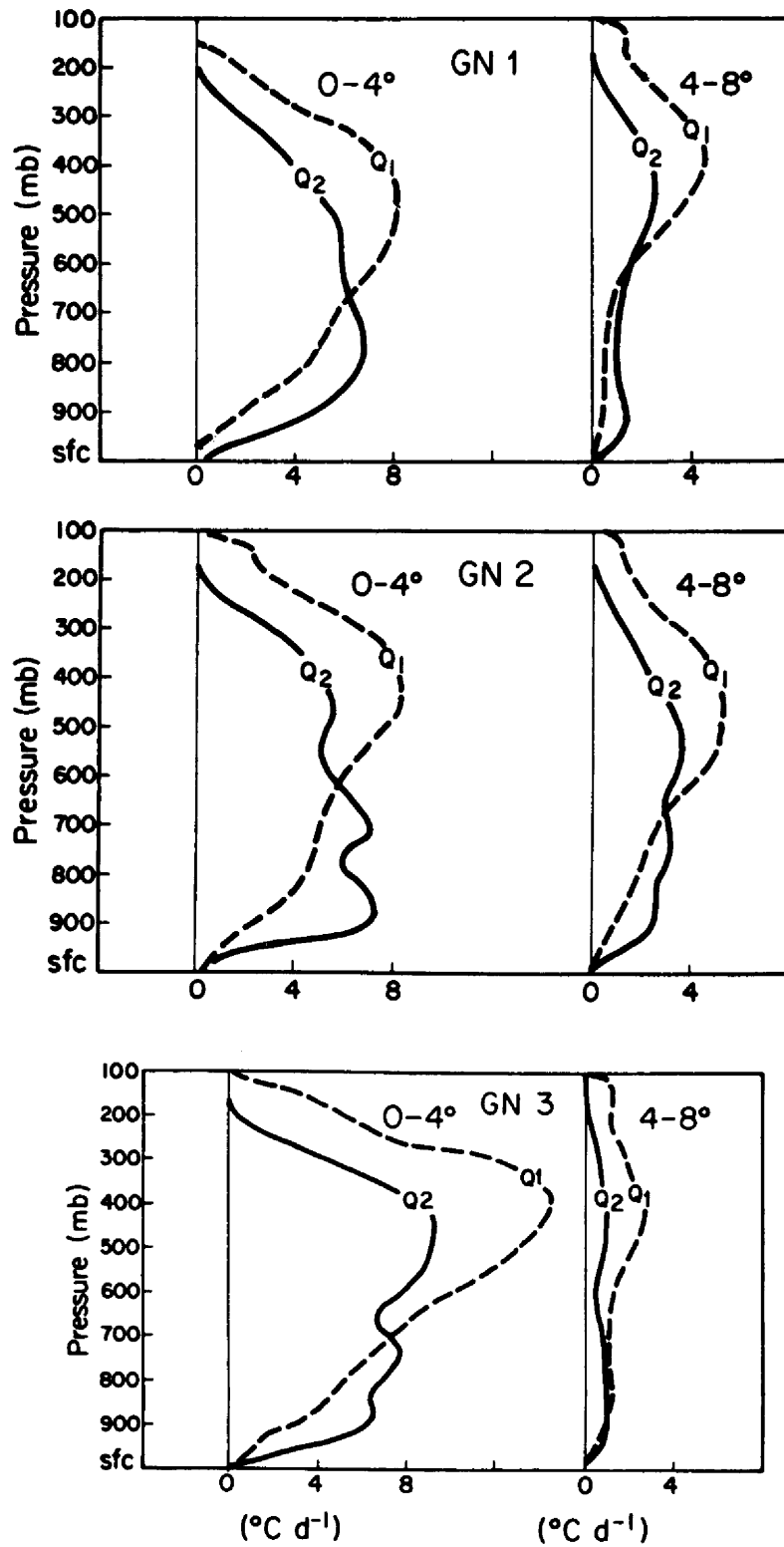
Fig. 43. The Q_1 and Q_2 profiles for the genesis case at the first 3 stages at the 0-4° and 4-8° regions.
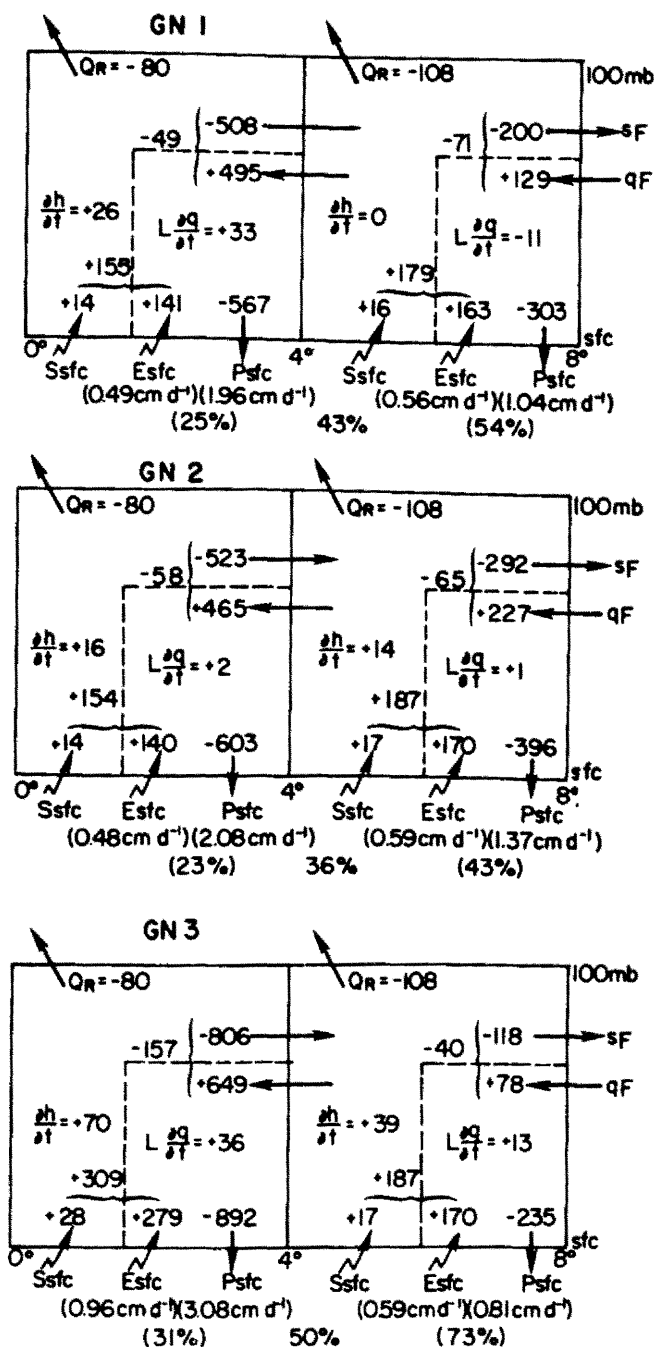
Fig. 44. Schematic diagram showing the energy and moisture budgets for the genesis case at the first 3 stages at the 0–4° and 4–8° regions. Unit is watt m^{-2} (or cm d^{-1} where so noted). The arrows within the dashed box (at the bottom, right corner) show terms for the moisture budget. The horizontal dry static energy and latent energy flux convergence are represented by sF and qF, respectively. The percentages of the total precipitation that comes from the local evaporation are shown for the 0–4°, 0–8°, and 4–8° regions.

during its transition period to a tropical cyclone (or from Stage 2 to Stage 3).

The surface evaporation for the pre-cyclone cloud cluster (at Stages 1 and 2) is about half a centimeter per day -- which is about the same as that of the background and the non-genesis cases. After the formation of a tropical cyclone (Stage 3), the surface evaporation increases greatly within the convective region (0-4° radius). It is thus speculated that the organized cumulus convection within a tropical cyclone is very efficient in increasing surface evaporation.

The precipitation at the 0-4° cloudy region is about 2 cm per day at Stages 1 and 2, but increases to 3 cm d^{-1} at Stage 3. At the 4-8° region, it increases from 1 cm d^{-1} at Stage 1 to 1.4 cm d^{-1} at Stage 2, but decreases to 0.8 cm d^{-1} at Stage 3. The average precipitation over the 0-8° region, however, drops from 1.54 cm d^{-1} at Stage 2 to 1.37 cm d^{-1} at Stage 3. Compared to the non-genesis cloud clusters, the genesis cloud clusters (at Stages 1 and 2) have more precipitation which also spreads over a larger region. Only about a quarter of the total precipitation of the genesis cloud cluster (at Stages 1 and 2) comes from local evaporation inside 4° radius. Even inside 8° radius, the local evaporation still accounts for only about 40% of the total local precipitation amount. These percentages are slightly less than those (about 50% inside 8° radius) of the non-genesis cases.

Results also indicate that the magnitudes of the net moist static energy (h) flux export for the genesis cloud clusters (49 and 58 watt m^{-2} for Stages 1 and 2) are much smaller than are those of the non-genesis cloud clusters (111 and 80 watt m^{-2} for non-persistent and persistent cases, respectively). The required surface energy flux for

tropospheric energy balance is about identical for both genesis (Stages 1 and 2) and persistent non-genesis cloud clusters at the 0-4° radius. The magnitude is 155, 154 and 160 watt m^{-2}, respectively. The non-persistent non-genesis cloud cluster, however, has a higher value of required surface energy flux (191 watt m^{-2} by assuming the local change rate is zero). However, there is no evidence that the non-persistent cloud cluster has a higher surface energy flux, especially since the other three composites all have about the same amount. It is thus more realistic to assume that the non-genesis cloud cluster agrees with the other composites (that is, it has about 155 watt m^{-2} surface energy flux). Under this assumption, the resulting local change rate is negative. In other words, the non-persistent, non-genesis cloud cluster is exporting more energy by the transverse circulation and radiational cooling than the surface energy flux can support, and thus is energy deficient. This might be one important reason why these cloud clusters form and die in a very short time period.

5.5 Cumulus Activities

Integrating $(Q_1-Q_2-Q_R)$ from 100 mb (assume $-\overline{\omega'h'} = 0$ there) downward to the surface gives the vertical eddy flux of moist static energy, that is, $-\overline{\omega'h'}/g$, which can be considered as the measure of the cumulus activity. The results for both the genesis and non-genesis cases at the 0-4° and 4-8° regions are shown in Fig. 45. The background profile, which decreases almost linearly with decreasing pressure, is also shown merely to illustrate the fact that cumulus activities decrease with height.

At the 0-4° region, the $-\overline{\omega'h'}$ is about the same for both the genesis (at Stages 1 and 2) and non-genesis cloud clusters. The cumulus

$$F = -\frac{1}{g}\,\widehat{\overline{\omega' h'}}$$
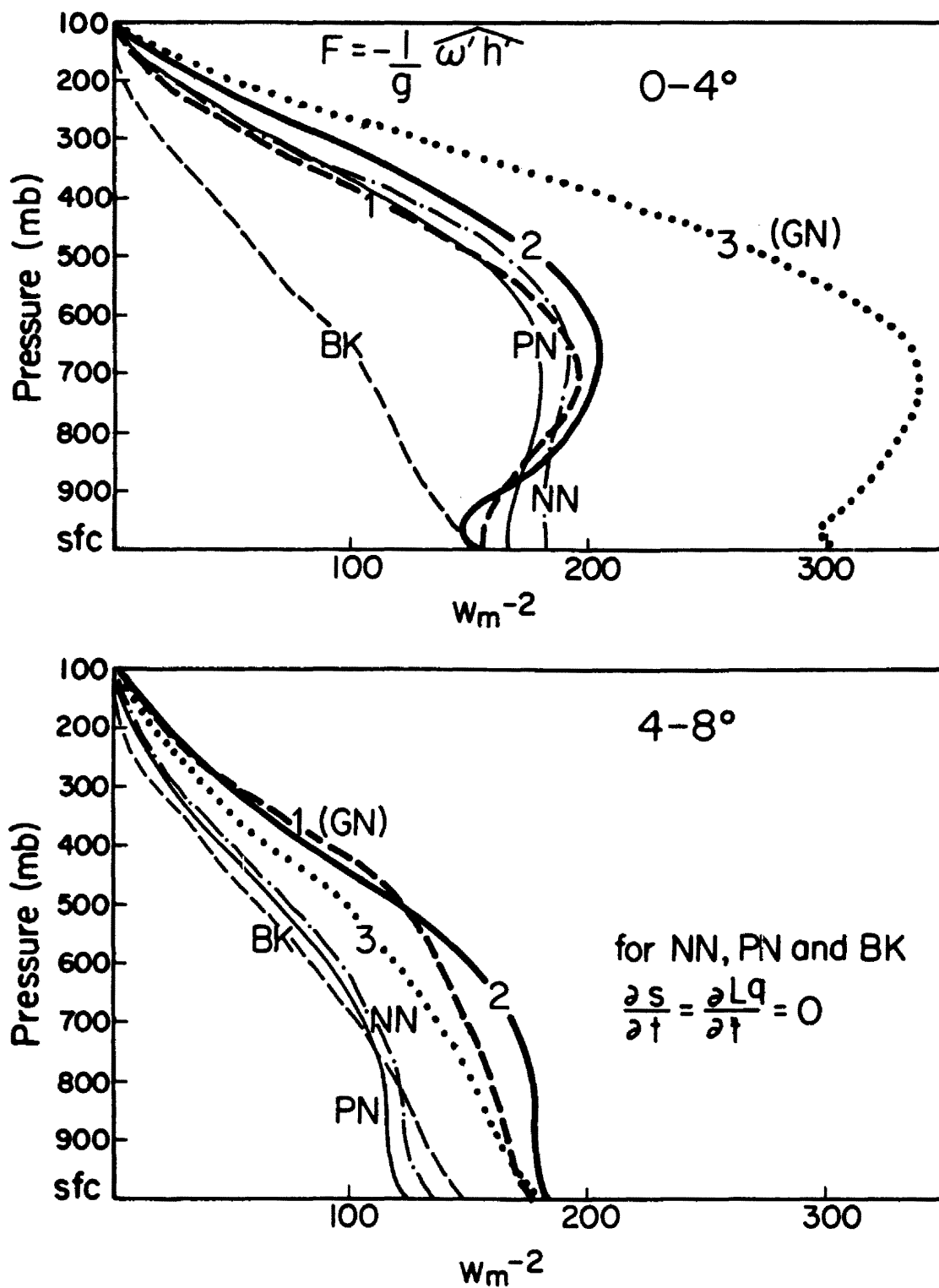
Fig. 45. The vertical prifles of $-(\overline{\omega'h'}/g)$ for both genesis and non-genesis (NG) composites at the 0-4° (top) and 4-8° (bottom) regions. The background (BK) profile is also shown.

convective transports of moist static energy do not become stronger until after the tropical cyclone was observed (Stage 3). At this stage, the cloud pattern is generally more organized. The increase in this cumulus convective transport from Stage 2 to Stage 3 appears fairly abruptly rather than gradually. Although the $-\overline{\omega'h'}$ for both the genesis and non-genesis cloud clusters is much larger than that for the background throughout the troposphere, the difference at the surface (surface energy flux) is small.

At the 4-8° radius, the profiles for both of the non-genesis cloud clusters are about the same as the background profile. The genesis case has a larger $-\overline{\omega'h'}$ compared to the non-genesis cases at all three stages. This indicates that genesis cloud clusters, on the average, have a greater radial and vertical extent of cumulus convection.

In summary, the non-genesis and the genesis cloud clusters have about the same amount of cumulus activities over the 0-4° radial domain. However, the genesis cloud clusters have more cumulus activities within the surrounding region.

6. TANGENTIAL (ANGULAR) MOMENTUM BUDGET

The tangential wind budget analysis is performed in a moving (or Lagrangian) coordinate. Vertical profiles of various horizontal and vertical transport terms will be presented for each composite at 4° radius to show the vertical distributions and individual case variation. Results will then be presented and discussed for two major areas: the 1-5° and 5-9° radial regions which are the most convective regions of the system and its surrounding environment. The discussion will include the relative importance of the different terms in contributing to the required total horizontal transport of tangential momentum and in the generation or maintenance of the vertical tangential wind shear. A residual term required for the balance of the tropospheric tangential momentum budget will be calculated and discussed.

6.1 Tangential Wind Equation in a Moving Coordinate

The tangential wind equation in a moving coordinate is, after taking the azimuthal average,

$$\frac{\partial \overline{V}_\theta}{\partial t} = \overline{V_r \frac{\partial V_\theta}{\partial r}} - \overline{V_r \frac{V_\theta}{r}} - \overline{(V_r + C_r)f} - \overline{\omega \frac{\partial V_\theta}{\partial p}} + \overline{F}_{sfc} \qquad (13)$$

where C_r is the radial component of the system (or the coordinate) motion, f the Coriolis parameter and F_{sfc} the surface friction. Note that V_r, and V_θ are in a moving coordinate; that is, the system motion has been subtracted out. The tangential wind equation essentially takes the same form in a moving coordinate or in a fixed coordinate, except

that the Coriolis force is calculated using the total wind speed $(V_{r-total} = V_r + C_r)$ in both coordinate frameworks.

Equation 13 can be rearranged to give

$$\frac{\partial \overline{V}_\theta}{\partial t} = - \overline{V_r \zeta_a} - \overline{\omega \frac{\partial V_\theta}{\partial p}} - \overline{C_r f} + \overline{F}_{sfc} \qquad (14)$$

where ζ_a is the absolute vorticity. This is a rather simple form which indicates that the local change of $\overline{V}_\theta$ in a moving coordinate is mainly due to the radial flux of absolute vorticity and vertical advection. The other two terms are the surface friction which is acting to slow down the tangential wind at the boundary layer, and the motion term or $\overline{-C_r f}$ which is due to the meridional motion of the system. This motion term is zero for east-west moving systems and is negative for northward moving systems. Therefore, these two terms, $-\overline{C_r f}$ and $\overline{F}_{sfc}$, are always negative for a tropical cloud cluster or cyclone which has a cyclonic circulation at the boundary layer and moves poleward. Thus for a developing system, the vertical integration of $(- \overline{V_r \zeta_a} - \overline{\omega \partial V_\theta / \partial p})$ has to be larger than the frictional dissipation and the northward motion spindown.

Note that the vertical advection term is not zero when integrating through the whole troposphere; rather,

$$\int_{sfc}^{100mb} (- \overline{\omega (\partial V_\theta / \partial p)}) \, dp = \int_{sfc}^{100mb} (- \overline{(\partial \omega V_\theta)/(\partial p)} + \overline{(V_\theta \, \partial \omega)/(\partial p)}) \, dp$$

$$= 0 + \int_{sfc}^{100mb} - \overline{V_\theta \cdot D} \, dp,$$

where D is the divergence or $= - \frac{\partial \omega}{\partial p}$. Since a convergent circulation (D < 0) generally occurs where the flow is more cyclonic and vice versa, this term is always positive when integrated vertically. The stronger the system, the larger is this term.

Equation 14 can also be decomposed into mean and eddy flux terms:

$$\frac{\partial \overline{V}_\theta}{\partial t} = -\overline{V}_r \overline{\zeta}_r - \overline{V_r' \zeta_r'} - \overline{V_r} \overline{f} - \overline{V_r' f'} - \overline{C_r' f'}$$

$$- \overline{\omega} \frac{\partial \overline{V}_\theta}{\partial p} + \overline{F}_{sfc} + \overline{F}_\theta \qquad (15)$$

where ζ_r is the relative vorticity and $\overline{F}_\theta$ is the residual subgrid scale effect (including cumulus friction and internal dissipation - the unresolvable horizontal and vertical eddies). In short, $\overline{F}_\theta$ is the residual required to have a balance of the tangential momentum budget. All the unresolvable effects, including data noise, go into this term. Note that the term $\overline{-C_r f}$ is due only to the Coriolis eddy effect because $\overline{C}_r = 0$.

The calculation of the mean terms and the surface friction is straightforward. As in Lee (1984) and Frank (1977b), the Deacon formula is used to determine surface stress:

$$\tau_o = -\rho C_D |V_{10}| V_{\theta 10},$$

where the drag coefficient $C_D = 1.18 \times 10^{-3} + 4.0 \times 10^{-5} |V_{10}|$. V_{10} in m s^{-1}, $|V_{10}|$ and $V_{\theta 10}$ are the total wind speed and the tangential wind speed at 10 meters height, respectively. The wind speed at 900 mb is scaled by 0.8 to approximate the wind speed at 10 m height. In addition, the τ_o is scaled by a factor to account for the variations in

the individual wind speed. This factor is determined by $\overline{v^2}/(\overline{V})^2$ where V^2 is calculated from each individual sounding. The magnitude is about 1.1 to 1.3 (or about the same as that used by Lee, 1984).

The eddy absolute vorticity flux term includes the eddy earth vorticity term and the eddy relative vorticity term which can be further decomposed into the shear and curvature vorticity terms; or,

$$-\overline{V_r'\zeta_a'} = -\overline{V_r'f'} - \overline{V_r'\zeta_r'}$$

$$= -\overline{V_r'f'} - \overline{V_r'\frac{\partial V_\theta'}{\partial r}} - \overline{V_r'\frac{V_\theta'}{r}} .$$

(Note that no azimuthal dependent term is considered). Unfortunately, there is no appropriate approach to estimate the eddy shear vorticity flux term $- \overline{V_r' (\partial V_\theta'/\partial p)}$. The only way is to calculate the value of $-V_r (\partial V_\theta/\partial r)$ at each grid point and then average all grid point values around the azimuth to represent the average total value. The eddy term is obtained by subtracting the mean from the total value. Obviously, this eddy term contains only the standing eddies, and thus greatly underestimates the transient eddies. (A more detailed discussion on transient eddies will be given later.)

For the two other eddy terms, $-V_r'\cdot\overline{\frac{V_\theta'}{r}}$ and $-\overline{V_r'f'}$, the approach used is to compute $- V_r f$ and $- V_r V_\theta$ from each individual sounding and average them with respect to each grid (box) for all 8 azimuthal boxes at any radius. An azimuthal average of values at all 8 grids is then taken to give the total terms, that is, $-\overline{V_r V_\theta}$ and $-\overline{V_r f}$ (or more precisely, $-\overline{[V_r V_\theta]}$ and $-\overline{[V_r f]}$). The eddy terms thus can be determined as:

$$-\overline{V_r'V_\theta'} = (-\overline{[V_rV_\theta]} - (\overline{[V_r]}\ \overline{[V_\theta]})\ \text{and}$$

$$-\overline{V_r'f'} = (-\overline{[V_rf]}) - (\overline{[V_r]}\ \overline{[f]}),$$

where the brackets ([ ]) represent the grid box average or the grid point value. Previously, it was shown that it is not feasible to use the total h flux calculated from each individual sounding for the energy budget analysis. However, those problems discussed earlier are not likely to cause a serious problem in the current calculations because the systematic latitudinal dependencies for wind are much less than those for the height and temperature.

As pointed out by Lee (1984), the term F_θ has included all the possible sub-grid scale effects that can not be properly calculated, as well as possible meteorological noise and data errors. However, the data sets used in the current budget analysis are much better than those previously used by Lee (1984) because the time evolution is more carefully treated. Therefore, the current analysis can likely address the horizontal transient eddies effect which Lee (1984) could not fully handle.

6.2 Vertical Distribution of Horizontal and Vertical Transport Terms

The calculated total horizontal and mean vertical transport terms of Eq. 14, $-\overline{V_r\zeta_a}$ and $-\bar{\omega}\,(\partial\overline{V}_\theta/\partial p)$, at 4° radius are shown in Fig. 46 for both the genesis (Stages 1, 2 and 3) and the non-genesis (NG) cases. Results indicate that the term $-\overline{V_r\zeta_a}$ is generally positive below 350 mb and negative aloft. For the genesis case, the negative value of $-\overline{V_r\zeta_a}$ increases at the upper levels as the system gets stronger. Near the surface, a slight increase occurs at Stage 1 to Stage 2 and no change
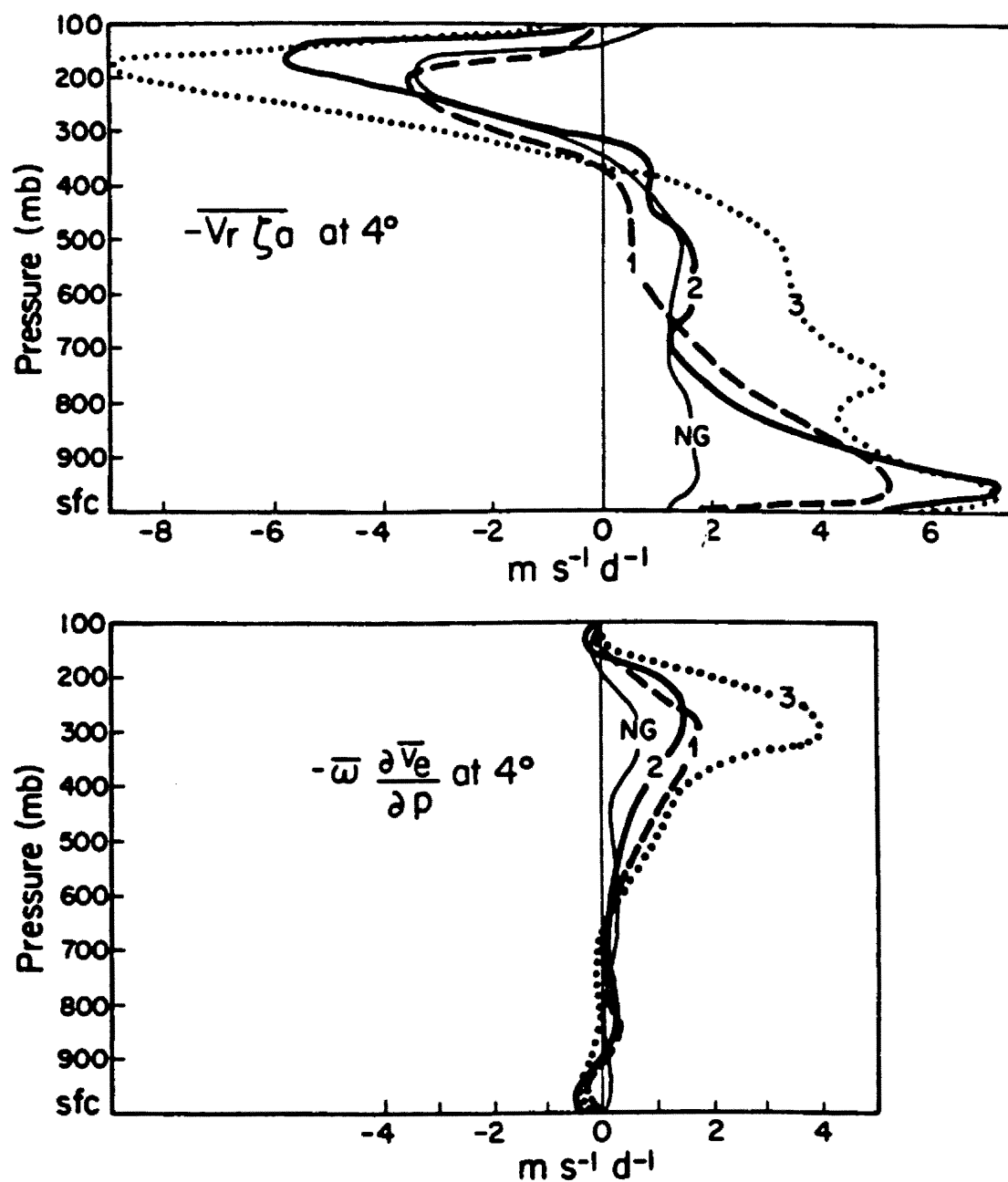
Fig. 46. Vertical profiles of $-\overline{V_r \zeta_a}$ and $-\overline{\omega} \, \partial \overline{V}_\theta / \partial p$ for the first 3 stages of genesis case and the non-genesis cloud cluster (NG) at $4°$ radius.

thereafter. At 350-650 mb, the positive value increases as the system develops. (The persistent non-genesis case also shows a slightly larger magnitude than the non-persistent case at these levels.) This might be a result of the convection induced inflow due to ice-phase sublimation and the freezing processes which gives extra buoyancy through the release of latent heat.

The major difference between the genesis (Stage 2) and the non-genesis cloud clusters occurs below 700 mb, where the genesis case has a stronger inward flux. Above 700 mb, the difference is small. Because of the stronger vertical wind shear associated with the genesis system, the genesis cloud cluster (Stage 2) has a stronger vertical advection than the non-genesis cases.

To show how the various horizontal flux terms can contribute to the total horizontal flux, the first four terms on the right hand side of Eq. 15 are shown at 4° radius for each case in Fig. 47. Note that term 4, $(-\overline{V'\zeta_r'})$, the eddy relative vorticity term, in the current analysis is primarily due to the eddy curvature vorticity. This is because the eddy shear vorticity term cannot be properly estimated. For the non-genesis cases, the mean earth vorticity term $(-\overline{V}_r\overline{f})$, though it averages to zero through the whole troposphere, appears to be the dominant term at all levels. Below 400 mb all three other terms are fairly small. In the upper level, these three terms show positive values which cancel out part of the large negative $-\overline{V}_r\overline{f}$ term.

For the genesis case, the mean earth vorticity term still plays a major role at all levels but other terms also contribute significantly. The most significant difference between the genesis and the non-genesis cases is that the genesis case mean relative vorticity term has larger
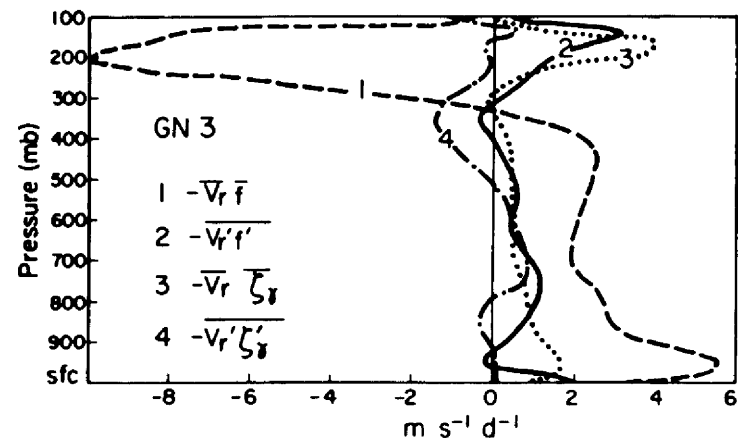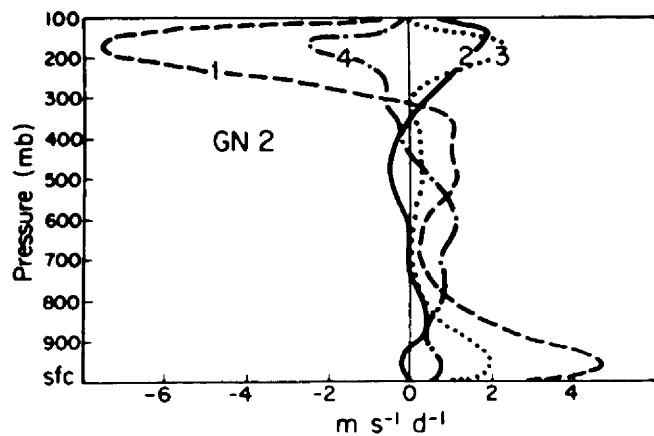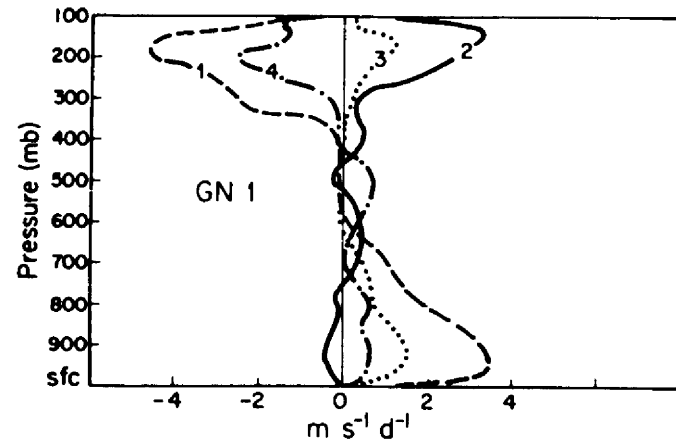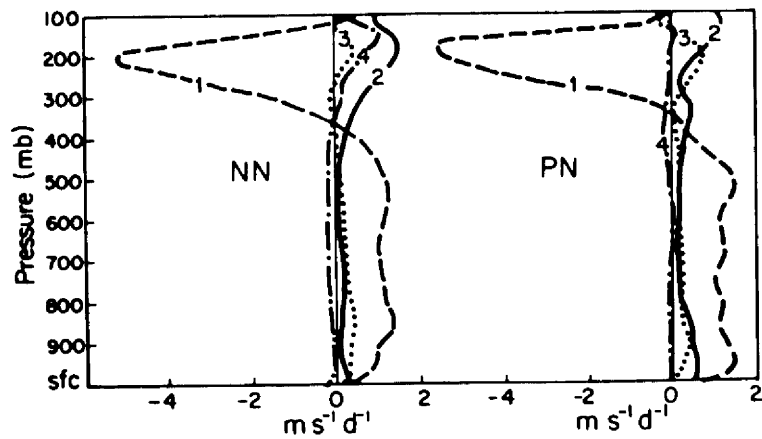
Fig. 47. The vertical profiles of $-\overline{V_r \zeta_r}$, $-\overline{V_r' \zeta_r'}$, $-\overline{V_r f}$ and $-\overline{V_r' f'}$ for the genesis case at the first three stages and the non-genesis cloud cluster (NG) at 4° radius. The horizontal eddy shear vorticity flux is not included in $-V_r' \zeta_r'$.
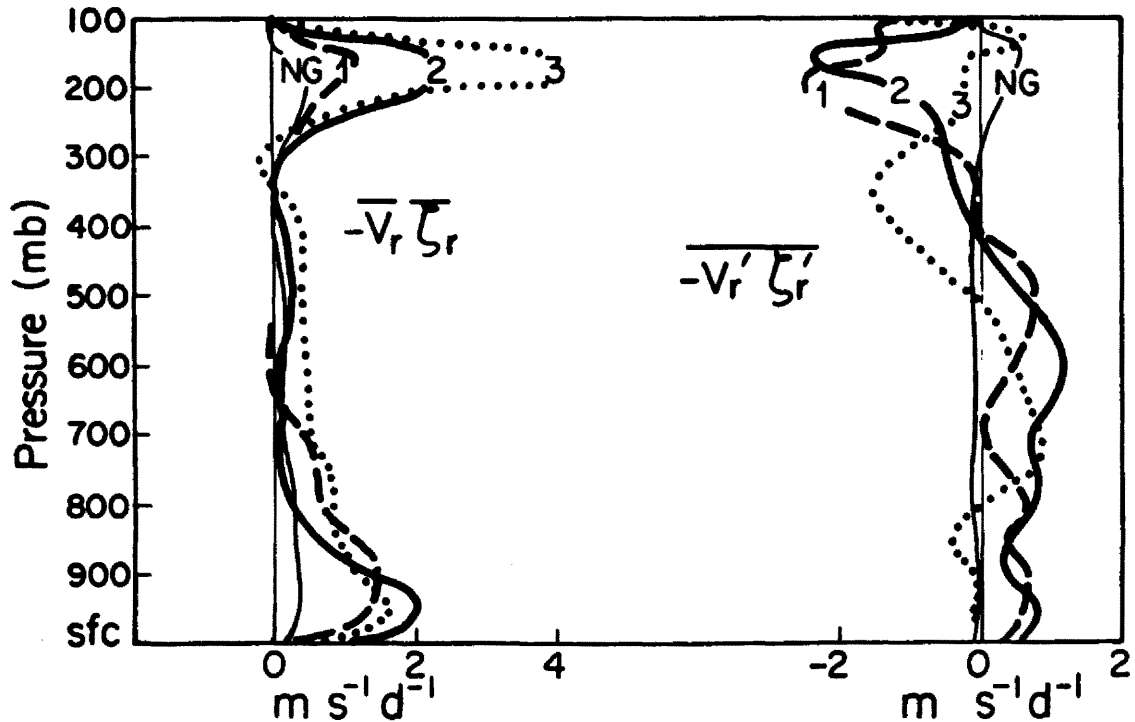
Fig. 48. The vertical profiles of $-\overline{V_r}\,\overline{\zeta_r}$ (top) and $-\overline{V_r'\zeta_r'}$ (bottom) for various composites at 4° radius. Note that the horizontal eddy shear vorticity flux is not included in the $-\overline{V_r'\zeta_r'}$ term.

values at the upper and lower levels, as shown in Fig. 48 (left diagram). The part of the eddy relative vorticity term which can be estimated is also quite different (Fig. 48b - right diagram). However, the tropospheric integrations of these profiles show that the difference in the total tangential momentum spinup due to this eddy effect is small. The eddy earth vorticity term shows a large positive value in the upper level and almost zero at middle and lower levels, which indicates an upper-level system relative flow from the north. The mean earth vorticity term is just a response to the mean radial wind.

6.3 Layer Budgets

For a cloud cluster to form a tropical cyclone it has to accumulate enough tangential momentum (or mean vorticity) over a domain of at least a few degrees latitude. Cyclone formation can then occur by drawing

enough tangential momentum from its immediate vicinity into the center region. However, this accumulation does not guarantee the formation of a tropical cyclone; other processes have to take place simultaneously. Even so, it is still vital to understand how this strong tangential momentum accumulation can happen in the first place.

Another important process that needs to be considered is the generation or maintenance of the anticyclonic vertical wind shear in the immediate vicinity of a tropical cyclone. This wind shear is necessary to maintain a reasonable middle-to upper—level warm core. From Fig. 31 (page 76), it is clear that the increase of the vertical wind shear is primarily due to the increase of the middle— to low-level cyclonic tangential wind within 5° radius (at 2° and 4° radii). At the outer radii (6° and 8°), the middle— to low-level cyclonic circulation buildup also plays an important role in the shear generation before the cyclone formation, and the upper-level anticyclonic circulation strengthens more significantly during and after the formation of the cyclone.

Figure 31 depicts different characteristics for the regions inside and outside 5° radius. Obviously, the region inside 5° radius is populated with organized cumulus convection associated with the system, whereas between $5-9^{\circ}$ in the system's immediate surrounding environment only scatter cumulus convection is present. Tables 7 and 8 give a summary of the various budget terms for the $1-5^{\circ}$ (2° and 4° area-weighted average) and the $5-9^{\circ}$ (6° and 8° area-weighted average) regions. In these tables, the whole troposphere is divided into three layers: the 100-300 mb major outflow layer, the 300-700 mb middle troposphere and the 700 mb to surface (~1000 mb) low-level major inflow

TABLE 7

Tangential momentum budgets at 1-5° (2° and 4° average) (unit: m s⁻¹d⁻¹)

$$\overline{\partial V}_\theta/\partial t = (-\overline{V_r \zeta_r})\ (-\overline{V_r'\zeta_r'})\ (-\overline{V_r\ f})\ (-\overline{V_r'f'})\ (-\overline{C_r f})\ (-\overline{\omega\ \partial V_\theta/\partial p})\ (+\overline{F}_{sfc})\ (+\overline{F}_\theta(res))$$

	$\overline{\partial V}_\theta/\partial t$	$(-\overline{V_r \zeta_r})$	$(-\overline{V_r'\zeta_r'})$	$(-\overline{V_r\ f})$	$(-\overline{V_r'f'})$	$(-\overline{C_r f})$	$(-\overline{\omega\ \partial V_\theta/\partial p})$	$(+\overline{F}_{sfc})$	$(+\overline{F}_\theta(res))$
100 to 300 mb									
Non-Non	0	+0.3	+0.3	-2.7	+0.9	-0.2	+0.1	+0	+1.3
Per-Non	0	+0.3	-0.2	-3.4	+0.6	-0.2	+0.2	+0	+2.7
Gen-S1	-0.5	+0.4	-1.7	-2.2	+1.7	-0.3	+0.6	+0	+1.0
Gen-S2	0.7	+1.4	-0.9	-5.2	+1.2	-0.4	+0.8	+0	+3.8
Gen-S3	1.3	+1.7	-0.7	-8.4	+1.2	-0.4	+2.2	+0	+5.7
300 to 700 mb									
Non-Non	0	+0.1	-0.1	+0.7	+0.2	-0.2	+0.3	+0	-1.0
Per-Non	0	+0.2	-0.1	+0.8	+0.3	-0.2	+0.4	+0	-1.4
Gen-S1	1.9	+0.0	+0.0	-0.1	+0.2	-0.3	+0.6	+0	+1.5
Gen-S2	2.3	+0.4	+0.2	+0.9	-0.2	-0.4	+0.7	+0	+0.7
Gen-S3	2.5	+0.1	-0.3	+0.9	+0.2	-0.4	+1.9	+0	+0.1
700 to Surface									
Non-Non	0	+0.3	-0.1	+0.9	+0.1	-0.2	+0.1	-0.4	-0.7
Per-Non	0	+0.3	-0.1	+1.1	-0.2	-0.2	+0.0	-0.4	-0.5
Gen-S1	2.7	+0.6	+0.5	+1.7	-0.2	-0.3	+0.0	-0.8	+1.2
Gen-S2	2.7	+1.2	+0.4	+2.2	-0.1	-0.4	+0.0	-1.7	+1.1
Gen-S3	1.4	+2.8	+0.4	+4.5	+0.5	-0.4	-0.1	-3.3	-3.0
100 to Surface									
Non-Non	0	+0.2	+0.0	+0.0	+0.3	-0.2	+0.2	-0.1	-0.4
Per-Non	0	+0.2	-0.1	+0.0	+0.3	-0.2	+0.2	-0.1	-0.3
Gen-S1	1.7	+0.3	-0.2	+0.0	+0.4	-0.3	+0.4	-0.3	+1.4
Gen-S2	2.0	+0.9	+0.0	+0.0	+0.1	-0.4	+0.5	-0.6	+1.5
Gen-S3	1.8	+1.3	-0.1	+0.0	+0.5	-0.4	+1.3	-1.1	+0.3

*The eddy shear vorticity transport by transient eddies is not included in the term $-\overline{V_r'\zeta_r'}$ but included in $\overline{F}_\theta$ (res).

TABLE 8

Tangential momentum budgets at 5-9° (6° and 8° average) (unit: m $s^{-1}d^{-1}$)

	$\partial V_\theta/\partial t=$	$(-\overline{V_r\zeta_r})$	$(-\overline{V_r'\zeta_r'})$	$(-\overline{V_r}\,\overline{f})$	$(-\overline{V_r'f'})$	$(-\overline{C_r f})$	$(-\overline{\omega}\,\partial\overline{V_\theta}/\partial p)$	$(+F_{sfc})$	$(+F_\theta(res))$
100 to 300 mb									
Non-Non	0 —	-0.1	-0.3	-2.6	+1.8	-0.4	+0.0	+0	+1.6
Per-Non	0 —	+0.5	+0.1	-3.2	+3.0	-0.4	-0.1	+0	+0.1
Gen-S1	+0.5 —	+0.8	-0.1	-4.7	+1.1	-0.8	+0.3	+0	+3.9
Gen-S2	-0.7 —	+0.7	+1.1	-5.6	+2.1	-0.9	+0.3	+0	+1.6
Gen-S3	-0.6 —	+1.7	+0.7	-7.2	+3.1	-1.0	+0.3	+0	+1.8
300 to 700 mb									
Non-Non	0 —	-0.1	-0.2	+0.4	+0.0	-0.4	+0.0	+0	+0.3
Per-Non	0 —	-0.2	-0.2	+0.8	+1.1	-0.4	+0.1	+0	-1.2
Gen-S1	1.4 —	+0.0	-0.1	+1.1	+0.1	-0.8	+0.4	+0	+0.7
Gen-S2	0.1 —	-0.1	+0.2	+0.9	-0.2	-0.9	+0.5	+0	-0.2
Gen-S3	0.4 —	-0.2	-0.2	+1.3	+0.0	-1.0	+0.2	+0	+0.3
700 to Surface									
Non-Non	0 —	-0.1	+0.0	+1.2	+0.2	-0.4	·0.0	-0.3	-0.6
Per-Non	0 —	+0.0	-0.2	+1.1	-0.7	-0.4	+0.0	-0.4	-0.8
Gen-S1	1.6 —	+0.1	+0.2	+1.6	-0.3	-0.8	+0.0	-1.1	+1.9
Gen-S2	0.3 —	+0.0	+0.4	+2.5	-0.3	-0.9	+0.0	-1.7	+0.3
Gen-S3	0.3 —	+0.0	-0.1	+2.9	+0.2	-1.0	+0.0	-1.8	+0.1
100 to Surface									
Non-Non	0 —	-0.1	-0.1	+0.0	+0.5	-0.4	+0.0	-0.1	+0.2
Per-Non	0 —	+0.1	-0.2	+0.0	+1.4	-0.4	+0.0	-0.1	-0.8
Gen-S1	1.2 —	+0.2	+0.0	+0.0	+0.2	-0.8	+0.2	-0.4	+1.8
Gen-S2	0.0 —	+0.1	+0.5	+0.0	+0.3	-0.9	+0.2	-0.6	+0.4
Gen-S3	0.2 —	+0.3	+0.0	+0.0	+0.8	-1.0	+0.1	-0.6	+0.6

*The eddy shear vorticity transport by transient eddies is not included in the term $-\overline{V_r'\zeta_r'}$ but included in $\overline{F}_\theta$ (res).

layer. The tropospheric average is also shown in the bottom panel.

Note that the term $-\overline{V_r'\zeta_r'}$ (eddy vorticity flux) does not include the

eddy shear vorticity flux $(-\overline{V_r' \dfrac{\partial V_\theta'}{\partial r}})$ by the transient eddies. Instead,

these transient eddies are included in F_θ, the residual term.

According to Lee (1984), the vertical cumulus momentum transports

$(-\overline{\dfrac{\partial \omega' V_\theta'}{\partial p}})$ are merely vertical rearranging processes and should average

to zero throughout the whole troposphere. The tropospheric average of

$\overline{F}_\theta$ of the bottom panel (in the right column) should include only the

internal dissipation and the unresolvable horizontal eddies, mainly

$-\overline{V_r' \dfrac{\partial V_\theta'}{\partial r}}$ and $-\overline{V_\theta' \cdot D'}$ where D' is the local perturbation of the

divergence. Note that this term is obtained by expanding the vertical

eddy advection term, or:

$$- \overline{\frac{\omega' \ \partial V_\theta'}{\partial p}} = - \overline{\frac{\partial \omega' V_\theta'}{\partial p}} + \overline{\frac{V_\theta' \ \partial \omega'}{\partial p}} = - \overline{V_\theta' \cdot D'}.$$

Since the tropospheric average of tangential wind is positive inside at

least 9° radius (Fig. 49), the internal dissipation should be negative

(or a spindown of cyclonic circulation). Its magnitude should also

increase as the system gets stronger, at least inside 5° radius.

a)   Inner region ($1-5^\circ$) budgets

Inside 5° radius, the cumulus momentum transports play a very

significant role in the vertical rearrangement of the tangential

momentum. The separation between the cumulus friction and the

unresolvable horizontal eddies is thus very difficult. The only clue is

that the cumulus momentum transport is mainly a down-gradient effect and

its magnitude increases as the vertical wind shear increases and/or the

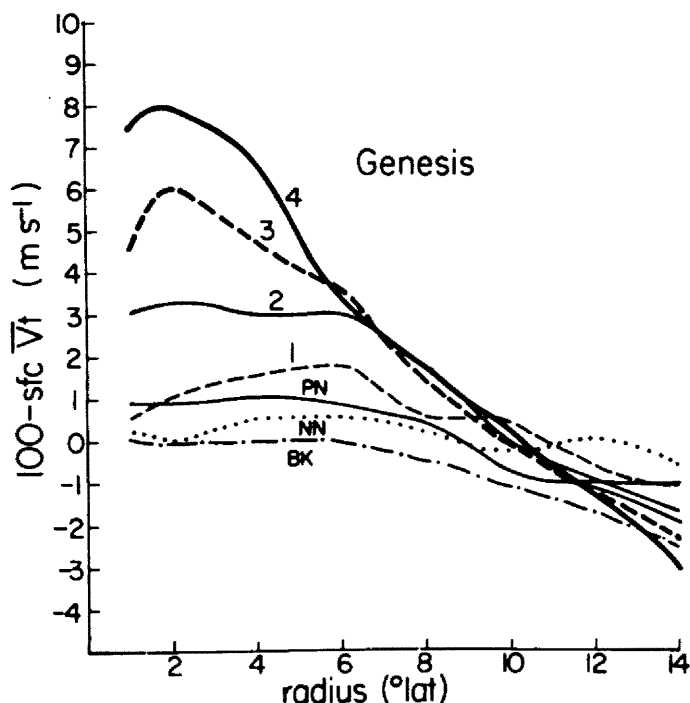cumulus convection strengthens. Therefore, a large positive cumulus

Fig. 49. The radial profiles of tropospheric averaged tangential winds for the genesis cases at Stages 1 (2 days before, $\leq$ 10 m s^{-1}), 2 (1 day before ~ 10 m s^{-1}), 3 (incipient tropical cyclone, ~ 15 m s^{-1}), and 4 (1 day after, ~ 22 m s^{-1}), the non-genesis cloud cluster (NG) and the background (BK).

friction should occur at the upper 100-300 mb layer and a negative one below that layer except near the surface.

Table 7 indicates that the mean earth vorticity term $(-\overline{V}_r\overline{f})$ is generally very important at any layer although its vertical integration is zero. It is interesting to see that the eddy earth vorticity term $(-\overline{V_r'f'})$ generally balances the meridional motion term $(-\overline{C_r f})$ except in the upper levels where a stronger northerly blowthrough brings about a larger positive eddy earth vorticity flux. The mean relative vorticity term $(-\overline{V}_r\overline{\zeta}_r)$] is generally larger for the genesis composite than for the non-genesis composite. The difference is primarily at the upper and lower layers where inflow (outflow) correlates with positive (negative) relative vorticity. The calculated eddy relative vorticity term (only

part of the total eddy) although averaged to about zero for the whole troposphere, acts in the same manner as the mean earth vorticity term to increase the vertical wind shear for the genesis case. The mean vertical advection term (or the correlation between the tangential momentum and the divergence) plays a significant role in the tangential momentum generation, especially for the stronger systems which have stronger vertical wind shear. The tropospheric average of this term is about the same as the mean relative vorticity term.

The residual term, F_θ(res) is generally positive in the upper level due to the cumulus friction. In the middle to lower levels, it is negative for the non-genesis cases and positive for the genesis case at Stages 1 and 2. Note that F_θ decreases from Stage 1 to Stage 3 for the genesis case. Since the cumulus convective transports are mainly negative at these levels, the unresolvable horizontal eddies should be positive and also are likely to decrease their magnitudes from Stage 1 to Stage 3. In other words, the unresolvable horizontal eddies, mainly ($- \overline{V_r' \, \partial V_\theta'/\partial r}$ and $- \overline{V_\theta' \cdot D'}$ account for a large generation of positive cyclonic vorticity at the middle to lower levels particularly in the early stages of genesis. These large eddy effects occur at the inner radii before the formation of the tropical cyclone. Note that the tropospheric average of $\overline{F_\theta}$ (no cumulus convective transports) drops from 1.7 m s^{-1} d^{-1} at Stage 2 to only 0.3 m s^{-1} d^{-1} at Stage 3. Also note that for the two non-genesis cases, the tropospheric averages of $\overline{F_\theta}$(res) are only −0.3 and −0.4 m s^{-1} d^{-1}. These small negative numbers for the non-genesis cases might be due to internal dissipation and to possible error in estimating other terms, mainly $\partial \overline{V_\theta}/\partial t$.

b.   Outer region (5-9°) budgets

At this region, the cumulus convection is not as intense as it is at the inner 1-5° region. The cumulus convective transports are obviously smaller. As shown in Table 8, the residual terms -- as well as all the mean terms -- are generally smaller than those at the inner region. However, the eddy earth vorticity term shows a slight increase in magnitude primarily due to the larger variation of f around the azimuth. The mean earth vorticity term is still dominant at each layer, but eddy terms play a more significant role -- especially at the upper levels. Note that for the genesis case, the tropospheric average of the residual term $(\overline{F}_\theta)$ has a rather large magnitude (1.8 m s^{-1} d^{-1}) at Stage 1 but drops to only 0.4 m s^{-1} d^{-1} at Stage 2 and then increases very slightly to 0.6 m s^{-1} d^{-1} at Stage 3.

6.4   Summary and Discussion

The tangential wind budgets presented in Tables 7 and 8 are rather extensive and complicated. Therefore, those results will be simplified and summarized in this section. Note that the tropospheric average of the tangential momentum equation (Eq. 15) eliminates the vertical cumulus rearrangement terms; or

$$\int_{Trop} \left(\frac{\partial \overline{V_\theta}}{\partial p}\right) dp = \text{mean terms + eddy terms + motion term + surface friction,}$$

where the mean terms $= \int_{Trop} \left(-\overline{V}_r \overline{\zeta}_r - \overline{V}_r \overline{f} - \overline{\omega}\frac{\partial \overline{V_\theta}}{\partial p}\right) dp$, or

$$= \int_{Trop} \left(-\overline{V}_r \overline{\zeta}_a - \overline{V}_\theta \overline{D}\right) dp \; ;$$

and the eddy terms $= \int_{Trop} (-\overline{V_r \zeta_a'} - \overline{V_\theta'D'})\, dp$, or

$$= \int_{Trop} (-\overline{V_r'f'} - \overline{V_r'\,(V_\theta'/r)} - \overline{V_r'\,(\partial V_\theta'/\partial r)} - \overline{V_\theta'D'})\, dp.$$

The first two eddy terms can be estimated from each sounding and the last two eddy terms are estimated by the residual. The results in Tables 7 and 8 are reconstructed in Table 9 to show the relative importance of these terms in contributing to the tropospheric cyclonic momentum spinup.

Table 9 indicates that for the non-genesis cloud clusters, the surface friction and meridional motion spindown effects are mainly balanced by the mean transports at the inner radii and by the eddy transports at the outer radii. For the genesis case at the outer radii (5-9° radius), the eddy transports account for about 80% of the total transport throughout the three stages. At Stage 1, about half of the total transport spinup (mean and eddy) goes to balance the two spindown effects and half goes to increase the tangential momentum. At Stage 2, the eddy transport drops from 2.0 m s^{-1} d^{-1} (at Stage 1) to 1.2 m s^{-1} d^{-1} and all the transports go to balance the spindown effects, leaving no change in the tangential momentum. The budget essentially remains unchanged from Stage 2 to Stage 3. At the inner radii (1-5°), the eddy transport still plays a significant role in the total tangential momentum transport. However, the percentage drops from 70% at Stage 1 to 53% at Stage 2 and to only 21% at Stage 3. This drop is primarily due to the increase of the mean transport and a significant decrease of

TABLE 9

Tropospheric tangential momentum budgets (unit: $m\ s^{-1}\ d^{-1}$). The numbers within parentheses are the percentage of the total tangential momentum spinup (or mean plus eddy terms) contributed by the eddies.

	$\partial\overline{V}_\theta/\partial t$	=	mean terms*1	+ eddy terms*2	+motion terms*3	+surface friction
(1-5°)						
Non-Non	0	=	+0.4	-0.1	-0.2	-0.1
Per-Non	0	=	+0.4	-0.1	-0.2	-0.1
Gen-S1	+1.7	=	+0.7	+1.6(70%)	-0.3	-0.3
Gen-S2	+2.0	=	+1.4	+1.6(53%)	-0.4	-0.6
Gen-S3	+1.8	=	+2.6	+0.7(21%)	-0.4	-1.1
(5-9°)						
Non-Non	0	=	-0.1	+0.6	-0.4	-0.1
Per-Non	0	=	+0.1	+0.4	-0.4	-0.1
Gen-S1	1.2	=	+0.4	+2.0(83%)	-0.8	-0.4
Gen-S2	0.0	=	+0.3	+1.2(80%)	-0.9	-0.6
Gen-S3	0.2	=	+0.4	+1.4(78%)	-1.0	-0.6

*1 mean term $= \overline{V}_r\overline{\zeta}_r - \overline{V}_r\overline{f} - \overline{\omega}\dfrac{\partial\overline{V}_\theta}{\partial p}$ or those transport terms which can be determined by the mean circulation.

*2 eddy term $= -\overline{V_r'\zeta_r'} - \overline{V_r'f'} - \overline{V_\theta'D'}$, or those transport terms which can not be determined by the mean circulation. The sum of these terms is estimated by the required residual. Note that the cumulus momentum transports do not appear in the tropospheric average.

*3 meridional motion term $= -\overline{C_r f} = \overline{C_r'f'}$

eddy transport from Stage 2 to Stage 3. Note that the local change rate remains about the same and the increase of the surface friction is primarily balanced by the increase of the mean transport.

These budget analyses have revealed the following important results:

(1) The mean circulation transport plays a more important role in the inner region than in the outer region. It is also more important at later stages than at earlier stages. In short, the mean circulation

transport is not efficient enough to give a large tropospheric cyclonic momentum spinup which is necessary for cyclone formation at the early stage when the mean vorticity is weak.

(2) The horizontal eddy transport plays a very important role in creating the tropospheric tangential momentum spinup, especially at the earlier stages or at the outer radii.

(3) The mean earth vorticity transport is the major process in maintaining or increasing the vertical wind shear. The cumulus momentum transport (primarily inside 5° radius), on the other hand, acts to reduce the vertical tangential wind shear. Therefore, the upper-level anticyclonic circulation experiences a slight decrease at inner radii and an increase at outer radii during the development of the system.

The horizontal eddy transport shown in Table 9 includes the earth vorticity, the relative vorticity and the eddy divergent term. The relative vorticity can further be broken down into the shear and curvature vorticity terms -- as shown in Table 10 in which the unresolvable eddy terms $\overline{- V_r' (\partial V_\theta'/\partial r)} - \overline{V_\theta' D'}$ are combined together and are represented by the calculated residual. The earth vorticity is mainly due to the meridional blow-through effect. (A meridional motion of the system will have a positive eddy effect too, but this will be cancelled out by the meridional motion term, or $-\overline{C_r f}$). This meridional system relative flow primarily occurs at the upper level and its effect is larger at the outer radii. The eddy curvature vorticity flux does not play an important role compared to other terms when averaged throughout the troposphere. The eddy shear vorticity term $(\overline{-V_r(\partial V_\theta/\partial r)}$ and the eddy divergent term $(-V_\theta' D')$ of the residual turn out to be very important in the horizontal momentum transports. Note that the large

residual effect appears at both regions of Stage 1, but only at the inner region of Stage 2, and disappears at Stage 3. This residual effect is due to an external large-scale forcing process which acts upon the cloud cluster center to cause a large cyclonic spinup. This process will be discussed in more detail in the next chapters.

TABLE 10

Tropospheric averaged horizontal eddy transports contributed by the earth, curvature and shear vorticities (plus the eddy divergent term). Unit: m s^1 d^{-1}. Note that eddy shear vorticity term and eddy divergent term are combined together and are respresented by the residual.

Total horizontal eddy transports	=	$\overline{-V_r'f'}$	$-\overline{V_r'\dfrac{V_\theta'}{r}}$	$-\overline{V_r'\dfrac{\partial V_\theta'}{\partial r} - V_\theta'D'}$
$(1-5^o)$				
Non-Non	-0.1	= +0.3	-0.1	-0.3
Per-Non	-0.1	= +0.3	-0.1	-0.3
Gen-S1	+1.6	= +0.4	-0.2	+1.4
Gen-S2	+1.6	= +0.1	+0.1	+1.4
Gen-S3	+0.7	= +0.5	-0.1	+0.3
$(5-9^o)$				
Non-Non	+0.6	= +0.5	+0.0	+0.1
Per-Non	+0.4	= +1.4	-0.1	-0.9
Gen-S1	2.0	= +0.2	+0.0	+1.8
Gen-S2	1.2	= +0.3	+0.3	+0.6
Gen-S3	1.4	= +0.8	+0.0	+0.6

7. SLOW AND FAST GENESIS COMPOSITES

We have previously studied the development of an average pre-cyclone cloud cluster. However, no special criteria regarding the characteristics of the pre-cyclone cloud clusters were used during case classification. It is thus highly desirable to classify all tropical cyclone formation cases into categories based on the different types of cyclogenesis. The most physically meaningful classification criterion is the large-scale environment in which the cloud clusters are embedded; that is, the monsoon type and trade wind type cloud clusters. However, this attempt is not really feasible based on the available data.

Another meaningful alternative is to classify all the systems according to their developing rate. Observations have indicated that some tropical cyclones experience a dramatic increase in intensity right after they become tropical cyclones, while others develop much more slowly. These two types of systems are defined as "fast genesis" and "slow genesis", respectively. Unfortunately, imposing this criterion has greatly reduced the number of cases included in these composites and many less soundings are used (refer to Appendix A). The dramatic reduction in the number of soundings has made the budget analysis less reliable. Therefore, the focus of the analysis is placed on the large-scale circulation influences on these systems, rather than on their budgets. It is expected that these composite analyses will help us better understand these two different types of tropical cyclone

formation cases and that this will aid in our basic understanding of the formation process.

7.1 Composite Classification Criteria

The data sample used in the slow and fast genesis composites is the same as that previously used in the genesis composite. Since the purpose of these composites is slightly different (no budget analyses for these composites), the selection methodology is somewhat different and is described as follows:

(a) Slow genesis composites: The incipient slow genesis tropical cyclone composite (Stage 3) can contain as many as three time periods from the first report (JTWC best track). Its intensity change is less than or equal to 5 kts in 12 hours or 10 kts in 24 hours. Other requirements are that the first reported maximum intensity is less than or equal to 30 kts and the first reported position is south of $20^{O}N$ and east of $120^{O}E$. A total of 206 cases were selected (about two-thirds of the genesis case composite).

The next composite (Stage 4) of the slow genesis case contains all the time periods after the Stage 3 composite until the intensity reaches 40 kts. Another requirement is that there is no weakening trend. Imposing a 40-kt maximum intensity has reduced the number of cases by about 15%. The purpose of this criterion is to keep a distinct intensity difference between slow and fast genesis composites at Stage 4 (refer to Appendix A for more information).

The Stage 2 composite contains two 12-hour time periods 24 and 36 hours (not 12 and 24 hours) before Stage 3; and the Stage 1 composite contains two 12-hour time periods before Stage 2. Persistence is also used to determine the positions at the first two stages.

These classification procedures for the slow genesis are somewhat different from those used for the genesis composites discussed in Chapter 4. However, they are similar to those classification criteria used by Zehr (1976) and McBride (1981), (i.e. no exact time separation is imposed). As will be shown later, the current composite analyses can better identify the important large-scale circulation patterns during cyclogenesis.

(b) Fast genesis composites: For a system to be classified as fast genesis, its initial intensity change has to be greater than or equal to 15 kts in 12 hours or 20 kts in 24 hours. (Note that there is a separation between the fast and slow genesis cases in the 12- and 24-hour intensity change.) Other requirements are that the first reported intensity be equal or less than 40 kts and the first position to be south of 25°N and east of 120°E. Only the first two 12-hour time periods are included in the incipient cyclone composite (Stage 3). The Stage 4 composite contains the two 12-hour time periods following Stage 3. For most of the systems, the intensity at Stage 4 is very strong or close to typhoon intensity. Stage 2 contains two 12-hour time periods, 24 and 36 hours before Stage 3; and Stage 1, two time periods 12 and 24 hours before Stage 2. The persistence is also used to determine the center positions at the first two stages.

The average intensity, positions, and other characteristics for these composites are shown in Appendix A. In order to have about the same number of cases included in both categories (especially to have enough of a case count for the fast genesis case), different latitude and intensity classification criteria were used in the selections. These two cases thus have slightly different average characteristics at

Stage 3. Note that regardless of the loose criteria used for the fast genesis composite, it still had fewer cases. In other words, the majority of the tropical cyclone formation cases are slow genesis rather than fast genesis.

Since both slow and fast genesis cases can be considered as subsets of the previously discussed genesis case, their characteristics should also be quite similar to those of the genesis case. Differences between slow and fast genesis cases are thus smaller than those between genesis and non-genesis cases. Besides, the rawinsonde composites tend to smooth out the extreme characteristics and leave only the mean conditions. Fortunately, because of the way the time classification was done, important large-scale characteristics can still be clearly identified. In the following sections, only those important characteristics which show obvious differences between the slow and fast genesis cases will be shown and discussed.

7.2 Structural Differences Between Slow and Fast Genesis Composites

The 950 mb height deviations from the east-west 9-15° average for both cases at these 4 stages are shown in Fig. 50. As in the full composite genesis case, a pressure drop of less than 1 mb occurred over a very large domain prior to tropical cyclone formation for both the slow and fast genesis cases. The slow genesis case shows a slow but rather uniform and continuous pressure drop over a domain as large as 8-9° radius from Stage 1 to Stage 4. The fast genesis, on the other hand, shows most of the pressure drop to be within 4° radius from Stage 2 to Stage 4, and its evolution pattern is more erratic. This apparent
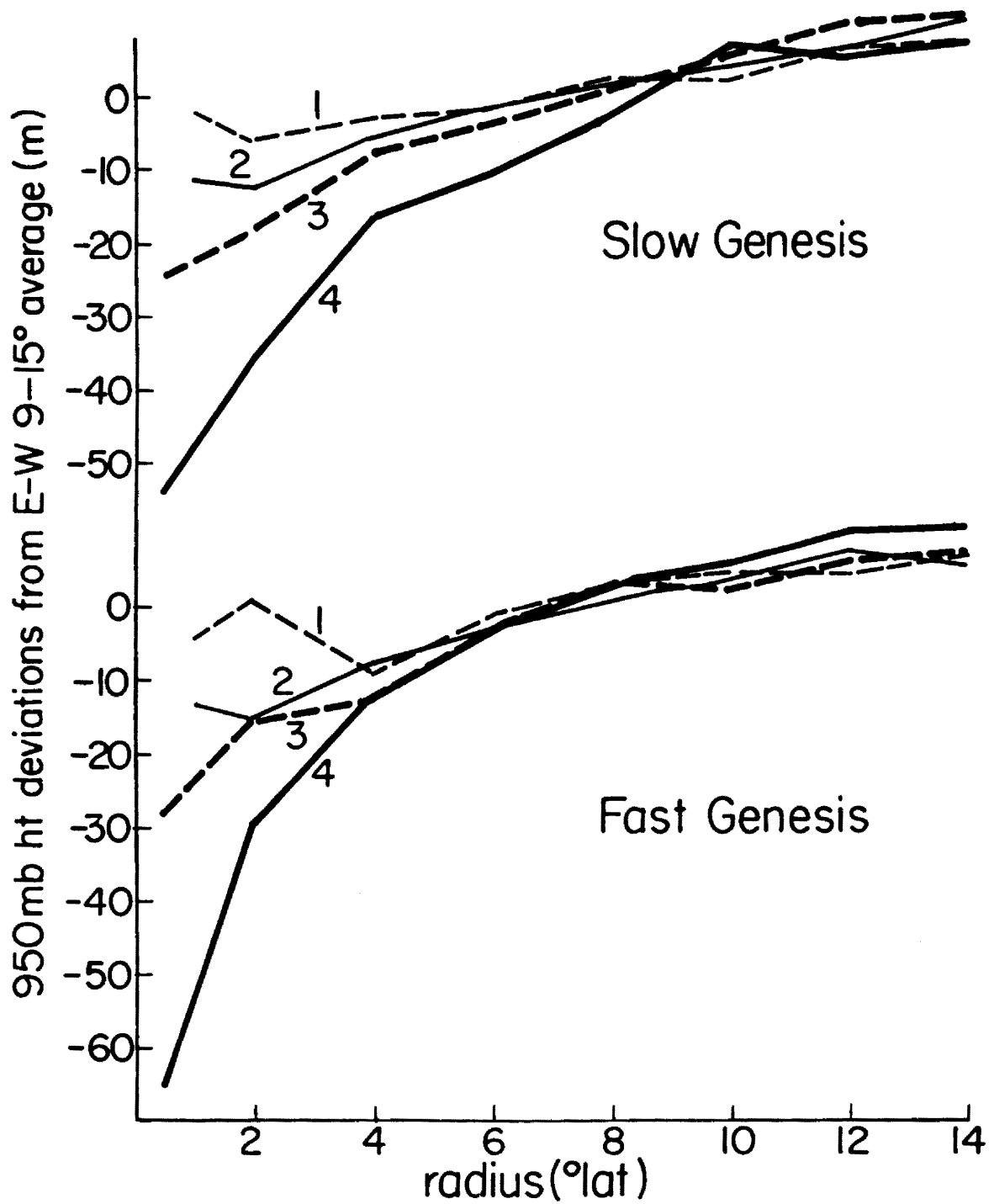
Fig. 50. The 950 mb height deviations from the east-west 9-15° average for both slow (top) and fast (bottom) genesis cases at Stage 1 (2 1/2 days before), Stage 2 (1 1/2 days before), Stage 3 (incipient tropical cyclone) and Stage 4 (1 day after).

difference in the surface pressure evolution suggests that slow and fast genesis cases are likely dictated by somewhat different physical processes.

Figure 51 shows the mean tangential wind profiles for the slow (upper panel) and fast (lower panel) genesis cases at 2°, 4°, 6°, and 8° radius. For the slow genesis case, the middle- to low-level tangential wind at the inner radii increases from Stage 1 to Stage 4. At 6° and 8° radius, the increase is smaller but rather steady. The large increase from Stage 2 to Stage 3 at 2° and 4° radius is somewhat caused by the longer time period between these two stages (one and half days as opposed to one day between Stages 1 and 2, Stages 3 and 4).

The fast genesis case shows pronounced middle- to low-level tangential wind pickup from Stage 1 to Stage 4 at 2° and 4° radius. At 6° and 8° radius, however, this increase is only observed from Stage 1 to Stage 2 or one and half days before the formation of the tropical cyclone. Almost no change is observed thereafter.

These results agree with the surface pressure pattern evolution – namely, that slow genesis is caused by a process that can increase the mean tangential wind (vorticity) over a rather large area while the fast genesis is mainly caused by a process that affects only the inner radii. It is also very interesting to find that, although the fast genesis case has a stronger inner core intensity than the slow genesis case at Stages 3 and 4, its outer circulation at 6° and 8° radius is actually weaker. The fast genesis case has an intensity of 61 kts (close to typhoon intensity) at Stage 4, while the slow genesis case has an intensity of only 33 kts. These results also imply that a slow developer tends to have stronger outer circulation.
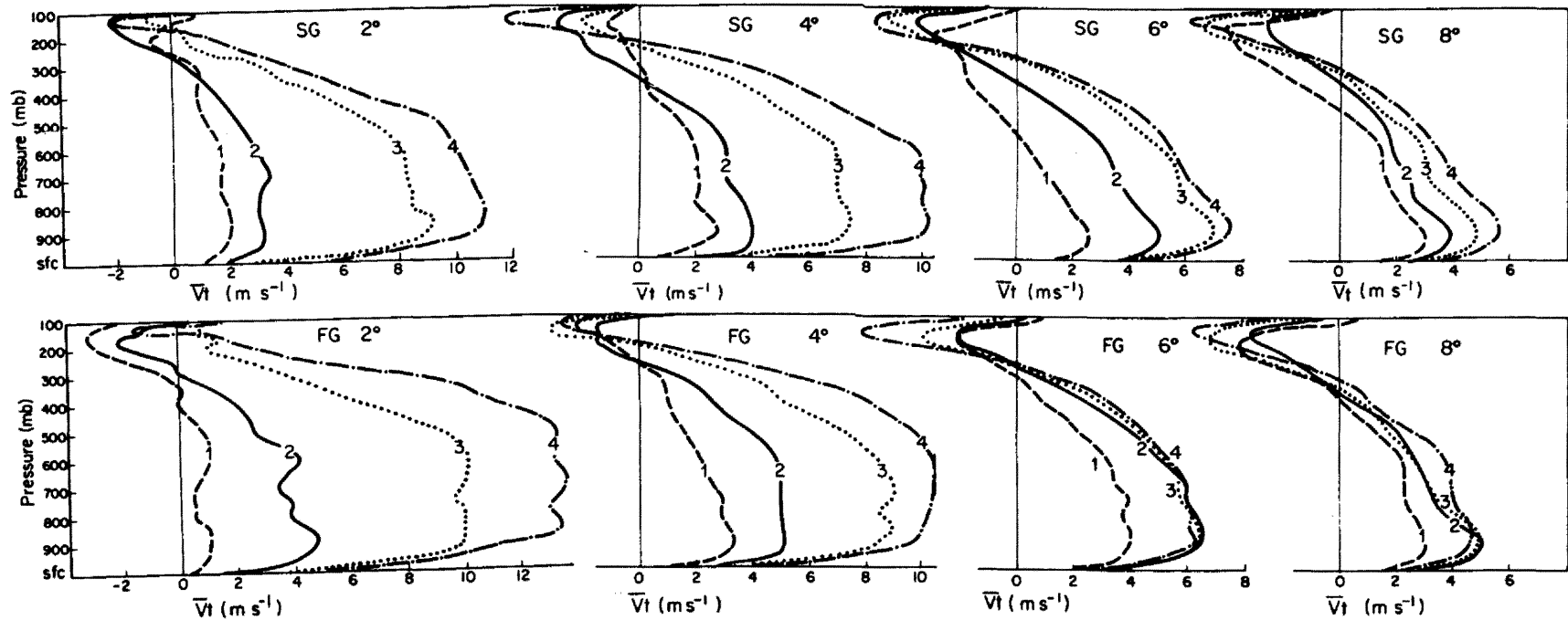
Fig. 51. The vertical profiles of the tangential wind at 2°, 4°, 6° and 8° radius for the slow (top) and fast (bottom) genesis cases at Stage 1 (2 1/2 days before), Stage 2 (1 1/2 days before), Stage 3 (incipient tropical cyclone) and Stage 4 (1 day after).

At upper levels, the evolution pattern is rather erratic at 2° and 4° radius. The reason why is that the local change rate in the upper level is the residual of two large effects (the cumulus convective transports and the radial earth vorticity transport), and a small change in either term can cause the local change rate to flip the sign. At 6° and 8° radius, the upper level anticyclonic circulation generally increases from Stage 1 to Stage 4. Note that both cases have similar evolution patterns in the upper-level anticyclonic circulation regardless of the differences in the middle- to low-level cyclonic circulation pattern evolution.

The mean $0-4^o$ and $0-6^o$ vertical motion shows somewhat different evolution patterns for these two cases (see Fig. 52). For the slow genesis, the $0-4^o$ radius mean upward vertical motion has a maximum of about 100 mb per day at 300 mb at Stages 1 and 2. A weak secondary maximum is located at 850 mb, suggesting that the primary inflow is below this level. Note that there is almost no inflow between 650 mb and 850 mb and the inflow between 600 and 400 mb is likely due to the freezing process. This upward motion increases slightly and only at low levels from Stage 1 to Stage 2, but the change is rather pronounced from Stage 2 to Stage 3. The maximum upward motion continues increasing after the formation of the tropical cyclone (Stage 3 to Stage 4). Note that this is the only case (in Figs. 28 and 52) which shows a continuous increase of mean vertical motion after the formation of tropical cyclone. The mean vertical motion generally decreases after the formation, which is what happens in the slow genesis case in the $0-6^o$ region. At this $0-6^o$ region, a steady increase in the mean upward
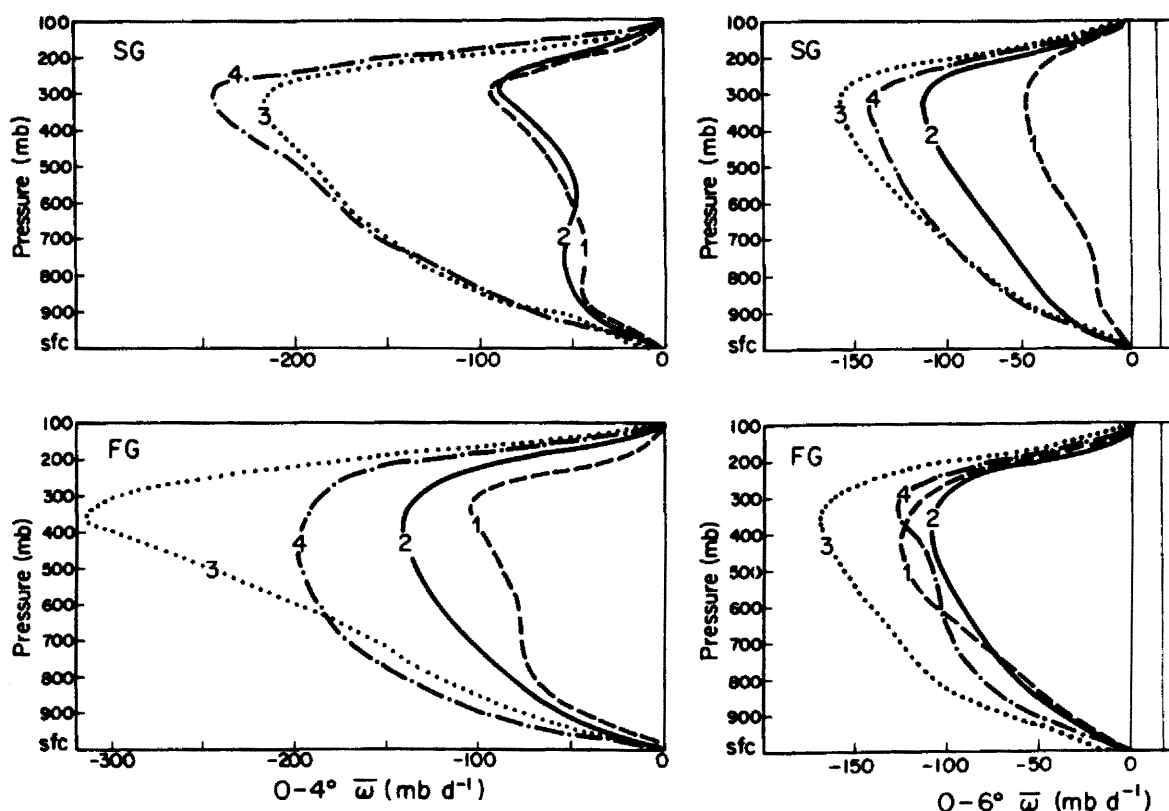
Fig. 52. The vertical profiles of the mean vertical motion 0-4° and 0-6° regions for the slow (top) and fast (bottom) genesis cases at Stage 1 (2 1/2 days before), Stage 2 (1 1/2 days before), Stage 3 (incipient tropical cyclone) and Stage 4 (1 day after).

motion is observed from Stage 1 to Stage 4; however, the increase is primarily from Stage 2 to Stage 3 for the 0-4° radius region.

For the fast genesis case, 0-4° mean vertical motion increases greatly from Stage 1 to Stage 3, and decreases significantly afterward. The 0-4° mean vertical motion at Stage 3 is the strongest of those calculated, with a maximum upward motion of 300 mb per day. At 0-6° radius, the mean vertical motion increases only during cyclone formation or from Stage 2 to Stage 3. The profiles at Stages 1, 2, and 4 are fairly similar.

These results reveal that the slow and fast genesis cases have different mean vertical motion evolution patterns. The only common feature is the increase of $\bar{\omega}$ from Stage 2 to Stage 3 in association with the tropical cyclone formation. From Stage 1 to Stage 2, the mean vertical motion increases primarily inside 4° radius for the fast genesis case and outside 4° radius for the slow genesis.

These results have indicated that the fast genesis is likely associated with processes which primarily influence the inner region and leave the outer region relatively undisturbed. Slow genesis, however, is likely associated with large-scale external processes which influence the outer region first. Note that the $\bar{\omega}$ increases mainly at $4-6^{\circ}$, not at $0-4^{\circ}$ at the early stage (Stage 1 to Stage 2). This forcing later reaches the inner region at Stage 3 (the cyclone formation stage) and causes a large increase in the $0-4^{\circ}$ mean vertical motion from Stage 2 to Stage 3. The $0-6^{\circ}$ mean vertical motion of the slow genesis also increases during this time period, but not as much as from Stage 1 to Stage 2, regardless of the longer time period between Stages 2 and 3. The continuous increase in the $0-4^{\circ}$ $\bar{\omega}$ from Stage 3 to Stage 4 for the slow genesis case is likely due to the remaining influence of this large-scale forcing. The $0-6^{\circ}$ $\bar{\omega}$ actually decreases slightly at this stage indicating a decrease in the $4-6^{\circ}$ $\bar{\omega}$.

7.3 Possible Processes Influencing Slow and Fast Genesis

The results presented in section 7.2 have revealed significant differences between the slow and fast genesis cases with regard to the evolution patterns of the surface pressure, the mean tangential wind and the mean vertical motion. These different evolution patterns may help us better understand the likely physical processes which dictate the

slow and possibly the fast genesis. These possible processes will be discussed in this section.

7.3.1 Slow Genesis

Slow genesis occurs in the majority of the cyclone formation cases. Slow genesis is primarily caused by a large-scale low-level process which initially builds a large cyclonic circulation over a large domain, as shown in Fig. 53. The 700-1000 mb averaged tangential wind has a magnitude of about 2 m s^{-1} from 2° up to almost 14° radius at Stage 1. The magnitude of the 2 m s^{-1} mean tangential wind at $10-12^{\circ}$ radius is very large (compare to Fig. 56 for the fast genesis). The uniform profile of $\overline{V}_t$ makes the vorticity increase linearly with decreasing radius. The 700-1000 mb radial wind (Fig. 54, bottom panel) shows a rather large inflow (-0.7 m s^{-1}) between 10 and 14° radius at Stage 1. A strong convergence is located between 6 and 10° radius where inflow decreases with decreasing radius.

Before the formation of the tropical cyclone (or from Stage 1 to Stage 2), this strong inflow pushes inward and causes a significant increase in the low-level inflow at 6° and 8° radius. The low-level mean tangential wind increases inside 9°, and the $0-6^{\circ}$ mean vertical motion also increases (Figs. 53 and 52). The low-level inflow inside 4° radius and the $0-4^{\circ}$ $\overline{\omega}$ essentially remain unchanged between Stage 1 and 2 except for the small increase in the low-level $\overline{\omega}$ (Figs. 54 and 52). The increase of 700-1000 mb $\overline{V}_t$ inside 4° radius is also smaller than that at $4-8^{\circ}$ radius. This low-level process eventually reaches the cloud cluster inner region and causes cyclogenesis (Stage 2 to Stage 3). The responses are dramatic increases in the mean vertical motion, the low-level inflow and the tangential wind at the inner radii. After cyclone
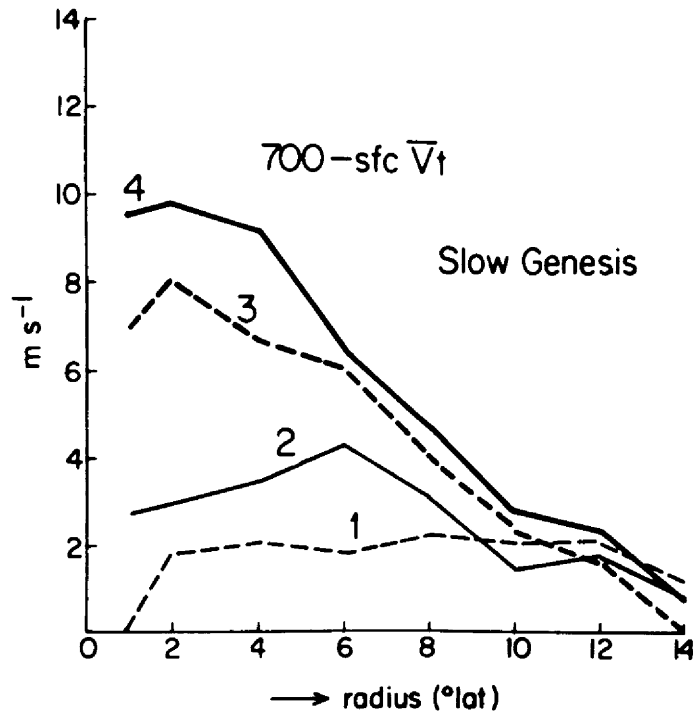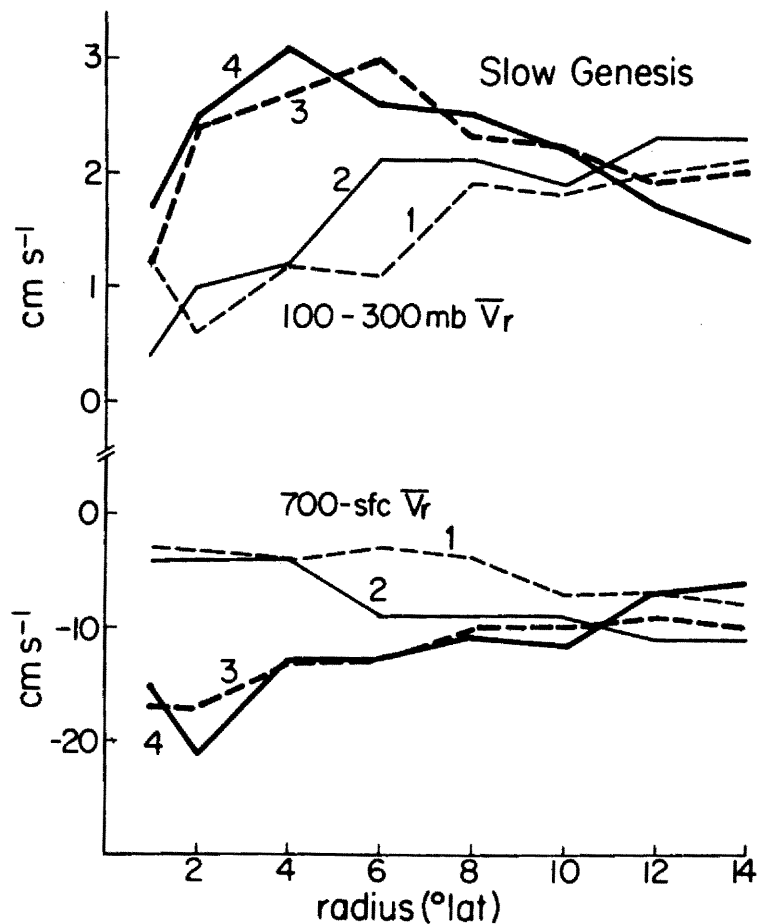
Fig. 53. The radial profiles of the 700 mb-surface mean tangential wind for the slow genesis case at Stage 1 (2 1/2 days before), Stage 2 (1 1/2 days before), Stage 3 (incipient tropical cyclone) and Stage 4 (1 day after).

formation (Stage 3 to Stage 4), the low-level inflow essentially remains the same; the low-level tangential wind, however, continues to increase - but slowly over a large domain. The 0-4° $\bar{\omega}$ still increases slightly in response to the remainder of this low-level forcing effect. The 0-6° $\bar{\omega}$, however, shows a slight decrease as this large-scale low-level inward forcing process reaches the inner region and fades away at outer region. In this process, the upper-level outflow (e.g. 100-300 mb $\bar{V}_r$ - as shown in Fig. 54, upper panel) is primarily a response to the low-level process. The whole process is one which leads to slow inward concentration.

Fig. 54. The radial profiles of the 100–300 mb (top) and 700 mb–surface (bottom) mean radial wind for the slow genesis case at Stage 1 (2 1/2 days before), Stage 2 (1 1/2 days before), Stage 3 (incipient tropical cyclone) and Stage 4 (1 day after).

The large-scale low-level forcing process described above is based only on the symmetric features. To illustrate this highly asymmetric forcing process, the circulation pattern (or streamlines) and the isotachs over a 14° radial domain in a moving coordinate are shown in Fig. 55 for 950, 850, 700, 500, and 200 mb. The shaded area is the strong wind region with a wind speed greater than 6 m s^{-1}.

At 850 mb, a strong southwest wind region is initially located beyond 6° radius at the southwest to south quadrant. Although the
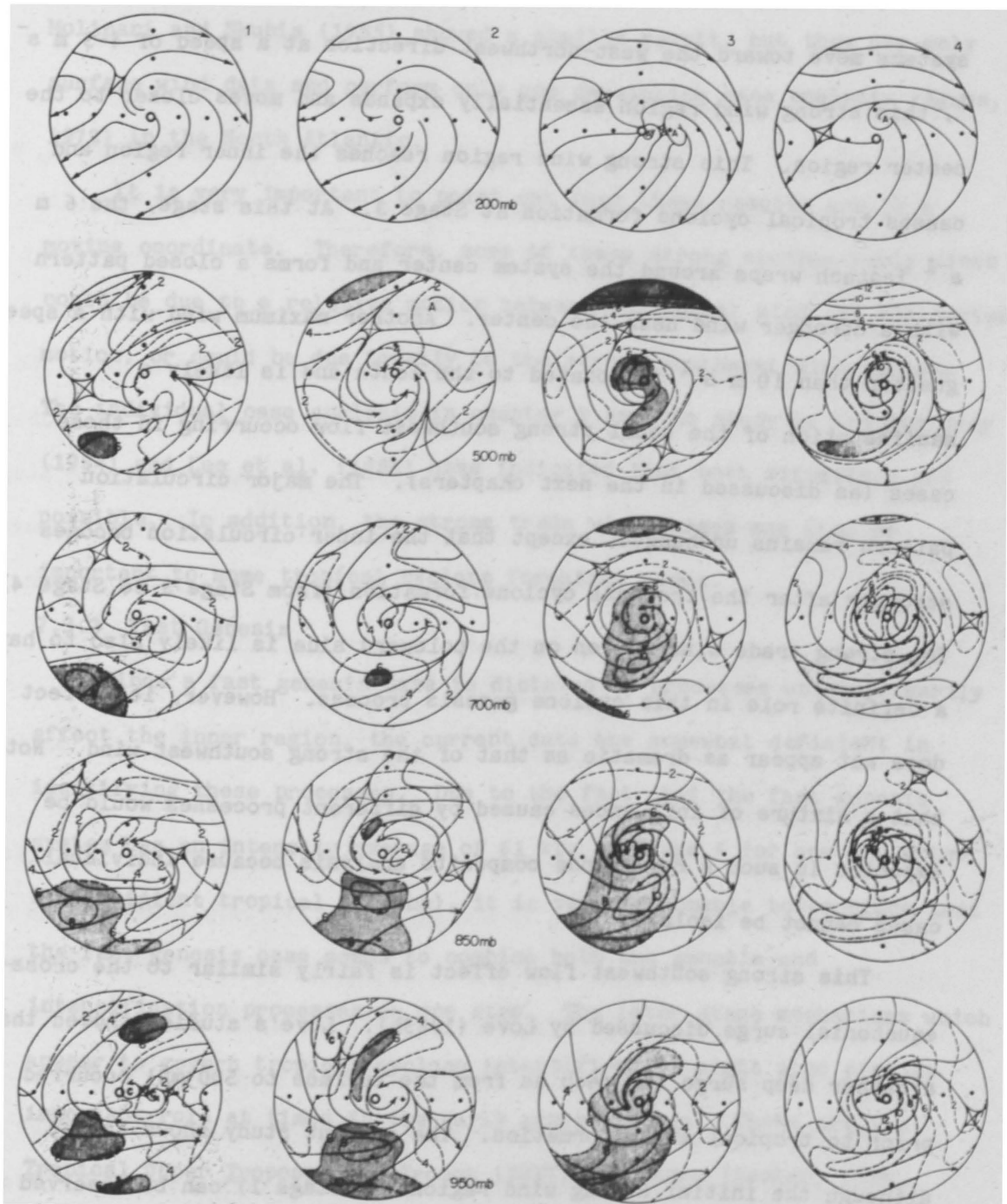
Fig. 55. The streamlines and isotachs in the moving or MOT system at
950 mb, 850 mb, 700 mb, 500 mb and 200 mb for the slow genesis
case at Stage 1 (2 1/2 days before), Stage 2 (1 1/2 days
before), Stage 3 (incipient tropical cyclone) and Stage 4 (1
day after). The shaded areas indicate a wind speed $\geq$ 6 m s^{-1}.

systems move toward the west-northwest direction at a speed of 4-5 m s^{-1}, this strong wind region essentially expands and moves closer to the center region. This strong wind region reaches the inner region and causes tropical cyclone formation at Stage 3. At this stage, the 6 m s^{-1} isotach wraps around the system center and forms a closed pattern with a stronger wind near the center. Another maximum wind with a speed greater than 10 m s^{-1} is located to the south and is likely a manifestation of the usual strong southwest flow occurring in these cases (as discussed in the next chapters). The major circulation pattern remains unchanged, except that the inner circulation becomes stronger after the tropical cyclone formation (from Stage 3 to Stage 4). The strong trade wind region on the poleward side is likely also to have a definite role in this cyclone genesis process. However, its effect does not appear as dramatic as that of the strong southwest wind. Note that a mixture of influences caused by different processes would be expected in such a rawinsonde composite analysis because individual cases cannot be isolated.

This strong southwest flow effect is fairly similar to the cross-equatorial surge discussed by Love (1985b). Love's studies showed that a rather deep surge (as deep as from the surface to 500 mb) occurred prior to tropical storm formation. The current study shows that although the initial strong wind region (at Stage 1) can be observed as high as 500 mb, the subsequent effect is primarily at low levels or below 700 mb (shown at 850 and 950 mb in Fig. 55). Note that the strong wind evolution pattern is not observed at 700 mb from Stages 1 to 2. The stronger wind speed at Stage 3 above 700 mb, however, probably is in

response to the tropical cyclone formation process. The study by Molinari and Skubis (1985) showed a similar result, but they use only surface wind data and perform only one developing case analysis (Agnes, 1972) in the North Atlantic.

It is very important to point out that these results are in a moving coordinate. Therefore, some of these strong southwesterly winds could be due to a relative motion between the actual wind and the system motion, or could be due totally to the strong southwest wind surges. The individual case analysis in chapter 9 and the study by Lee and Gray (1984) and Lee et al. (1986) have indicated that both situations are possible. In addition, the strong trade wind surges may also be important to some tropical cyclone formation cases.

7.3.2 Fast Genesis

Since a fast genesis case is dictated by processes which primarily affect the inner region, the current data are somewhat deficient in identifying these processes. Due to the fact that the fast genesis system has an intensity average of 61 kts at Stage 4 (or one day after the incipient tropical cyclone), it is very reasonable to conclude that the fast genesis case seems to combine both the genesis and intensification processes as one step. The later stage mechanisms which appear to govern tropical cyclone intensification might also play an important role at times in the early genesis stage. These are the Tropical Upper Tropospheric Trough (TUTT) influence (Sadler, 1976, 1978), upper-level outflow jet characteristics (Chen and Gray, 1985; Merrill, 1985), the non-linear increase of the heating efficiency due to the increased vorticity (Hack and Schubert, 1986) and the CISK mechanism (Charney, 1964; Ooyama, 1969, 1982).

It is impossible to examine the applicability of these effects in the current study. Therefore, only observational evidence will be presented for the fast genesis. Figures 56 and 57 show the radial profiles of the 700-1000 mb $\bar{V}_t$, and the 100-300 mb and 700-1000 mb $\bar{V}_r$ at all four fast genesis stages, respectively. The low-level tangential wind shows a maximum at 6° radius initially - which is quite different from that of the slow genesis at Stage 1. A buildup of this low-level $\bar{V}_t$ occurs over the 8-10° radius domain before cyclogenesis (Stage 1 to Stage 2). However, the increase is limited to only inside of 4° radius during the formation and the later intensifying stages (Stage 2 to Stage 4). Figures 56 and 53 show the important characteristic that, although the processes affecting the slow and fast genesis are different, both cases require a buildup of large-scale tangential wind prior to the formation (or from Stage 1 to Stage 2).

The radial wind profiles of the fast genesis case (Fig. 57) do not show the progressive inflow surges prior to cyclogenesis that were evident for the slow genesis case. The pattern evolutions of the upper- and low-level radial winds at 2° and 4° radius are very similar, but the upper-level pattern is more distinct. It is hypothesized that besides the possible internal dynamics, favorable surrounding system upper-level features can also influence the inner region later stage intensity, especially because of the low inertial stability and the high static stability in these levels (Holland and Merrill, 1984). Flow is rather quasi-horizontal at these levels.

It is surprising to find that a composite trough is located to the east and northeast of the system center at 200 mb before the cyclogenesis stage, that is, at Stages 1 and 2 (Fig. 58). Although this
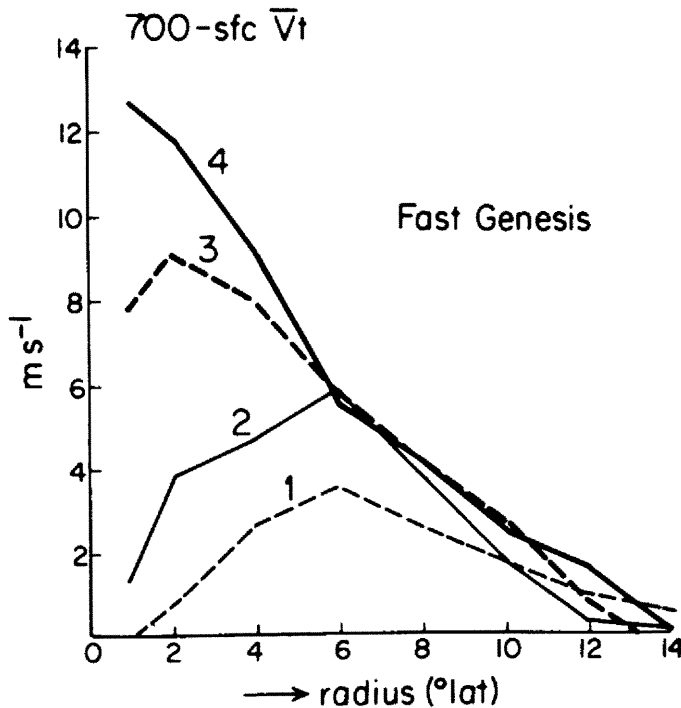
Fig. 56. The radial profiles of the 700 mb-surface mean tangential wind for the fast genesis case at Stage 1 (2 1/2 days before), Stage 2 (1 1/2 days before), Stage 3 (incipient tropical cyclone) and Stage 4 (1 day after).

trough does not look the same as the upper-level trough in the real atmosphere, it does suggest the possible influence of the upper-level trough on the fast genesis case. Also to be noted is that the 200 mb wind vectors on the northeastern quadrant show a tendency to change sign with radius and have a weaker wind speed. This might be due to the fact that TUTTs (or upper troughs) at different configurations have been composited together, yielding these results. As discussed by Merrill (1985), it is necessary to rotate the outflow axis before compositing in order to help eliminate this problem.

At 850 mb (lower pannel of Fig. 58), strong wind regions initially (Stage 1) are located to the southwest and to the north. These strong wind regions strengthen before tropical cyclone formation
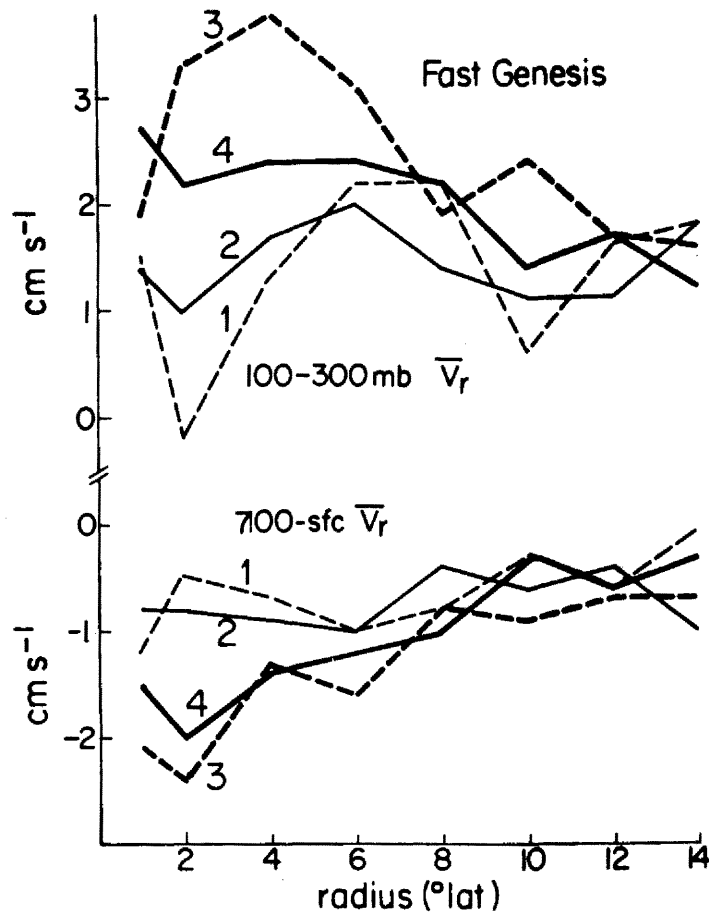
Fig. 57. The radial profiles of the 100-300 mb (top) and 700 mb-surface (bottom) mean radial wind for the fast genesis case at Stage 1 (2 1/2 days before), Stage 2 (1 1/2 days before), Stage 3 (incipient tropical cyclone) and Stage 4 (1 day after).

(Stage 1 to Stage 2). However, unlike the process described for the slow genesis, this strengthening process seems to develop in situ rather than due to inward progressive processes. These fast and slow genesis class differences are worthy of note and of further study.

7.3.3 Summary

The slow and fast genesis are influenced by different physical processes and have different structural evolution patterns. The slow genesis is generally caused by large-scale forcing processes, such as
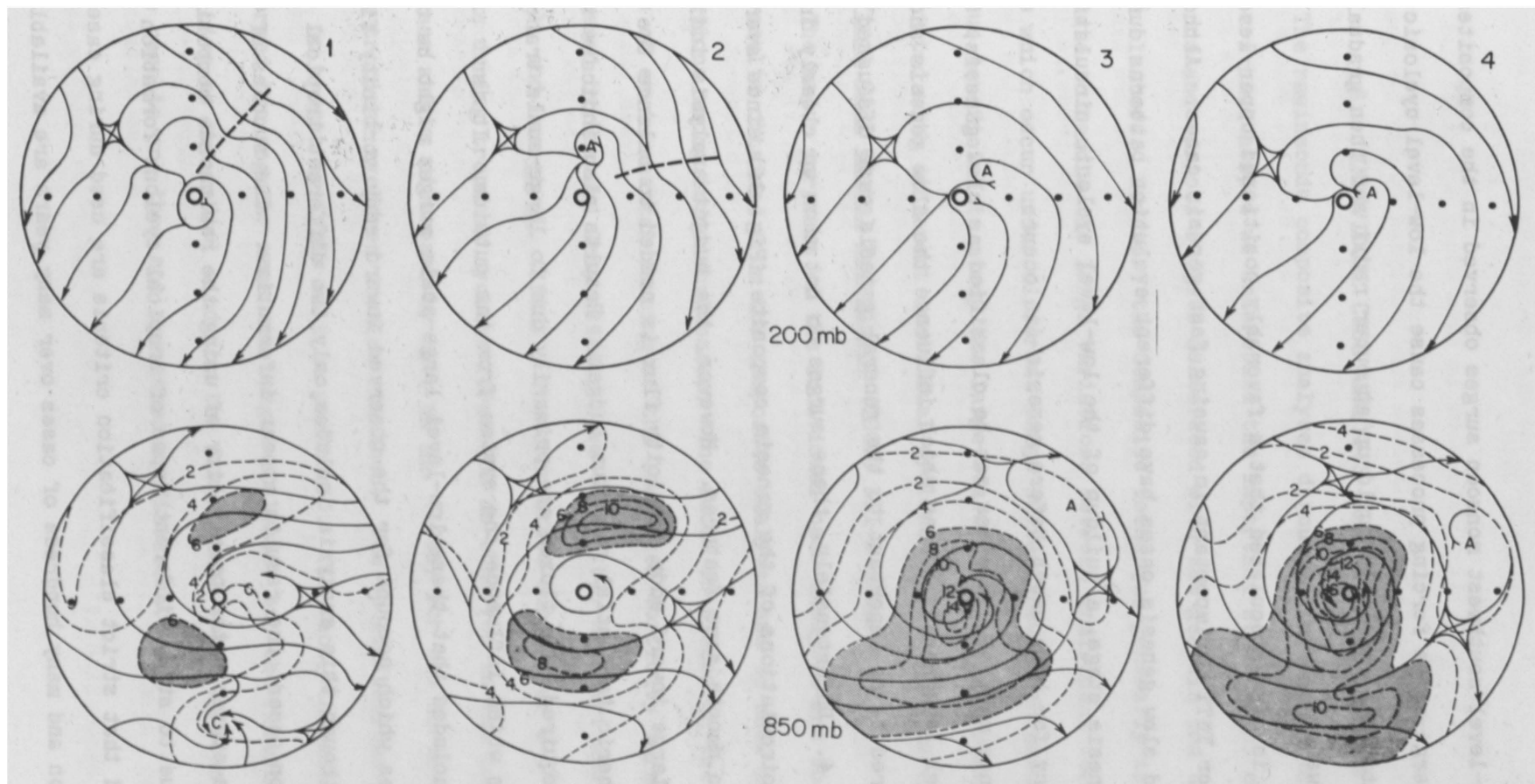
Fig. 58. The streamlines and isotachs at 850 mb and 200 mb for the fast genesis case at Stage 1 (2 1/2 days before), Stage 2 (1 1/2 days before), Stage 3 (incipient tropical cyclone) and Stage 4 (1 day after). The shaded areas indicate a wind speed ≥ 6 m s^{-1}.

the low-level southwest monsoon surges observed in the composites. These large-scale forcing processes cause the low-level cyclonic circulation to initially build up at outer radii and then gradually to move inward.

It is also speculated that a favorably positioned upper-level trough or TUTT is important in causing fast genesis cases. Although the fast and slow genesis cases have different evolution patterns during the cyclogenesis stage, a buildup of the low-level cyclonic circulation is necessary for both cases before genesis can occur.

Since most of the cases can be classified as slow genesis, the low-level large-scale surges which influence the slow genesis should be considered to be important to the general genesis case discussed in Chapter 4. Unfortunately, these surges do not show up clearly in the 850 mb circulations of the genesis composite (Fig. 36) since averaging tends to smooth some features. However, the budget analysis indicates that a large inward eddy vorticity flux is needed to balance the tropospheric tangential momentum budget. Results also indicate that these required eddy fluxes are primarily due to large-scale transient features which influence the system from the outside. It is thus concluded that these low-level large-scale surges might be the primary processes which account for the observed inward eddy vorticity fluxes.

Although this analysis includes only two different tropical cyclone formation cases, the results appear informative. The success of this analysis suggests the possibility of using the rawinsonde composite technique to study different types of tropical cyclone formation events, provided that strict classification criteria are used during case selection and many hundreds of cases over many years are available.

8. INDIVIDUAL CASE ANALYSIS USING FGGE III-b DATA

The rawinsonde composite analyses discussed in the previous chapters have helped us understand the important structures, circulation patterns and various budgets associated with the genesis and non-genesis cloud clusters. However, the composite technique generally is not adequate to handle the large variations between individual formation cases which occur under different large-scale circulation patterns. It is thus beneficial to study the large-scale circulation variations associated with different individual cyclone formation cases by using the First GARP Global Experiment (FGGE) III-b data.

The major purposes of the individual case analyses are to verify the results obtained from the composite analyses and to show the large variations among individual cases. The focus is placed on the different types of environmental forcing of the low-level vorticity buildup, as discussed by Lee and Gray (1984), Love (1985a,b), Molinari and Skubis (1985), and Lee et al. (1986). The convective burst over $0-4^{\circ}$ or $0-6^{\circ}$ radius during tropical cyclone formation as observed in the composite analyses and as discussed by Lee, et al. (1986) for the North Indian Ocean tropical cyclones is also examined. Due to limitations of the data, no budget analysis will be performed. (In fact, the author has performed the angular momentum budget analysis, but the results are very sensitive to the radial wind (or the divergence) which is less reliable. These results are thus not presented or discussed.)

8.1 Use of FGGE Level III-b Data

The FGGE Level III-b data used in this study are zonal and meridional components of horizontal wind analyzed by the European Center for Medium-Range Weather Forecasts (ECMWF). These data are extracted directly from the analyzed pressure levels, and have not been subjected to any vertical interpolation. The analysis procedure used a primitive equation forecast for the first guess, but after the initial analysis step, no model initialization has taken place. The data are available at 1.875° latitude/longitude grids and at 15 vertical pressure levels. A cylindrical coordinate is often preferable for studying the radial and tangential circulations associated with a tropical cyclone. The original gridded wind analyses are thus interpolated linearly onto a cylindrical grid system with 2° latitude radial and 22.5° azimuthal grid spacings. The zonal and meridional wind components (u, v) are then converted to radial and tangential winds (V_r, V_t) with respect to the moving cyclone center.

Although there are 15 vertical levels in the analyses, this study relies heavily on the upper and lower troposphere because raw data (from SMS satellite winds) are more numerous there. Most tropical cyclone development is influenced by the large-scale circulations at these levels too. The satellite-derived cloud winds are very useful information in the FGGE III-b analyses. Unfortunately, there exists an uncertainty in determining the heights of these cloud winds. Therefore, the 150 mb, 200 mb (weighted by a factor of two) and 250 mb wind vectors (weighting factor one) are averaged to represent the upper-level flow. This also takes into account the different heights of the maximum outflow associated with tropical cyclones. Equatorial outflow layers

are typically 25-50 mb higher than poleward outflow layers. By averaging 150, 200, and 250 mb levels together, we obtain a measure of the outflow which can be compared at all azimuths. On the other hand, the low-level circulation is represented by the layer average from 700 mb to 1000 mb.

A very important question that needs to be answered when using the FGGE analyses is how well can they represent the individual tropical cyclone surrounding circulation. Since there is no direct answer to this question, a reasonable substitute is to look at how well the FGGE analyses compare against the rawinsonde composites. Therefore, a radius-pressure cross section of the mean tangential wind for some composites and three FGGE cases are shown in Fig. 59. Typhoons Cecil and Ellis are chosen because they have maximum intensity similar to the typhoon composite. Typhoon Judy is chosen because of its unusually strong intensity. In Fig. 59, the top panel is the very early cloud cluster stage. The middle panel shows conditions at the depression stage or just reaching tropical storm intensity. The bottom panel shows conditions at their mature stage or maximum intensity.

These results indicate that the FGGE analyses are generally quite reasonable in representing a tropical cyclone's mean surrounding circulation at its early stage. As the cyclone systems get organized and become stronger, FGGE analyses become less and less capable of resolving the stronger circulation at the inner radii. However, beyond 5-6° radius, the FGGE analyses are still quite realistic. For the major application in this study -- which is to examine the early formation stage -- it can be assumed that the FGGE analyses are reasonably good as
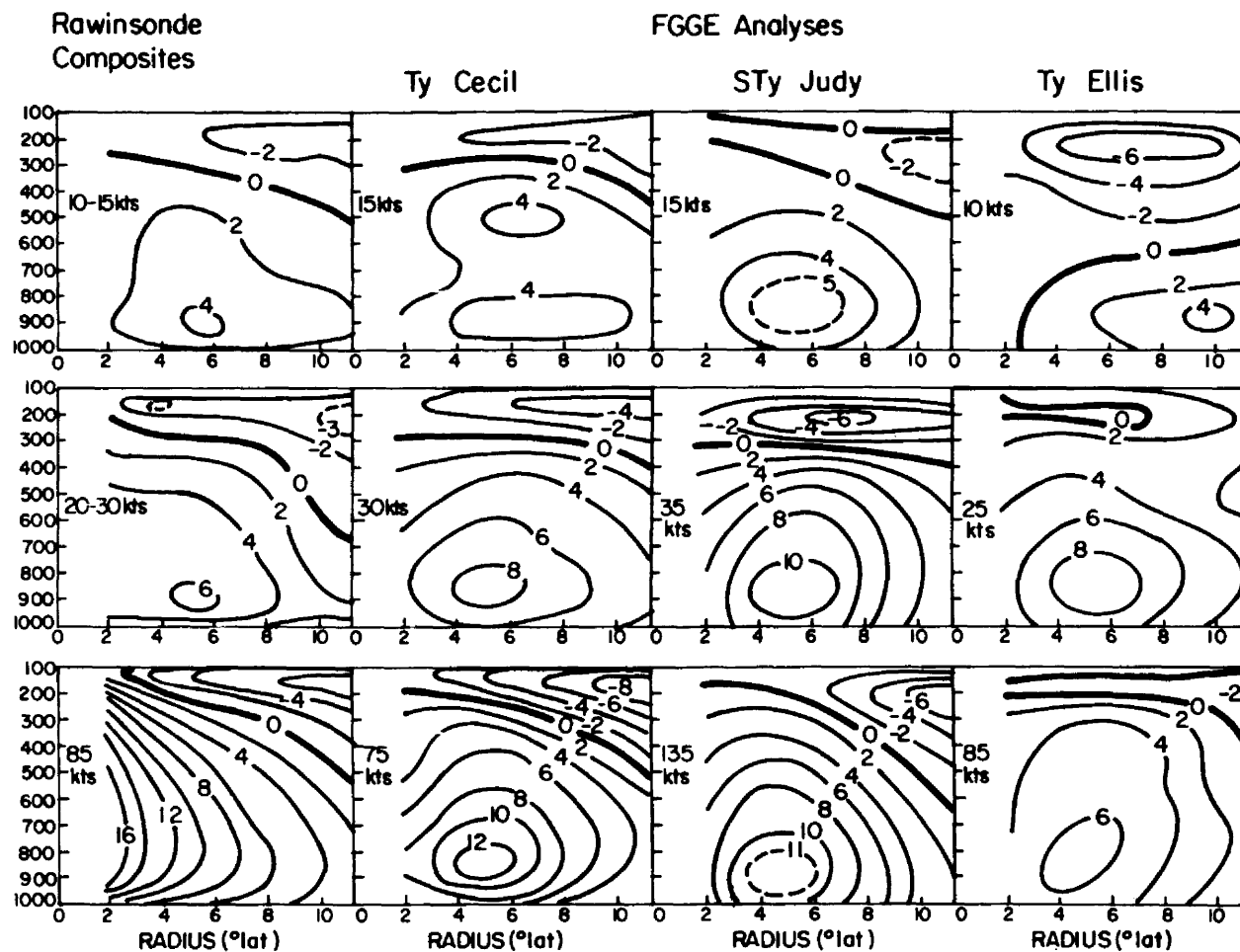
Fig. 59. The radius-pressure cross section of the mean tangential wind for the rawinsonde composites and three FGGE cases: Typhoon Cecil, Typhoon Ellis and Supertyphoon Judy at 3 different intensity stages. The intensity is shown for each case.

close as 3-4° radius from the center. For Typhoon Ellis, the upper level shows a large change between different time periods, and this has caused some concern. It might be more profitable to study the time evolution of these patterns, not just the patterns at one particular time period.

The radial wind profiles at 6° radius for the same aforementioned cases are shown in Fig. 60. The FGGE analyses show profiles generally similar to the composites. Because of the vertical resolution, the maximum inflow values for the FGEE analyses occur at the surface. (Note that the level above 1000 mb is 850 mb in the FGGE analyses). The upper-level outflow generally increases from the cluster stage (marked as 1) to the mature typhoon stage (marked as 3). However, it appears that the FGGE analyses have smeared out the peak outflow magnitude (again, because of the vertical resolution) and have somewhat underestimated the overall outflows.

Many individuals have claimed that the FGGE analyses underestimate the tropical divergence field. The comparisons done in the current analysis, however, do not support this claim - at least not for the divergence field over such a large area (12° latitude in diameter), especially when a layer average is taken. For the 0-4° divergence field, the FGGE analyses do show a reduction in the 0-4° divergence in comparison with the rawinsonde data, especially at later stages. Nevertheless, for the current application, especially when analyzing the time series, the FGGE analyses can be considered reasonably realistic.

8.2 Tropical Cyclones in the Western North Pacific During the 1979 FGGE Year

Twenty-four tropical cyclones that developed during 1979 in the western North Pacific are studied. A list of these cyclones are shown in
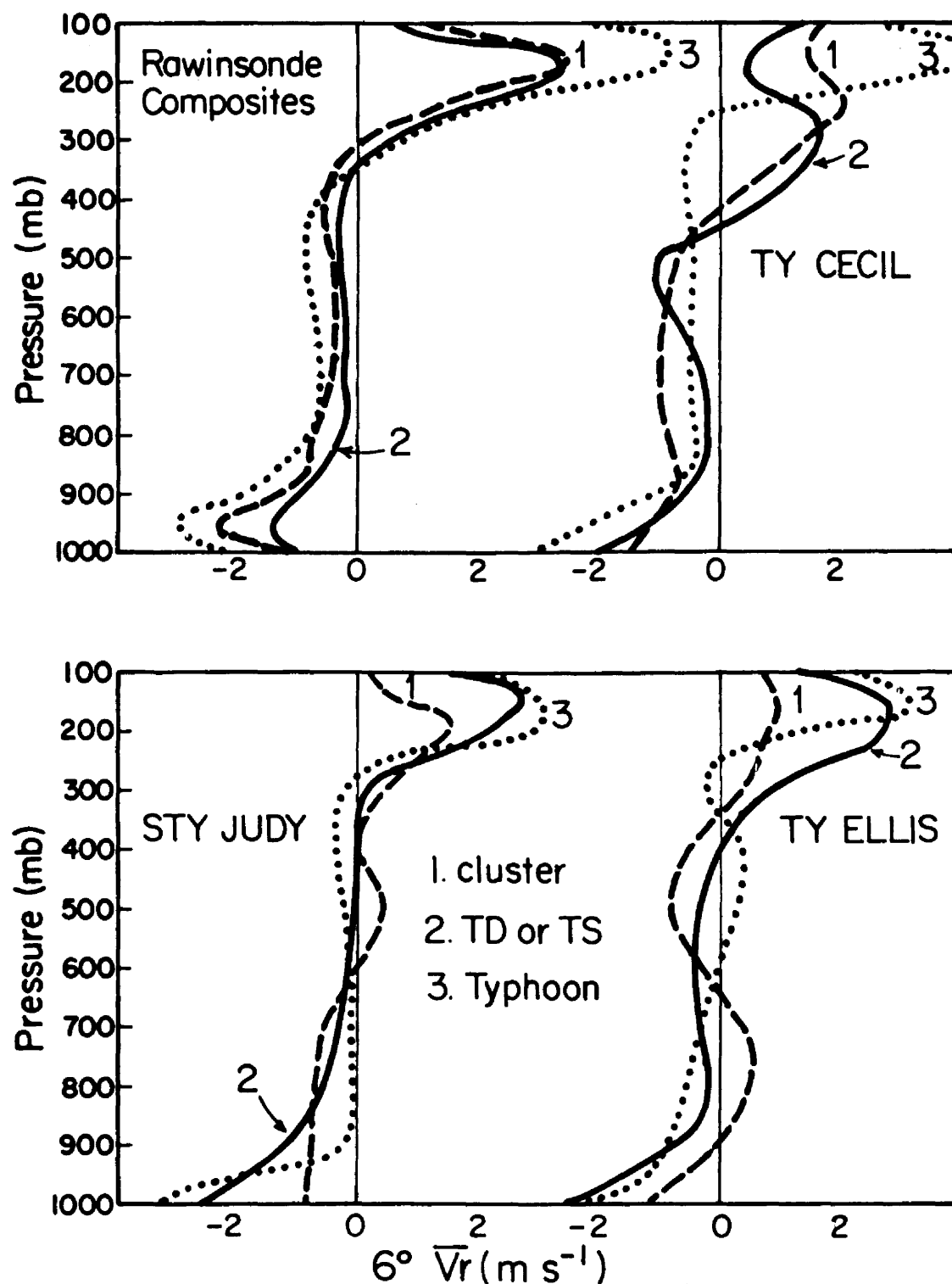
Fig. 60. The $6°$ radial wind profiles for the rawinsonde composites and three FGGE cases: Typhoon Cecil, Typhoon Ellis and Supertyphoon Judy at 3 different intensity stages. The intensity is shown for each case in Fig. 59.

Table 11. (Four systems that occurred in December and January are not
included). Included in the table are the period and the number of days
each system lasts, and the maximum sustained surface wind (kts) and
minimum sea-level pressure (mb). This intensity information is all
based on the Joint Typhoon Warning Center (JTWC) in Guam, Annual Typhoon
Report (ATR). The last two columns list the intensity at the first time
period and the number of days for each system to reach its maximum
intensity.

The ATR best track is obtained by a post analysis that uses all the
possible data including the aircraft reconnaissance flight observations,
the satellite images, the land radar observations and the
surface/gradient level synoptic data. Because 1979 is the first year
the Japanese GMS satellite was available, JTWC best track analyses
positioned some systems from an early time period when they were still
tropical disturbances and not yet tropical cyclones. This seems to have
helped in the current study because the positions at earlier stages for
some systems are better defined. Nevertheless, the data presented in
Table 11 have been adjusted for some systems (marked by a star) to start
at the time periods when they were upgraded to tropical depressions. In
some cases, the NOAA satellite mosaics are used to determine the
positions that precede the start of the best track.

8.3 Time Series

The greatest advantage the FGGE analyses offer is that continuous
time series of any important parameter can be constructed for each
individual tropical cyclone throughout its life cycle. (A continuous
trend of parameters would add to the credibility of the FGGE data.)

TABLE 11

Summary of 1979 Tropical Cyclones in NW Pacific

System Name	Period (No. of days)	Maximum surface winds (kts) and minimum sea-level pressure (mb)	V_{max} (kts) at initial time	No. of days to reach maximum intensity
NW Pacific				
TY Bess	March 20-25 (6)	90(958)	30*	3.0
TY Cecil	April 09-20 (12)	80(965)	15*	6.5
TS Dot	May 08-15 (8)	40(984)	20*	6.0
TD 05	May 17-24 (8)	30(998)	20	7.0
TY Ellis	June 29-Judy 05 (7)	85(955)	20	4.0
TS Faye	July 01-07 (7)	40(998)	20*	5.0
TD 08	July 23-26 (3.5)	20(1004)	15	0.5
TS Gordon	July 25-29 (5)	60(980)	15	2.5
STY Hope	July 25-Aug 03 (10)	130(898)	25*	6.0
TD 11	Aug 04-06 (3)	25(997)	20*	2.0
TY Irving	Aug 09-17 (9)	90(954)	30*	5.5
STY Judy	Aug 15-26 (12)	135(887)	15	5.5
TD 14	Aug 18-20 (3)	20(1006)	15	0.5
TS Ken	Aug 31-Sept 04 (6)	60(985)	20*	4.0
TY Lola	Sept 02-08 (7)	90(950)	25	4.5
TY Mac	Sept 15-24 (10)	70(984)	15*	2.0
TS Nancy	Sept 18-22 (5)	45(993)	25*	1.5
TY Owen	Sept 22-30 (9)	110(918)	20	4.0
TS Pamela	Sept 24-26 (3)	45(1002)	20*	1.0
TS Roger	Oct 02-07 (6)	45(985)	20	3.0
TY Sarah	Oct 04-15 (12)	110(929)	20*	6.0
STY Tip	Oct 04-19 (16)	160(870)	20	8.0
STY Vera	Nov 02-07 (6)	140(915)	25	2.0
TS Wayne	Nov 08-13 (6)	50(990)	25*	2.0

* The JTWC best tracks for these systems start when the systems were still disturbances. The data presented here have been adjusted to start from the time when these systems were upgraded to tropical depressions.

Because of the importance of the upper-level and lower-level mean tangential winds (or the mean vorticity) -- as emphasized by McBride and Zehr (1981) and also observed in the current study -- their time series are constructed for 4° and 6° radius. Two other important parameters included in the time series analysis are the intensity of the system (represented by the maximum sustained surface wind) and the upper-level mean radial wind (or mean divergence) at 4° and 6° radius. To smooth out the short variations over time, especially the diurnal variation, a center weighted three successive 12-hour period running mean in time has been taken for the radial and tangential winds.

Two examples of these time series at 4° and 6° for the first two systems in 1979, that is, Typhoon Bess and Typhoon Cecil, are shown in Fig. 61. Here, the circle represents the time at which the system was upgraded from a tropical disturbance to a tropical depression (cyclone), and the triangle is the first time when the center position was fixed by the aircraft reconnaissance flight data. Note that in most situations the intensity before this point could only be estimated by the synoptic data and satellite Dvorak (1975) method cloud pattern determination. Seven other cases are shown in Chapter 9 and eight more cases are shown in Appendix B. Seven cases are not shown because they are weaker systems or do not last long. Note that the time series for the other cases are shown only at 6° because their patterns are similar at both radii (shown in Fig. 61).

These time series reveal that the individual case variations are very large. However, there are still important characteristics which are common to most cases. These common characteristics will be summarized in this section. To highlight the different large-scale
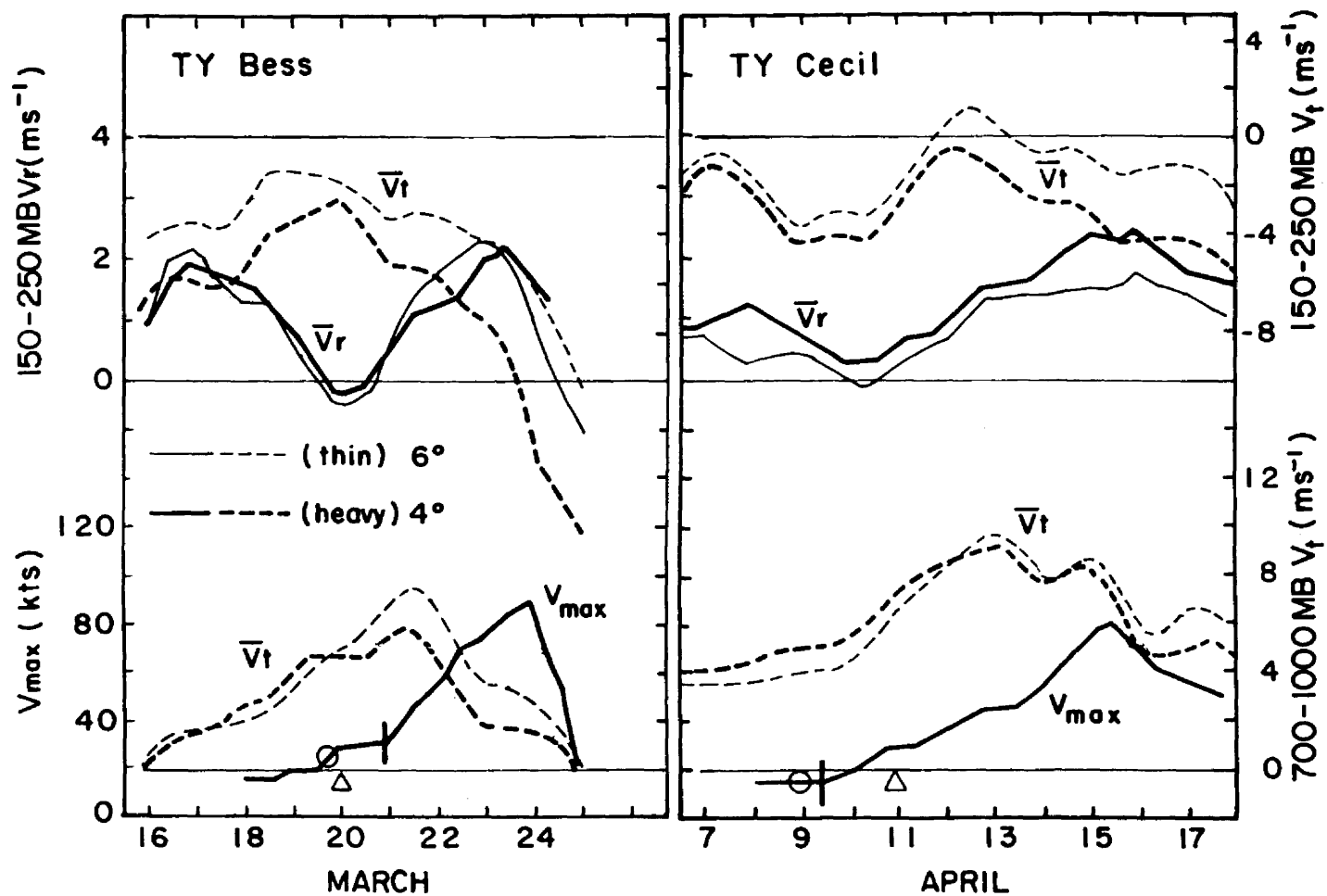
Fig. 61. Time series of the upper-level and low-level mean tangential winds and the upper-level mean radial wind at 4° and 6° radius for Typhoon Bess and Typhoon Cecil. The maximum intensity is also shown. The circle is the time period when the system was upgraded to a tropical cyclone and the triangle is the first time period when the center of the system was fixed by the aircraft reconnaissance flight.

circulation patterns during tropical cyclone formation and development,
seven cases will be discussed in detail in the next chapter.

8.3.1 Cyclone Intensity vs. Low-Level Mean Vorticity

Analysis indicates that a majority of tropical cyclones experience
a time period (ranging from 1 to 4 days) with little or no intensity
change before a large intensification, as shown in the bottom panel of
Fig. 62. Intensification information was obtained from Guam based
aircraft reconnaissance data. In this figure each intensity curve has
been normalized with respect to the time period when a major increase in
intensity is about to occur. This time period is marked by a short
straight vertical bar in the time series of maximum intensity for each
case and, for convenience, is called the ''transition point.'' This
''transition point'' is often very close to the time period when the
system was upgraded to a tropical cyclone. Although the system's
intensity does not change much before this point, the outer 4-6°
circulation (or the mean vorticity over 0-4° or 0-6° radius) generally
increases greatly -- as is shown in the middle panel of Fig. 62 in which
the magnitude of $\bar{V}_t$ has also been normalized with respect to the
magnitude at the transition point. After the transition point, the
outer circulation can experience quite different wind change patterns.
Three systematic patterns have been identified and are synthesized as
shown in Table 12.

The first change pattern (Category 1) in the outer circulation
shows primarily no change or an increase trend in the 4-6° tangential
wind after this transition point. This change pattern occurred with 9
cases which tended to have a weaker intensification rate, averaging 13
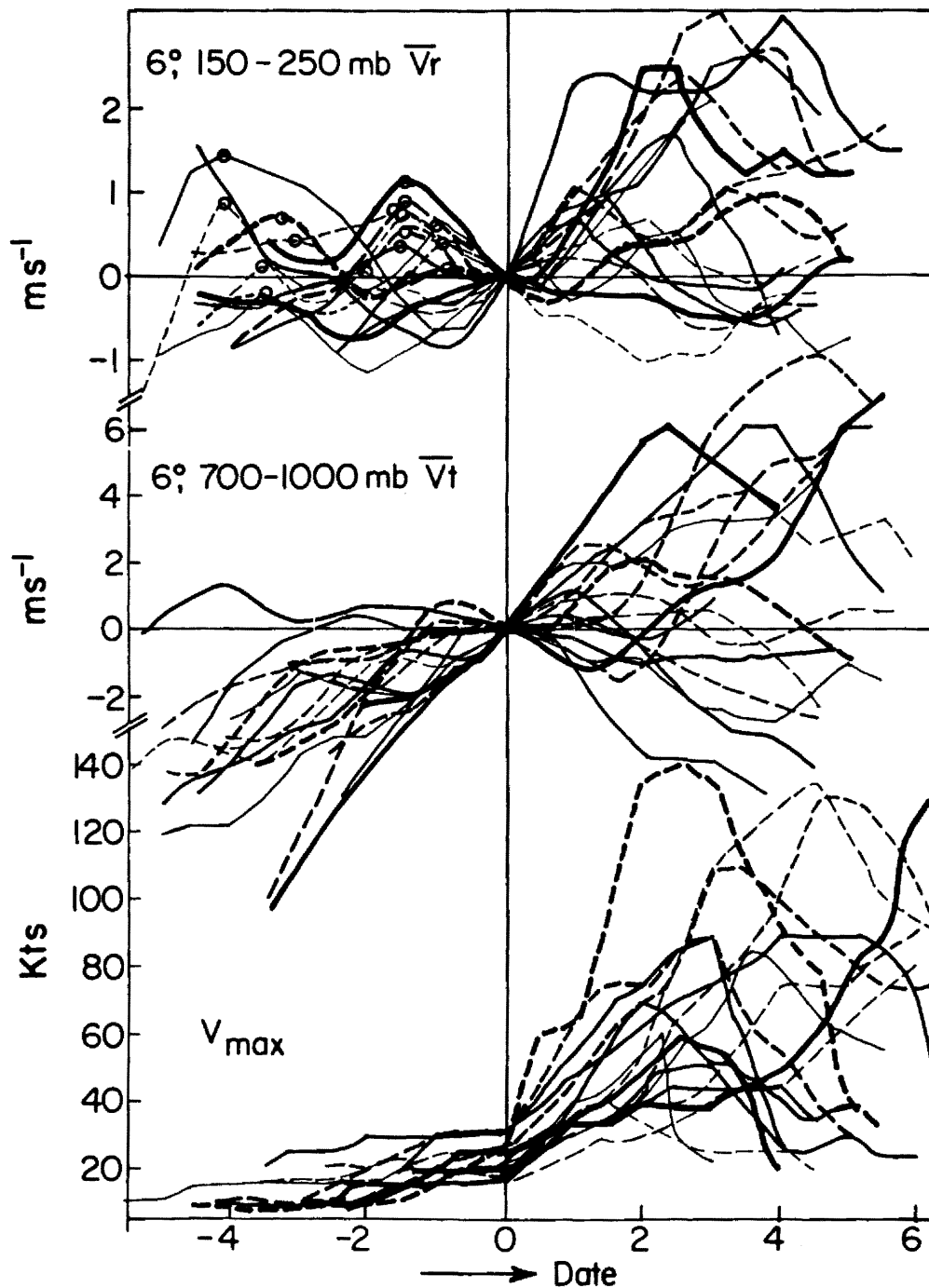kts per day (left column). The two other change patterns (categories 2

Fig. 62. Time series of the upper-level $\overline{V}_r$ (upper panel) and low-level $\overline{V}_t$ (middle panel) at 6° radius and of the maximum intensity (bottom panel). Note that time has been normalized with respect to the transition time period which is marked as the straight bar in the time series diagram (see text for definition of transition point). The magnitudes of $\overline{V}_r$ and $\overline{V}_t$, have also been normalized with respect to the magnitudes at the transition time period for each individual case.

TABLE 12

Typical variations of low-level outer 4-6° circulation after the transition point (see text) and before reaching maximum cyclone intensity. The intensification rate (in kts per day) for every case in each category is shown. Numbers within parentheses are the total intensity increase (in kts) and numbers of days for each system to reach its maximum intensity. For example, Typhoon Cecil increases 65 kts in 6.0 days or 11 kts every day.

Category 1 No Change or Increasing	Category 2 Decreasing	Category 3 Decreasing then Increasing
Cecil (65/6.0) 11	Bess (60/3.0) 20	Hope (115/4.5) 26
Faye (15/1.5) 10	Ellis (65/3.5) 19	July (120/4.5) 27
Gordon (45/2.5) 18	Lola (60/3.0) 20	Owen (85/3.0) 28
Irving (60/4.0) 15	Mac (55/2.0) 28	Tip (140/7.5) 19
Ken (35/2.25) 16	Wayne (35/2.5) 14	Vera (115/2.5) 46
Roger (25/2.5) 10	Average 20	Average 29
Sarah (95/6.5) 15		
Average 13	Average 24	

and 3) show a decreasing or a break in the increase of 4-6° tangential wind around (or after) this transition point has been reached. These cases generally have a stronger intensification rate, averaging 24 kts per day or a 70% higher rate than that of category 1. Category 3 includes those typhoons which have a much stronger intensification rate and/or last longer to allow their inner strong circulation to build up and expand outward, thus causing the outer circulation to first decrease and then to increase again.

These results agree very well with the composite information. For the systems to undergo stronger developing rates (fast genesis), the circulation primarily increases at the inner radii. There is little change (or even decreasing) in the tangential wind at the outer radii

during the early developing stage (that is, from Stage 3 to Stage 4 of the composites). The slow developer (slow genesis), however, shows a circulation increase over a much larger radius; thus an increase in the $4-6^{\circ}$ outer circulation is observed before and after the transition point.

8.3.2 Upper-Level Mean Vorticity and Divergence

The upper-level $4-6^{\circ}$ tangential wind and radial wind (or mean vorticity and divergence) show much larger variations with time in responding to the rapidly changing upper-level flow features. Weak anticyclonic vorticity is generally present at the early stage. However, the evolution of the upper-level vorticity (not shown) is frequently erratic. For some strong systems, the upper-level circulation tends to become less and less anticyclonic, or even becomes cyclonic, due to the strong vertical transport of cyclonic vorticity from low levels.

The upper-level mean divergence (or radial wind) shows a more consistent pattern than does the vorticity field. In general, the divergence (or radial wind) at $4-6^{\circ}$ radius increases as the system intensifies during its developing phase. For some cases, the mean radial wind peaked before the maximum intensity was reached. R. Edson (personal communication) also found similar features in his analysis. An interesting phenomena is that a radial wind or upper-level inward horizontal transport maximum is frequently observed during the early formation stage (before the ''transition point'') of the system. To illustrate this feature, the normalized upper-level radial winds for all 17 cases are shown in the upper panel of Fig. 62. Circles represent the local maximum of divergence before the transition point is reached. In

ten systems, this local maximum (or a convection burst) occurs at one to one and a half days before the transition point. Five systems have this convection burst at three to four days before the transition point.

These convective bursts are very similar to those of the composite cases except for a slight difference in time. The composite cases show the convective bursts occurring at the tropical cyclone formation time period (or Stage 3). The individual case time series, however, shows greater individual case variations and the convection burst generally occurs slightly before the disturbance was upgraded to a tropical depression. (Note that this intensification point is generally within one day after the time period when the system was upgraded to a tropical depression.) This difference in time may just be the result of the composite smoothing effect. The importance of the convective burst is that it appears to be an indicator that the low-level large-scale inward surge forcings has reached the vicinity of the disturbance and is acting to concentrate the convection. Associated with this low-level large-scale forcing is a large increase of the low-level large-scale vorticity. The next chapter will give a more detailed discussion of this process for individual cases.

The results discussed above are based on the symmetric features. However, the asymmetric features are often more important because the circulation is usually quite asymmetric in the early formation stages. This is discussed in the next chapter.

9. EXAMPLES OF LARGE-SCALE CIRCULATION PATTERN CHANGES ASSOCIATED
WITH INDIVIDUAL TROPICAL CYCLONE FORMATION DURING THE FGGE YEAR

This chapter discusses seven cases of tropical cyclone formation which occurred during four time periods in the 1979 FGGE year. The first time period is from late June to early July 1979 during which typhoon Ellis and tropical storm Faye formed. Both cross-equatorial surges and trade wind surges were observed during this period. The second time period is late July 1979. Circulation patterns were complicated during this period but three tropical cyclones formed - Supertyphoon Hope, Tropical Storm Gordon and a tropical depression (No. 08). The third time period is between late August and early September 1979 during which Typhoon Lola and Tropical Storm Ken occurred almost simultaneously along the periphery of a TUTT system. The last time period studied was early November 1979 when Supertyphoon Vera formed as a tropical cyclone on 2 November with an intensity of only 25 kts but then intensified by 110 kts in the next two days, reaching a supertyphoon intensity of 135 kts.

The following discussion will be divided into four sections corresponding to these four time periods. A detailed analysis of Typhoon Ellis and Supertyphoon Vera is given. Other cases are presented primarily to show the influence of different large-scale conditions. The focus of the discussion is on the systematic characteristics and the large variabilities of the environmental wind forcing between cases. Although the emphasis is on tropical cyclone formation, the important

large-scale characteristics during these cyclones' later development phase are also discussed. Of special interest is the relationship between the cyclone intensification and the upper-level outflow jet as discussed by Chen and Gray (1985) and Merrill (1985). For convenience, the given name of each system will be used during the discussion even if it is only a weak cloud cluster or depression at that time. (Note that a tropical cyclone is not given a name unless it reaches tropical storm intensity.)

9.1 Ellis and Faye

Formation Stage. Although the Annual Typhoon Report (ATR) best track of Typhoon Ellis starts from 23 June (as shown in Fig. 63), the time series shows that Ellis did not really develop until after the 30th (Fig. 64). (Ellis was upgraded to a tropical cyclone or depression on the 29th.) The cloudiness associated with the pre-Ellis disturbance was not noticeable until 25 June (see Fig. 65, diagrams a and b). The cloud pattern is reasonably organized by the 26th. In the time series (Fig. 64), a significant increase of both upper-level divergence and low-level vorticity over 4° to 6° radius is observed from the 24th to the 26th. This is primarily due to a low-level cross-equatorial surge, (see Fig. 66 diagrams a-d).

On 24 June the trade winds in both hemispheres (near the equator) are strong to the east of the Dateline (180°), and are split into two branches west of the Dateline. The Northern Hemisphere branch extends westward toward the Asian continent and maintains approximately the same strength through 27 June. The pre-Ellis disturbance is located south-southwest of a moderately strong trade wind zone (wind speed greater than 5 m s^{-1}). In the Southern Hemisphere, the trade winds (south
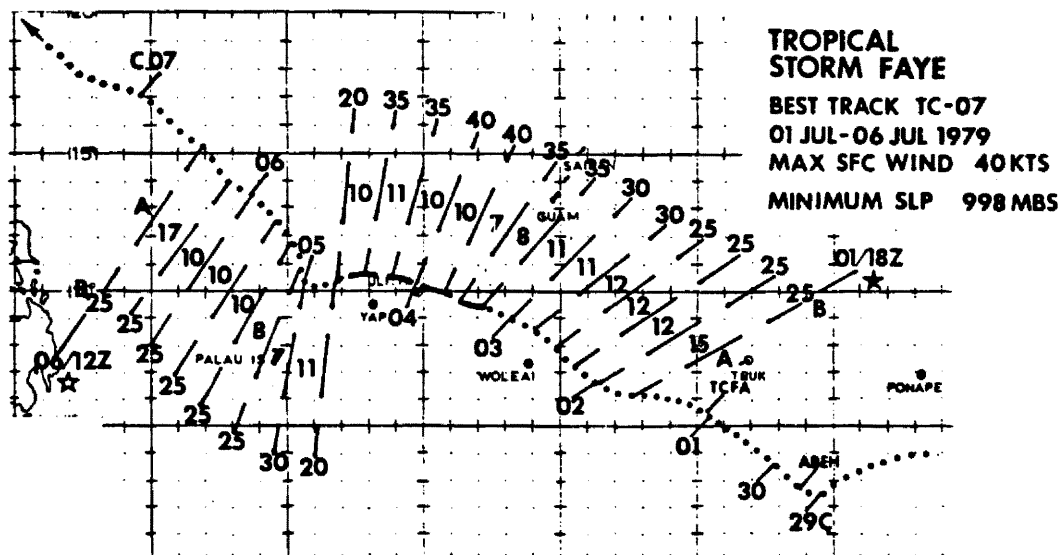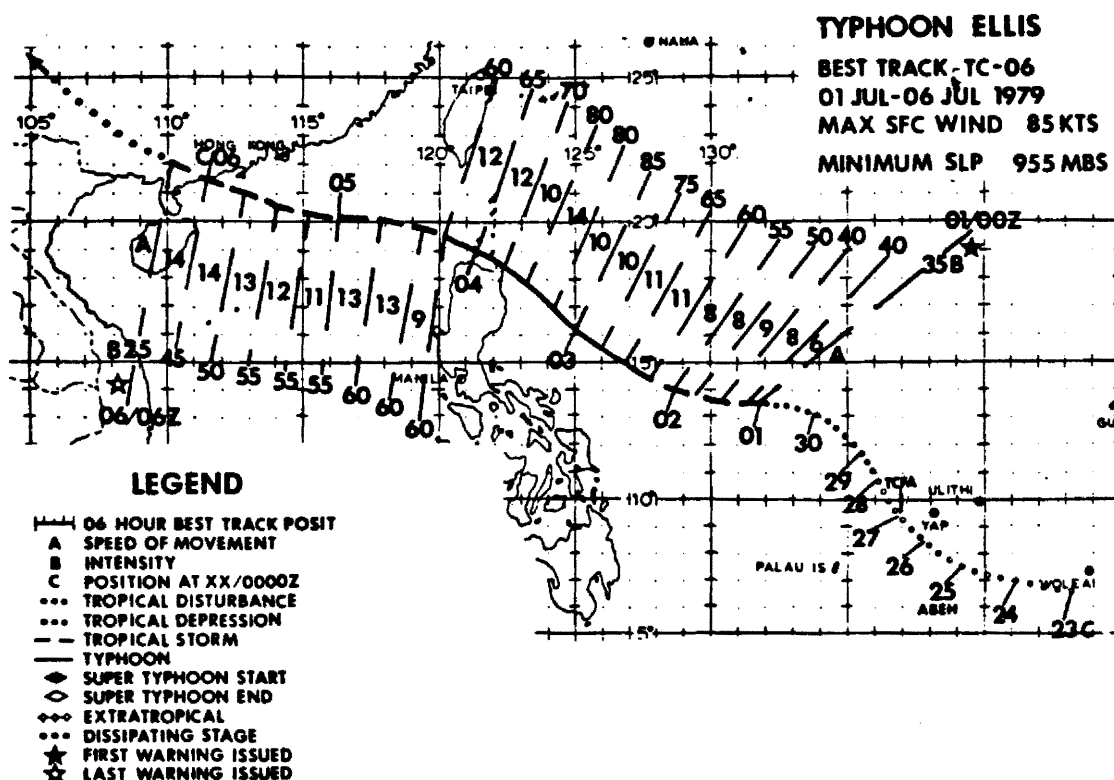
TYPHOON ELLIS

BEST TRACK TC-06
01 JUL-06 JUL 1979
MAX SFC WIND 85 KTS

MINIMUM SLP 955 MBS

LEGEND

|←—| 06 HOUR BEST TRACK POSIT
A SPEED OF MOVEMENT
B INTENSITY
C POSITION AT XX/0000Z
••• TROPICAL DISTURBANCE
••• TROPICAL DEPRESSION
— — TROPICAL STORM
—— TYPHOON
◆ SUPER TYPHOON START
◇ SUPER TYPHOON END
✦✦◇ EXTRATROPICAL
••• DISSIPATING STAGE
★ FIRST WARNING ISSUED
☆ LAST WARNING ISSUED

**TROPICAL
STORM FAYE**

BEST TRACK TC-07
01 JUL-06 JUL 1979
MAX SFC WIND 40 KTS

MINIMUM SLP 998 MBS

Fig. 63. The best tracks for Typhoon Ellis and Tropical Storm Faye
(1979). The data are taken from JTWC ATR best tracks.
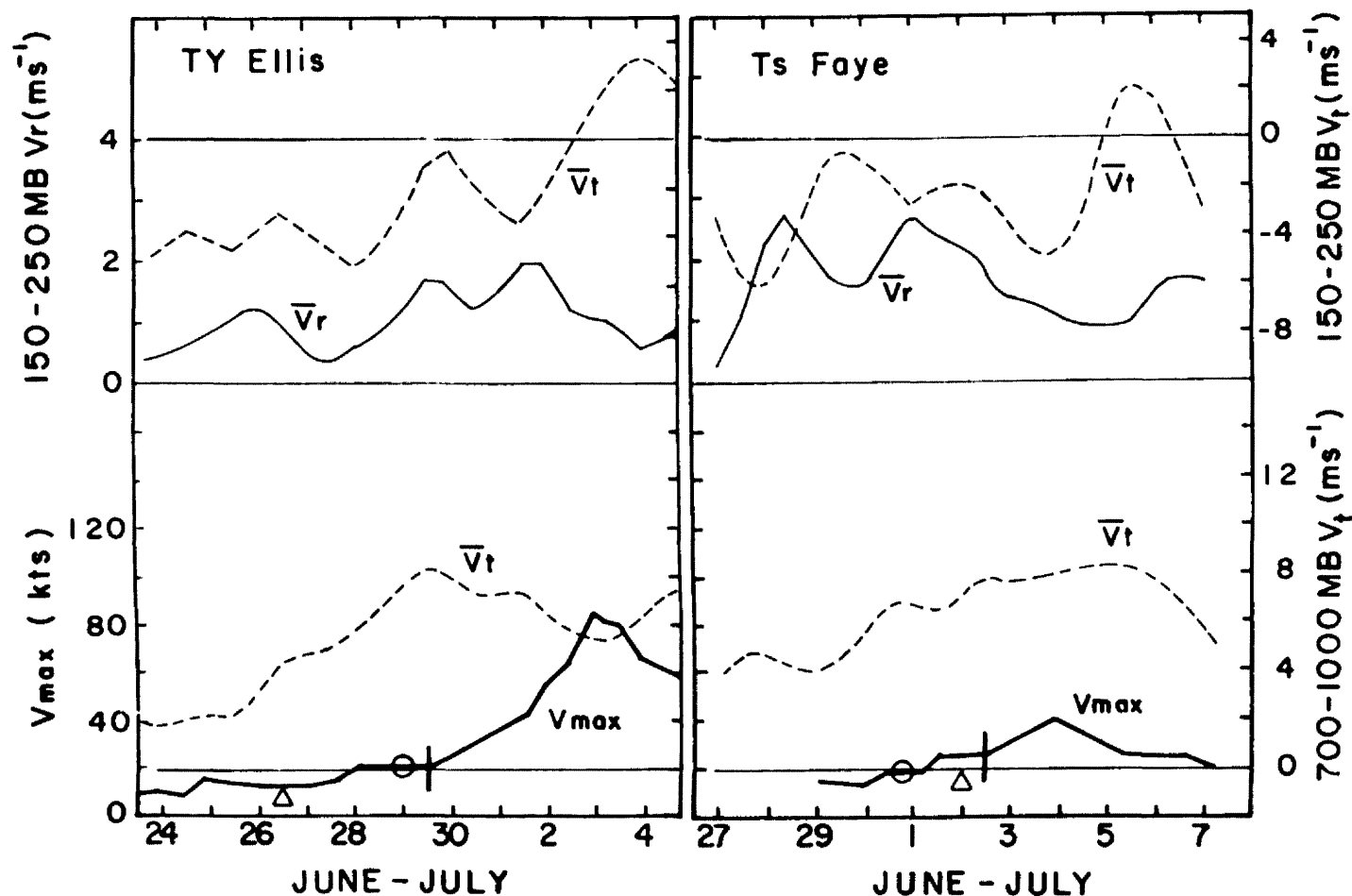
Fig. 64. Time series of the upper-level and low-level mean tangential winds and the upper-level mean radial wind at 6° radius for Typhoon Ellis and Tropical Storm Faye. The maximum intensity is also shown. The circle is the time period when the system was upgraded to a tropical cyclone or depression. The triangle shown is the first time period when the center of the system was fixed by the aircraft reconnaissance flight.
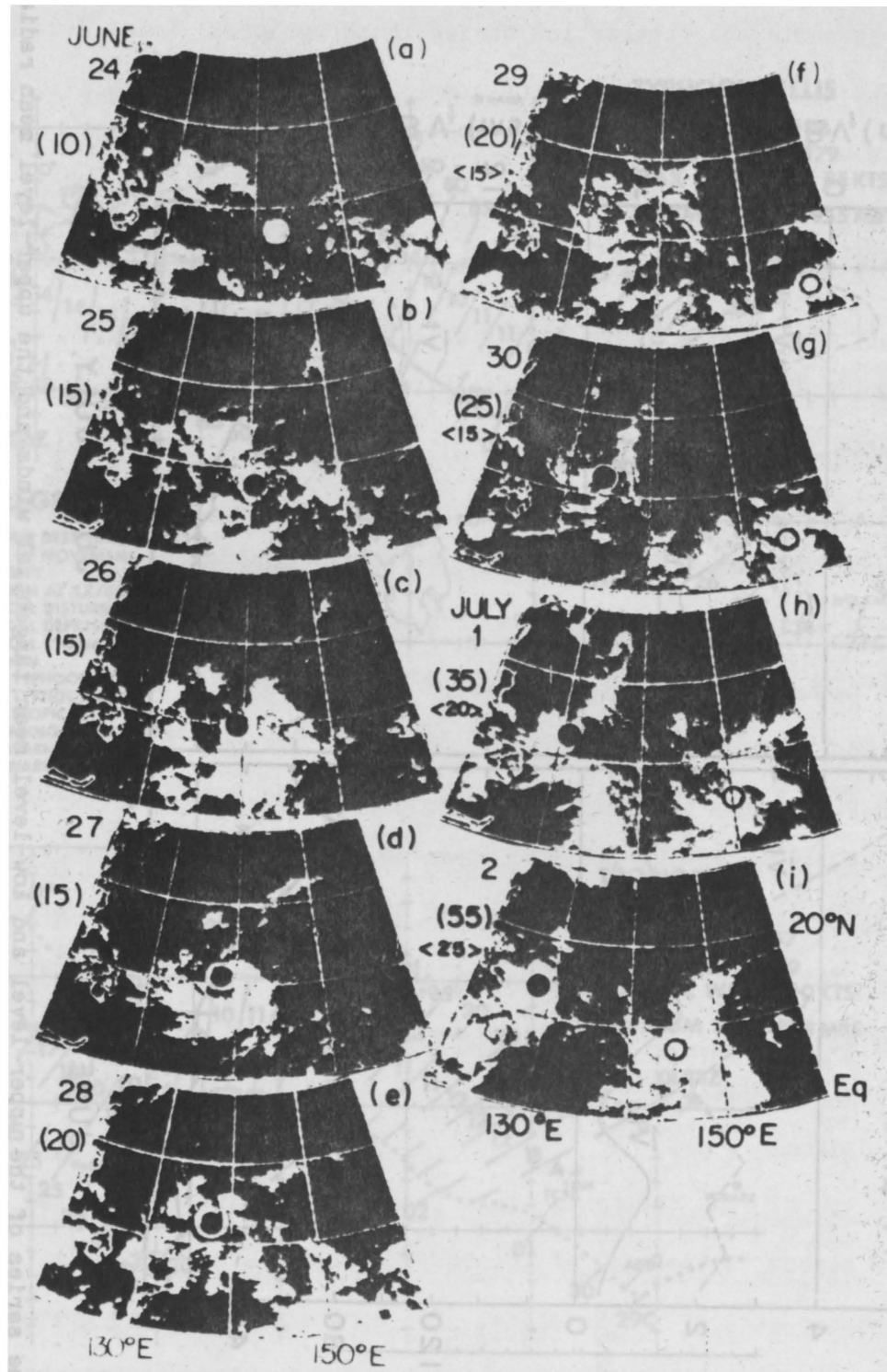
Fig. 65. The NOAA satellite pictures from 24 June, 03Z to 2 July, 03Z. Centers of Ellis and Faye are shown as dots and circles, respectively. Intensities of Ellis and Faye are shown within parentheses and brackets (in kt), respectively.
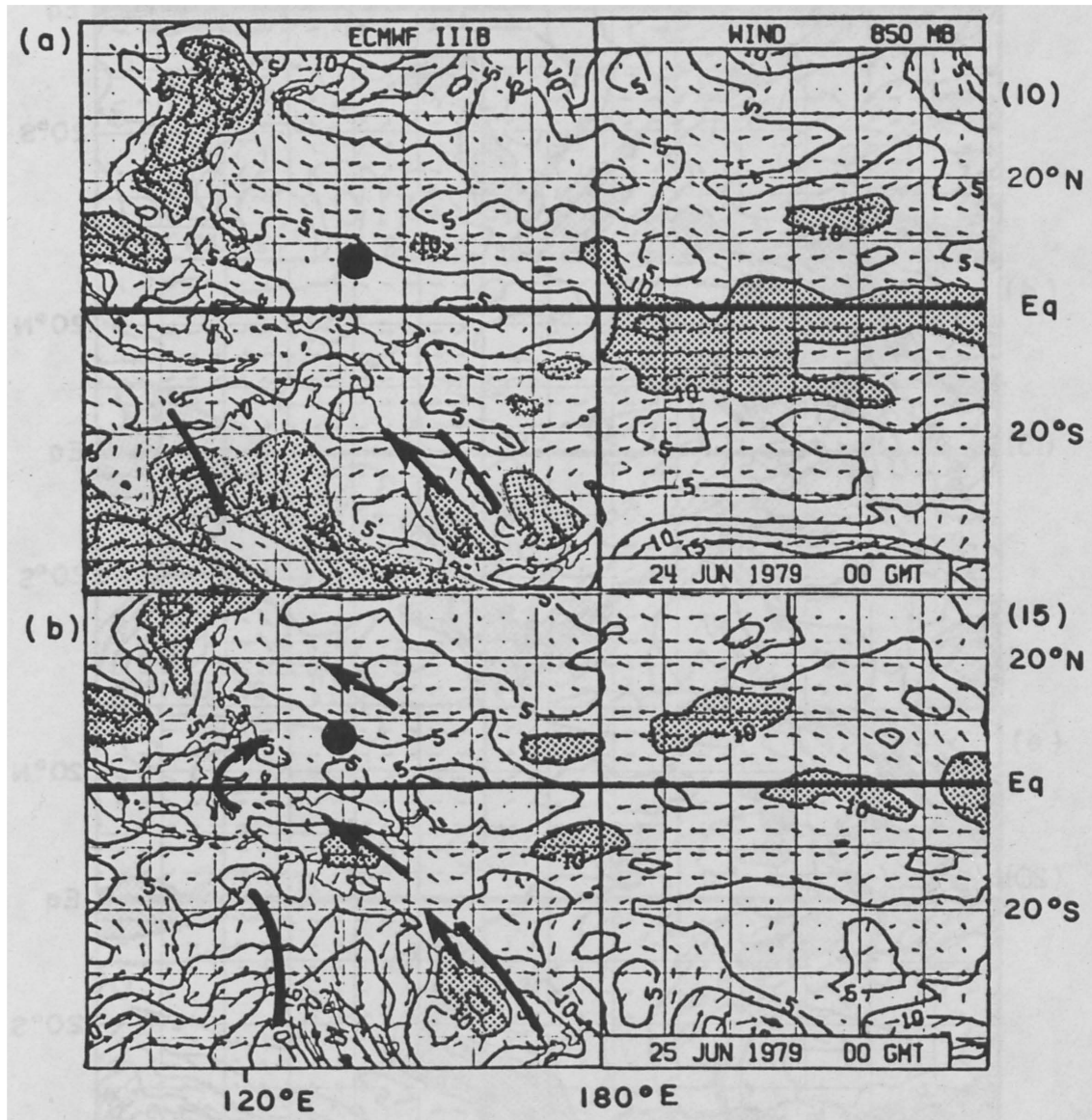
Fig. 66. The 850 mb flow pattern and isotachs on 24 June–1 July, 00Z. The shaded areas are the regions with a wind speed $\geq$ 10 m s^{-1}. The dots and circles show the center positions of Ellis and Faye, respectively. Intensities of Ellis and Faye are shown within parentheses and brackets (in kt), respectively.

Fig. 66. Continued.

178
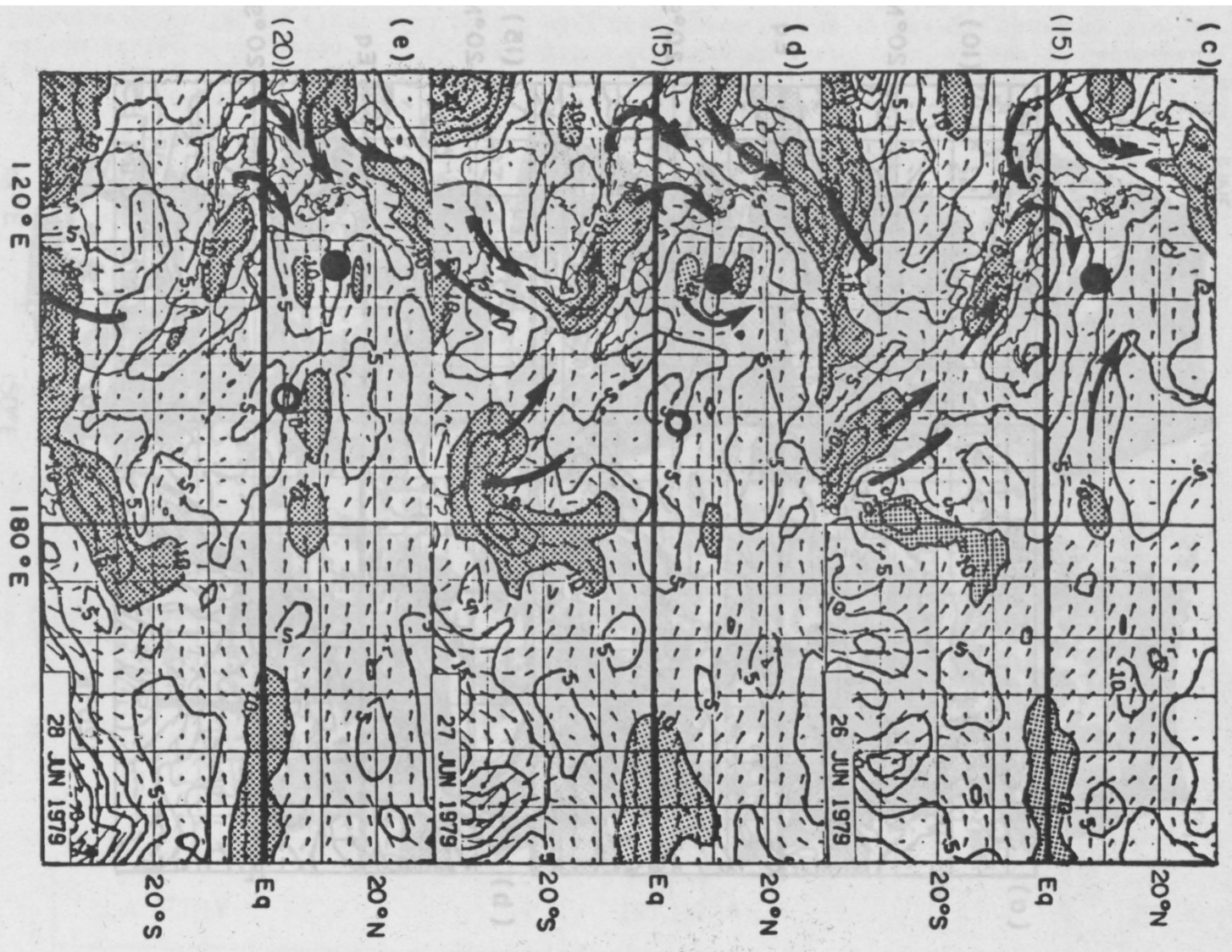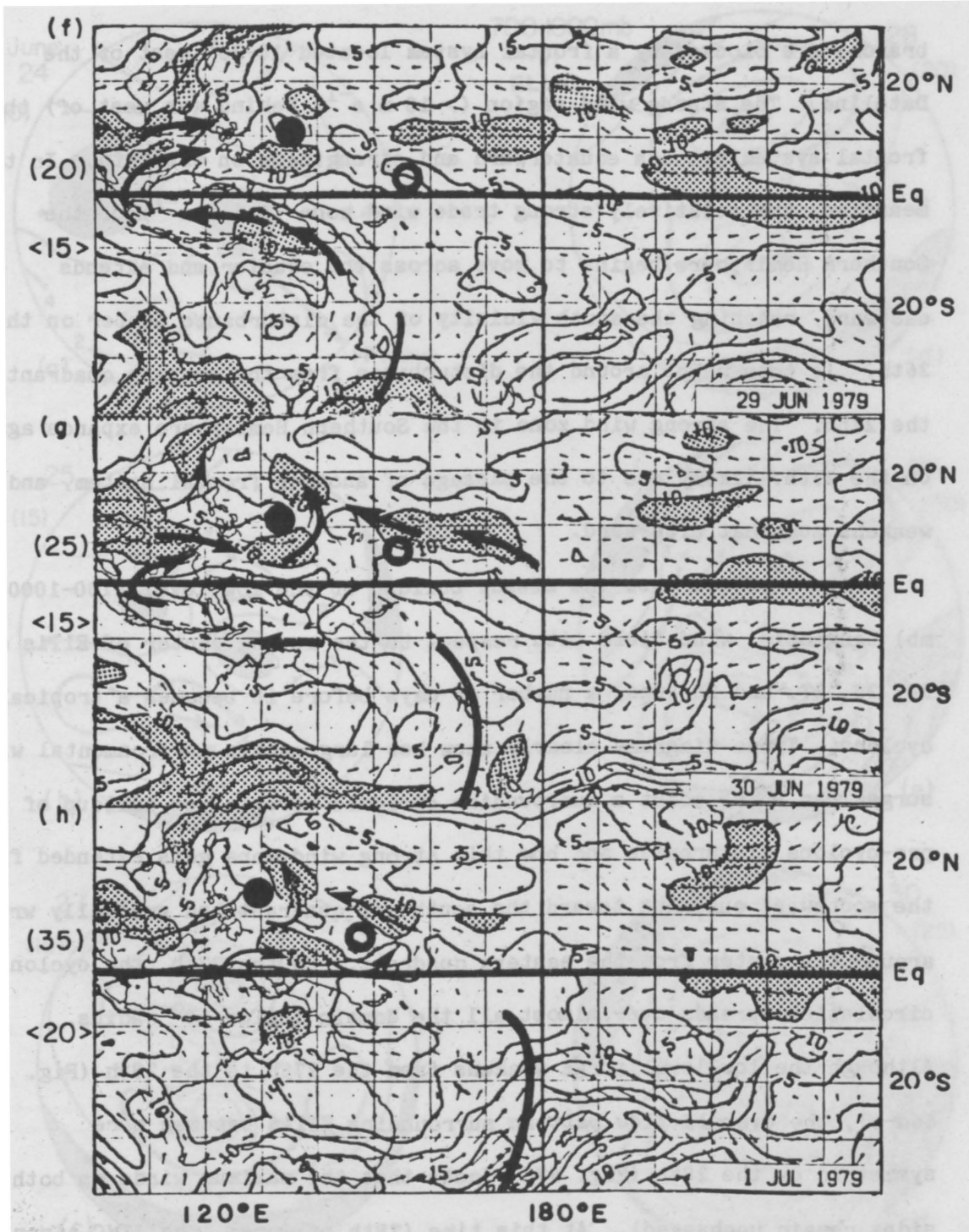
Fig. 66. Continued.

branch) are blocked by a frontal system located 10-30° west of the
Dateline. The strong wind region (> 10 m s^{-1}) behind (or west of) this
frontal system extends equatorward and strengthens on the 26th. In the
meantime, the relatively strong trade wind zone (> 5 m s^{-1}) of the
Southern Hemisphere begins to move across the equator and extends
eastward, reaching the south vicinity of the disturbance center on the
26th. It then wraps around the disturbance from the eastern quadrant on
the 27th. The strong wind zone in the Southern Hemisphere expands again
on the 27th, likely due to the passage of another frontal system, and
weakens somewhat afterward.

Figures 67a-d show the steady buildup of the low-level (700-1000
mb) tangential wind field with respect to the moving center of Ellis on
24, 25, 27, and 28 June, a number of days before it becomes a tropical
cyclone. These diagrams clearly show how large-scale environmental wind
surges can bring about a surrounding cyclonic circulation buildup of the
pre-cyclone disturbance and how this strong wind zone gets extended from
the southwest quadrant toward the southeast quadrant and gradually wraps
around the center from the eastern quadrant. On the 27th, the cyclonic
circulation spreads over almost all the domain inside 10° radius.
Although the low-level surge weakens from the 27th to the 28th (Fig.
66d-e), the overall flow pattern surrounding Ellis becomes more
symmetric on the 28th (Fig. 67d) (note that the maximum winds on both
sides remain unchanged). At this time (28th of June), the JTWC aircraft
reconnaissance flights could find only a very broad surface circulation
with a relatively high surface pressure (JTWC ATR, 1979).

On the 26th, a Tropical Upper Tropospheric Trough (TUTT) was
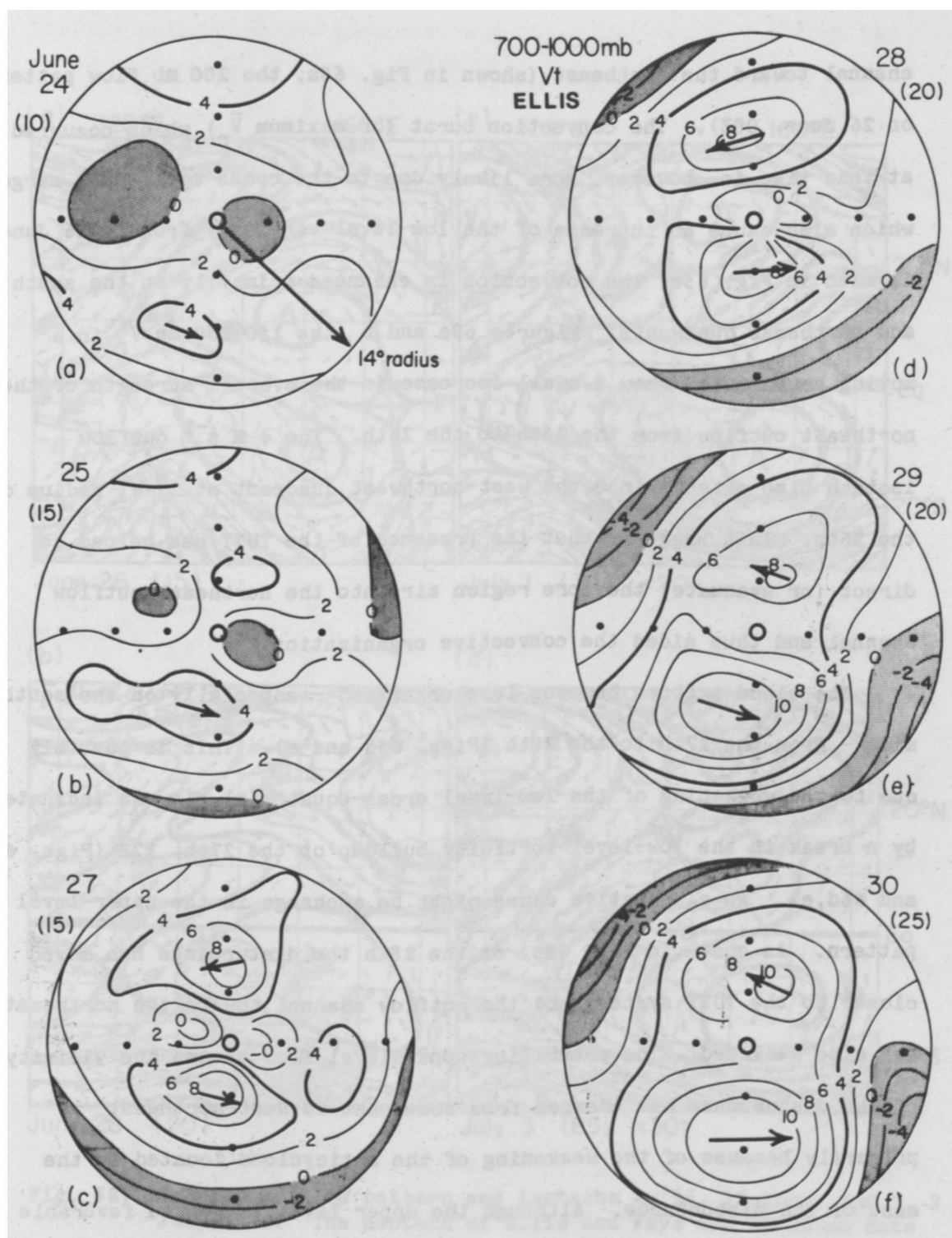located north of the disturbance center, providing a good outflow

Fig. 67. The 700-1000 mb average V_t in moving or MOT coordinate for Ellis on 24, 25, 27, 28, 29, and 30 June, 00Z. The shaded areas are the negative V_t regions and the heavy curves are 4 m s^{-1} isotachs. The radial grid spacing is 4° latitude. The intensity is shown within parentheses.

channel toward the northeast (shown in Fig. 68a, the 200 mb flow pattern on 26 June, 00Z). The convection burst (or maximum $\bar{V}_r$) which occurred at this time is, however, more likely due to the cross-equatorial surges which also cause an increase of the low-level vorticity from 24-26 June. As seen in Fig. 65c, the convection is enhanced primarily on the south and southeast quadrants. Figures 69a and b (the 150-250 mb V_r in a moving coordinate) show a small increase in the overall strength of the northeast outflow from the 25th to the 26th. The 4 m s^{-1} outflow isotach also extends into the west-northwest quadrant at 2°-6° radius on the 26th. This suggests that the presence of the TUTT has helped to direct (or evacuate) the core region air into the northeast outflow channel and thus aided the convective organization.

The cloud pattern becomes less organized - especially on the south side - from the 27th to the 28th (Figs. 65d and e). This is possibly due to the weakening of the low-level cross-equatorial flow as indicated by a break in the low-level vorticity buildup on the 27th, 12Z (Figs. 64 and 66d,e). An alternative cause might be a change in the upper-level pattern. As shown in Fig. 68b, on the 28th the disturbance has moved closer to the TUTT system, and the outflow channel toward the northeast has also weakened. The prevailing upper-level flow around the vicinity of the disturbance has changed from southeast to west-northwest primarily because of the weakening of the anticyclone located to the east of the disturbance. Although the upper level is not so favorable (large-scale divergence decreases to almost zero), the low-level vorticity remains strong, about 2 x 10^{-5} s^{-1} over an area of 4-6° radius. (Note that f = 2.5 x 10^{-5} s^{-1} at 10°N.) It is this strong
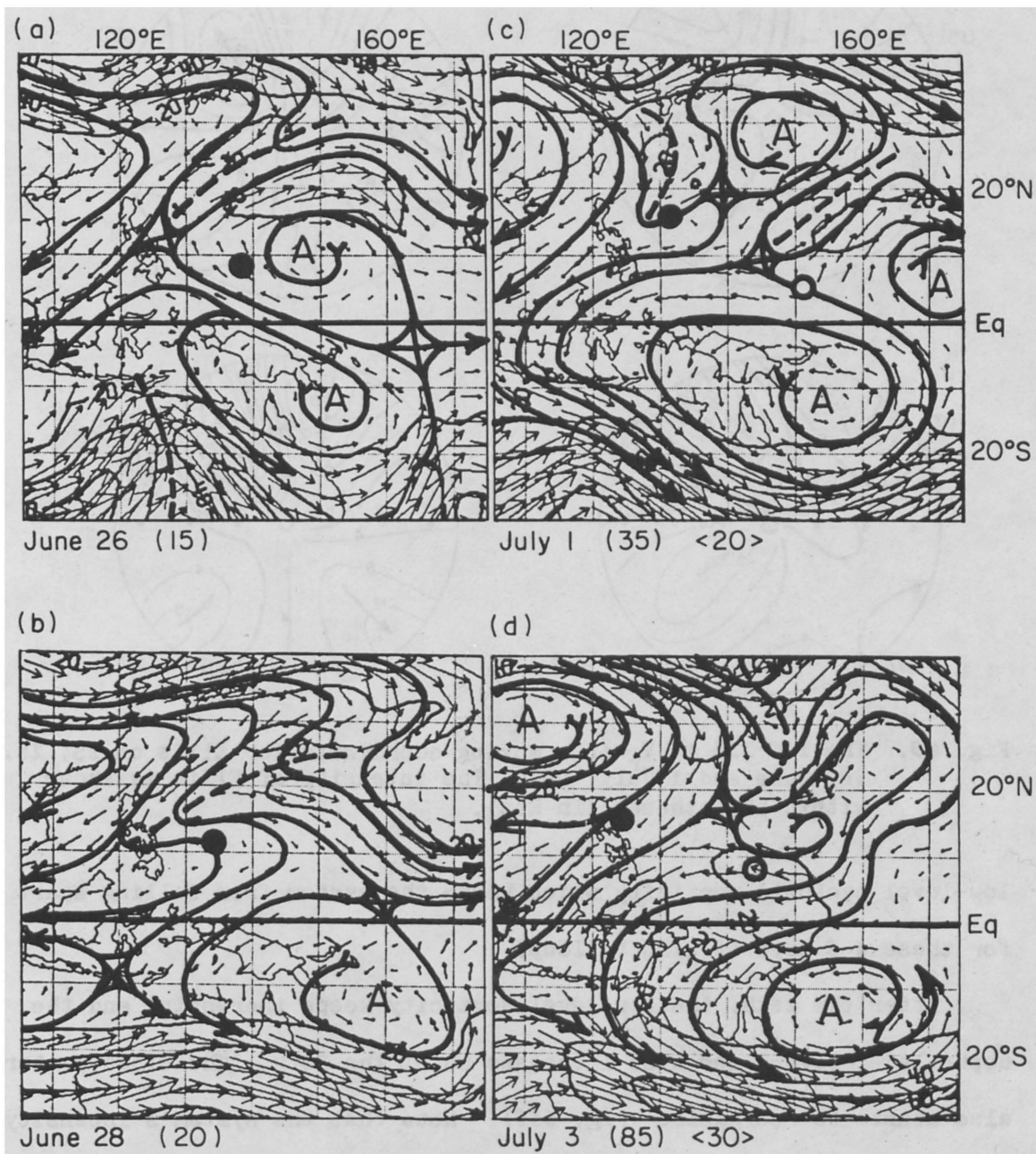
Fig. 68. The 200 mb flow pattern and isotachs on 26, 28 June, and 1, 3 July, 00Z. The centers of Ellis and Faye are shown as dots and circles, respectively. Intensities of Ellis and Faye ae shown within parentheses and brackets (in kt), respectively.
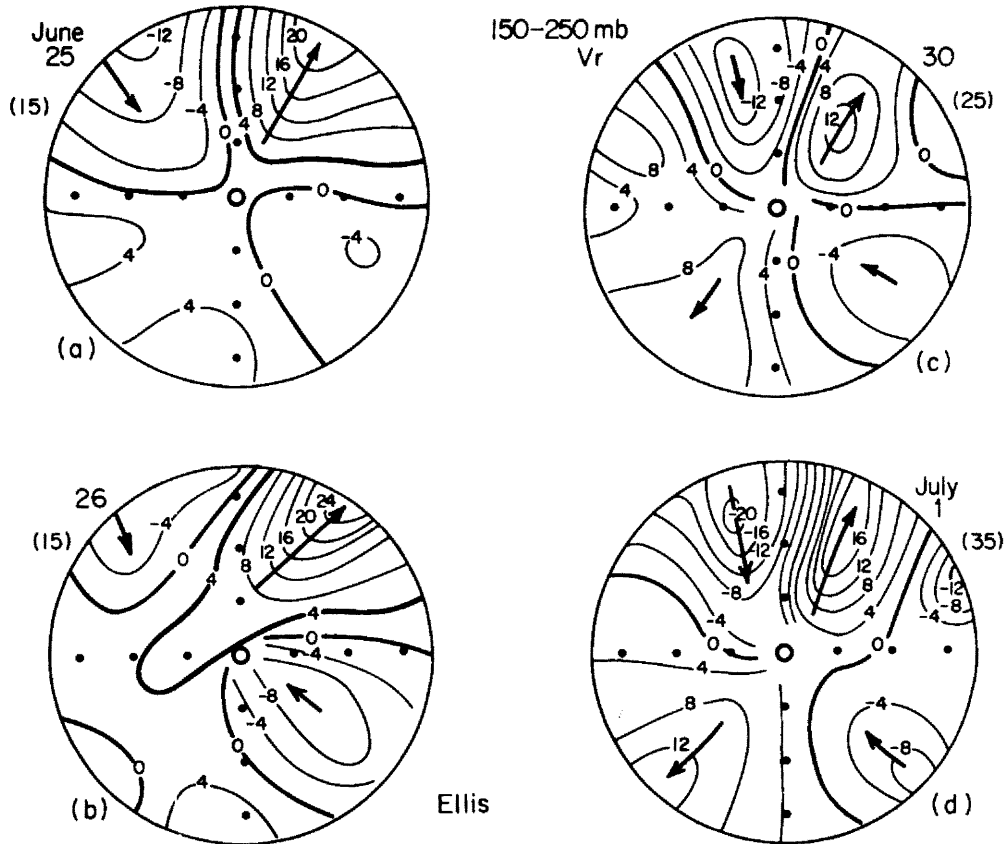
Fig. 69. The 150-250 mb V_r in a moving coordinate for Ellis on 25, 26, 30, June and 1 July, 00Z. The intensity of Ellis is shown within parentheses (in kts).

low-level cyclonic vorticity which keeps the system from falling apart for these 4-5 days of wind buildup.

After the 28th, the low-level vorticity keeps increasing and the upper-level divergence also increases until the 30th. The cloud pattern also starts to reorganize (Fig. 65f). Note that the system's intensity is still pretty weak and remains almost unchanged until the 30th, but the low-level vorticity experiences a steady increase throughout the whole period. From the 28th to the 30th, the system is influenced by a combination of the strengthening of the trade wind surge in the North Pacific and a monsoon surge from the North Indian Ocean rather than by the cross-equatorial surge.

The pattern of the southwest monsoon (which originated from the North Indian Ocean summer monsoon) remains unchanged over the southeastern Asian coast region from the 24th to the 28th (see Figs. 66a-e). A split of this monsoon is observed on the 29th, and the south branch extends eastward toward the southern vicinity of Ellis on 30 June. The strengthening and eastward stretching of the monsoon from the 28th to 30th (Figs. 66e-g) helps the buildup of the cyclonic circulation on the equatorward side of Ellis. Another convection burst is found on the 30th (Fig. 64a). Figures 67d-f (the 700-1000 mb V_t) show that between 28-30 June, the cyclonic circulation increases significantly on the equatorward side, but remains relatively unchanged on the poleward side.

Although the monsoon surge from North Indian Ocean appears to be the major process causing this strong westerly flow, the western branch of the cross-equatorial flow (between 105-110°E) might also have helped to redirect the flow toward the vicinity of Ellis. Note that due to the topographic effect, the cross-equatorial flow generally can split into two or three branches in this region. The positions where cross-equatorial surges usually take place in the western Pacific are east and west of New Guinea (150-160°E and 120-130°E) and between Singapore and Borneo (105-110°E). The cross-equatorial surge during the 25th to the 27th is at 120-130°E.

A strengthening of the trade winds is also observed west of the Dateline between the 26th and 30th. Whether this trade wind surge is caused by the westward stretching of the strong trades over the eastern central Pacific or by the strengthening of the Northern Hemisphere subtropical high is not clear. (Note that there are less data in the

Pacific region east of the Dateline.) Although the increase in the cyclonic circulation on the poleward side of Ellis from the 29th to the 30th (Figs. 66f, g and 67e, f) might have been boosted by the trade wind surge, it is also possible that this increase is due to the development of the system itself.

The strengthening of this trade wind, on the other hand, might have helped the formation of the pre-Faye cloud cluster on the 28th (shown in the southeast corner of Fig. 65e). Note that a maximum upper level $\overline{V}_r$ is observed on the 28th (Fig. 64b). The monsoon surge that affected Ellis on 30 June appears to spread its influence eastward on 1 July and increases the cyclonic circulation on the equatorward side of the pre-Faye disturbance (Figs. 66g and h). Another convection burst is found at that time period (Fig. 64b). Note that the best track of Faye started on the 29th, but JTWC did not upgrade the disturbance to a tropical depression (a tropical cyclone) until shortly before 1 July.

The discussion presented above shows various low-level large-scale forcings that can cause the buildup of the low-level cyclonic vorticity around the disturbance center during the cyclone formation stage. A convection burst is generally found when a wind surge reaches the vicinity of the disturbance. These large-scale low-level forcings in the western North Pacific can be due to the cross-equatorial surges, Indian monsoon surges and trade wind surges. It has to be noted that the FGGE analyses have smoothed out many smaller-scale features, and the peak strength of the surges (especially the shear vorticity) probably have been considerably underestimated. As discussed in the composite tangential momentum budget analysis, a very large horizontal eddy vorticity flux is required to spin up the cyclonic circulation during the formation stage.

It is thus hypothesized that this horizontal eddy vorticity flux is produced by smaller scale processes (such as convective activities in conjunction with the strong shear vorticity) associated with these low-level large-scale asymmetric wind forcings.

Developing Stage. Ellis experiences a much stronger developing trend after 30 June; that is, its intensity increases faster especially after 1 July, 12Z. The low-level cyclonic circulation over 4-6° radius decreases after this point primarily because the system has moved away from the strong monsoon and trade wind regions. The large-scale forced inward eddy vorticity flux thus is decreased. Still, the cyclone now has a well established symmetric circulation pattern with a very high vorticity (Fig. 67f), and thus is able to maintain itself. The low-level large-scale forcing is becoming less and less capable of influencing the cyclone's inner region because of the increased inertial stability associated with the vorticity pick up. Other observations have indicated that upper-level features are more likely to influence the cyclone's development at this later stage (Chen and Gray, 1985; Merrill, 1985).

The upper-level divergence increases greatly from 28 June to 30 June, and maintains approximately the same strength for the next couple of days (Fig. 64a). A significant feature is the deepening and the eastward movement of an upper-level trough which provides an excellent outflow channel toward the northeast quadrant on July 1 (Fig. 68c) Note that the outflow region on the northeast quadrant actually narrows, but the strength of the outflow increases or an outflow channel forms from 30 June to 1 July (Figs. 69c-d). As discussed by Chen and Gray (1985), an upper-level outflow channel is generally favorable for tropical

cyclone intensification. Ellis intensifies from a minimal tropical
storm to a typhoon in the next two days (the maximum intensity changes
from 35 kts on 1 July to 85 kts on 3 July). By 3 July, the upper trough
has moved to the east of Ellis (Ellis is also moving toward the west-
northwest), and a strong northeasterly shearing flow prevails over
Ellis' inner region (Fig. 68d) causing its intensity to weaken after
this time.

Although this eastward moving trough helps Ellis develop into a
typhoon, it does not help Tropical Storm Faye develop. Note that Faye's
intensity increases by only 20 kts from 1 July to 4 July. This is
probably due to the fact that Faye is located at a lower latitude, and
thus is less affected by the trough (Fig. 68d). The upper-level V_r for
Faye (in moving coordinates) on 3 July (Fig. 70a) shows that the outflow
associated with the large-scale trough on the northeast quadrant is not
very strong and does not really reach the inner region of TS Faye. Note
that a TUTT is located to the north of Faye on 1 July and provides a
reasonably good outflow channel toward the northeast direction, as shown
in Fig. 68c. Unfortunately, the eastward propagating trough causes this
TUTT system to disappear on 3 July (Fig. 68d). The broad outflow toward
the southwest on 3 July is just a blow-through due to the prevailing
easterly flow over the system's center (Fig. 70a). By 4 July an overall
wind blow-through is evident over the whole region, as shown in Fig. 70b
in which inflow is observed on the east-northeastern side and outflow on
the opposite side. This blow-through shearing effect causes Faye to
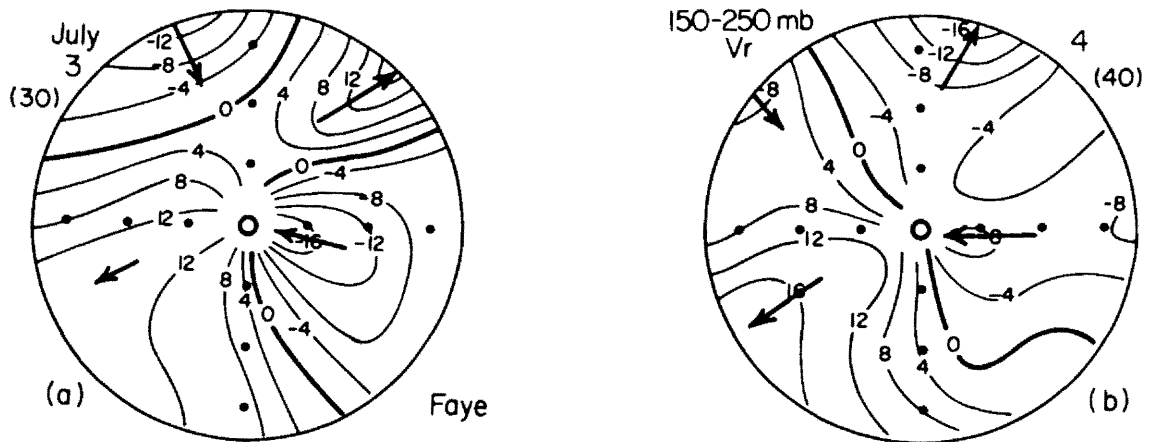weaken after 4 July.

Fig. 70.   The 150-250 mb V_r in a moving coordinate for Faye on 3, 4
July, 00Z.   The intensity of Faye is shown within parentheses
(in kts).

9.2   Hope and Gordon

From 20-26 July, three tropical cyclones formed around the
Philippine Sea.   They are TD 08, Tropical Storm Gordon and Supertyphoon
Hope.   The best tracks and the time series of Gordon and Hope are shown
in Figs. 71 and 72.   (TD 08 is not shown.)   From 20-22 July, strong
trade winds and a strong cross-equatorial flow occurred around the
region $20^\circ N$, $140^\circ E$ and TD 08 formed at the merging region of these two
strong flows on 23 July (see Figs. 73a and 74a).   On the next two days,
TD 08 moved northwestward and was better separated from the cloudiness
generated by the strong cross-equatorial flow (Figs. 73b and c).   No
significant development associated with TD 08 was observed.   This
cross-equatorial flow did not weaken but reintensified from 24-26 July
due to another surge (Figs. 74b-d) and caused the remaining cloud
cluster of TD 08 to form TS Gordon on 25 July, 12Z (Figs. 73b-d).

Before the formation of Gordon, the cloud cluster east of the pre-
Gordon cloud cluster formed a tropical cyclone (Hope) at 12Z of 24 July
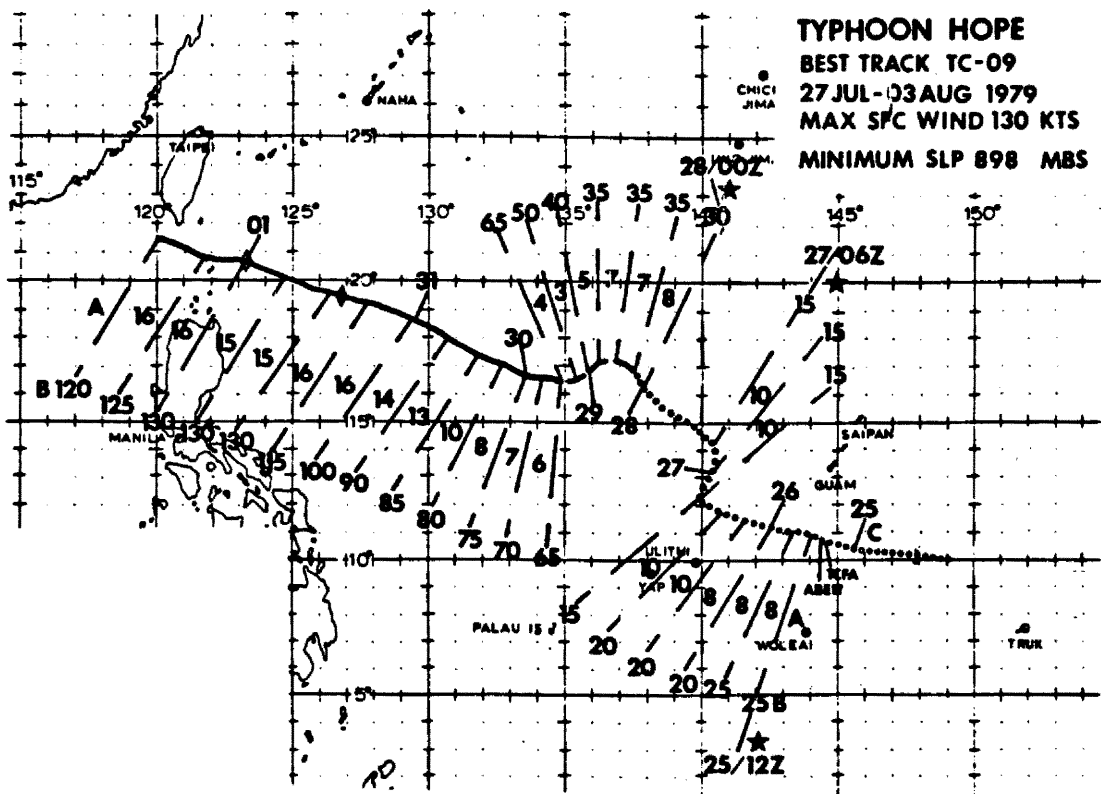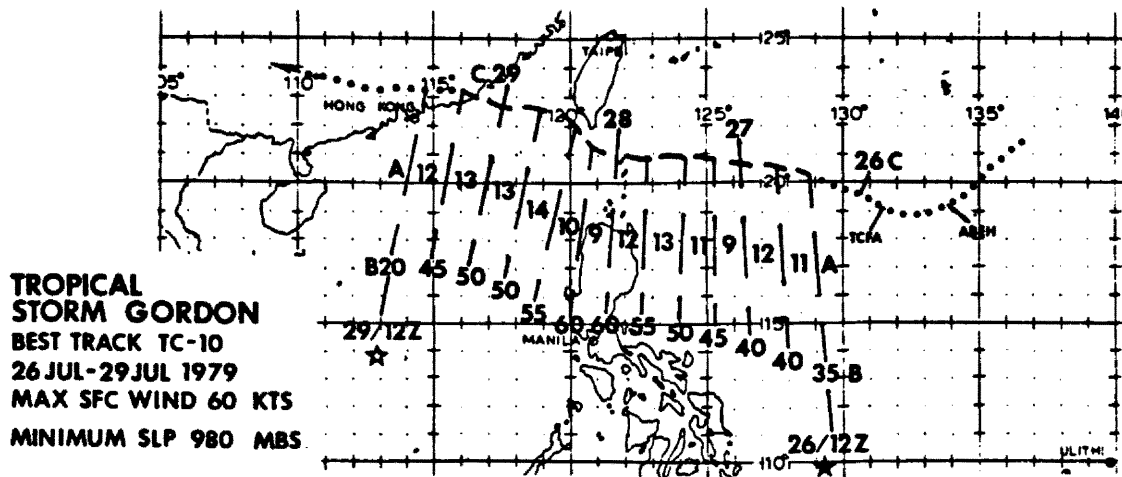(Figs. 73b and c).   The strong trade wind to the north of Hope extended

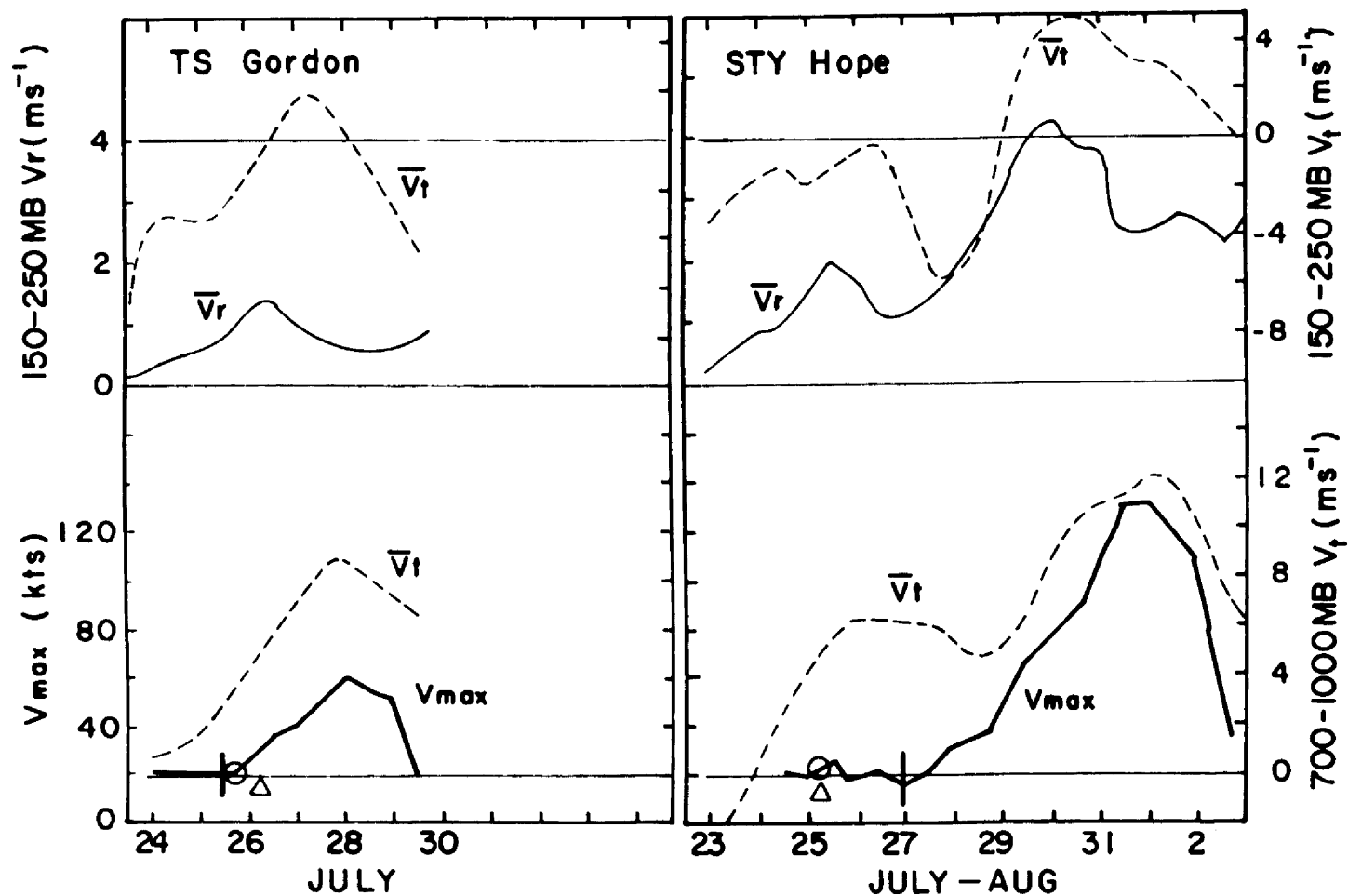**Fig. 71.** The best tracks of TS Gordon and STY Hope (1979).

Fig. 72. Time series of the upper-level and low-level mean tangential winds and the upper-level mean radial wind at 6° radius for Tropical Storm Gordon and Supertyphoon Hope. The maximum intensity is also shown. The circle is the time period when the system was upgraded to a tropical cyclone and the triangle is the first time period when the center of the system was fixed by the aircraft reconnaissance flight.
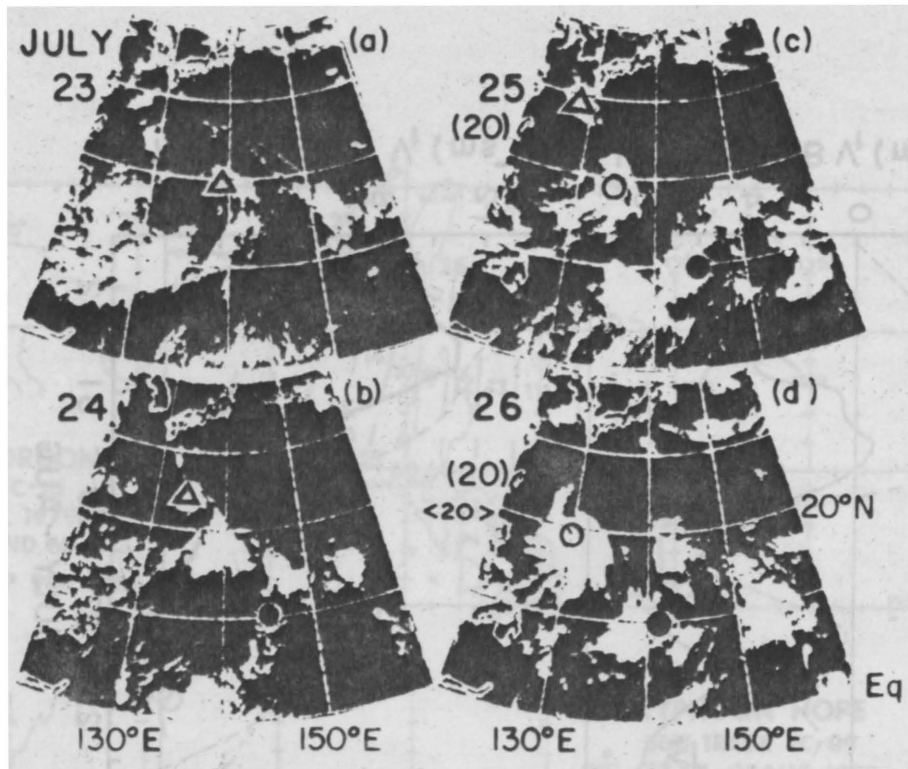
Fig. 73. The NOAA satellite pictures on 23-26 July, 03Z. The centers of TD08, Tropical Storm Gordon and Supertyphoon Hope are indicated by the triangles, the open circles, and the dots, respectively. Intensities of Hope and Gordon are shown within parentheses and brackets (in kt), respectively.

southward and curved cyclonically around the system from the 24th to 25th, as shown in Figs. 74b,c and d. In the upper level, the TUTT north of the disturbance on the 23rd (Fig. 75a) deepened and moved southward on the 24th (Fig. 75b). This upper-level configuration created an outflow to the east-northeast and to the southwest directions for the pre-Hope disturbance. These upper-level outflow channels apparently caused the organization of the cloud cluster (Figs. 73b and c) and the formation of the tropical cyclone.

The pre-typhoon Hope tropical cyclone moved close to the TUTT on the 26th (Figs. 75c and d) and the cyclone-associated convection fell apart (Fig. 73d). Fortunate for its later development, a low-level strong cross-equatorial flow occurred east of New Guinea on the 25th and
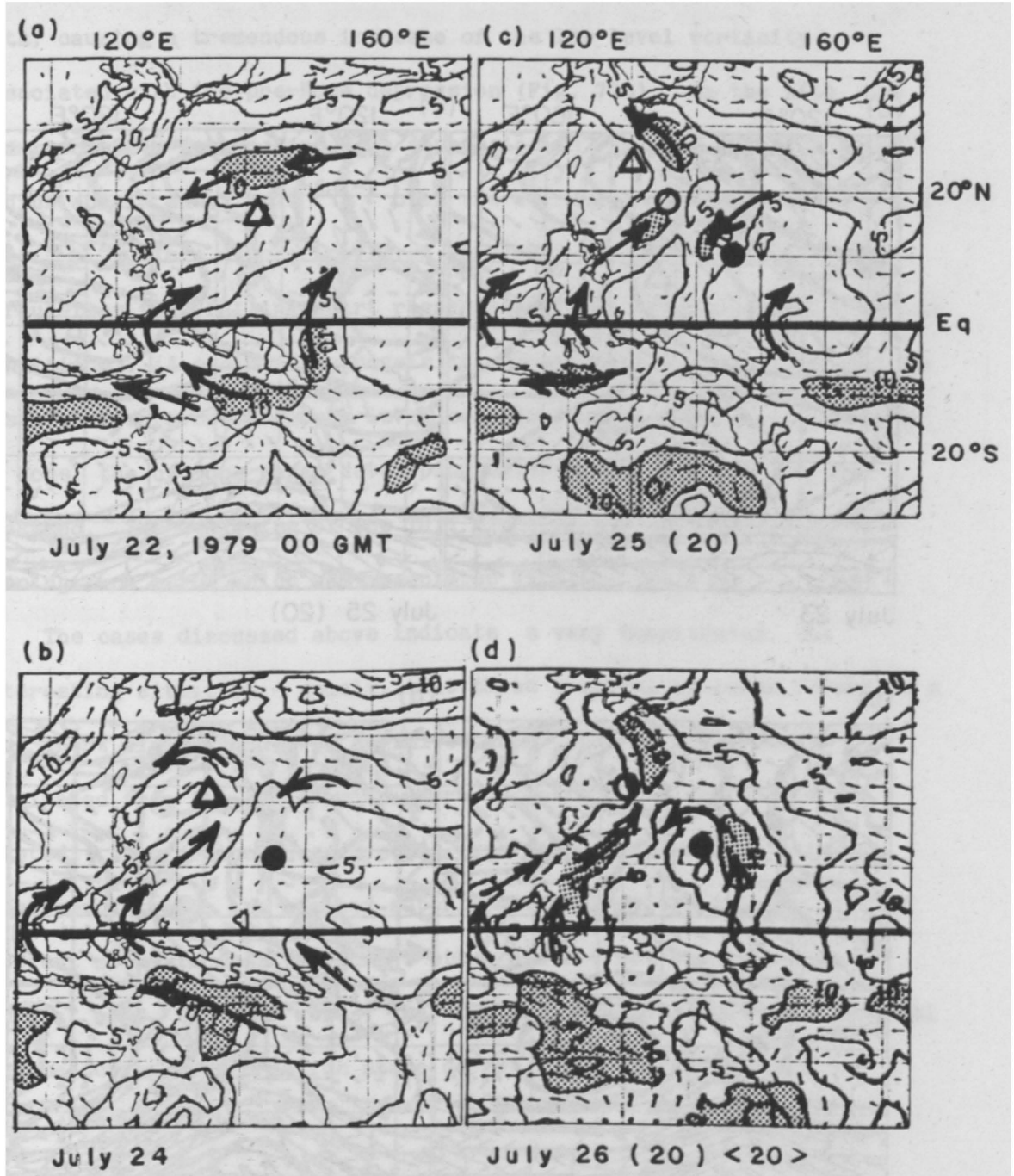
Fig. 74. The 850 mb flow pattern on 22, 24, 25, and 26 July, 06Z. The centers of TD08, Tropical Storm Gordon and Supertyphoon Hope are indicated by the triangles, the open circles, and the dots, respectively. The shaded areas are the regions with a wind speed $\geq$ 10 m s^{-1}. Intensities of Hope and Gordon are shown within parentheses and brackets (in kt), respectively.

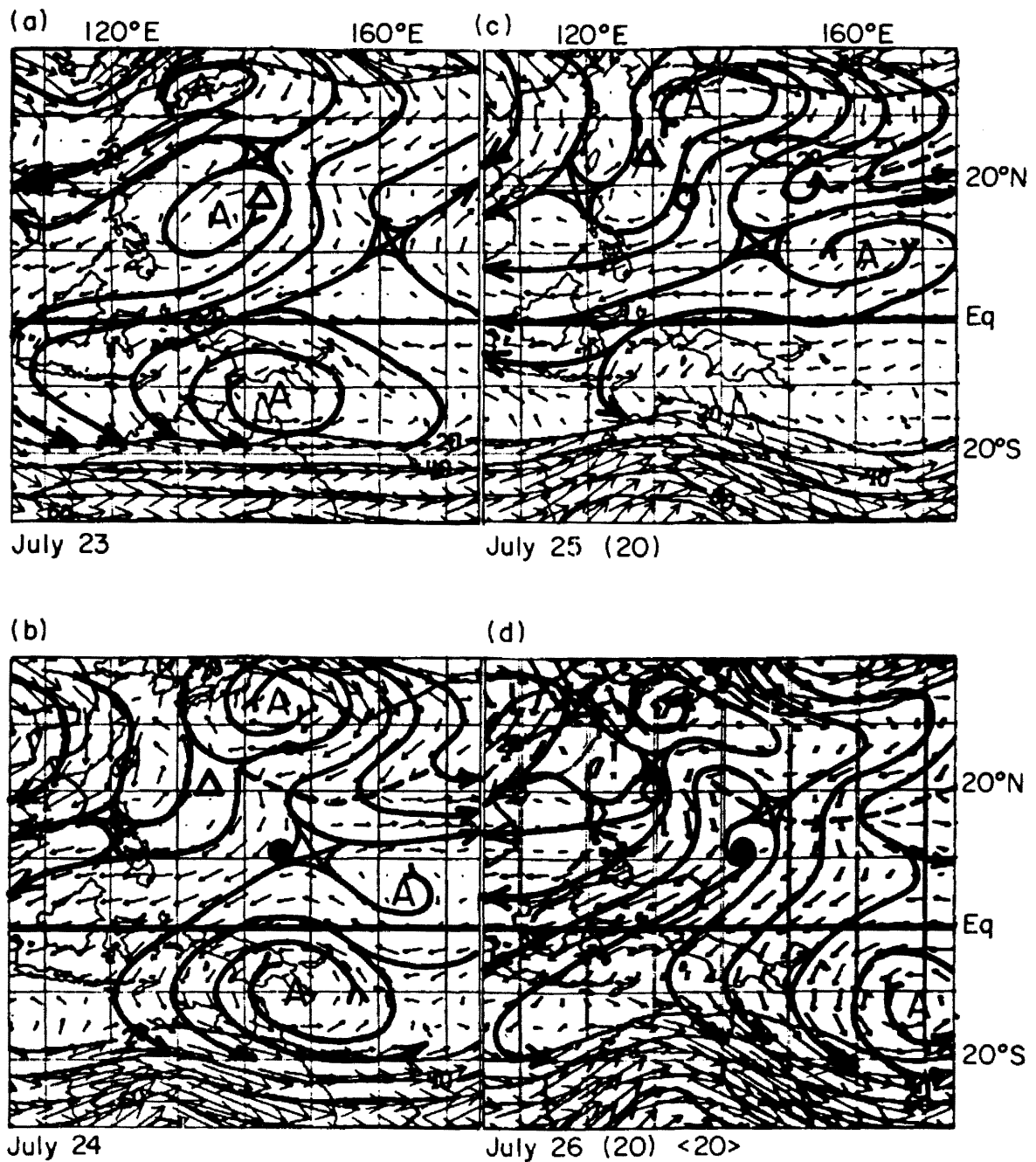Fig. 75. The 200 mb flow pattern on 23-26 July, 00Z. The centers of
TD08, Tropical Storm Gordon and Supertyphoon Hope are
indicated by the triangles, the open circles, and the dots,
respectively. Intensities of Hope and Gordon are shown within
parentheses and brackets (in kt), respectively.

reached the cyclone's inner region from the southeast direction on the 26th, causing a tremendous increase of the low-level vorticity associated with the pre-Hope depression (Fig. 72b). On the 26th, the mean vorticity for the pre-Hope depression is 2×10^{-5} s^{-1} over the 6° radius domain and 3×10^{-5} s^{-1} over the 4° radius domain; f is only 2.5 $\times 10^{-5}$ s^{-1}. This strong low-level vorticity keeps the cyclone circulation from falling apart regardless of the unfavorable upper-level conditions. (A cyclone can regain its development trend as soon as its associated unfavorable upper-level conditions disappear.) In the case of Hope, the cyclone began developing after the 27th, when the TUTT weakened. The weakening of the TUTT might be due to the convective forcing from below which was associated with the cyclone.

The cases discussed above indicate a very complicated, but interesting situation - namely, that three tropical cyclones formed in a very short time period over a limited area. Two of the systems originated from the same region where surge-forced cloud clusters existed. Each of the three systems experienced a different later development trend: one reached supertyphoon intensity, another reached tropical storm intensity, and the other did not develop into a major storm at all. In other words, the initial characteristics of a tropical cyclone during its formation stage do not necessarily determine its later development trend.

9.3 Ken and Lola

In the mid-season, tropical cyclone formation and development are often affected by the TUTT in the western North Pacific region. Tropical Storm Ken and Typhoon Lola developed almost concurrently along the periphery of a TUTT system during late August and early September.

Their best tracks and time series are shown in Figs. 76 and 77. Figures 78a-e show satellite pictures from 31 August to 4 September in which the TUTT axis is also shown. The upper-level (200 mb) flow patterns for the same time period are shown in Figs. 79a-e. As seen in Figs. 78a and b, a number of disturbances are arranged into a line of convection ringing the TUTT system on 31 August and 1 September. The TUTT system deepened in the next 24 hours (Figs. 79b and c) and divided the convective line into two distinctive systems (Figs. 78c and d - Ken and Lola). Both systems intensify by 10 kts from 1 to 2 Augusut, but they have not reached tropical storm intensity yet.

Prior to the formation of Ken, the strong low-level northeast wind behind or west of a low-level trough caused a surge of the momentum field near the vicinity of the pre-Ken disturbance during the period from 30 August to 1 September (see Figs. 80a-d). This momentum surge helped the buildup of the large-scale vorticity associated with Ken. Ken was upgraded from a disturbance to a tropical cyclone on 31 August. In the upper level, the circulation changed from weak cyclonic to strong anticyclonic and the divergence increased slightly at this time period (Figs. 77a). No major outflow channel was observed until after 2 September when an eastward moving upper-level trough approached the cyclone (Figs. 79c and d). The alignment of the large-scale low-level cyclonic circulation and the upper-level anticyclonic circulation was very good throughout the whole period. This might be the most important
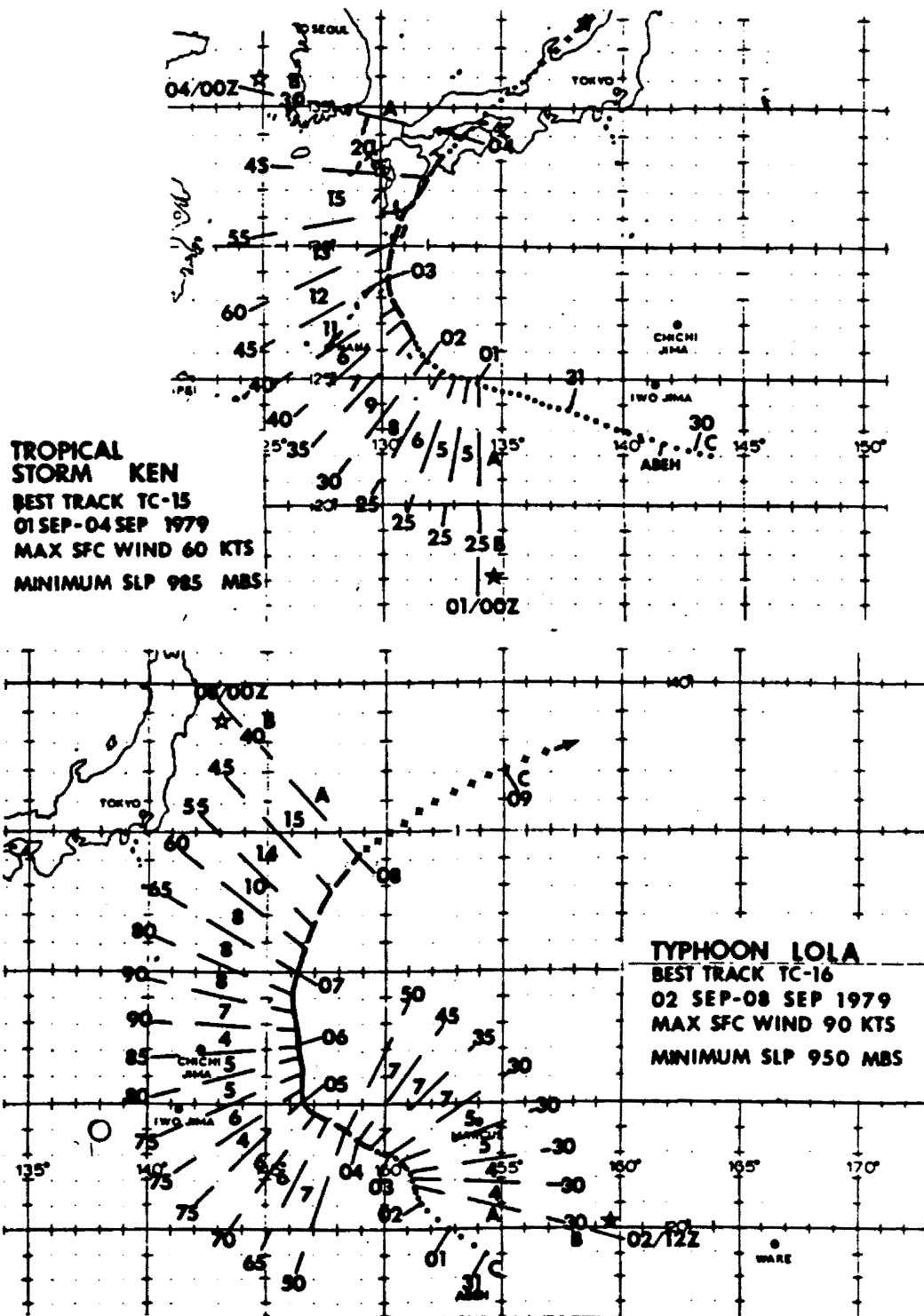
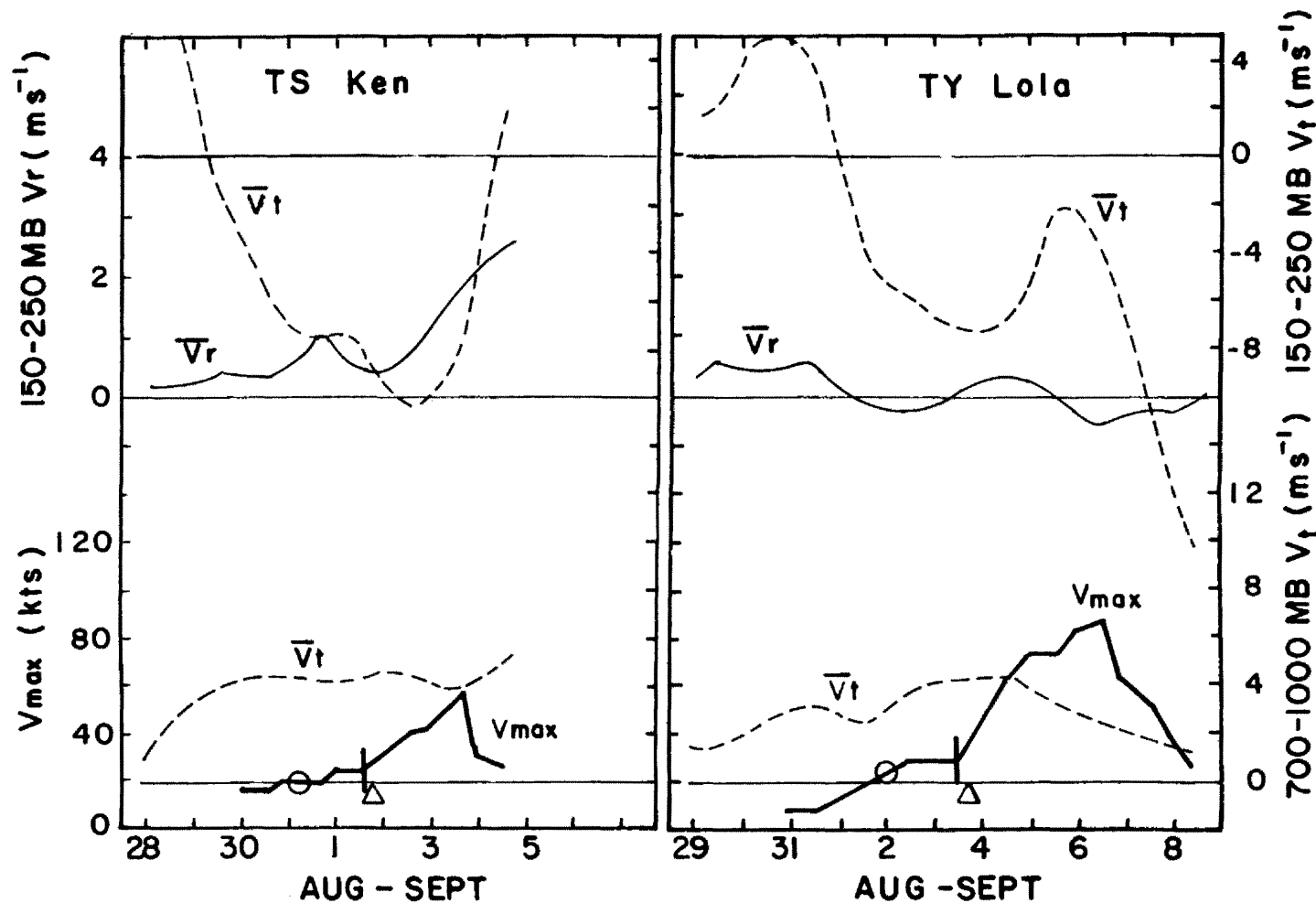Fig. 76. The best tracks of TS Ken and TY Lola (1979).

Fig. 77. Time series of the upper-level and low-level mean tangential winds and the upper-level mean radial wind at 4° and 6° radius for Tropical Storm Ken and Typhoon Lola. The maximum intensity is also shown. The circle is the time period when the system was upgraded to a tropical cyclone and the triangle is the first time period when the center of the system was fixed by the aircraft reconnaissance flight.
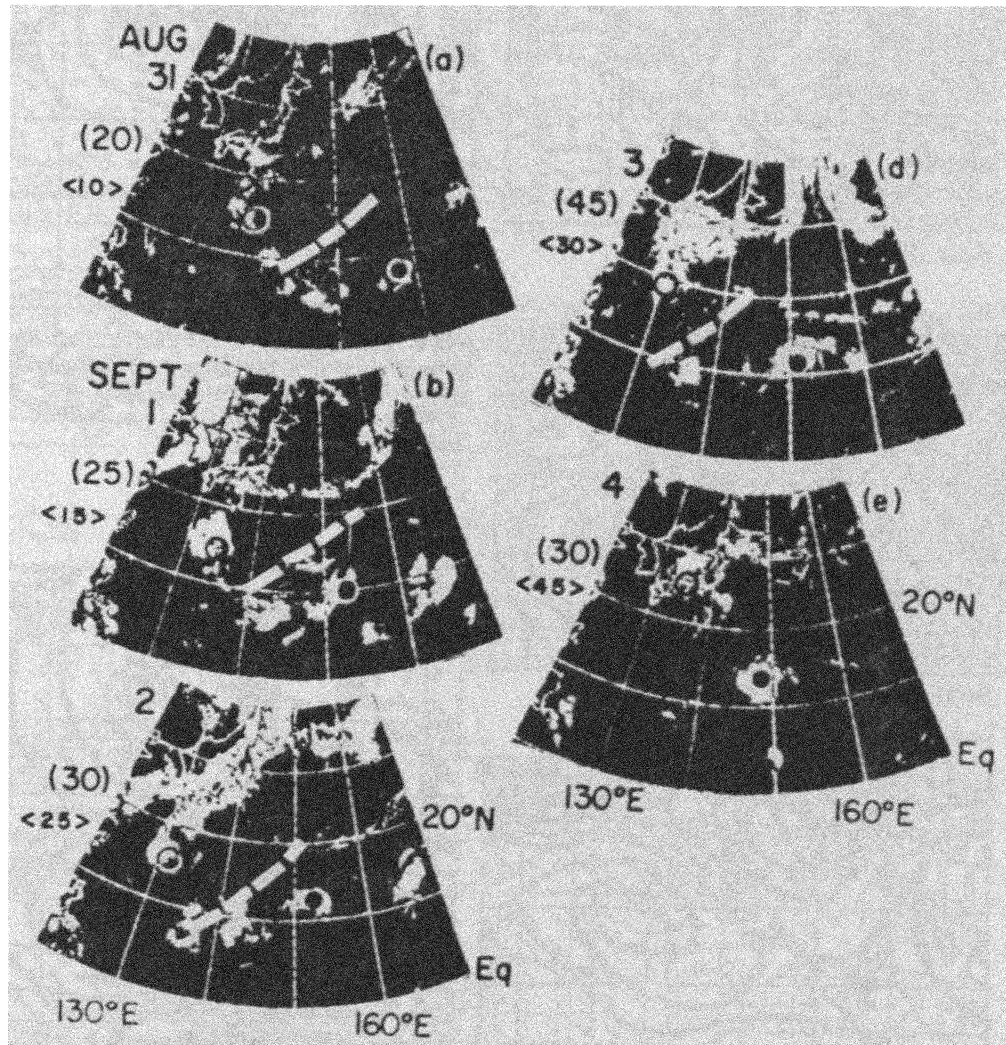
Fig. 78. The NOAA satellite on 31 August–4 September, 03Z. The centers of Ken and Lola are shown in open circles and dots, respectively. The wide dashed white line shows the axis position of the TUTT. Intensities of Ken and Lola are shown within parentheses and brackets (in kt) at the left of each diagram, respectively.
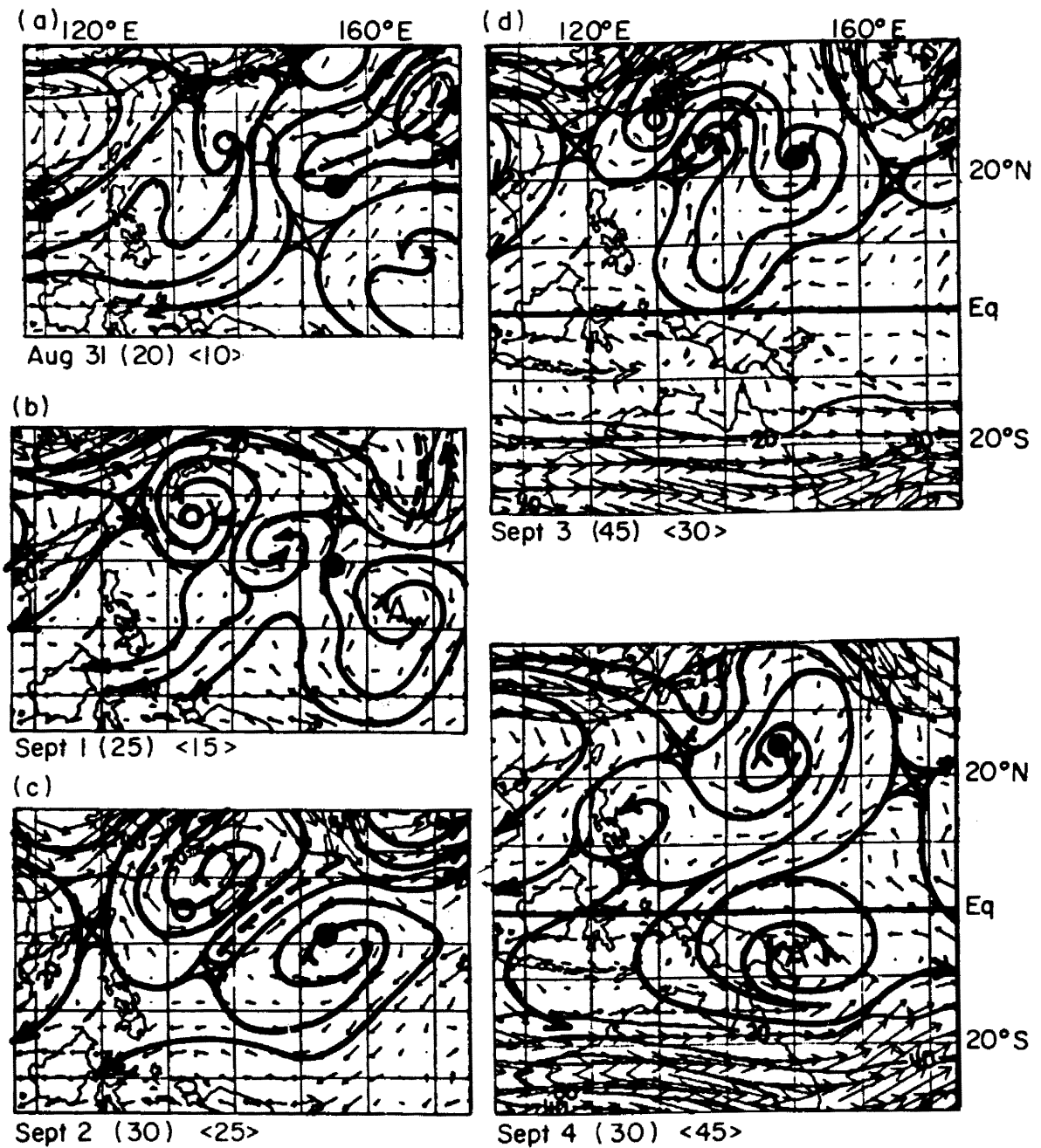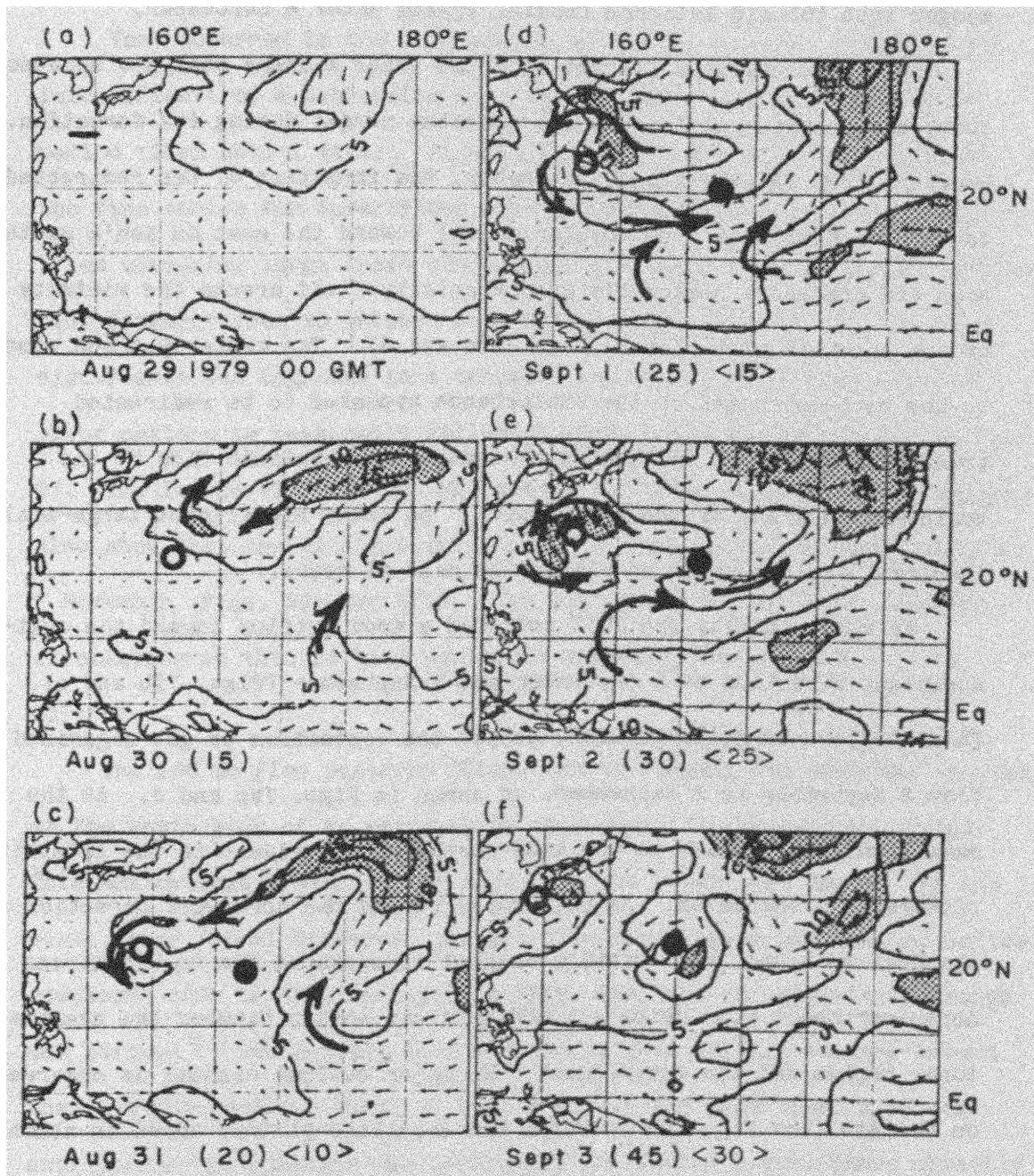
Fig. 79. The 200 mb flow pattern on 31 August-4 September, 00Z. The centers of Ken and Lola are shown in open circles and dots, respectively. Intensities of Ken and Lola are shown within parentheses and brackets (in kt) underneath each figure, respectively.

Fig. 80. The 850 mb flow pattern and isotachs on 29 August–3 September, 00Z. The shaded areas are the regions with a wind speed ≥ 10 m s^{-1}. The centers of Ken and Lola are shown in open circles and dots, respectively. Intensities of Ken and Lola are shown within parentheses and brackets (in kt), respectively.

feature in causing the slow but steady development of Ken before it merged into the mid-latitude frontal system after 4 September.

Lola is somewhat different from the other systems analyzed because there are no apparent large-scale momentum surges during its formation. However, from 31 August to 1 September, the formation of Ken redirected the strong northeast flow (cyclonically) toward the east on Ken's south side and created a reasonably good vorticity field around the vicinity of the pre-Lola disturbance (Figs. 80c and d). The easterly trade wind to the east-southeast of the disturbance appeared to be redirected toward the northeast and helped strengthen the cyclonic flow to the southeast quadrant of the disturbance. No other significant large-scale low-level feature occurred within the next 48 hours.

At upper levels, the TUTT provided a good outflow toward the east-northeast direction on 1 September and 2 September (Figs. 79b and c). This outflow channel apparently helped the convection to get organized from 2 September to 3 September, as shown in Figs. 78c and d. At the same time, the outflow to the east-northeast is evident in the satellite picture on 3 September. As Lola moved toward the northwest direction in the next 24 hours, this outflow channel disappeared due to the strong north-northeast flow which cut off this connection between the cyclone's inner region and its environment. No major outflow channel is observed on the 4th (see Fig. 78e in which the satellite picture shows an almost circular cloud pattern except for a very weak outflow in the southeast direction). However, the large-scale low-level cyclonic circulation is now aligned with the upper-level anticyclonic circulation and Lola developed from 45 kts to 85 kts from the 4th to the 6th. Note that the upper-level large-scale divergence (or the mean radial wind) did not

really increase throughout Lola's whole life cycle (Fig. 77b).

9.4 Vera

Vera occurred in the late season (October-November) of 1979. It intensified from a depression to a supertyphoon in a very short time period (less than 2 days). Figures 81 and 82 show the best track and the time series for Supertyphoon Vera. The formation of Vera is forced by an unusually large trade wind surge (see Figs. 83a-d, in which 850 mb flow patterns from 30 October to 2 November are shown). The pre-Vera disturbance was upgraded to a tropical depression on the 2nd, but its cloud pattern is reasonably well-organized on 1 November (Figs. 84a and b). The low-level (700-1000 mb) tangential winds in a moving coordinate also show that the cyclonic circulation was already well established by 1 November (Figs. 85a and 85b). The buildup of the low-level cyclonic circulation in this 24 hour period is unusually large and fast (Fig. 82).

The 200 mb flow patterns (Figs. 86a-d) reveal that Vera was located on the south side of an anticyclone throughout its developing period. This anticyclone prevented any major outflow toward the north. At the early stage (30-31 October), the pre-Vera disturbance was located on the southeast side of this anticyclone (Fig. 86a) and an upper-level trough was located to its north. This provided a good outflow channel toward the east-northeast as shown in Fig. 87a. At the same time, a strong anticyclonic circulation was located in the Southern Hemisphere directly south of the disturbance and steered the flow toward the west-southwest.

In the next 24-48 hours (1-2 November), the disturbance moved westward and lost its connection with the jet to the northeast (Figs. 86b and c). The upper-level (150-250 mb) radial winds (Figs. 87b and c)
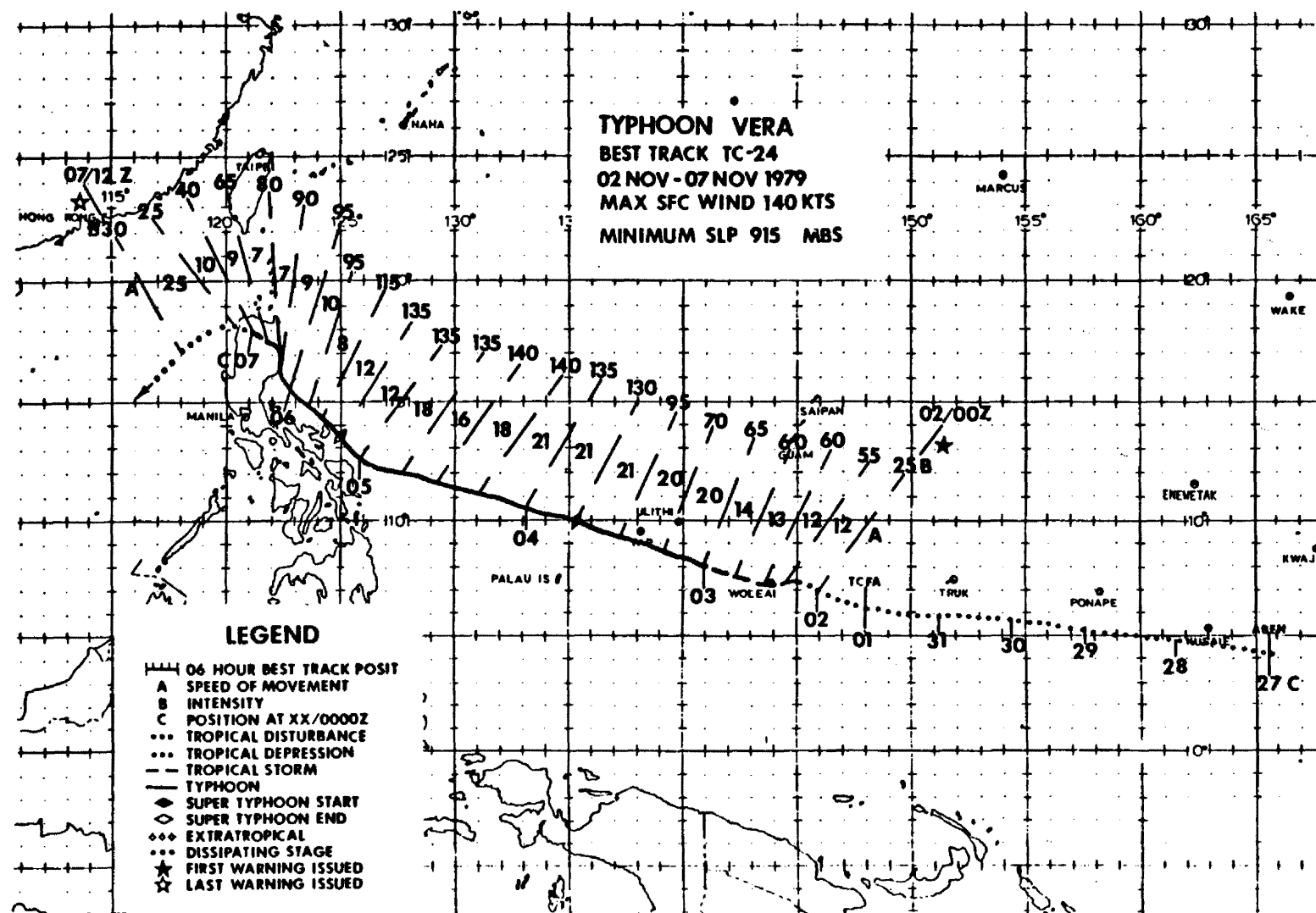
TYPHOON VERA
BEST TRACK TC-24
02 NOV - 07 NOV 1979
MAX SFC WIND 140 KTS
MINIMUM SLP 915 MBS

LEGEND
⊢┼┼┤ 06 HOUR BEST TRACK POSIT
A   SPEED OF MOVEMENT
B   INTENSITY
C   POSITION AT XX/0000Z
••• TROPICAL DISTURBANCE
••• TROPICAL DEPRESSION
— — TROPICAL STORM
——   TYPHOON
◆   SUPER TYPHOON START
◇   SUPER TYPHOON END
◆◆◆ EXTRATROPICAL
••• DISSIPATING STAGE
★   FIRST WARNING ISSUED
☆   LAST WARNING ISSUED

Fig. 81.   The best track of STY Vera (1979).
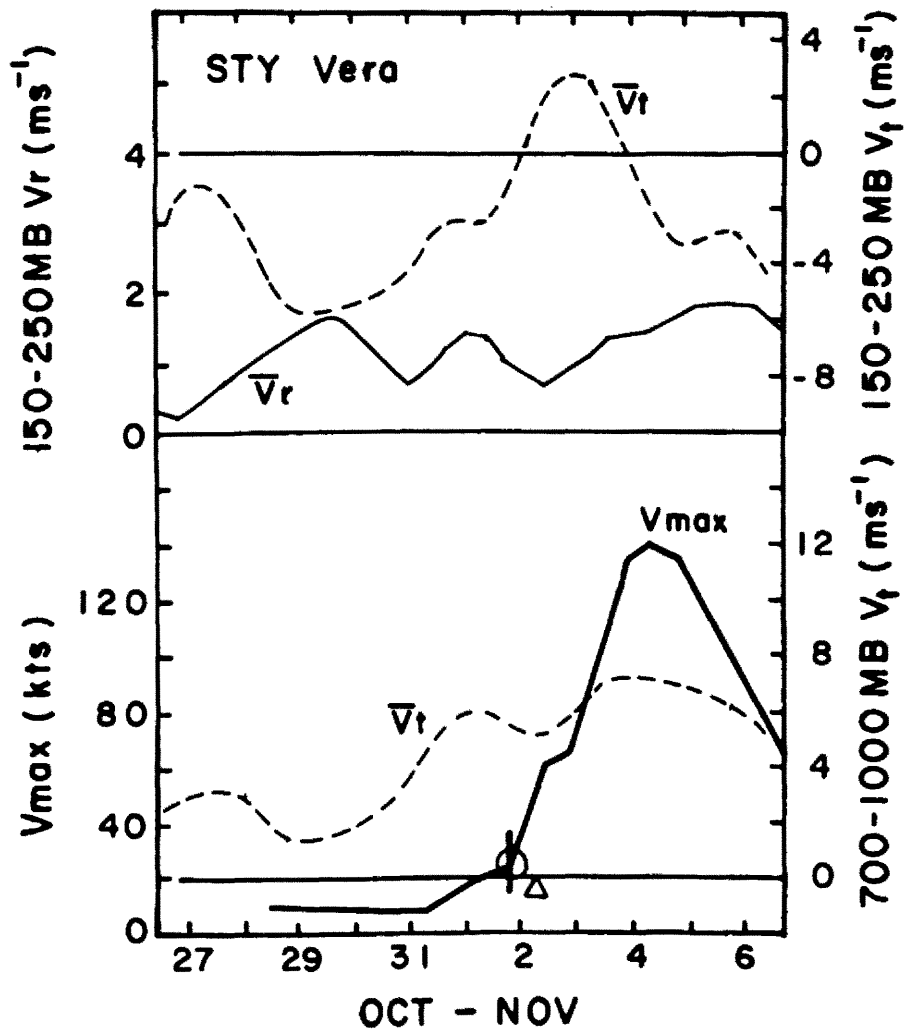
Fig. 82. Time series of the upper- and low-level mean tangential winds and the upper-level mean radial wind at 6° radius for Supertyphoon Vera. The maximum intensity is also shown. The circle is the time period when the system was upgraded to a tropical cyclone and the triangle is the first time period when the system's center was fixed by the aircraft reconnaissance flight.
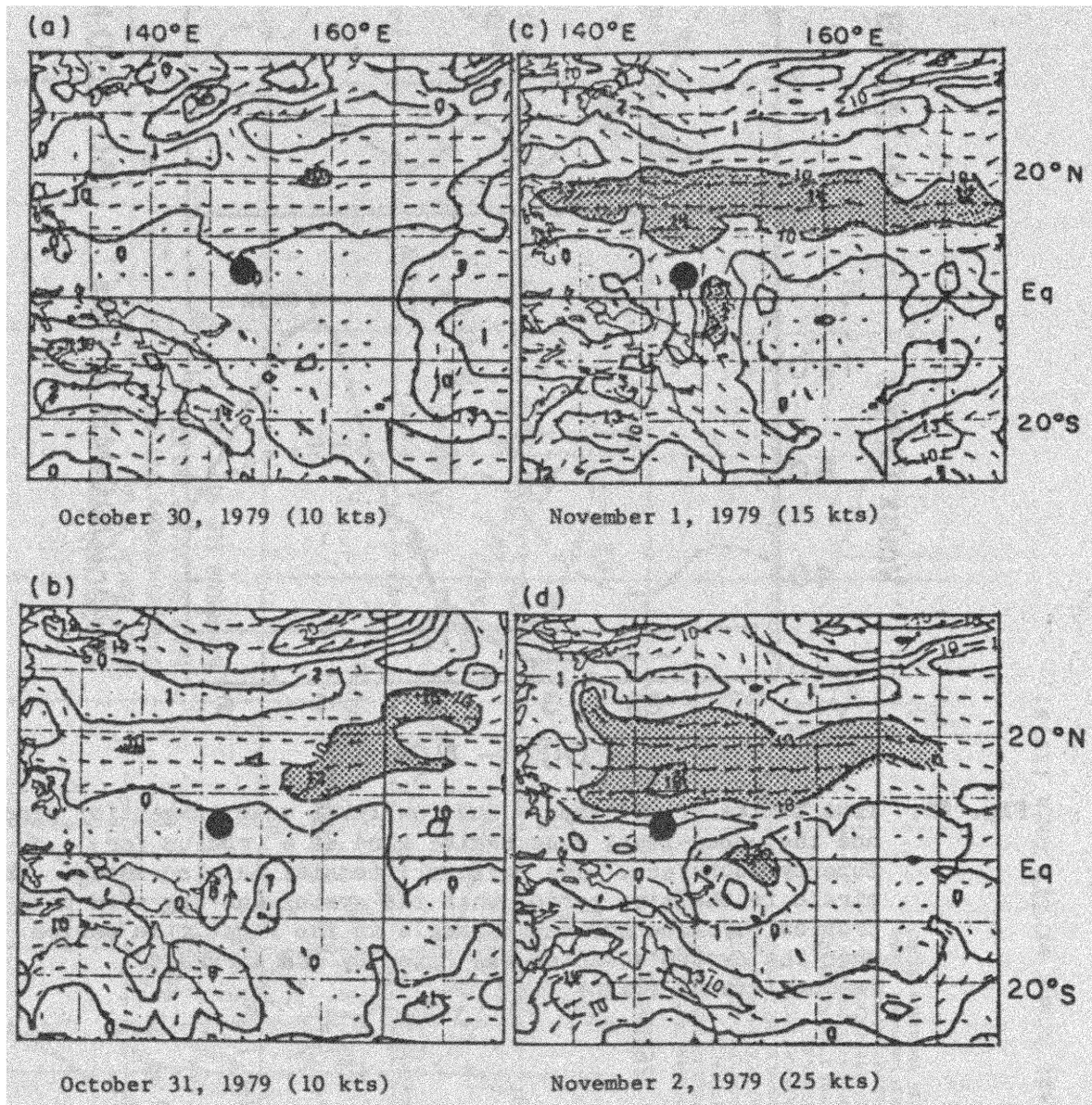
Fig. 83. The 850 mb flow pattern and isotachs on 30 October-2 November, 00Z. The shaded areas are the regions with a wind speed $\geq$ 10 m s^{-1}. The centers of STY Vera are shown in dots. The intensity of Vera is shown in parentheses underneath the diagram.
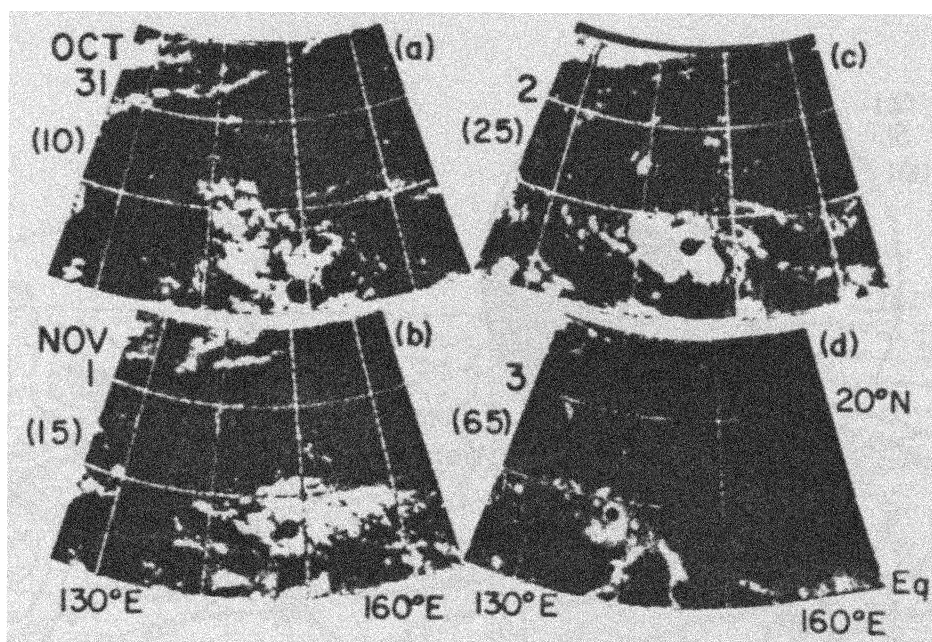
Fig. 84. The NOAA satellite pictures on 31 October-3 November, 03Z. The centers of STY Vera are shown in dots. The intensity of Vera is shown within parentheses (in kts).

show that this northeastward outflow had weakened considerably by 1 November and almost disappeared on 2 November. At the same time, the Southern Hemisphere anticyclone weakened and allowed the air to detrain from the system toward the south. Figures 87b and c show an increased outflow toward the south-southeast. The intensity of Vera increased by 40 kts in the next 24 hours or from 25 kts on 2 November to 65 kts on 3 November.

The anticyclone in the Northern Hemisphere weakened somewhat on 3 November and its center had moved eastward. Vera was located at the southwestern edge of this anticyclone (Fig. 86d). This new configuration caused the outflow to be directed toward the northwest. The anticyclone in the Southern Hemisphere broke into two weaker anticyclones. The outflow air (in moving coordinates) was thus directed
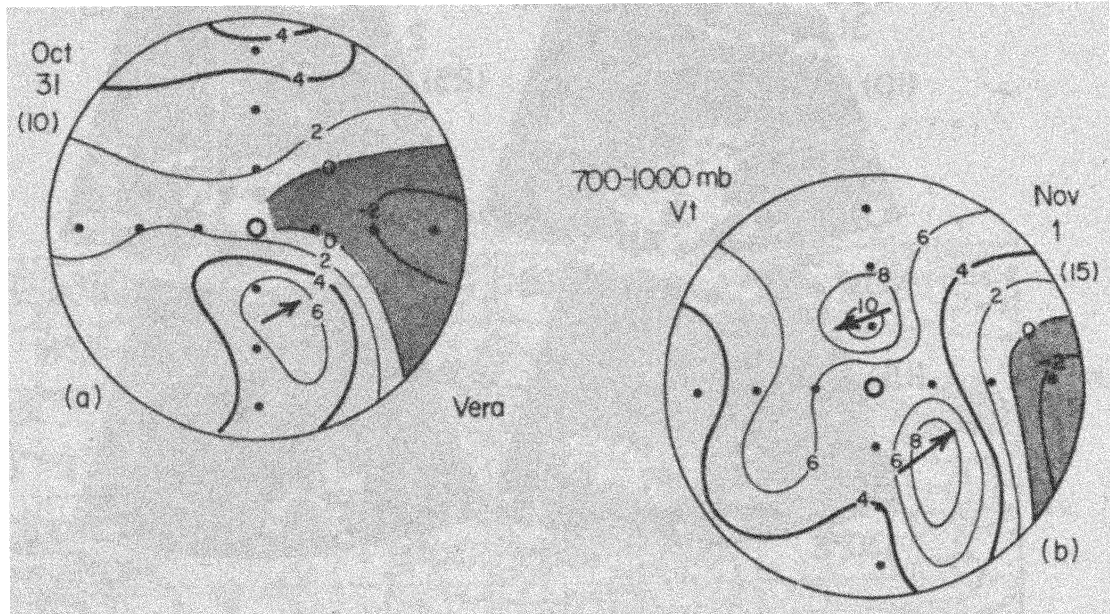
Fig. 85. The 700-1000 mb V_t in a moving coordinate for Supertyphoon
Vera on 31 October 31 and 1 November, 00Z. The shaded areas
are the regions with an anticyclonic circulation or negative
V_t. The heavy curves are the 4 m s^{-1} isotachs. The intensity
of Vera is shown within parentheses (in kts).

toward the south-southeast (Fig. 87d). Figure 84d shows a fairly tight

and circular cloud pattern associated with Vera on 1 November, with the

major outflow toward the south-southeast in this data. Vera intensified

into a supertyphoon in the next 24 hours by increasing its intensity

from 65 kts to 135 kts (or intensified by 110 kts in 48 hours from 2

November to 4 November). This is a rather unusually high

intensification rate. However, the large-scale circulations did not

exhibit any unusual strong upper-level outflow channels. The upper-

level mean divergence is also relatively unchanged throughout this time

period. It appears that the cyclone's internal dynamics were the

dominant factor in this unusual cyclone development event. It is also

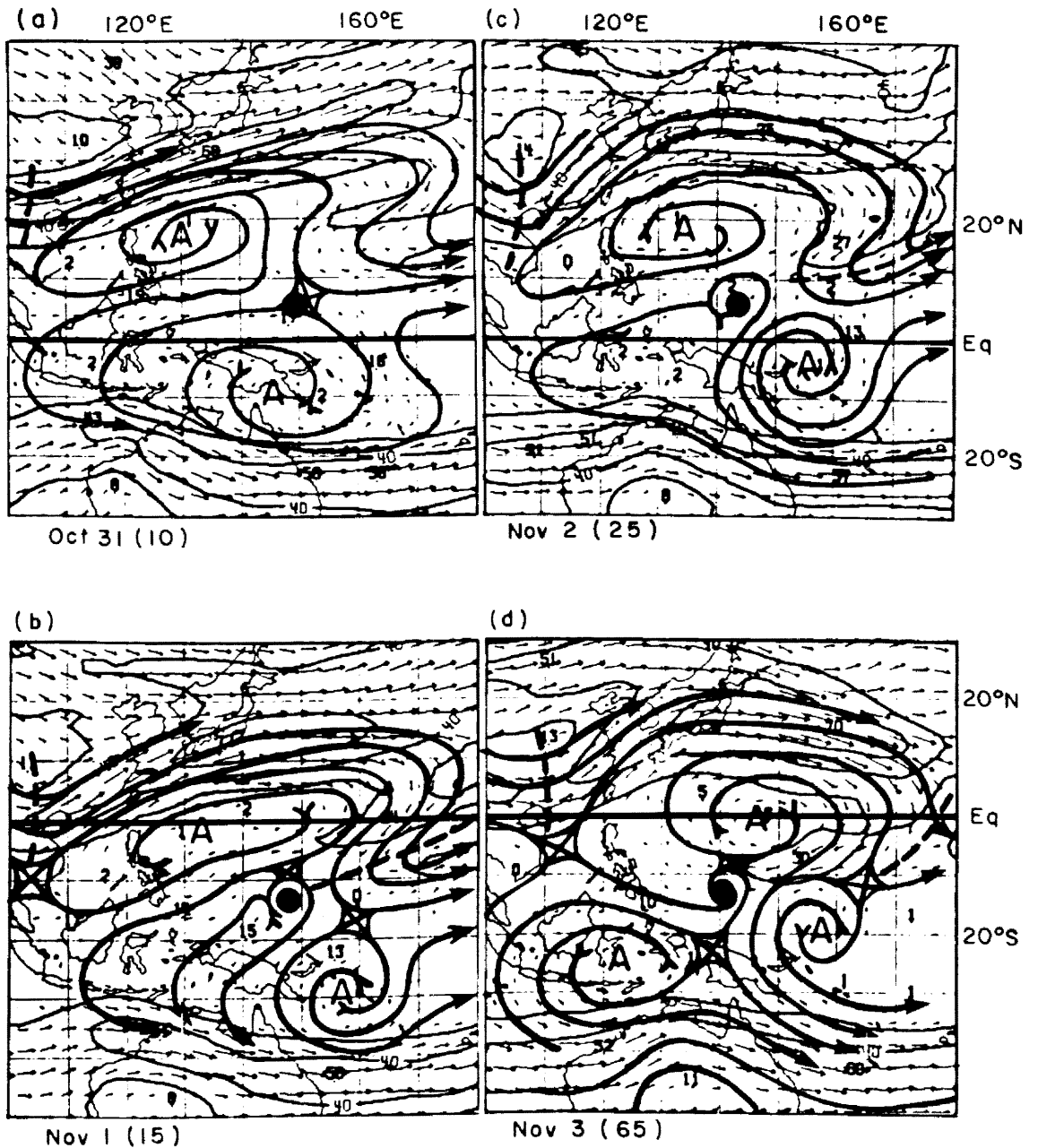possible that the low-level forcing might have played a more important

Fig. 86. The 200 mb flow pattern on 31 October–3 November, 00Z. The centers of STY Vera are shown in dots. The intensity of Vera is shown within parentheses (in kts).
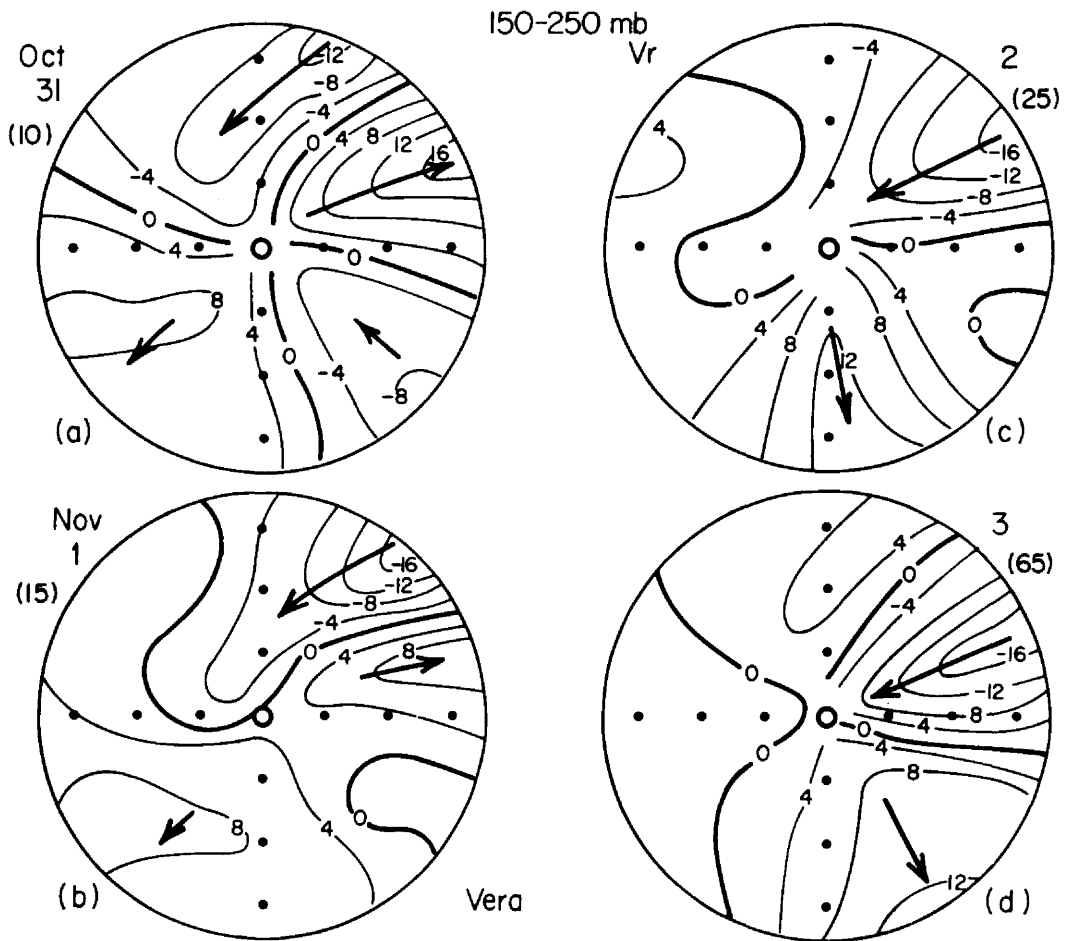
Fig. 87. The 150-250 mb V_t in a moving coordinate for STY Vera on 31 October-3 November, 00Z. The intensity of Vera is shown within parentheses (in kts).

role during Vera's development due to the unusually large trade wind surge which preceeded this development.

9.5 Summary

The discussions presented above indicate many important characteristics of the formation and development processes of the tropical cyclone. They also portray the very common and important pre-cyclone large-scale circulation patterns which are usually associated with the genesis process. This analysis indicates that:

1) Low-level large-scale circulations play a very important role

during the tropical cyclone formation stage, while upper-level circulation and divergent features appear more dominant during the later development and intensification stages.

2) There is (are) often low-level large-scale momentum surge(s) during the formation stage which cause a buildup of the large-scale low-level cyclonic vorticity around the pre-cyclone disturbance. These surges can be trade wind surges, cross-equatorial surges or monsoon surges from the North Indian Ocean. (The term ''surge'' is used to represent a large increase in the momentum field.) A convection burst often occurred when these surges reached the vicinity of the cloud cluster.

3) Good upper-level outflow channels can cause cloud clusters to better organize their convection patterns provided that the cloud clusters are already located within a favorable region with a strong low-level large-scale vorticity.

4) Although not crucial for initial genesis a favorable alignment of both the large-scale low-level cyclonic vorticity and the upper-level anticyclonic vorticity is favorable for later stage cyclone development or intensification.

5) Upper-level outflow channel(s) or jet(s) are generally favorable for cyclone intensification. Fast intensification does not necessarily require an extremely good upper-level outflow channel.

6) Low-level momentum surges and upper-level outflow channels are quite asymmetric transient features. Eddy processes are extremely important in these situations.

7) There appear to be very large variations among individual tropical cyclone formation and intensification cases.

10.   SUMMARY DISCUSSION

The observational analyses presented in the previous chapters have
shown the important structural changes taking place as cloud clusters
begin to evolve into tropical cyclones. Although individual case
variations can be large, common large-scale circulation influences on
tropical cyclone formation have been documented. This chapter will
summarize these results and compare them to previous observational
studies by McBride (1981a, b), McBride and Zehr (1981), and Love (1985a,
b). Various theories regarding tropical cyclogenesis will also be
discussed and verified against the current results. The necessary
conditions for tropical cyclone formation will then be synthesized.

10.1   Observed Structural and Large-scale Circulation Changes During Tropical Cloud Clusters' Evolution

Conservative, non-intensifying tropical cloud clusters are observed
to have a weak middle- to upper-tropospheric warm core (about half a
degree) and a lower tropospheric cold core. A small surface pressure
drop (less than half a millibar) and a weak, but deep, cyclonic
circulation is present. Inflow occurs through a very deep layer and the
upper-level outflow is concentrated within a shallow layer. The
middle-level inflow is about as strong as that of the boundary layer
inflow.

Almost no change in the surface pressure field is observed during
cloud cluster formation and dissipation. The change in the cyclonic
circulation is also small during and after cloud cluster convection.
However, after cloud cluster convection, there is a moistening process

occurring at the middle troposphere and a drying out at the lower troposphere. Before the prominent cloud cluster is observed, the mean vertical motion over the $0-4^{\circ}$ or $0-6^{\circ}$ radial domain has already become very large (much larger than the mean background ω-profile). The vertical profile of $\bar{\omega}$ is near constant with height at this pre-cluster stage, indicating that the large-scale low-level convergence is larger while the middle-level convergence is almost zero. The middle-level convergence then increases significantly during the cloud cluster stage. These results suggest that tropical cloud clusters are likely to be forced primarily by environmental low-level convergence while the middle-level inflow is more a feedback response to the cumulus convection. It is suspected that ice-phase processes associated with the convective-scale and meso-scale ascent updraft act as an important mechanism to the development of the middle-level inflow (as discussed by Cotton and Anthes, 1986). The entrainment of the middle-level low θ_e air and the re-evaporation of the downdrafts (Johnson, 1976) are also likely important mechanisms in causing this middle level inflow.

The rawinsonde composite analyses also have shown that pre-cyclone cloud clusters usually have a stronger middle- to lower-level cyclonic circulation (or mean vorticity) than the non-genesis cloud clusters. These circulation differences extend over a domain as large as $6-8^{\circ}$ radius. Pre-cyclone cloud clusters also have a slightly warmer middle- to upper-tropospheric warm core and slightly lower surface pressure over a larger domain which occurs in response to such circulation differences. Developing systems have a slightly higher moisture content, as well. However, the pre-cyclone and non-genesis cloud clusters both have about the same amount of maximum mean vertical motion

and cumulus convection over the 0-4° or 0-6° radial domain. These observed characteristic differences between the genesis and non-genesis cloud clusters are in good agreement with those found by Zehr (1976), Erickson (1977), McBride (1981a, 1981b) and McBride and Zehr (1981).

The most important characteristic of the pre-cyclone cloud cluster during the formation process is the increase of the middle- to low-level cyclonic circulation (or mean vorticity). This increase appears to occur as far out as 8° radius before the cyclogenesis stage but is limited to inside of 5° radius at later stages when the cloud cluster has been upgraded to a tropical cyclone. A convection burst is often observed during the transition phase of a cloud cluster to a tropical cyclone. The middle- to upper-level warming, the surface pressure drop, the moistening process and the mean vertical motion also become more concentrated at the inner radii (inside 2-3° radius). The low-level circulation also changes gradually from an east-west elongated pattern to a more circular and symmetric pattern.

The tangential momentum (or angular momentum) budget at this critical genesis period indicates that the mean transverse circulation is not large enough both to produce the observed tangential wind increase and to balance the surface frictional loss. It is necessary to hypothesize a very large positive residual momentum source in order to make the tropospheric tangential momentum budget balance. This required residual is observed in early stages at both the inner (1-5°) and outer (5-9°) regions, but soon becomes weak as the formation process proceeds. This study's results indicate that this residual effect is likely due to large-scale forcing processes which create large inward eddy vorticity fluxes (especially on eddy shear vorticity flux). Due to the limitations

the rawinsonde composite technique, the space and time transient feature
of this eddy flux cannot be directly measured. However, the detailed
time stratification of the composites has made it possible to estimate
this effect as a residual for the tropospheric tangential momentum
budget. None of the previous composite studies (e.g. Zehr, 1976;
McBride 1981a, 1981b; McBride and Zehr, 1981; and Love, 1985a, 1985b)
were capable of resolving this transient eddy effect.

The composite analysis has further shown that a large number of
cyclone formation cases (slow genesis composite) have some type of low-
level cross-equatorial surge influences. Observations indicate that the
original wind surge can be as deep as 500 mb, but the cross-equatorial
flow is typically limited to below 700 mb. The composite data show that
surges are primarily from the southwest direction, where a strong
horizontal wind shear is typically observed. It appears that the
horizontal wind shear can be much stronger in the individual cases and
that cumulus or meso-scale activities associated with this strong shear
vorticity are primarily responsible for the large inward eddy vorticity
flux. These results agree with the studies by Love (1985), regarding
the observed cross-equatorial surge or large-scale influences on the
tropical cyclone formation process, and the case study of Molinari and
Skubis (1985). The current study, however, provides important and much
more detailed quantitative information on the important terms of the
tangential momentum budget.

Although the composite analyses show that the large-scale momentum
surges are mainly from the southwest direction, the individual case
analyses using FGGE III-b data show that three types of large-scale
momentum surge are possible:

i) cross-equatorial surges which are often affected by the island topography in the western Pacific;

ii) monsoon surges originating in the North Indian Ocean (in the summer when the monsoon is strong); and

iii) trade wind surges which might play an important role in the early and late seasons when the cross-equatorial surge typically has less influence.

In the western North Pacific, the trade winds on the poleward side are always a potential source for surges. It is thus possible to have two surge sources influencing a formation event or to have a series of surges from the same source. Under favorable large-scale circulation patterns, it is thus possible to have multiple disturbance formations which can influence each other, as has been discussed in the Lola and Ken cases. Although an investigation of the possible cause for these surges was not the intent of this study, it appears clear that these surges are often brought about by same or opposite hemisphere mid-latitude frontal systems penetrating into the tropics, as discussed by Love (1985a, 1985b).

Another possible situation, discussed by Lee et al. (1986) for cyclone formation in the North Indian Ocean, is that of dual cyclone cases. When a strong cyclone in the opposite-hemisphere intensifies and builds up its outer circulation, this can cause an increase of vorticity in the vicinity of a tropical disturbance in the other hemisphere. Keen (1982) has discussed cyclone pairs over the Pacific Ocean during the southern oscillation. However, there were no apparent dual opposite hemispheric cyclone pair influences in this region during the 1979 FGGE year period of this study.

The genesis situations discussed in this paper all involve some type of low-level large-scale environmental influences which are hypothesized to act to increase the surrounding pre-cyclone vorticity through some sort of (transient) eddy vorticity transport process. However, it is not necessarily true that every cyclone formation event requires these surges, as the case of Lola indicates. Here the low-level large-scale relative vorticity is sufficiently large at the initial stage to bring about cyclone formation. (Possibly, this is because Lola is located at a higher latitude where f is larger.) Under these conditions, a favorably positioned upper-level outflow channel can help the cloud cluster to organize its convection patterns and to increase its inward eddy vorticity transports without the need for a major low-level wind surge. This might be a common situation for higher latitude TUTT-influenced cyclone developments embedded within the trade winds. Precisely how these favorable upper-level outflow channels can influence the early stage formation of a tropical cyclone has yet to be fully studied, though there have been many observational studies regarding the influence of upper-level outflow on tropical cyclone intensity change (e.g., Sadler, 1976, 1978; Chen and Gray, 1985; and Merrill, 1985).

A large inward eddy vorticity flux is important because it allows the tropical disturbance to increase its surrounding vorticity or cyclonic circulation without actually increasing its transverse circulation. Due to the vertical energy distribution (referred to as θ_e profile), the transverse circulation associated with a tropical disturbance imports low θ_e air inward (from the surface to 350 mb) and exports higher values θ_e air at the higher levels. The tropical

disturbance's mean transverse circulation is thus always bringing about an energy export from the system. It is thus necessary that a sufficiently large amount of sea-surface energy flux occurs within the disturbance to balance its net energy (or θ_e) export and radiational cooling. For each incremental increase in transverse circulation, a similar incremental increase in the amount of sea-surface energy flux is required for energy balance. If a disturbance can increase its vorticity through horizontal eddy flux without having to increase its transverse circulation, then a more efficient energy budget can be obtained. Such increased vorticity or cyclonic circulation spinup is also needed for a better organization of the deep cumulus into squall lines. As proposed by Gray (1982) the downdrafts from such line convection can lead to a more efficient surface energy flux.

A stronger warm core will hydrostatically give lower surface pressure and the possibility for a stronger transverse circulation. Due to the increase of the low-level cyclonic vorticity, the low-level inflow is more efficient in producing more and more inward vorticity transports (Hack and Schubert, 1986). The eddy vorticity transport can then become less and less important as the system develops. At the same time, the convection is becoming much better organized. A higher surface energy flux is thus possible through more intense and organized convective scale downdraft activity. Such a high surface energy flux must occur in order to balance the ever higher energy export caused by the stronger transverse circulation. The strong cloud-scale downdrafts within the convective cells or squall lines will become dry and cool as they descend to the boundary layer due to the re-evaporational cooling (Johnson, 1980; Zipser, 1977). These cool and dry downdrafts further

enhance surface energy flux.

10.2 Dynamics of Tropical Cyclone Formation

As the vorticity of the vortex is low at the early tropical cyclone formation stage, the energetical efficiency of cloud cluster heating in producing warming and a balanced vortex flow is very low, while the efficiency of the cloud cluster forcing of the vorticity field is very high (Schubert, et al. 1980; Hack and Schubert, 1986). Shapiro (1977) also pointed out that thermodynamic processes appear to be of secondary importance at this early stage of formation.

The current study also found that non-genesis cloud clusters have about as much mean vertical motion and apparent condensation heat release over the $0-4^{\circ}$ or $0-6^{\circ}$ radial domain as the genesis cloud clusters. However, almost no apparent spinup of the circulation or significant pressure drop was observed. Therefore, it does not appear physically realistic for a weak vortex to spin up purely from diabatic heating without resorting to the processes which can affect the dynamical field; namely, the cumulus momentum mixing and the horizontal (eddy) momentum transports. This argument, however, does not entirely rule out the diabatic heating as one necessary ingredient for cyclone formation, particularly later stage formation. Instead it points out the fact that the cumulus heating or apparent heat source is about $10-15^{\circ}C$ d^{-1} while the observed temperature change is less than $1^{\circ}C$ d^{-1} at the formation stage.

Shapiro (1977) emphasized the likely importance of the non-linear vorticity advection, and pointed out that its increase might be a result of the changes in the environmental circulation. The numerical model simulation by Kurihara and Kawase (1985), on the other hand, compared

the relative importance of the cumulus heating to that of the non-linear vorticity advection and concluded that cumulus heating is more important for cyclogenesis. However, Kurihara and Kawase (1985) did not include in their model simulation the possible influences of environmental forcing on the vorticity field or of the retarding effect of cumulus vertical momentum mixing processes. Their conclusions that a CISK-type heating is more efficient in causing early stage vortex spinup than the non-linear vorticity advection is not supported by this study's analysis.

10.2.1 Scale-dependent Dynamics and Environmental Forcing

As discussed by Ooyama (1982), the dynamics of the tropical cyclone formation process is related to the scale-dependent dynamics of the atmosphere. If the vortex's horizontal scale of motion is greater than the Rossby's radius of deformation, the flow is quasi-horizontal and nearly in geostrophic balance (the pressure field is being strongly constrained by the earth's rotation). This condition is generally met during the early formation stage of a tropical cyclone when the relative vorticity is weak. If the large-scale relative vorticity and rotation associated with the disturbance are increased, the disturbance environment is stiffened by the increased inertial stability. In other words, the Rossby's radius of deformation is locally decreased due to increased relative vorticity, and the lower-scale limit of the quasi-balanced flow regime is brought down closer to the mesoscale. If by any chance this trend (increasing relative vorticity) would continue, the more deterministic dynamics of the balanced flow would begin to take

over the control of the meso-scale convection associated with the pre-
cyclone disturbance.

As is apparent, the current study deals only with the environmental
influences that increase the relative vorticity during the early
formation stage. No attempt is made at the present time to examine the
complicated interaction between the meso-scale convective system and its
environment (which really can only be properly addressed through a 3-D
nested numerical model simulation incorporating both the environmental
and the convective scale influences). Nevertheless, the current study
appears to have rather successfully identified the most prominent
environmental features during the early stage cyclogenesis process. It
is very important to be able to distinguish and understand the physical
processes associated with both cyclogenesis and non-cyclogenesis;
otherwise any attempt to study the internal dynamics and to do a
numerical simulation will likely fail because this fundamental physical
linkage will be missing. A tropical cyclone cannot be realistically
modeled in a tin can!

The present study demonstrates that low-level large-scale
disturbance forcing is a quite common feature during the early formation
stage, while the upper-level outflow channel influences are likely a
more dominant influence during the later cyclone intensification stage.
During the early formation stage, the upper-level circulation pattern
may be more of a hindering mechanism if strong middle- to upper-level
shearing features are present or if the system is underneath an upper-
level trough. Otherwise, a weak divergent anticyclonic circulation has
proven to be favorable enough for formation. Even under a rather
unfavorable upper-level condition, the low-level cyclonic circulation

can still maintain itself if the low-level vorticity is large enough. Once the unfavorable upper-level condition disappears, the convection can reorganize itself and the system can develop again.

The relative importance of the upper- and lower-level environmental influences is greatly affected by the inertial stability and the static stability of the system's surrounding circulation. Throughout the life cycle of a tropical cyclone, the static stability is relatively invariant except near the inner core region. The inertial stability, however, experiences a significant increase - especially at close-in radii - as shown for the genesis composites at stage 1 (early cloud cluster) and stage 4 (tropical storm - typhoon intensity) in Fig. 88. In the upper level, the inertial stability does not change much (actually decreases slightly) from Stage 1 to Stage 4. In the middle- to lower-levels and inside $1-2^{\circ}$ radius, however, it increases greatly. These changes are relatively small outside 6° radius.

There have been a few studies regarding the effects of inertial and static stability changes on the development of a hurricane-like vortex (e.g. Schubert and Hack, 1982; Willoughby, 1979; Willoughby et al., 1982 and Holland and Merrill, 1984). However, these studies were directed toward the hurricane intensification rather than toward the initial formation stage. Holland and Merrill (1984) pointed out that upper level environmental (momentum) forcing can more easily reach the hurricane's inner region because of the low inertial stability and high static stability there. On the other hand, the low-level forcing is more confined at the outer region due to the rather strong inertial stability at the inner region and to the fact that the static stability is relatively low. However, at the early formation stage, the inertial
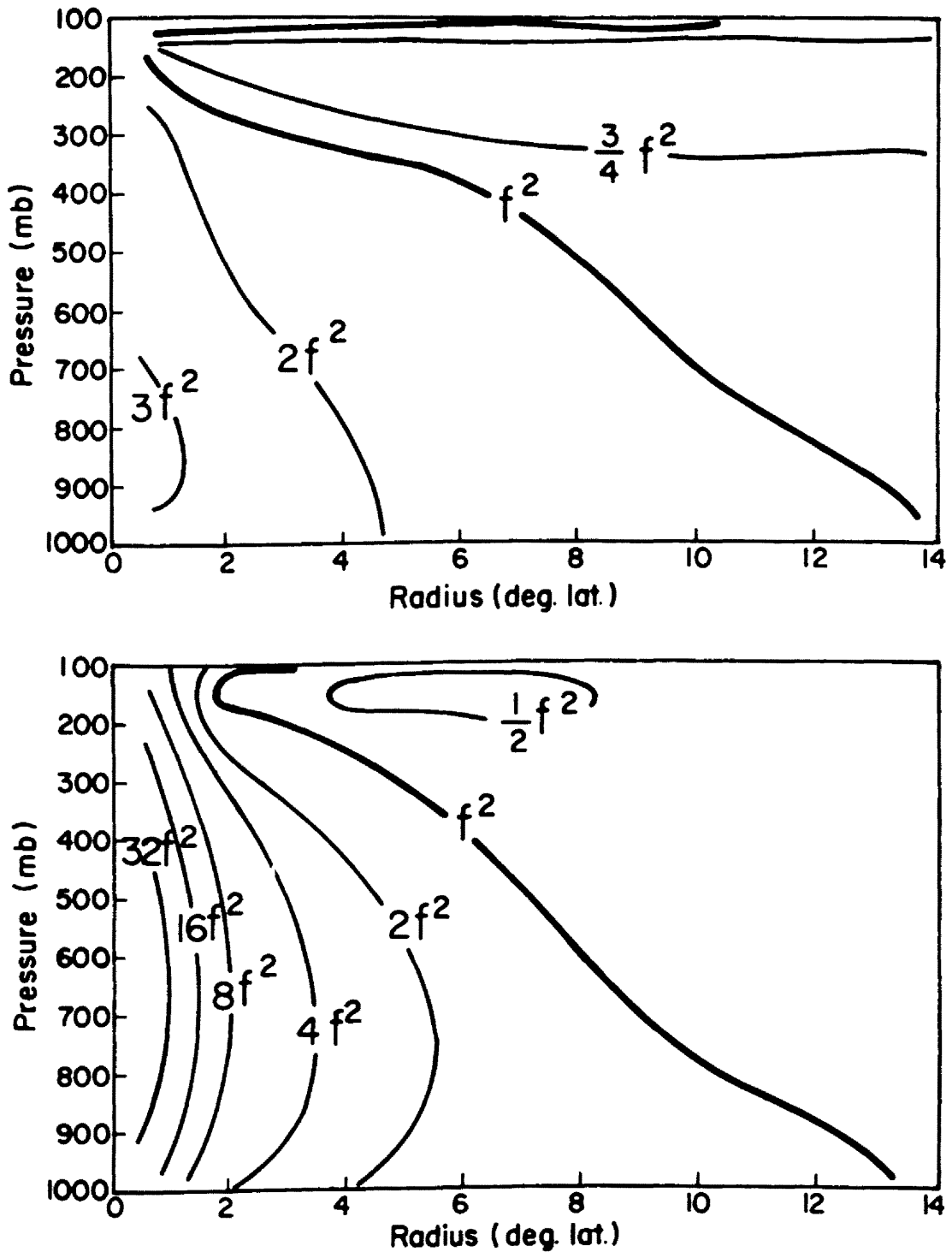
Fig. 88. The inertial stability for the genesis case at the Stage 1 (top) cloud cluster stage and Stage 4 (bottom) tropical storm – typhoon stage.

stability is much smaller compared to that of the later stage (see Fig. 88). Therefore, it is much easier for the low-level environmental forcing to reach and act upon the inner region if this forcing is strong enough. This may help explain why low-level forcing may be more dominant at the formation stage, while the upper-level forcing dominates at the later development/intensification stage.

10.2.2 Numerical Model Vortex Spinup and the Horizontal Eddy Vorticity Flux

Fingerhut (1980) pointed out that many numerical model simulations have overestimated the mean vertical motion by a factor of 2-3 or more. In other words, those models are deficient in producing a reasonable vortex spinup rate given a realistic mean vertical motion or of a realistic cumulus diabatic heating function. Besides, most of the previous numerical model simulations (for example, Kurihara and Kawase, 1985) have so far failed to incorporate the cumulus momentum mixing, though the cumulus diabatic heating is always included. Since the cumulus momentum mixing is primarily a downgradient mixing process and acts to reduce the vertical shear (Lee, 1984), it is a retarding or slowdown mechanism for vortex spinup (Challa and Pfeffer, 1984). If cumulus momentum mixing were to be included in these numerical model simulations together with a more realistic vertical motion profile, it would be expected that most previous model vortex spinup rates would be greatly reduced and that vortex spinup in a realistic time scale could not be achieved. Numerical model simulations of the early stage genesis would thus be impossible unless some type of efficient horizontal eddy flux was included. This may be the reason why most previous tropical cyclone model simulations have been initialized with unrealistically high vorticity fields, as shown in Table 1.

The deficiency of most of the numerical model simulations in producing a realistic tropical cyclone in a reasonable time period from a weak disturbance is likely due to the lack of observed horizontal eddy vorticity fluxes. The studies by Fingerhut (1980) and Challa and Pfeffer (1980) did include horizontal eddies obtained from a crude composite estimation (not from a complete budget analysis). Their results suggested that an extra angular momentum or vorticity source did help the spinup of the vortex.

Fingerhut (1980) further showed that it is necessary to have a cyclonic vorticity source over a very deep layer in order to produce a realistic model tropical cyclone in a reasonable time period. Unfortunately, he did not have other information on how this vorticity source can be produced. He attributed it to cumulus induced momentum generation. Since his model included all the physical processes: cumulus heating, cumulus friction, horizontal eddies estimated by composites; radiational cooling, etc.), it was not fully understood at that time as to why an initial deep layer of cyclonic vorticity was necessary for cyclone spinup.

The current studies have made it clear that the large-scale environmentally forced inward (transient) eddy vorticity flux is the key factor in most early stage tropical formation situations. This transient eddy vorticity flux could not be properly addressed in previous composite analyses because no strict classification in time was made for those composites. Therefore, the horizontal eddy fluxes included in Fingerhut (1980) and Challa and Pfeffer (1980) are not so appropriate. The present study appears to have cleared up the unknowns concerning the numerical model results of Fingerhut (1980).

The importance of this large-scale environmentally forced (transient) eddy vorticity flux is that it can give the necessary vorticity spinup without requiring an increase of the mean transverse circulation and its corresponding extra h-energy export plus the extra retarding influences of cumulus downgradient momentum mixing. As previously discussed, mean transverse circulation is exporting moist static energy from the system in proportion to its magnitude. Therefore, an increased transverse circulation will require more compensating surface energy flux in order to satisfy energy budget requirements - and this can only be produced by stronger surface winds or better-organized cumulus downdrafts. Eddy vorticity flux from the environment gives the system a greater potential for development because momentum spinup can be accomplished without the need of increasing the transverse circulation.

These results are in qualitative agreement with a theory proposed by Shapiro (1977) which emphasized the likely importance of some type of non-linear vorticity flux in producing an imbalanced state favorable for disturbance growth. Yanai (1961) also pointed out the importance of the non-linear advection in producing the observed vorticity increase. This can be produced by changes in the disturbance's inward environmental vorticity flux. The current study indicates that the required inward eddy vorticity flux primarily occurs from large-scale environmentally forced momentum surges. Such eddy vorticity fluxes appear to have been inadvertently included in the non-linear vorticity advection ideas of Shapiro (1977). He failed, however, to specifically comment on this. Nevertheless, the gist of many of this paper's observational results in a general sense agree with some of the ideas proposed by Shapiro (1977).

10.3 Genesis Potential and the Necessary Conditions for Tropical Cyclone Formation

McBride and Zehr (1981) have proposed that tropical cyclone genesis potential is related to the $0-6^{\circ}$ mean vorticity (or the mean tangential wind at 6° radius) difference between 900 mb and 200 mb. The stronger the low-level cyclonic circulation and/or the upper-level anticyclonic circulation, the higher the possibility for tropical cyclone formation to occur. However, the current results only confirm the importance of a strong middle- to low-level vorticity. A strong upper-level anticyclonic circulation appears not to be a general and necessary condition for early stage cyclogenesis. This is also in agreement with Fingerhut's (1980) modeling results. A very strong anticyclone might even be unfavorable for early stage genesis because it tends to cause outflow air parcels to move more anticyclonically than radially outward in order to conserve absolute angular momentum (Lee, 1984). As Lee's 1984 results indicated, a mean outflow will create an anticyclonic circulation in the upper level, which is approximately balanced by the cumulus momentum transports inside 5° radius. Outside 5° radius, however, the outflow circulation (without deep convection) will be required to become more anticyclonic as the vortex develops into a tropical cyclone. Kurihara and Tuleya (1981) have also found that the appearance of an upper-level anticyclonic disturbance in their model was caused entirely by the outflow forcing from cumulus convection below.

Another important characteristic which the genesis cloud cluster generally requires is a weak middle- to upper-level vertical wind shear near where the center is going to form. Since this is the layer where most of the warming occurs, a strong vertical wind shear would tend to

prevent the accumulation of the enthalpy in a vertical column and thus could hinder the development of the early stage vortex, as discussed by Gray (1968). As shown previously in Fig. 33, the non-genesis cloud clusters do show a strong zonal wind shear between 200 and 500 mb, while the genesis cloud clusters have almost no vertical wind shear at this layer. It is more realistic, however, to treat the vertical wind shear as a hindering mechanism. The strong middle- to low-level cyclonic circulation and the upper-level divergent flow, however, are conducive to the cloud cluster development and cyclogenesis.

Although this study discusses the importance of the middle- to low-level cyclonic vorticity, the upper-level divergence and the vertical wind shear, it does not imply that other genesis parameters - e.g., the sea-surface temperature, the Coriolis parameter, the middle-level relative humidity and the static stability (Gray, 1981) - are not important. However, such conditions are generally satisfied during the summer-autumn period in the western North Pacific.

10.4 Concluding Remarks and Recommendations for Future Research

This observational analysis has attempted a better understanding of the large-scale characteristics associated with early stage tropical cyclone formation. However, the internal dynamics of the meso-scale convection associated with the tropical cloud cluster, the details of the physical links between the surrounding circulation, and the forming cyclone's internal dynamics have yet to be addressed. Tropical cyclone formation cannot be fully understood until both the internal dynamics and the large-scale characteristics, as well as their interactions, are properly ascertained. A 3-dimensional nested-grid model which incorporates both the cloud-scale and synoptic-scale processes is

necessary to completely explore these subjects and their complicated interactions. But, a simplified model (e.q. Hack and Schubert, 1986) can often be as valuable in advancing our knowledge of the tropical cyclone formation process.

The most significant result in this analysis is that there are often large-scale low-level (momentum) surges acting upon pre-cyclone cloud clusters right before they develop into tropical cyclones. These surges can conceivably create large inward eddy vorticity flux and help spin up the pre-cyclone cloud cluster's vorticity. The FGGE individual case analysis in this study has indicated three possible surges in the western North Pacific: the cross-equatorial surges, the trade wind surges and the southwest monsoon surges from North Indian Ocean. Lee, et al., (1986) found similar large-scale surges during cyclogenesis stage in the North Indian Ocean. Love (1985) has also found that a cold outbreak in the opposite hemisphere can cause cross-equatorial surges which can be important for cyclogenesis in the western Pacific and the Australia region. (The current analysis found that strong momentum surges behind a cold front is often sufficient enough to produce cross-equatorial surges. A cold outbreak is not necessarily required.) However, the triggering mechanism for the trade wind surges is not well understood. It is also desirable to know if such surge-influenced cyclogenesis events are a common feature in the other ocean basins (e.g. eastern North Pacific, North Atlantic, etc.)

In the tangential momentum budget analysis, a large residual effect (which includes the eddy shear vorticity flux and the eddy divergence effect) is found to be required for tropospheric budget balance. However, whether this residual effect is primarily due to the strong

shear vorticity associated with the transient large-cale momentum surges or is due to the eddy divergence effect associated with cumulus activities remains to be answered.

In short, there is still much more research needed to fully understand tropical cyclogenesis. For those who are interested in tropical cyclones, this might be a good place to start.

ACKNOWLEDGEMENTS

REFERENCES

Alaka, M. A., 1962: On the occurrence of dynamic instability in incipient and developing hurricanes. Mon. Wea. Rev., 90, 49-58.

Anthes, R., 1970: The role of large-scale asymmetries and internal mixing in computing meridional circulations associated with the steady-state hurricane. Mon. Wea. Rev., 98, 521-528.

Anthes, R. A., 1972: The development of asymmetries in a three-dimensional numerical model of the tropical cyclone. Mon. Wea. Rev., 100, 461-476.

Anthes, R. A., 1977: Hurricane model experiments with a new cumulus parameterization scheme. Mon. Wea. Rev., 105, 287-300.

Anthes, R. A., S. L. Rosenthal and J. W. Trout, 1971a: Preliminary results from an asymmetric model of the tropical cyclone. Mon. Wea. Rev., 99, 744-758.

Anthes, R. A., J. W. Trouth and S. L. Rosenthal, 1971b: Comparisons of tropical cyclone simulation with and without the assumption of circular symmetry. Mon. Wea. Rev., 99, 759-766.

Arnold, C. P., 1977: Tropical cyclone cloud and intensity relationships. Dept. of Atmos. Sci. Paper No. 277, Colo. State Univ., Ft. Collins, CO 154 pp.

Carrier, G. F., 1971: The intensification of hurricanes. J. Fluid Mech., 49, 145-158.

Ceselski, B. F., 1974: Cumulus convection in weak and strong tropical disturbances. J. Atmos. Sci., 31, 1241-1255.

Charney, J. G., and A. Eliassen, 1964: On the growth of the hurricane depression. J. Atmos. Sci., 21, 68-75.

Challa, M. and R. L. Pfeffer, 1980: Effects of eddy fluxes of angular momentum and model hurricane development. J. Atmos. Sci., 37, 1603-1618.

Challa, M. and R. L. Pfeffer, 1984: The effect of cumulus momentum mixing on the development of a symmetric model hurricane. J. Atmos. Sci., 41, 1313-1319.

Chen, L. and W. M. Gray, 1985: Global view of the upper level outflow patterns associated with tropical cyclone intensity changes during FGGE. Dept. of Atmos. Sci. Paper No. 392, Colo. State Univ., Ft. Collins, CO, 126 pp.

Cotton, W. R. and R. A. Anthes, 1986: Dynamics of cloud and precipitating systems. Academic Press. (In preparation).

Dvorak, V. F., 1975: Tropical cyclone intensity analysis and forecasting from satellite imagery. Mon. Wea. Rev., 103, 420-430.

Erickson, Steven L., 1977: Comparison of developing vs. non-developing tropical disturbances. Dept. of Atmos. Sci. Paper No. 274, Colo. State Univ., Ft. Collins, CO, 81 pp.

Fingerhut, W. A., 1980: Tropical cyclone genesis - numerical modeling inferences. Dept. of Atmos. Sci. Ph.D. Dissertation, Colo. State Univ., Ft. Collins, CO, 155 pp.

Frank, W. M., 1976: The structure and energetics of the tropical cyclone. Dept. of Atmos. Sci. Paper No. 258, Colo. State Univ., Ft. Collins, CO, 180 pp.

Frank, W. M., 1977a: The structure and energetics of the tropical cyclone, I: Storm structure. Mon. Wea. Rev., 105, 1119-1135.

Frank, W. M., 1977b: The structure and energetics of the tropical cyclone, II: Dynamics and energetics. Mon. Wea. Rev., 105, 1136-1150.

Frank, W. M., 1977c: Convective fluxes in tropical cyclones. J. Atmos. Sci., 34, 1554-1568.

Gamache, J.F. and R. A. House, 1982: Mesoscale air motions associated with a tropical squall line. Mon. Wea. Rev., 110, 118-135.

Gray, W. M., 1968: Global view of the origin of tropical disturbances and storms. Mon. Wea. Rev., 96, 669-700.

Gray, W. M., 1975: Tropical Cyclone Genesis. Dept. of Atmos. Sci. Paper No. 234, Colo. State Univ., Ft. Collins, CO, 121 pp.

Gray, W. M., 1979: Hurricanes: their formation, structure, and likely role in the tropical cyclone. Meteorology over the tropical oceans. D. B. Shaw, Editor, Roy. Meteor. Soc., 155-218.

Gray, W. M., 1981: Recent advances in tropical cyclone research from rawinsonde composite analysis. Paper prepared for the WMO Committee of Atmospheric Science, Geneva, Switzerland, 407 pp.

Gray, W. M., 1982: Tropical cyclone genesis and intensification. Topics in Atmospheric and Oceanographic Sciences, Intense Atmospheric Vortices, (Ed. by L. Bengtsson/J. Lighthill), Springer-Verlag Berlin Heidelberg (ISPN 3-540-11657-5), 3-20.

Hack, J. and W. Schubert, 1986: On the non-linear response of atmospheric vortices to heating by organized cumulus convection. Submitted to J. Atmos. Sci.

Harrison, E. J., Jr., 1973: Three-dimensional numerical simulation of tropical systems utilizing nested finite grids. J. Atmos. Sci., 30, 1528-1543.

Holland, G. J., 1983: Angular momentum transports in tropical cyclones. Quart. J. Roy. Meteor. Soc., 109, 187-209.

Holland, G. J., and R. T. Merrill, 1984: On the dynamics of tropical cyclone structural changes. Quart. J. Roy. Met. Soc., 110, 723-745.

Izawa, T., 1964: On the mean wind structure of typhoon. Japan Meteorological Agency, Meteorological Research Institute, Typhoon Research Laboratory, Technical Note No. 2, Mabashi, Suginami, Tokyo, Japan.

Johnson, R. H., 1976: The role of convective-scale precipitation downdrafts in cumulus and synoptic scale interactions. J. Atmos. Sci., 33, 1890-1910.

Johnson, R. H., 1980: Diagnosis of convective and meso-scale motions during Phase III of GATE. J. Atmos. Sci., 37, 733-753.

Joint Typhoon Warning Center, 1979: Annual Typhoon Report. NAVOCEANCOMCEN/JTWC. Guam, 191 pp.

Keen, R. A., 1982: The role of cross-equatorial tropical cyclone pairs in the southern oscillation. Mon. Wea. Rev., 110, 1405-1416.

Kuo, H. L., 1965: On formation and intensification of tropical cyclones through latent heat release by cumulus convection. J. Atmos. Sci., 22, 40-63.

Kurihara, Y., 1975: Budget analysis of a tropical cyclone simulated in an axisymmetric numerical model. J. Atmos. Sci., 32, 25-59.

Kurihara, Y. and M. Kawase, 1985: On the transformation of a tropical easterly wave into a tropical depression: A simple numerical study. J. Atmos. Sci., 42, 68-77.

Kurihara, Y. and R. E. Tuleya, 1974: Structure of a tropical cyclone developed in a three-dimensional numerical simulation model. J. Atmos. Sci., 31, 893-919.

Kurihara, Y. and R. E. Tuleya, 1981: A numerical simulation study on the genesis of a tropical storm. Mon. Wea. Rev., 109, 1629-1653.

Lee, C.-S, 1984: The bulk effects of cumulus momentum transports in tropical cyclones. J. Atmos. Sci., 41, 590-603.

Lee, C.-S., R. Edson, W. M. Gray, 1986: Large scale characteristics associated with tropical cyclone development in the northern Indian Ocean during FGGE. To be submitted to Mon. Wea. Rev.

Lee, C.-S., and W. M. Gray, 1984: Characteristics of North Indian Ocean Tropical Cyclone Activity. (108 pp.). US Navy Environmental Prediction Research Facility Report No. CR 84-11. (Available from the US Navy, Monterey, CA). Navy Support.

Love, G., 1982: The role of the general circulation in western Pacific tropical cyclone genesis. Dept. of Atmos. Sci., Paper No. 340, Colo. State Univ., Ft. Collins, CO, 215 pp.

Love, G., 1985a: Cross-equatorial influence of winter hemisphere subtropical cold surges. Mon. Wea. Rev., 113, 1487-1498.

Love, G., 1985b: Cross-equatorial interactions during tropical cyclone genesis. Mon. Wea. Rev., 113, 1499-1509.

Madala, R. V., 1975: Numerical simulation of a three dimensional hurricane using a semi-implicit time integration scheme. G.F.D.I. contribution No. 999, Florida State Univ., Tallahassee, FL, 60 pp.

Mathur, M. B., 1972: Simulation of an asymmetric hurricane with a fine mesh multiple grid primitive equation model. Ph.D. Dissertation, Florida State Univ., Tallahassee, FL, 162 pp.

McBride, J. L., 1979: Observational analysis of tropical cyclone formation. Dept. of Atmos. Sci. Paper No. 308, Colo. State Univ., Ft. Collins, CO, 230 pp.

McBride, J. L., 1981a: Observational analysis of tropical cyclone formation. Part I: Basic description of data sets. J. Atmos. Sci., 38, 1117-1131.

McBride, J. L., 1981b: Observational analysis of tropical cyclone formation. Part III: Budget analysis. J. Atmos. Sci., 38, 1152-1166.

McBride, J. L., and R. Zehr, 1981: Observational analysis of tropical cyclone formation. Part II: Comparison of non-developing versus developing systems. J. Atmos. Sci., 38, 1132-1151.

Merrill, Robert T., 1985: Environmental influences on hurricane intensification. Dept. of Atmos. Sci. Paper No. 394, Colo. State Univ., Ft. Collins, CO, 156 pp.

Miller, B. I., 1969: Experiment in forecasting hurricane development with real data. ESSA Tech. Memorandum ERLTM-NHRL 85, Miami, FL, 28 pp.

Molinari, J. and S. Skubis, 1985: Evolution of the surface wind field in an intensifying tropical cyclone. Mon. Wea. Rev., 42, 2856-2864.

Ooyama, K. V., 1969: Numerical simulation of the life cycle of tropical cyclones. J. Atmos. Sci., 26, 3-40.

Ooyama, K. V., 1982: Conceptual evaluation of the theory and modeling of the tropical cyclone. J. Meteor. Soc. of Japan, 60, 369-380.

Pfeffer, R. L., 1958: Concerning the mechanics of hurricanes. J. Meteor., 113-120.

Pfeffer, R. L., and M. Challa, 1981: A numerical study of the role of eddy fluxes of momentum in the development of Atlantic hurricanes. J. Atmos. Sci., 38, 2393-2398.

Reed, R. J. and E. E. Recker, 1971: Structure and properties of synoptic-scale wave disturbances in the equatorial western Pacific. J. Atmos. Sci., 28, 1117-1133.

Reed, R. J., D. Norquist and E. E. Recker, 1977: The structure and properties of African wave disturbances as observed during Phase III of GATE. Mon. Wea. Rev., 105, 317-333.

Riehl, H., 1948: On the formation of typhoons. J. Meteor., 5, 247-264.

Riehl, H., 1961: On the mechanisms of angular momentum transport in hurricanes. J. Meteor., 18, 113-115.

Rosenthal, S. L., 1970: A circularly symmetric primitive equation model of tropical cyclone development containing an explicit water vapor cycle. Mon. Wea. Rev., 98, 643-663.

Rosenthal, S. L., 1978: Numerical simulation of tropical cyclone development with latent heat release by the resolvable scales I: Model description and preliminary results. J. Atmos. Sci., 35, 258-271.

Ruprecht, E. and W. M. Gray, 1976: Analysis of satellite-observed tropical cloud clusters, I: Wind and dynamic fields. Tellus, 28, 391-413.

Sadler, J. C., 1976: A role of the tropical upper tropospheric trough in early season typhoon development. Mon. Wea. Rev., 104, 1266-1278.

Sadler, J. C., 1978: Mid-season typhoon development and intensity changes and the tropical upper tropospheric trough. Mon. Wea. Rev., 106, 1137-1152.

Schubert, W. H., J. J. Hack, P. L. Silva Dias and S. R. Fulton, 1980: Geostrophic adjustment in an axisymmetric vortex. *J. Atmos. Sci.*, 37, 1464-1484.

Schubert, W. H. and J. J. Hack, 1982: Inertial stability and tropical cyclone development. *J. Atmos. Sci.*, 39, 1687-1697.

Shapiro, L. J., 1977: Tropical storm formation from easterly waves: a criterion for development. *J. Atmos. Sci.*, 34, 1007-1021.

Sundquist, H., 1970: Numerical simulation of the development of tropical cyclones with a ten-layer model, Part I. *Tellus*, 22, 359-390.

Thompson, R. M., S. W. Payne, E. E. Recker and R. J. Reed, 1979: Structure and properties of synoptic-scale wave disturbances in the intertropical convergence zone of the eastern Atlantic. *J. Atmos. Sci.*, 36, 53-72.

Tollerud, E. I. and S. K. Esbensen, 1985: A composite life cycle of non-squall mesoscale convective systems over the tropical ocean. Part I: Kinematic fields. *J. Atmos. Sci.*, 42, 823-837.

Tuleya, R. E., 1986: The simulation of the genesis of tropical storms using the FGGE III-b data set. Preprints, National Conference on Scientific Results of the First GARP Global Experiment, AMS, Jan. 14-17, 1986, Miami, FL, 78-81.

Tuleya, R. E., and Y. Kurihara, 1981: A numerical study on the effects of environmental flow on tropical storm genesis. *Mon. Wea. Rev.*, 109, 2487-2506.

Williams, K. T. and W. M. Gray, 1973: Statistical analysis of satellite observed cloud clusters in the western North Pacific. *Tellus*, 25, 178-201.

Willoughby, H. E., 1979: Some aspects of the dynamics in Hurricane Anita of 1977. *NOAA Tech. Memo. ERL NHEML-5*, 30 pp.

Willoughby, H. E., J. A. Clos and M. G. Shoreibah, 1982: Concentric eye walls, secondary wind maxima, and the evolution of the hurricane vortex. *J. Atmos. Sci.*, 39, 395-411.

Yamasaki, M., 1968: Numerical simulation of tropical cyclone development with the use of primitive equations. *J. Meteor. Soc. Japan*, 46, 178-201.

Yamasaki, M., 1977: A preliminary experiment of the tropical cyclone without parameterizing the effects of cumulus convection. *J. Meteor. Soc. Japan*, 55, 11-30.

Yanai, M., 1961: A detailed analysis of typhoon formation. *J. Meteor. Soc. Japan*, 39, 4, 187-214.

Yanai, M., S. Esbensen and J. Chu, 1973: Determination of bulk properties of tropical cloud clusters from large-scale heat and moisture budgets. J. Atmos. Sci., 30, 611-627.

Zehr, R., 1976: Tropical disturbance intensification. Dept. of Atmos. Sci. Paper No. 259, Colo. State Univ., Ft. Collins, CO, 91 pp.

Zipser, E. J., 1977: Mesoscale and convective scale downdrafts as distinct components of squall-line circulation. Mon. Wea. Rev., 105, 1568-1589.

APPENDIX A

APPENDIX A

Average Characteristics of all Composites

	Number of System	Time Period	Min. Press. (mb)	Max. Wind Speed (kts)	Average Lat. (°N)	Long. (°E)	Average Direction (toward)	Moving Speed (m s^{-1})	Number of Soundings Inside 5° radius (200mb)	15° radius (200mb)
Background	----	1621	----	----	11.5	143.4	298	4.0	1701	14146
Non-Persistent, Non-Genesis										
Stage 1	332	664	----	----	7.4	150.3	283	4.0	451	2063
Stage 2	332	664	----	----	8.2	147.2	283	4.0	457	2176
Stage 3	332	664	----	----	8.9	143.9	283	4.0	424	2358
Persistent, Non-Genesis										
Stage 1	328	741	----	----	8.3	149.2	280	4.3	539	2584
Stage 2	328	1094	----	----	9.5	144.6	283	4.5	767	4512
Stage 3	326	756	----	----	10.3	140.0	283	4.4	462	3440
All Genesis										
Stage 1	341	682	----	----	10.9	147.1	295	4.7	421	3201
Stage 2	341	682	----	----	12.3	144.6	299	4.9	404	3745
Stage 3	341	682	999.9	30.6	13.9	142.0	301	5.0	415	4653
Stage 4	341	682	993.3	43.2	15.5	139.2	304	5.1	466	5690

Average Characteristics of all Composites

| | Number of | | Average | | Average | | Average Moving | | Number of Soundings Inside | |
	System	Time Period	Min. Press. (mb)	Max. Wind Speed (kts)	Lat. (^{o}N)	Long. (^{o}E)	Direction (toward)	Speed (m/s)	5° radius (200mb)	15° radius (200mb)
Slow Genesis										
Stage 1	206	411	---	---	9.4	147.4	291	4.4	210	1555
Stage 2	206	412	---	---	10.4	144.9	297	4.7	255	1888
Stage 3	206	417	1002.5	26.5	12.2	141.2	298	4.7	255	2509
Stage 4	171	327	997.9	32.7	13.7	138.7	297	4.9	189	2354
Fast Genesis										
Stage 1	164	328	---	---	10.6	148.6	295	4.9	174	1409
Stage 2	164	328	---	---	12.0	145.9	299	5.1	189	1757
Stage 3	164	328	996.5	36.5	14.3	141.7	301	5.3	191	2406
Stage 4	164	328	984.0	61.0	16.2	138.9	307	5.6	227	2895

APPENDIX B
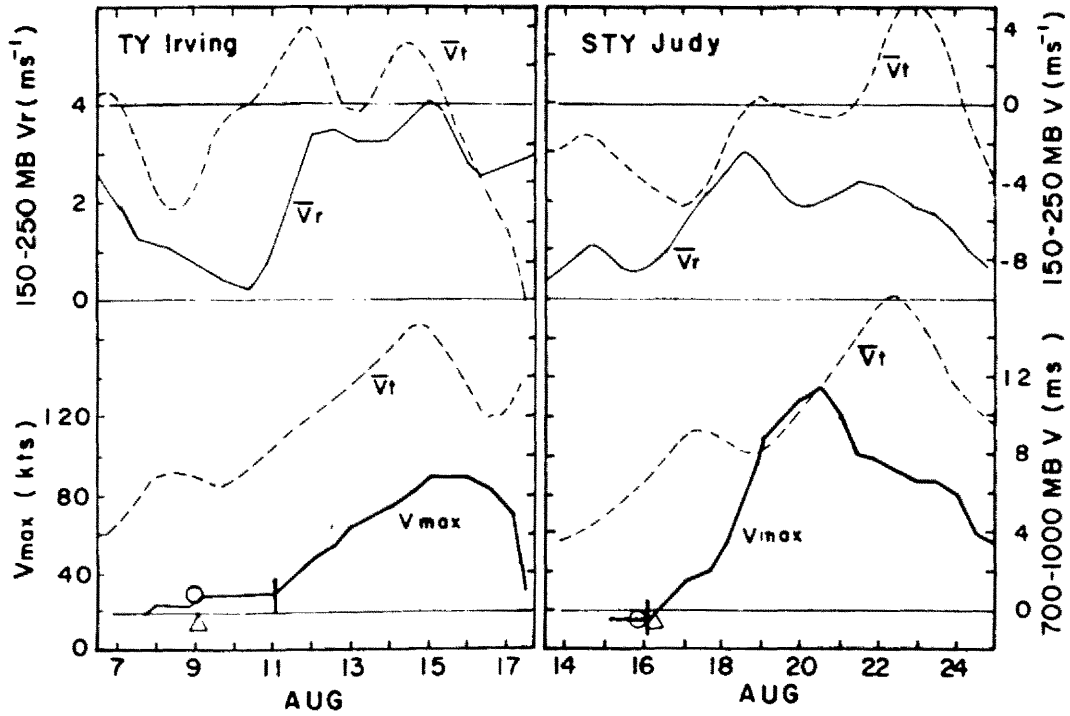
Fig. B.1.   TY Irving.

Fig. B.2.   STY Judy.
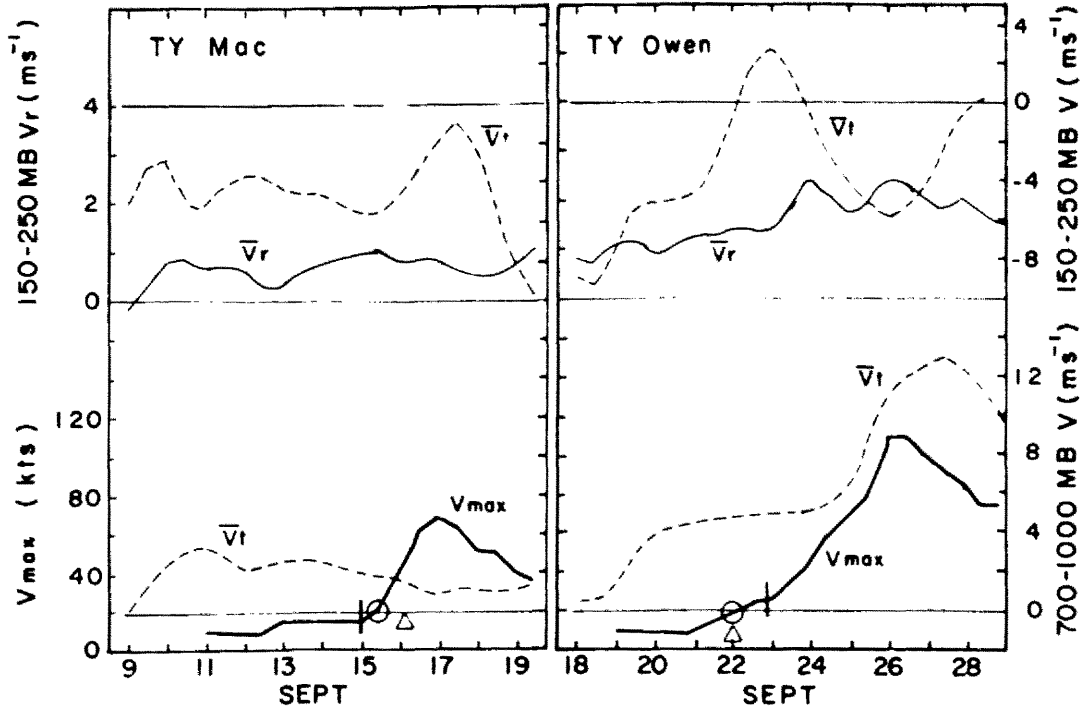
Fig. B.3.   TY Mac.

Fig. B.4.   TY Owen.
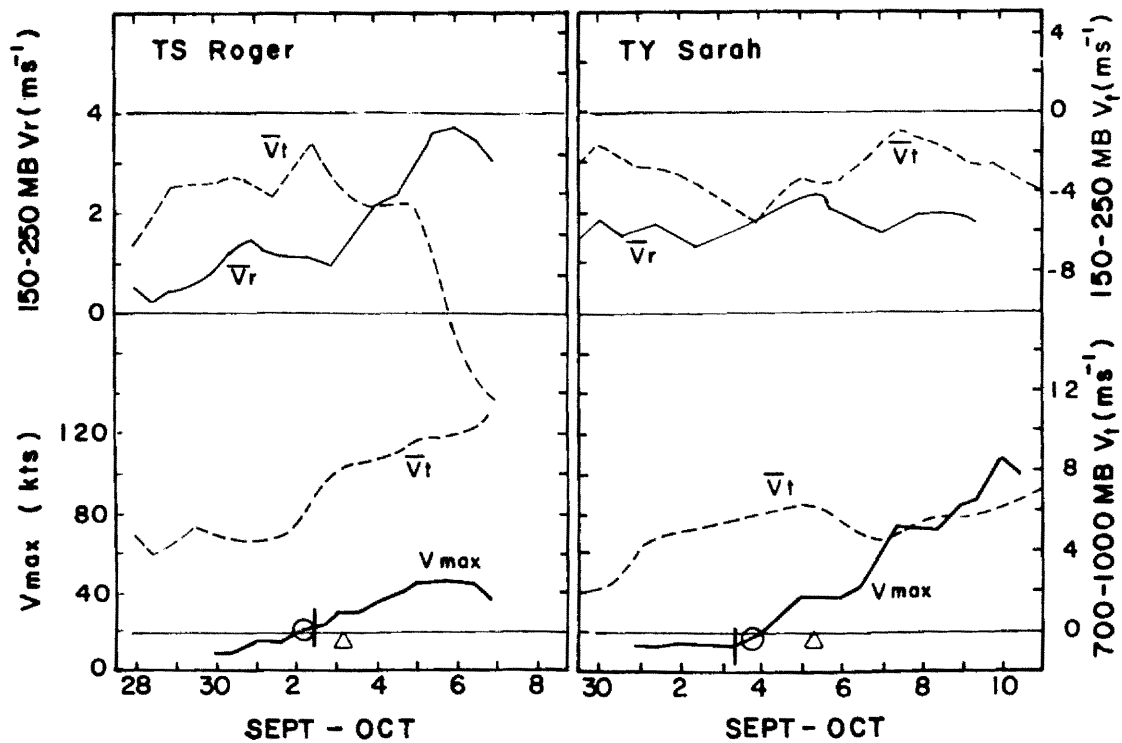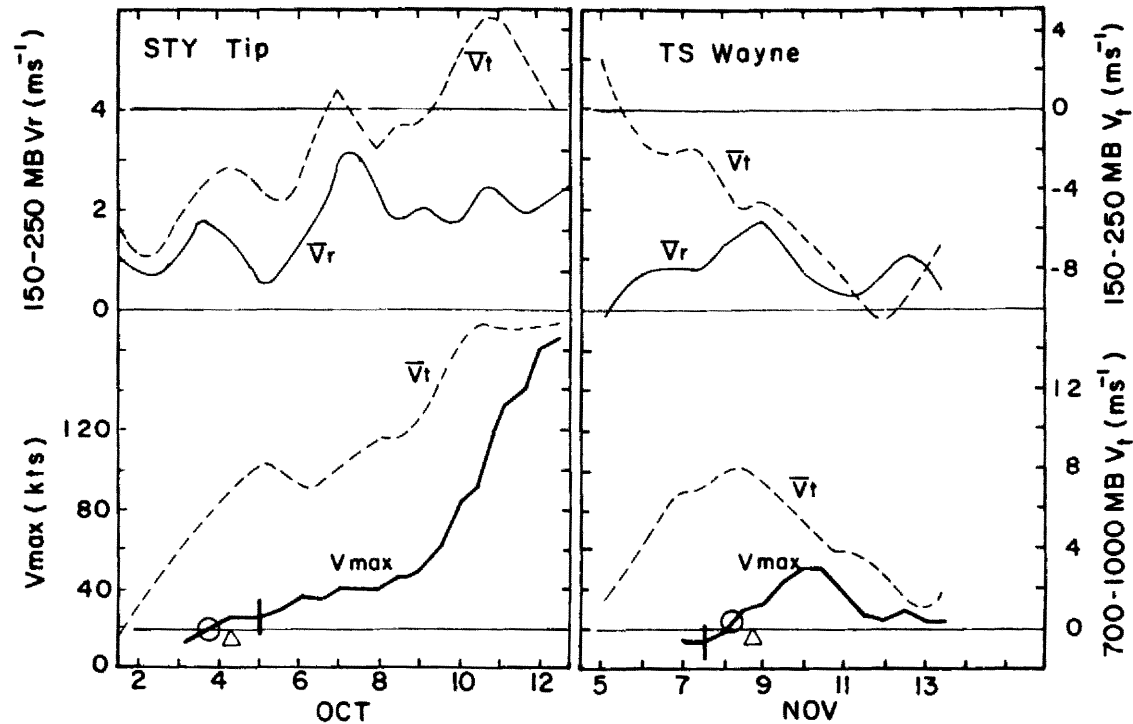
Fig. B.5. TS Roger.
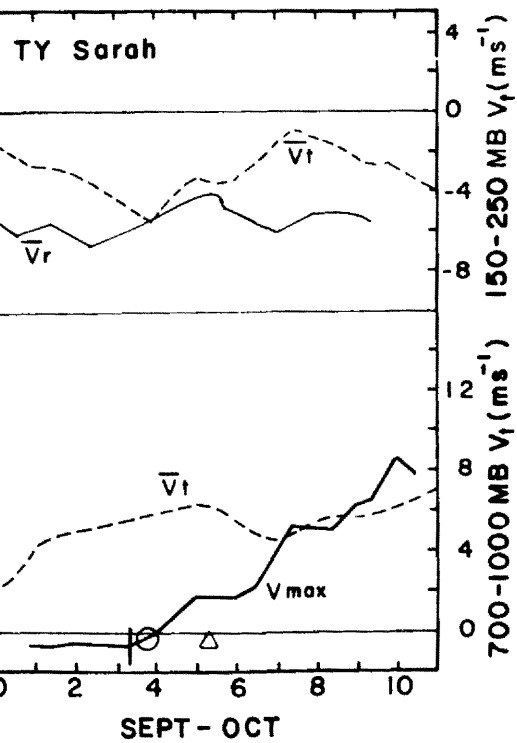
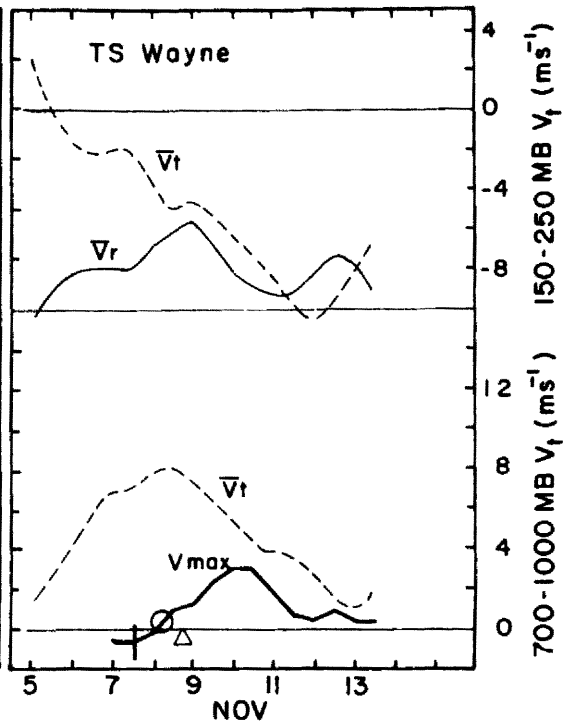Fig. B.6. TY Sarah.

Fig. B.7. STY Tip.

Fig. B.8. TS Wayne.

W. M. GRAY'S FEDERALLY SUPPORTED RESEARCH PROJECT REPORTS SINCE 1967

CSU Dept. of Atmos. Sci. Report No.	Report Title, Author, Date, Agency Support
104	The Mutual Variation of Wind, Shear and Baroclinicity in the Cumulus Convective Atmosphere of the Hurricane (69 pp.). W. M. Gray. February 1967. NSF Support.
114	Global View of the Origin of Tropical Disturbances and Storms (105 pp.). W. M. Gray. October 1967. NSF Support.
116	A Statistical Study of the Frictional Wind Veering in the Planetary Boundary Layer (57 pp.). B. Mendenhall. December 1967. NSF and ESSA Support.
124	Investigation of the Importance of Cumulus Convection and Ventilation in Early Tropical Storm Development (88 pp.). R. Lopez. June 1968. ESSA Satellite Lab. Support.
Unnumbered	Role of Angular Momentum Transports in Tropical Storm Dissipation over Tropical Oceans (46 pp.). R. F. Wachtmann. December 1968. NSF and ESSA Support.
Unnumbered	Monthly Climatological Wind Fields Associated with Tropical Storm Genesis in the West Indies (34 pp.). J. W. Sartor. December 1968. NSF Support.
140	Characteristics of the Tornado Environment as Deduced from Proximity Soundings (55 pp.). T. G. Wills. June 1969. NOAA and NSF Support.
161	Statistical Analysis of Trade Wind Cloud Clusters in the Western North Pacific (80 pp.). K. Williams. June 1970. ESSA Satellite Lab. Support.
——	A Climatology of Tropical Cyclones and Disturbances of the Western Pacific with a Suggested Theory for Their Genesis/Maintenance (225 pp.). W. M. Gray. NAVWEARSCHFAC Tech. Paper No. 19-70. November 1970. (Available from US Navy, Monterey, CA). US Navy Support.
179	A diagnostic Study of the Planetary Boundary Layer over the Oceans (95 pp.). W. M. Gray. February 1972. Navy and NSF Support.
182	The Structure and Dynamics of the Hurricane's Inner Core Area (105 pp.). D. J. Shea. April 1972. NOAA and NSF Support.

CSU Dept. of
Atmos. Sci.
Report No.   Report Title, Author, Date, Agency Support

188   Cumulus Convection and Larger-scale Circulations, Part I:
          A Parametric Model of Cumulus Convection (100 pp.).
          R. E. Lopez. June 1972. NSF Support.

189   Cumulus Convection and Larger-scale Circulations, Part II:
          Cumulus and Meso-scale Interactions (63 pp.). R. E. Lopez.
          June 1972. NSF Support.

190   Cumulus Convection and Larger-scale Circulations, Part III:
          Broadscale and Meso-scale Considerations (80 pp.). W. M.
          Gray. July 1972. NOAA-NESS Support.

195   Characteristics of Carbon Black Dust as a Tropospheric Heat
          Source for Weather Modification (55 pp.). W. M. Frank.
          January 1973. NSF Support.

196   Feasibility of Beneficial Hurricane Modification by Carbon
          Black Seeding (130 pp.). W. M. Gray. April 1973. NOAA
          Support.

199   Variability of Planetary Boundary Layer Winds (157 pp.).
          L. R. Hoxit. May 1973. NSF Support.

200   Hurricane Spawned Tornadoes (57 pp.). D. J. Novlan. May
          1973. NOAA and NSF Support.

212   A Study of Tornado Proximity Data and an Observationally
          Derived Model of Tornado Genesis (101 pp.). R. Maddox.
          November 1973. NOAA Support.

219   Analysis of Satellite Observed Tropical Cloud Clusters
          (91 pp.). E. Ruprecht and W. M. Gray. May 1974. NOAA/
          NESS Support.

224   Precipitation Characteristics in the Northeast Brazil Dry
          Region (56 pp.). R. P. L. Ramos. May 1974. NSF Support.

225   Weather Modification through Carbon Dust Absorption of
          Solar Energy (190 pp.). W. M. Gray, W. M. Frank, M. L.
          Corrin, and C. A. Stokes. July 1974.

234   Tropical Cyclone Genesis (121 pp.). W. M. Gray. March
          1975. NSF Support.

CSU Dept. of Atmos. Sci. Report No.	Report Title, Author, Date, Agency Support
——	Tropical Cyclone Genesis in the Western North Pacific (66 pp.). W. M. Gray. March 1975. US Navy Environmental Prediction Research Facility Report. Tech. Paper No. 16-75. (Available from the US Navy, Monterey, CA). Navy Support.
241	Tropical Cyclone Motion and Surrounding Parameter Relationships (105 pp.). J. E. George. December 1975. NOAA Support.
243	Diurnal Variation of Oceanic Deep Cumulus Convection. Paper I: Observational Evidence, Paper II: Physical Hypothesis (106 pp.). R. W. Jacobson, Jr. and W. M. Gray. February 1976. NOAA-NESS Support.
257	Data Summary of NOAA's Hurricanes Inner-Core Radial Leg Flight Penetrations 1957-1967, and 1969 (245 pp.). W. M. Gray and D. J. Shea. October 1976. NSF and NOAA Support.
258	The Structure and Energetics of the Tropical Cyclone (180 pp.). W. M. Frank. October 1976. NOAA-NHEML, NOAA-NESS and NSF Support.
259	Typhoon Genesis and Pre-typhoon Cloud Clusters (79 pp.). R. M. Zehr. November 1976. NSF Support.
Unnumbered	Severe Thunderstorm Wind Gusts (81 pp.). G. W. Walters. December 1976. NSF Support.
262	Diurnal Variation of the Tropospheric Energy Budget (141 pp.). G. S. Foltz. November 1976. NSF Support.
274	Comparison of Developing and Non-developing Tropical Disturbances (81 pp.). S. L. Erickson. July 1977. US Army Support.
——	Tropical Cyclone Research by Data Compositing (79 pp.). W. M. Gray and W. M. Frank. July 1977. US Navy Environmental Prediction Research Facility Report. Tech. Paper No. 77-01. (Available from the US Navy, Monterey, CA). Navy Support.
277	Tropical Cyclone Cloud and Intensity Relationships (154 pp.). C. P. Arnold. November 1977. US Army and NHEML Support.
297	Diagnostic Analyses of the GATE A/B-scale Area at Individual Time Periods (102 pp.). W. M. Frank. November 1978. NSF Support.

248

CSU Dept. of
Atmos. Sci.
Report No.   Report Title, Author, Date, Agency Support

298   Diurnal Variability in the GATE Region (80 pp.). J. M.
                 Dewart. November 1978. NSF Support.

299   Mass Divergence in Tropical Weather Systems, Paper I:
                 Diurnal Variation; Paper II: Large-scale Controls on
                 Convection (109 pp.). J. L. McBride and W. M. Gray.
                 November 1978. NOAA-NHEML Support.

——   New Results of Tropical Cyclone Research from Observational
                 Analysis (108 pp.). W. M. Gray and W. M. Frank.
                 June 1978. US Navy Environmental Prediction Research
                 Facility Report. Tech. Paper No. 78-01.
                 (Available from the US Navy, Monterey, CA). Navy Support.

305   Convection Induced Temperature Change in GATE (128 pp.).
                 P. G. Grube. February 1979. NSF Support.

308   Observational Analysis of Tropical Cyclone Formation
                 (230 pp.). J. L. McBride. April 1979. NOAA-NHEML, NSF
                 and NEPRF Support.

——   Tropical Cyclone Origin, Movement and Intensity
                 Characteristics Based on Data Compositing Techniques
                 (124 pp.). W. M. Gray. August 1979.
                 US Navy Environmental Prediction Research Facility Report.
                 Tech. Paper No. CR-79-06. (Available from the US Navy,
                 Monterey, CA). Navy Support.

——   Further Analysis of Tropical Cyclone Characteristics from
                 Rawinsonde Compositing Techniques (129 pp.). W. M. Gray.
                 March 1981. US Navy Environmental Prediction Research
                 Facility Report. Tech. Paper No. CR-81-02.
                 (Available from the US Navy, Monterey, CA). Navy Support.

333   Tropical Cyclone Intensity Change - A Quantitative
                 Forecasting Scheme. K. M. Dropco. May 1981. NOAA Support.

——   Recent Advances in Tropical Cyclone Research from
                 Rawinsonde Composite Analysis (407 pp.). WMO Publication.
                 W. M. Gray. 1981.

340   The Role of the General Circulation in Tropical Cyclone
                 Genesis (230 pp.). G. Love. April 1982. NSF Support.

341   Cumulus Momentum Transports in Tropical Cyclones (78 pp.).
                 C. S. Lee. May 1982. ONR Support.

CSU Dept. of
Atmos. Sci.
Report No.   Report Title, Author, Date, Agency Support

343   Tropical Cyclone Movement and Surrounding Flow Relationships
          (68 pp.). J. C. L. Chan and W. M. Gray. May 1982. ONR
          Support.

346   Environmental Circulations Associated with Tropical Cyclones
          Experiencing Fast, Slow and Looping Motions (273 pp.).
          J. Xu and W. M. Gray. May 1982. NOAA and NSF Support.

348   Tropical Cyclone Motion: Environmental Interaction Plus a
          Beta Effect (47 pp.). G. J. Holland. May 1982. ONR
          Support.

----   Tropical Cyclone and Related Meteorological Data Sets
          Available at CSU and Their Utilization (186 pp.). W. M.
          Gray, E. Buzzell, G. Burton and Other Project Personnel.
          February 1982. NSF, ONR, NOAA, and NEPRF Support.

352   A Comparison of Large and Small Tropical Cyclones (75 pp.).
          R. T. Merrill. July 1982. NOAA and NSF Support.

358   On the Physical Processes Responsible for Tropical Cyclone
          Motion (200 pp.). Johnny C. L. Chan. November 1982.
          NSF, NOAA/NHRL and NEPRF Support.

363   Tropical Cyclones in the Australian/Southwest Pacific
          Region (264 pp.). Greg J. Holland. March 1983.
          NSF, NOAA/NHRL and Australian Government Support.

370   Atlantic Seasonal Hurricane Frequency, Part I: El Nino
          and 30 mb QBO Influences; Part II: Forecasting Its
          Variability (105 pp.). W. M. Gray. July 1983. NSF
          Support.

379   A Statistical Method for One- to Three-Day Tropical
          Cyclone Track Prediction (201 pp). Clifford R.
          Matsumoto. December, 1984. NSF/NOAA and NEPRF support.

----   Varying Structure and Intensity Change Characteristics
          of Four Western North Pacific Tropical Cyclones. (100 pp.).
          Cecilia A. Askue and W. M. Gray. October 1984. US Navy
          Environmental Prediction Research Facility Report
          No. CR 84-08. (Available from the US Navy, Monterey, CA).
          Navy Support.

CSU Dept. of
Atmos. Sci.
Report No.   Report Title, Author, Date, Agency Support

---   Characteristics of North Indian Ocean Tropical Cyclone
             Activity. (108 pp.). Cheng-Shang Lee and W. M. Gray.
             December 1984. US Navy Environmental Prediction Research
             Facility Report No. CR 84-11. (Available from the US
             Navy, Monterey, CA). Navy Support.

391   Typhoon Structural Variability. (77 pp.). Candis L.
             Weatherford. October, 1985. NSF/NOAA Support.

392   Global View of the Upper Level Outflow Patterns Associated
             with Tropical Cyclone Intensity Change During FGGE. (126 pp.).
             L. Chen and W. Gray. October, 1985. NASA support.

394   Environmental Influences on Hurricane Intensification.
             (156 pp.). Robert T. Merrill. December, 1985. NSF/NOAA
             support.

Author: Cheng Shang Lee
         (P.I.: William M. Gray)

AN OBSERVATIONAL STUDY OF TROPICAL CLOUD CLUSTER EVOLUTION
AND CYCLOGENESIS IN THE WESTERN NORTH PACIFIC

Colorado State University
Department of Atmospheric Science
Fort Collins, Colorado 80523

Subject Headings:
Tropical Cloud Clusters
Tropical Cyclones
Cyclogenesis

A combination of rawinsonde composite and individual case analyses using FGGE III-b data have been used to study the evolution of pre-cyclone tropical cloud clusters and those prominent cloud clusters which do not develop into tropical cyclones in the western North Pacific. These two types of cloud clusters are defined as genesis and non-genesis cases. Results show that the non-genesis cloud clusters have about the same magnitude of maximum-mean upward vertical motion and the same amount of cumulus activities as those of the genesis cloud clusters. The convection associated with the non-genesis cloud clusters do not necessarily alter the temperature, pressure or the vorticity fields, but do transport moisture from the lower troposphere to the middle troposphere. These cloud clusters generally form due to a large-scale low-level forced convergence and dissipate due to a strong middle-to upper-level shearing effect.

16. Abstracts

   A combination of rawinsonde composite and individual case analyses using FGGE III-b data have been used to study the evolution of pre-cyclone tropical cloud clusters and those prominent cloud clusters which do not develop into tropical cyclones in the western North Pacific. These two types of cloud clusters are defined as genesis and non-genesis cases. Results show that the non-genesis cloud clusters have about the same magnitude of maximun mean upward vertical motion and the same amount of cumulus activities as those of the genesis cloud clusters. The convection associated with the non-genesis cloud clusters do not necessarily alter the temperature, pressure or the vorticity fields, but do transport moisture from the lower troposphere to the middle troposphere. These cloud clusters generally form due to a large-scale low-level forced convergence and dissipate due to a strong middle- to upper-level shearing effect.

17. Key Words and Document Analysis. 17a. Descriptors

   Tropical Cloud Clusters
   Tropical Cyclones
   Cyclogenesis

17b. Identifiers/Open-Ended Terms

17c. COSATI Field/Group